Title
The Removal of Nutrients from Wastewater Effluent in Horizontal Levees

Author
Cecchetti, Aidan

Publication Date
2020

Peer reviewed|Thesis/dissertation

The Removal of Nutrients from Wastewater Effluent in Horizontal Levees

by

Aidan R. Cecchetti

A dissertation submitted in partial satisfaction of the
requirements for the degree of
Doctor of Philosophy

In

Civil and Environmental Engineering

in the

Graduate Division

of the

University of California, Berkeley

Committee in charge:

Professor David L. Sedlak, Chair
Professor Kara L. Nelson
Professor Todd E. Dawson

Summer 2020

The Removal of Nutrients from Wastewater Effluent in Horizontal Levees

Abstract

The Removal of Nutrients from Wastewater Effluent in Horizontal Levees

by

Aidan R. Cecchetti

Doctor of Philosophy in Civil and Environmental Engineering

University of California, Berkeley

Professor David L. Sedlak, Chair

Municipal wastewater treatment plants in coastal areas are facing numerous challenges, including the need to provide cost-effective approaches for removing nutrients from wastewater, as well as adapting to the effects of climate change. Retrofitting conventional wastewater treatment plants to remove nutrients can be expensive and is technically challenging. Moreover, wastewater treatment facilities are often situated along coasts, leaving them uniquely susceptible to sea level rise. For these reasons, innovative wastewater utilities have begun to consider more seriously the use of nature-based approaches, such as horizontal levees, to manage these simultaneous pressures. Horizontal levees consist of sloped subsurface wetlands that are built between storm control levees and tidal marshes. When combined with tidal marshes, these systems can help attenuate storm surges and provide space for wetland transgression to higher elevations as sea levels rise. At the same time, removal of residual wastewater-derived contaminants (i.e., nutrients and trace organic contaminants) from treated wastewater effluent can be achieved in the subsurface of these systems.

In the research detailed within this dissertation, we evaluated the ability of horizontal levees to improve water quality. Specifically, we focused on the ability of these systems to remove nutrients (i.e., nitrogen and phosphorus) from nitrified secondary wastewater effluent. To identify optimal operating conditions, we monitored water quality improvements at a 0.7-ha experimental horizontal levee system. First, we assessed the impact of design and operational parameters on contaminant removal, as detailed in Chapter 2. The removal of nitrogen and trace organic contaminants was particularly sensitive to hydrology in this system: rapid and near complete removal (>97%) was observed in water flowing through the subsurface of this system, whereas water flowing over the surface did not receive treatment. When overland flow was eliminated, removal of F+ coliphage (>99%) and phosphate (>83%) was also significant. However, phosphate removal was not as sensitive to hydrology as was removal of other contaminants.

Using porewater sampling, isotope measurements and mass balances on nitrogen and other redox active species, we investigated the mechanisms responsible for nitrogen removal in this system. As detailed in Chapter 3, we identified that microbial metabolic processes (i.e., denitrification and anammox) were responsible for the majority (approximately 80%) of nitrogen removal in this system. The addition of labile organic carbon in the form of wood chips to this system stimulated heterotrophic microorganisms, leading to a progression of reduction of dissolved oxygen, nitrate,

Mn-oxides, Fe-oxides and sulfate within the first 15 m of the subsurface. This progression was especially rapid in the summer. $Fe(II)_{(aq)}$ and sulfide produced from these processes precipitated to form a reservoir of sulfide minerals in the wetland sediments. During cooler winter months, autotrophic denitrifiers paired oxidation of those Fe(II)-sulfides to nitrate reduction, consuming as much as 30% of the nitrate removed in the wetland during the winter. To project long-term removal of nitrogen in horizontal levees, we developed an electron transfer model, described in Chapter 3, to account for production and consumption of electron donors (e.g., organic carbon) that are required to fuel denitrification. Results indicated that horizontal levees could remove nitrate from wastewater effluent for at least 50 years before the carbon amended to the system (e.g., as wood chips) would be depleted. After the wood chips are depleted, sulfide minerals, decaying vegetation and root exudates may provide enough electrons to fuel long-term nitrogen removal.

Plant uptake can also be a significant removal pathway for nitrogen in nature-based treatment systems. However, past methods for quantifying plant uptake have often relied on harvesting plants and assuming that all nitrogen stored in plant biomass is derived from wastewater. This assumption is inappropriate in pilot- or full-scale systems where other sources of nitrogen are available. Moreover, harvesting methods can be laborious and inaccurate when extrapolated to large wetland areas due to heterogeneous distributions of plant biomass. To improve our understanding of this removal mechanism, we developed a new method for quantifying plant uptake, detailed in Chapter 4, in which we used a stable isotope mixing model to distinguish between nitrogen sources. We applied this new method at the field site and found that 14% of nitrogen in plants was derived from wastewater with the remaining nitrogen obtained from the soil. By combining these results with remote-sensing derived biomass measurements, it was determined that 8% of nitrogen removal in this system was due to plant uptake. There were large variations in plant uptake along the wetland slope, both seasonally and with plant maturity. Plant uptake also varied significantly based on design parameters, suggesting that design decisions can have an important impact on this removal pathway. We present this new method as a useful way to inform our understanding of nitrogen cycling and optimization of nature-based nutrient control systems.

We also assessed the cycling of phosphorus in the horizontal levee test facility (Chapter 5). Despite observing significant phosphate removal, removal of phosphate was largely offset by export of dissolved organic phosphorus from the pilot system. This suggested that phosphate may be consumed by microorganisms or assimilated into plant biomass and then exported in other forms. However, preliminary experiments were conducted to investigate the possible use of aerated ponds to convert $Fe(II)_{(aq)}$ in the effluent from these systems to Fe(III)-oxide flocs that can settle out of the water column and have a high capacity for adsorption of phosphorus. This presents a relatively simple method for increasing phosphorus removal and recovery from these systems.

Overall, our work identifies horizontal levees as a promising alternative to conventional treatment systems for the removal of nitrogen and other contaminants from wastewater effluent. Our findings provide us with a better understanding of the impact of design and operational parameters on contaminant removal in these systems and can be used to inform the design of future systems. Further work is needed to test the ability of these systems to treat a variety of additional contaminants (e.g., trace metals), to characterize removal mechanisms for many contaminants (e.g., trace organic contaminants), and to understand the impact of alternative water matrices (i.e., reverse osmosis concentrate) on contaminant removal in these systems.

Table of Contents

LIST OF FIGURES

LIST OF TABLES

Acknowledgements

It would be impossible to acknowledge all the crucial contributions that my family, friends and colleagues have made to this work. Without the input, support and love of the following people, none of this research would have been possible. Compiling this dissertation has simultaneously been one of the most demanding and most gratifying challenges of my life and I am eternally grateful to everyone who has helped make this possible.

First and foremost, I am deeply grateful to my doctoral advisor, David Sedlak, whose incomparable intellect, steadfast support and guidance, and critical feedback have made my research incalculably better than it would have been otherwise. Without David's talent for identifying critical research needs and acquiring necessary funding, my work literally could not have been completed. During graduate school, David gave me the freedom to launch myself headfirst wherever my intellectual curiosity took me. David's mentorship has been instrumental to my development as an independent researcher and I am eternally grateful for the foundational experiences and skills he has helped me to cultivate. I am also immensely grateful to Angela Stiegler, with whom I have worked closely these past few years. Angela was my companion on many long days of field sampling. Together, we fell into sampling trenches, conquered seemingly impenetrable willow stands, and cultivated one of the most meaningful and impactful friendships that I have. In many ways, Angela's contributions to the experimental development, analysis and interpretation of my results have been unmatched. Without her keen analytical acumen, many of the ideas within this dissertation would remain isolated fragments within our respective minds. I cannot thank Angela enough for her contributions to this work and I will follow her research and career with great excitement.

I am also thankful for the vital contributions provided by my other co-authors: Todd Dawson, Anneliese Sytsma, Emily Gonthier, and Katherine Graham. This work has also depended greatly on the collective skills of many members of the Sedlak Research group. In particular, Justin Jasper and Samantha Bear were instrumental in laying the foundation of my research, while Rachel Scholes gave extensive and insightful feedback on my research and large portions of this dissertation. Additional research support was provided by Jessica Ray, Tom Bruton, Tim Rodgers, Florence Bonvin, Jean Van Buren, Marc Teixido, Emily Marron, Carsten Prasse, Joe Charbonnet, Tom Hennebel, Martin Hansen, Aurora Yueng, Amy Cuthbertson, James Barazesh, Daniel Ocasio, Yanghua Duan, Emily Kraemer, Griffin Walsh, Ila Shimabuku, Donald Dillard, and Yue Wen. Many other members of the Berkeley Water Center were crucial to my successful completion of this dissertation, specifically Siva Rama Satyam Bandaru, Sasha Harris-Lovett, Jess Goddard, Jennifer Lawrence, Will Tarpeh, Mi Nguyen, Emily Cook, Shan Yi, Mason King, Ned Antell, Ileana Wald, Lauren Kennedy, Erica Fuhrmeister, Rose Kantor, and Negassi Hadgu. I also want to thank my collaborators through the NSF ERC ReNUWIt, who contributed to my research, as well as the work I have engaged with to promote diversity, equity and inclusion. Specifically, I thank Kara Nelson, Skuyler Herzog, John McCray, Patricia Gonzales, Shaila Kotadia, Kirin Furst, Ali Boehm, Juliana Berglund-Brown, Josh Sharp, Lisa Alvarez-Cohen and Pamela McLeod. The support of staff, including Shamealle Bostic, Sang Oum, and Shelley Okimoto, has also been invaluable. I am grateful to my colleagues through the Center for Stable Isotope Biogeochemistry, Stefania Mambelli and Wenbo Yang, as well as Andrew Weitz and Juliana Wu, without whom the 4th chapter of this work would not exist. I also thank Whendee Silver, Heather Dang and Summer Ahmed for their assistance developing methods for processing soil and plant samples. Carol Kendall, Miriam Diamond, and Joia Fishman have all contributed valuably to this work, as well.

I have learned a lot from the many students I have mentored or co-mentored during my doctoral studies, whose unbridled intellectual curiosity has introduced me to new areas of inquiry. These researchers included Soliver Fusi, who helped introduce me to the idea of coupled elemental cycles and whose friendship I have valued tremendously since we met back in the summer of 2015, and Jean-Paul Wallis, whose work on phosphorus cycling in the horizontal levee laid the foundation for the 5th chapter of this dissertation. I am also deeply thankful for the countless contributions of Devansh Jalota, Sandra Maw, Mhara Coffman, Cayla Anderson and Sara Jones, who I only hope were able to gain as much from our interactions as they contributed to my research.

I am grateful to the entire Oro Loma Horizontal Levee Project team, who developed, designed, implemented, operated and maintained the field site where I conducted my research. Carlos Diaz, Mark Lindley, Jeremy Lowe, Christina Toms, Alex Horne and Peter Baye played critical roles in the development and design of the experimental system where Donna Ball, Jessie Olson and many volunteers from Save the Bay worked tirelessly to cultivate a thriving plant community. I am also grateful to Marc Holmes, Jacqueline Zipkin, Jennifer Krebs, Adrien Baudrimont, Heidi Nutters, Christian Nilsen, Eric Haas-Stapleton, and Mike Connor for their roles in the implementation of this project. I also want to thank Jason Warner, Jimmy Dang, Kristopher Decker, Manuel Talledo-Garcia and everyone at Oro Loma Sanitary District who helped maintain the experimental system.

I cannot imagine graduate school without the friendships of Sara Gushgari-Doyle and Scott Miller, who provided insightful feedback and were also lifelines of cheer and amusement throughout what was often a lonely and frustrating process. Lastly, and in many ways most importantly, I want to thank my family and close friends for their love, advice and encouragement. In particular, I want to thank my parents, Lynda and Rick, whose faith in my abilities, strong connection to the environment, and deep appreciation of science instilled in me from an early age the values and drive that motivated me to complete this dissertation. I am also deeply grateful to my older sister Katy, who has always been one of my closest friends and has frequently given me empathy, strength and comfort when I needed it most. My close friends Jihyon Im, Brianna Jean, Morgan Hilow, and Michelle Gelinas, as well as Dina Beigelman and Remi Preux, provided love, encouragement, and sorely needed help maintaining my mental health when my work felt too daunting. I will always be grateful for my unique and cherished friendship with Brianna Wentworth, who frequently answered my frantic messages in need of advice at all hours of the night. Without these special relationships, I never would have been able to complete this work.

Finally, I dedicate this work to my partner (in crime, in life and otherwise), Michael Charles Greenberg, who has steadfastly stood by me with love and compassion throughout this process, even when it has been painful. I could not have completed this work without his loving care, his frequent reminders to maintain a healthy work-life balance, and our shared love of adventures – both geographical and culinary. Michael and our affectionate cat, Torple, have brought unparalleled joy to my life, which has sustained me throughout this arduous journey.

This dissertation was made possible by a UC Berkeley Civil and Environmental Engineering graduate research fellowship, the National Science Foundation Graduate Research Fellowship Program (GRFP) under Grant No. DGE-1106400, and the National Science Foundation's Engineering Research Center for Reinventing the Nation's Urban Water Infrastructure (ReNUWIt) EEC-1028968. Additional support was provided by a Bay Area Integrated Regional Water Management Plant (IRWMP) grant and through a grant provided by Oro Loma Sanitary District.

Chapter 1. Introduction

1.1 Background

1.1.1 Problems Faced by Wastewater Treatment Plants in Urbanized Estuaries

Over the past two centuries, humans have transformed the global nitrogen (Seitzinger et al., 2006; Galloway et al., 2008) and phosphorus cycles (Childers et al., 2011). These changes have been driven largely by agricultural fertilizers (Galloway et al., 2008), which consist of ammonia from the Haber-Bosch process and phosphate mined from nonrenewable mineral deposits (Cordell et al., 2009). The Haber-Bosch process requires large inputs of energy and has more than doubled the amount of fixed nitrogen entering terrestrial systems (Gruber and Galloway, 2008). Human activities have also nearly tripled the global mobilization of phosphorus (Smil, 2000). Release of these nutrients into aquatic ecosystems via agricultural runoff and municipal wastewater effluent has led to negative impacts on natural ecosystems globally, such as harmful algal blooms (Paerl and Scott, 2010) and eutrophication (Kadlec and Wallace, 2009). For example, in 2008 nearly two-thirds of estuaries in the United States assessed by Bricker et al. (2008) were determined to have moderate to high levels of eutrophication due to nutrient enrichment caused by human activities. Furthermore, the eutrophic status of the majority of assessed estuaries was predicted to worsen in coming decades due to improper management of human activities (Bricker et al., 2008). To make matters worse, increasing temperatures associated with climate change are creating conditions that are more favorable for the algal growth caused by nutrient pollution (Paerl and Scott, 2010).

In the San Francisco Bay estuary, urbanization has combined increasing contaminant loads from wastewater treatment plants with another problem: the destruction of ecologically important and historically extensive wetland systems (Lowe et al., 2013). Natural wetlands are vital habitats for a variety of animals and migratory birds. Wetlands also play important roles in hydrological and nutrient cycles, earning them the nickname “nature’s kidneys” due to their ability to reduce contaminant loads (e.g., dissolved nitrogen) that can negatively impact aquatic ecosystems (Young, 1996). It is therefore concerning that an estimated 30% of wetlands in the United States (Young, 1996) and >90% of the coastal marshes in the San Francisco Bay Area (Williams and Faber, 2001) have disappeared over the past 200 years.

Despite increasing nutrient loading, algal growth in the San Francisco Bay has been suppressed historically due to high suspended sediment concentrations that limit light penetration into the water column (Cloern, 1999). For that reason, discharges of nutrients from wastewater treatment plants, which are the primary source of nutrients to the southern portion of the Bay (Cloern and Jassby, 2012), have remained largely unregulated. These discharges are high compared to other urbanized estuaries throughout the U.S. (e.g., nitrogen and phosphorus discharges per area are higher in San Francisco Bay than ~80% of reported estuaries along the East and Gulf Coasts; Table 1-1). However, decreasing sediment loads to the Bay appear to have ended the period in which algal growth was not a major concern despite high nutrient loading (Cloern and Jassby, 2012) because algal blooms are becoming more frequent and severe (Cloern, 2005; Lehman et al., 2008).

Additional issues associated with climate change, such as sea level rise, threaten critical water infrastructure. This is a significant issue in the Bay Area, especially because of the loss of coastal

wetlands that play a protective role in reducing coastal flooding (Shepard et al., 2011). Additionally, of the 28 wastewater treatment plants that are most vulnerable to sea level rise in California, 21 are in the San Francisco Bay area (Heberger et al., 2009). Increasing climate variability and storm severity over the next century is of particular concern for these facilities (Cayan et al., 2008) and threatens their ability to provide services (Hummel et al. 2018). Loss of service at wastewater treatment plants could lead to a variety of problems, such as discharges of untreated wastewater, which are made worse by a lack of coastal wetlands to regulate hydrological conditions and contaminant levels in estuaries.

Table 1-1: Loading of total nitrogen (TN) and total phosphorus (TP) to urbanized and impacted estuaries across the United States.

Estuary	TN load per estuary area, kg km^{-2} yr^{-1}	TP load per estuary area, kg km^{-2} yr^{-1}	Surface area, km^2	Source
East Coast				
Great Bay, NH	22,500	1,570	47	Moorman et al., 2014
Massachusetts Bay	1,150	75.2	2,393	Moorman et al., 2014
Long Island Sound	12,100	1,150	3,301	Moorman et al., 2014
Hudson River	89,900	10,400	799	Moorman et al., 2014
Pamlico Sound, NC	1,900	197	5,588	Moorman et al., 2014
Chesapeake Bay	11,500	713	11,263	Moorman et al., 2014
Median Value	**8,420**	**625**	**206**	
Gulf Coast				
Tampa Bay	3,400	1,320	1,000	USGS, 2014
Mobile Bay	39,900	4,200	1,070	USGS, 2014
Mississippi River Basin	735,000	88,200	1,700	Aulenbach et al., 2007
Galveston Bay	25,300	3,970	1,600	USGS, 2014
Corpus Christi Bay	4,520	702	497	USGS, 2014
Laguna Madre	1,120	110	2,500	USGS, 2014
Median Value	**9,080**	**1,400**	**540**	
Pacific Coast				
Santa Monica Bay	16,000	1,040	1070	Sengupta et al., 2013
Elkhorn Slough	3,940	836	4	Tetra Tech, 2018
San Francisco Bay	**24,700**	**2,070**	**1100**	**Novick and Senn, 2013**
Humboldt-Arcata Bay	9,600	3,400	50	Swanson, 2015
Puget Sound	10,200	n.r.	2600	Mohamedali et al., 2011
Median Value	**10,000**	**1,555**	**1000**	

n.r. = value not reported within cited study

Engineering approaches for dealing with these challenges can be costly and may not provide permanent solutions. For example, seawall and levee construction in California has been projected to cost $14 billion (in year 2000 dollars) with an additional $1.4 billion required yearly for maintenance (Heberger et al., 2009). Additionally, at wastewater treatment plants, nutrient control processes often require large capital investments (Ko et al., 2004) and can increase operation and maintenance costs by as much as 20% (Molinos-Senante et al., 2010). Because of their interdependent nature and the inability of individualized approaches to resolve them appropriately, these combined challenges (i.e., coastal flooding, loss of coastal wetlands and coastal nutrient pollution) have been labeled as a "wicked problem" – an adverse situation that overwhelms existing practices and persists even with the application of best-known practices (Thornton et al., 2013).

1.1.2 Constructed Wetlands and the Horizontal Levee Concept

The high costs associated with traditional approaches for dealing with these challenges have spurred a growing interest in multi-benefit alternatives, such as constructed wetlands (Ko et al., 2004). Constructed wetlands are engineered systems that are designed to utilize processes found in natural wetlands to treat wastewater. These systems have been used since at least the 1950s (Vymazal, 2010) and have commonly been applied for control of wastewater-derived nutrients (Vymazal, 2007), while providing many other benefits such as the removal of additional wastewater-derived contaminants, water storage, habitat restoration, and recreational opportunities (Young, 1996; Kadlec and Wallace, 2009).

A new type of subsurface constructed wetland – the horizontal levee – shows significant promise both as a flood control system and as a final treatment step (i.e., polishing) for nitrified wastewater effluent (Lowe et al., 2013). Horizontal levees consist of sloped subsurface treatment wetlands that are built on the seaward side of storm control levees. These systems can provide restored wetland habitat while protecting levees by attenuating storm surges that can overtop them (Figure 1-1). Municipal wastewater effluent is discharged to the subsurface of these wetland systems where it provides a source of freshwater for plants growing in the restored wetlands. In the subsurface, the wastewater effluent concurrently receives treatment of wastewater-derived contaminants while providing water and nutrients to plants.

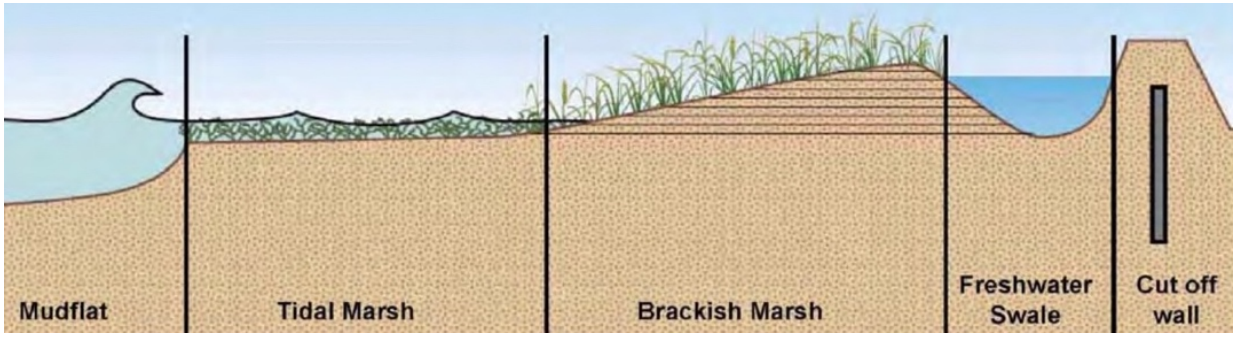

Figure 1-1: Sketch of a recreated wetland gradient used to buttress a storm control levee (reproduced from Lowe, et al., 2013).

The capacity of coastal wetlands to attenuate storm surges is well established (Wamsley et al., 2010; Gedan et al., 2011; Shepard et al., 2011; Möller et al., 2014), but research has not been conducted on the ability of horizontal levees to remove nutrients. Some insight can be gained from research on the nutrient removal capabilities of similar nature-based systems, such as subsurface treatment wetlands, which have traditionally consisted of gravel beds planted with cattails or bulrushes (Kadlec and Wallace, 2009), as well as riparian wetlands (Hill, 1996; Willems et al., 1997; Piñón-Villarreal et al., 2013) and denitrification walls (Schipper and Vojvodic-Vukovic, 2001; Shipper et al., 2004; Schipper et al., 2010; Schmidt and Clark, 2012). The horizontal levee incorporates many design features of these systems, but there remain major differences in the hydrological conditions, plant communities, construction materials and influent water matrices. Additionally, the lack of robust, well-parameterized models for estimating nutrient removal in these natural treatment systems makes it difficult to extrapolate the results of past research to newly constructed horizontal levees.

1.2 Nutrient Transformations in Constructed Wetlands

In natural and constructed wetlands, a range of processes control the fate and transport of nutrients (Table 1-2). These processes are in turn controlled by a suite of design and operational parameters (e.g., hydrological conditions). There are fundamental differences between the major processes controlling the removal of nitrogen and phosphorus respectively in wetlands, as detailed in Table 1-2.

Table 1-2: Key processes in the nitrogen and phosphorus cycles in constructed wetlands. Processes expected to dominate in horizontal levees receiving nitrified wastewater effluent are in bold.

Species	Nutrient Cycle Processes		
	Conversion	Storage	Removal
Nitrogen	Ammonification Nitrification **DNRA** **Feammox, Mnammox**	**Plant uptake** Microbial assimilation Adsorption Burial of particulate nitrogen	**Denitrification** **Anammox** **Feammox** Ammonia volatilization
Phosphorus	Mineralization	**Plant uptake** Microbial assimilation **Adsorption** **Precipitation of phosphate minerals** Burial of particulate phosphorus	

1.2.1 Nitrogen Cycling

The nitrogen cycle is typically dominated by microbial processes that convert nitrogen among a variety of oxidation states, such as nitrification and denitrification (Vymazal, 2007; García et al., 2010). Only a limited number of these processes remove nitrogen from the aqueous matrix, with the majority contributing to an internal cycle of conversion between oxidation states and nitrogen species (Vymazal, 2007). In subsurface wetlands similar to the horizontal levee, strong biological activity and low dissolved oxygen concentrations favor anaerobic processes like denitrification, anaerobic ammonium oxidation processes (i.e., anammox, Feammox, and Mnammox), and dissimilatory nitrate reduction to ammonium (DNRA). Additionally, because wastewater flows through the rooting zones of wetland plants in these systems, plant uptake of nitrogen (and its subsequent deposition and burial) can play a significant role in nitrogen cycling as well (Mayo and Bigambo, 2005).

Despite previous research efforts, the relative importance of different nitrogen cycle processes in subsurface wetlands is still unclear. There are wide and unexplained variations in reported denitrification rates in natural ecosystems (Seitzinger et al., 2006) and constructed wetlands (Kadlec and Wallace, 2009). This is likely due in part to inadequacies in methods for measuring and reporting denitrification (Groffman et al., 2006). Recent recognition of the potential importance of processes such as anammox (Strous et al., 1999), Feammox (Yang et al., 2012a), and DNRA (Tiedje, 1988) to the nitrogen cycle in natural ecosystems has also called into question past analyses and has led to important advances in methods to quantify nitrogen cycle processes (Groffman et al., 2006; Salk et al., 2017). Additionally, despite a large body of evidence linking denitrification rates to specific variables (e.g., hydrology) (Seitzinger et al., 2006) and the development of a suite of models for predicting denitrification rates (Boyer et al., 2006), relatively little effort has been made to apply this knowledge or these models to constructed wetlands.

Past studies have also provided conflicting information about the relative magnitude of plant uptake in constructed wetlands (Saeed and Sun, 2012). This is partly because many plant uptake rates reported in the literature have been determined in systems without fully developed plant communities, which can be problematic because plant nutrient sources and requirements often change with plant age

(Tanner, 2001). Additionally, estimates have often been made using methods that have the potential to overestimate or underestimate plant uptake rates, such as assuming that all nitrogen stored in plant biomass is derived from the wastewater source (Healy and Cawley, 2002; Kantawanichkul et al., 2009) or by simply attributing differences in nitrogen removal between planted and unplanted wetland cells to uptake (Drizo et al., 1997; Meers et al., 2005). Despite the ostensible consensus within the literature that plant uptake in constructed wetlands typically accounts for 0.5-40% of nitrogen removal (Meers et al., 2008; Saeed and Sun, 2012), reported fractions of nitrogen removal attributable to plant uptake span three orders of magnitude (Table 1-3). These possible discrepancies make it clear that plant uptake must be studied in wetlands of variable plant age using more robust quantification methods.

Table 1-3: Observed fractions of nitrogen removal attributed to plant uptake in subsurface wetlands. Abbreviations: VSSF – vertical subsurface flow, FWS – free-water surface, SSF – subsurface flow, and HSSF – horizontal subsurface flow.

Wetland Type	Nitrogen Removal as Plant Uptake (%)	Source
VSSF Wetlands (*Typha*)	0.5-3.3	Kantawanichkul et al., 2009
VSSF Wetlands (*Cyperus*)	6.7-16.9	
Mixed FWS and SSF Wetlands	9	Meers et al., 2008
HSSF Wetlands	2-4	Lee et al., 2004
HSSF Wetlands	7-18	Meers et al., 2005
SSF Microcosms	90	Rogers et al., 1991
HSSF Wetlands	20-60	Drizo et al., 1997
HSSF Wetlands	10	Mayo and Bigambo, 2005

1.2.2 Phosphorus Cycling

The biogeochemistry of phosphorus differs significantly from that of nitrogen. Similarities between the cycling of nitrogen and phosphorus are limited to physical storage of particulate forms of phosphorus and nitrogen, and assimilatory processes, such as microbial assimilation and plant uptake. However, the magnitude of these assimilatory processes differs between the two species by approximately an order of magnitude based on the nutritional requirements of plants and microorganisms.

During the initial stages of wetland development, phosphorus is often removed rapidly by plant uptake and adsorption onto mineral surfaces, though the importance of these processes typically changes over time and can vary widely both across and within wetlands (Kadlec and Wallace, 2009). Phosphorus removal in subsurface wetlands frequently depends on substrate geology because phosphate has a high affinity for Al-, Fe- and Mn-oxides in the subsurface (Evans and Smillie, 1976; Parfitt, 1978; Holtan et al., 1988; Darke and Walbridge, 2000). Additionally, adsorption to calcite and formation of Ca-phosphate minerals can also affect phosphate concentrations under certain conditions (Illmer and Schinner, 1995). However, adsorption processes often do not constitute long-term removal mechanisms because they have a finite capacity (Illmer and Schinner, 1995; Kadlec and Wallace, 2009) and can be susceptible to reversal during fluctuations in redox conditions. For example, biological redox reactions can affect phosphorus cycling indirectly when iron oxides are present. During reductive dissolution of Fe(III)-oxides, adsorbed phosphate can be released (Chacón et al., 2005; Liptzin and Silver, 2009). A similar phenomenon can occur during reductive dissolution of Mn(III/IV)-oxides (Yao and Millero, 1996). Removal of phosphorus by plant uptake is partly offset over time by deposition and decay of dead plant biomass on the wetland surface, which can lead to reintegration of assimilated phosphorus into the aqueous phase unless labor-intensive practices like

plant harvesting are conducted. Because these processes can vary widely over time and space, further research is required to understand how design and operational parameters can be modified to optimize removal.

Over the long-term, sustainable phosphorus removal is achieved through accretion processes, such as precipitation of phosphorus minerals, deposition of particulate phosphorus and accumulation of recalcitrant soil organic phosphorus. Because these processes tend to occur at much lower rates than the processes that dominate the beginning stages of wetland development, subsurface wetlands are rarely intended specifically for phosphorus removal (Kadlec and Wallace, 2009). For this reason, innovative design and operational features may be required to achieve long-term phosphorus removal in horizontal levees.

1.3 Motivation and Research Objectives

1.3.1 Motivation

Horizontal levees have multiple advantages, such as providing wetland habitat and flood control for low-lying treatment facilities and urban areas, as well as a suite of additional benefits (e.g., recreational opportunities). These systems represent a promising alternative to conventional nutrient management strategies for wastewater treatment plants. However, little is known about their optimization for nutrient removal. There is uncertainty regarding the contribution of various processes to nutrient removal in constructed wetlands, such as denitrification and plant uptake of nitrogen. Nitrogen removal is controlled by a complex set of interconnected processes that transform nitrogen in a cyclical nature and it can be difficult to quantify individual processes precisely. Past research has been marred by inadequate measurement methods and an incomplete understanding of the complexity of this cycle, making it difficult to extrapolate past results to new wetlands. New methods are needed to provide more precise data for nitrogen cycle processes, such as plant uptake, which has been poorly constrained by past research. In contrast to the nitrogen cycle, the dominant processes in the phosphorus cycle and the lack of ultimate removal mechanisms make long-term removal of phosphorus difficult without innovative design features. By developing a more complete understanding of the contribution of various nutrient removal mechanisms and their controls, horizontal levees can be optimized to provide effective treatment of municipal wastewater effluent.

To determine the impact of design parameters on contaminant removal and develop a mechanistic understanding of that removal, we applied a set of new methods, including porewater sampling and isotope fingerprinting, to study nutrient removal in an experimental horizontal levee system. Our research is detailed in the five subsequent chapters of this publication. Chapters 2-5 detail the results of individual studies we conducted to address the four objectives detailed in subsections 1.3.2, 1.3.3, 1.3.4 and 1.3.5, below. Finally, in Chapter 6 we summarize the key results of these studies and their implications for the design and implementation of horizontal levees, while detailing important next steps for research on these systems.

1.3.2 Objective 1: Evaluate the Impact of Design and Operational Parameters on Removal of Nutrients in a Horizontal Levee

To determine optimum design and operational parameters to enhance nutrient removal in horizontal levees, contaminant removal (i.e., removal of nutrients and trace organic contaminants) was evaluated in a set of experimental horizontal levee cells, as described in Chapter 2. Design and operational parameters, such as topsoil texture, plant community composition, cell topography, and applied flow

rates, were varied among wetland cells that were monitored over a 2-year period to test the impact of those parameters on contaminant removal. Water quality parameters were tracked in the influent and effluent to wetland cells, as well as in water flowing through the subsurface and over the wetland surface, to construct mass balances on contaminants and to understand how hydrological conditions impact contaminant removal in a horizontal levee. The relative influence of the above parameters on contaminant removal were tested using various statistical methods. The area needed for removal of 90% of nitrate was used as a measurable metric for comparison with other treatment systems.

1.3.3 Objective 2: Characterize Subsurface Nitrogen Biogeochemistry in a Horizontal Levee

Removal of nitrogen from wastewater effluent is a primary objective of horizontal levees. In subsurface wetlands, nitrogen removal is typically achieved primarily by plant uptake and a suite of microbially-mediated biogeochemical cycles in the subsurface. To evaluate the relative importance of microbial nitrogen cycle processes to the removal of nitrogen, changes in the concentration and speciation of nitrogen (and other relevant elements) were tracked in subsurface porewater samples. Subsurface mass balances were constructed using porewater sampling and a variety of solid phase characterizations for nitrogen, carbon, sulfur, manganese and iron to evaluate the relative importance of different microbial processes (e.g., denitrification and anammox) and to understand the impact of other chemical species on nitrogen cycle processes (e.g., sulfide-driven denitrification). An overall mass balance on nitrogen was conducted to understand the relative contribution of subsurface microbial processes to nitrogen removal, as described in Chapter 3.

1.3.4 Objective 3: Evaluate Plant Uptake of Wastewater-Derived Nitrogen in a Horizontal Levee

Plant uptake of nitrogen is among the most important nitrogen removal mechanisms in constructed wetlands, but the relative importance of this process is currently unclear. There are wide discrepancies among the results reported in past studies of constructed subsurface wetlands, suggesting that there are either deficiencies in plant uptake measurement methodologies or that there are additional factors creating an unexpectedly large amount of variation in these measurements. To quantify plant uptake in a horizontal levee, we developed and applied a new plant uptake measurement method to the pilot-scale horizontal levee system, as described in Chapter 4. This new method involves the measurement of stable isotope ratios of nitrogen ($\delta^{15}N$) in plants, soils, and influent wastewater and the application of a set of mixing models, commonly used in ecology to quantify diets of animals, to determine the fraction of plant nitrogen that is derived from wastewater. The fraction determined from these models was multiplied by the total mass of nitrogen stored in plants to calculate uptake of wastewater-derived nitrogen. Plant uptake measurements were combined with the characterization of subsurface microbial processes (Objective 2) to estimate an overall mass balance on nitrogen (Chapter 3).

1.3.5 Objective 4: Evaluate Phosphorus Removal Mechanisms in a Horizontal Levee

Phosphorus removal in subsurface constructed wetlands is controlled primarily by a suite of physical and chemical processes such as adsorption and precipitation of phosphate minerals but is also impacted by microbial processes and plant uptake of phosphorus. Unlike nitrogen, which can be converted to $N_{2(g)}$ and released to the atmosphere as an ultimate sink, phosphorus removal is better characterized as a set of short to long-term storage mechanisms. Many of these mechanisms, such as adsorption of phosphate onto iron-oxide minerals, are susceptible to shifts in redox conditions, which can lead to the re-release of adsorbed phosphate. To study phosphorus biogeochemistry in a horizontal levee,

mass balances were evaluated for phosphorus and related species (e.g., iron) to estimate the relative importance of phosphorus removal mechanisms, as described in Chapter 5. Additionally, dissolved Fe(II) produced by iron-reducing microorganisms in the subsurface has the potential to form Fe(II)-phosphate minerals (e.g., vivianite) or Fe(III)-oxides with a high affinity for phosphate upon oxidation. Experiments were performed to investigate the potential for these mechanisms in effluent water from a horizontal levee and the affinity of formed precipitates for dissolved phosphate.

Chapter 2. The Horizontal Levee: A Multi-Benefit Nature-Based Treatment System that Improves Water Quality and Protects Coastal Levees from the Effects of Sea Level Rise

Reproduced with permission from Stiegler, A.N., Graham, K.E., Sedlak, D.L. The horizontal levee: a multi-benefit nature-based treatment system that improves water quality and protects coastal levees from the effects of sea level rise. *Water Research X*. **2020**, 7, 100052.

ABSTRACT

Municipal wastewater treatment plants in coastal areas are facing numerous challenges, including the need to provide a cost-effective approach for removing nutrients and trace organic contaminants from wastewater, as well as adapting to the effects of climate change. The horizontal levee is a multi-benefit response to these issues that consists of a sloped subsurface treatment wetland built between a coastal levee and tidal marshes. The wetland attenuates storm surges and can provide space for wetland transgression to higher elevations as sea levels rise, while simultaneously removing contaminants from treated wastewater effluent. To assess the ability of the horizontal levee to improve water quality and to identify optimal operating conditions, a 0.7-ha experimental system was studied over a two-year period. The removal of nitrate and trace organic contaminants was particularly sensitive to hydrology; rapid and near complete removal (>97%) of these contaminants was observed in water flowing through the subsurface, whereas surface flows did not exhibit measurable contaminant removal. Removal of F+ coliphage also appeared to be sensitive to hydrology, with up to 99% removal of these indicator viruses in subsurface flow. For phosphate, removal was not as sensitive to hydrology, but significant removal (>83%) was still observed when overland flow was eliminated. Although removal of contaminants did not appear to be sensitive to other design considerations, parameters such as soil texture and planting regimes affected the maximum subsurface flows, which in turn controlled contaminant mass loadings. Rapid subsurface removal of contaminants suggests that water quality benefits of these systems are limited by physical constraints (i.e., the ability of the system to maintain subsurface flow) and not chemical or biological conditions in the subsurface.

2.1 Introduction

Municipal wastewater treatment plants located in coastal environments are facing numerous challenges. Nutrient (i.e., nitrogen and phosphorus) discharges can impact marine and estuarine ecosystems by causing harmful algal blooms and eutrophication (Heisler et al., 2008). In addition, trace organic contaminants, such as pharmaceuticals, personal care products and household pesticides, have been detected in treated wastewater effluent at concentrations that pose risks to aquatic ecosystems (Sumpter and Johnson, 2005). Although future regulations may require additional treatment for these contaminants, retrofitting conventional treatment plants to remove them is expensive and technically challenging (Schwarzenbach et al., 2006; Foley et al., 2010). To further complicate matters, coastal wastewater treatment facilities are susceptible to flooding. As sea-level rises and the frequency of severe storms increases, wastewater treatment plants and other coastal infrastructure, as well as sensitive coastal ecosystems, will be threatened (Heberger et al., 2011). For example, in the United States, 30 cm of sea-level rise would result in flooding and loss of service at wastewater treatment plants serving more than 4 million people (Hummel et al., 2018).

The traditional approach for protecting coastal infrastructure from flooding involves the construction of seawalls and levees, at significant cost (Heberger et al., 2011). In 2013, a new approach for reducing the need to raise existing levees as sea-level rises, while simultaneously reducing the mass of contaminants discharged by municipal wastewater treatment plants, was designed. This system, which is referred to as the horizontal levee, consists of a sloped subsurface treatment wetland built between coastal levees and tidal marshes. The horizontal levee provides transitional wetland habitat consisting of native vegetation that protects existing levees from erosion and reduces the threat of coastal flooding by attenuating storm waves (Wamsley et al., 2010; Gedan et al., 2011; Shepard et al., 2011). Treated municipal wastewater effluent is discharged to the subsurface of these wetlands through a perforated pipe to provide water for plants growing on this elevated wedge of land. As the water flows though the subsurface wastewater-derived contaminants are attenuated. To accommodate greater applied flows, the subsurface consists of multiple layers. A surficial layer of low permeability soil (i.e., clay or loam) that is suitable for cultivating wetland plants, is underlain by coarse layers (i.e., sand and gravel) with higher hydraulic conductivities to achieve greater subsurface flows.

In natural and constructed wetlands, hydrology plays a significant role in contaminant removal. This is especially true for contaminants that are removed through microbial processes, as exemplified by nitrate. Across diverse aquatic ecosystems, variation in the proportion of nitrate removed appears to be largely explained by hydrological variables, such as residence times and water depth (Seitzinger et al., 2006). Hydraulic short-circuiting is common in constructed wetlands (Knowles et al., 2010), and can adversely impact treatment efficacy (Headley and Kadlec, 2007) by routing flows (and nitrate contained therein) around quiescent suboxic zones where denitrification activity is more significant (Seitzinger et al., 2006). For example, while denitrification walls can remove nitrate from groundwater (Schipper and Vojvodic-Vukovic, 2001; Schmidt and Clark, 2012), treatment efficiency decreases if water bypasses regions of biological activity by flowing through zones with higher hydraulic conductivity (Schipper et al., 2004). Additionally, overland flow in riparian wetlands often leads to less nitrate removal (Hill, 2000), likely due to decreased contact with plant roots and denitrifying communities in the subsurface (Willems et al., 1997). Similar effects are expected for trace organic contaminants that are susceptible to biotransformation in wetlands.

To assess the potential for using a horizontal levee to remove contaminants from treated wastewater effluent, we studied water quality and hydrological conditions over two years of operation in an experimental horizontal levee consisting of various combinations of design parameters (e.g., sediment

texture, planting regimes). We monitored nutrients (i.e., nitrogen and phosphorus) and wastewater-derived trace organic contaminants because they are difficult to remove in existing treatment systems and frequently are present above concentrations of concern for aquatic ecosystems. We also monitored F+ coliphage to assess the ability of these systems to remove enteric pathogen indicators. Results from these analyses inform the design and operation of horizontal levee systems and provide a basis for assessing the performance of full-scale subsurface treatment systems.

2.2 Materials and Methods

2.2.1 Field site

A 0.7-hectare experimental horizontal levee was constructed in San Lorenzo, CA (37.67°N by 122.16°W) to treat a small portion (i.e., <1%) of the secondary effluent from a conventional activated sludge wastewater treatment plant operated by the Oro Loma Sanitary District (https://oroloma.org/sewage-treatment/), which has a total treatment capacity of 76,000 m^3 d^{-1}. The effluent was nitrified in a gravel trench upstream of the wetland system. Water quality characteristics for nitrified secondary effluent are summarized in Table 2-1. Native wetland plants (section A.1.3 of Appendix A), mainly consisting of members of the families *Cyperaceae* (sedges), *Juncaceae* (rushes) and *Salicaceae* (willows), were planted in the horizontal levee between November 2015 and February 2016. Native plants were propagated from cuttings (typically less than 3 cm) in the surficial soil approximately 15 months before nitrified wastewater effluent was introduced into the subsurface. During this period, the sloped wetland was irrigated via sprinklers using shallow groundwater from a well located approximately 50 m from the wetland. In April 2017, treated effluent from the wastewater treatment plant was first introduced to the horizontal levee at a total flow of 265 m^3 d^{-1}.

Table 2-1: Water quality characteristics of nitrified secondary wastewater effluent at the horizontal levee test facility.

Constituent	Units	Average (± S.D.)
pH	-	8.2 ± 0.8
Temperature	ºC	19 ± 2.2
Dissolved Oxygen	mg O_2/L	6.0 ± 3.6
Conductivity	mS/cm	0.9 ± 0.5
Total nitrogen	mg N/L	30 ± 13
Nitrate	mg N/L	25 ± 11
Nitrite	mg N/L	0.7 ± 0.7
Ammonium	mg N/L	2.9 ± 2.6
Organic nitrogen	mg N/L	2.1 ± 1.4
Dissolved organic carbon	mg C/L	10.1 ± 5.4
Chloride	mg/L	97 ± 27
Bromide	mg/L	0.4 ± 0.3
Phosphate	mg P/L	1.6 ± 1.4
Sulfate	mg/L	49 ± 17
Sodium	mg/L	120 ± 58
Potassium	mg/L	12 ± 3.4
Magnesium	mg/L	11 ± 3.8
Calcium	mg/L	26 ± 12

Prior to entering the horizontal levee, wastewater effluent passed through a gravel nitrification trench and a 0.8-hectare surface-flow wetland planted with cattails and bulrushes (*Typhaceae* spp.) (Figure

2-1). The nitrification trench converted >90% of the ammonia in the effluent into nitrate and nitrite (i.e., average applied ammonia concentrations were 31 ± 5.1 mg N L^{-1}). Between April and November 2017, the hydraulic residence time in the surface flow wetland was approximately 11 days. Under these conditions, an average of 63% of influent nitrate was removed before entering the horizontal levee (i.e., average influent nitrate concentrations were 11 ± 4.2 mg N/L from April to October 2017). In November of 2017, the flow from the nitrification trench was rerouted directly into the influent pump station to the subsurface wetland to assure that higher concentrations of nitrate entered the horizontal levee. After November 2017, mean nitrate concentrations were 31 ± 6.3 mg N L^{-1} in the influent to the horizontal levee.

Figure 2-1: The site layout of the experimental horizontal levee test facility (Baye and ESA, 2012). The site included a surface-flow treatment wetland, which doubled as a wet weather equalization basin, a nitrification facility and the horizontal levee slope. The two flow paths correspond to the two flow regimes employed over the monitoring period, in which: (1) nitrified secondary effluent passed through the freshwater treatment wetland prior to being distributed in the horizontal levee slope (blue path) and (2) nitrified secondary effluent bypassed the treatment wetland was fed directly into the horizontal levee slope, in which case a parallel flow of water was also pumped backward through the freshwater treatment wetland (not shown) before returning to the headworks of the wastewater treatment facility (orange path). In both regimes, effluent from the horizonal levee slope was also returned to the headworks of the wastewater treatment plant. A timeline of operational changes is presented in Figure 2-3. The influent sampling location was at the distribution pump preceding the horizontal levee slope.

The subsurface wetland was divided into 12 parallel treatment cells, each having dimensions of 1 m deep x 12 m wide x 46 m long. The cells were hydraulically isolated from each other with clay berms and were underlain with a geotextile liner and a low permeability compacted clay layer ($K_{sat} < 10^{-6}$ cm s^{-1}). The 12 cells provided an ability to test four different wetland configurations in triplicate (Figure 2-2 and section A.1 of Appendix A). The four treatments (i.e., swale-depression cells, wet meadows with fine or coarse topsoil, and willow/riparian cells) varied in terms of their topography, soil type and plant community.

Figure 2-2: Layout of the horizontal levee slope at the test facility showing the individual cells. The four treatments are labeled in the center of each cell. Influent water enters each cell through perforated pipes at the top of the slope represented by the green line. Intermediate wells 15 and 30 m along the slope were located in the center of each cell (denoted by a red X). The effluent was collected in a gravel trench at the end of each slope, represented by the blue line, with effluent sampling ports and flow meters denoted by a yellow X for each cell. The yellow line indicates the direction of flow.

The horizontal levee was gently sloped (1:30) and consisted of three granular media layers. From the bottom to the top, these included gravel, coarse sand and loam topsoil layers with hydraulic conductivities of approximately 0.25 cm s^{-1}, 0.1 cm s^{-1} and 10^{-3} cm s^{-1} respectively. The topsoil layers consisted of various mixtures of fine clay loam consisting of clay excavated onsite mixed with coarse sand (section A.1.2 of Appendix A). The topsoil layer supported plant roots and prevented rapid diffusion of oxygen into the subsurface. The higher hydraulic conductivities of the underlying layers were integrated to allow for a greater flow of water through the system. All subsurface layers were amended with organic carbon (i.e., wood chips) to promote microbial conversion of nitrate (NO_3^-) to nitrogen gas (N_2) via denitrification. Redwood wood chips (*Sequoia sempervirens* or *Pseudotsuga menziesii*) of less than 2 cm in their greatest dimension were mixed into the sand and gravel layers by disking at 30% v/v prior to installing the loamy soil surface layer. Wood fines of less than 0.5 cm in size were mixed into the topsoil layer at 10% v/v. Wood fines were composted for 12 months prior to use. See section A.1 of Appendix A for further details.

Nitrified treated municipal wastewater effluent was introduced into each wetland cell via perforated 5-cm diameter PVC pipes located at a depth of 5 cm below the surface within 0.6-m wide gravel trenches at the top of the slope.

Several features were incorporated into the design of the subsurface wetland to minimize hydraulic short-circuiting and to provide a means of collecting representative water samples. 0.6-m wide vertical

gravel walls, oriented perpendicular to the direction of water flow, were installed in each cell at 15 and 30 m along the slope (i.e., 33 and 66% of the length of the slope). 5-cm diameter monitoring wells, screened at depths from 0.9 to 0.3 m, were installed in the center of each trench (Figure 2-2). The effluent from each cell flowed into a 0.6-m wide gravel trench at the end of the cell where it was collected in perforated 7-cm diameter pipes (located at the bottom of the trench). These pipes conveyed treated water to a monitoring well in each individual cell, where samples were collected. Water flowing out of the horizontal levee was pumped back to the headworks of the wastewater treatment plant and constituted less than 0.6% on average of the overall flow to the plant. Ultrasonic flow meters (Master Meter, Mansfield, TX, USA) collected flow data continuously in the influent piping prior to each cell and in treated water leaving monitoring wells at the southwest corner of each treatment cell.

Over the course of the 24-month study, operational parameters were varied to assess their impact on system performance (Figure 2-3). During the first phase of the study, from April to November 2017, the total applied flow setting was 265 m^3 d^{-1} (~22 m^3 d^{-1} per cell) and water flowed from the nitrification facility into the surface flow wetland before being applied to the subsurface wetland cells, as described previously. In July 2017, the applied flows going into each cell were adjusted to achieve similar levels of treatment across cells. During the second phase, between November 2017 and July 2018, the overall applied flow setting decreased to 190 m^3 d^{-1} (~16 m^3 d^{-1} per cell) and water flowed directly from the nitrification facility into the subsurface wetland cells. During the third and final phase, between July 2018 and April 2019, the flow setting decreased to 95 m^3 d^{-1} (~7.9 m^3 d^{-1} per cell). During this last phase, applied flows to individual cells were again adjusted to eliminate overland flow in the majority of cells (D-L) (details are included in section A.2 of Appendix A).

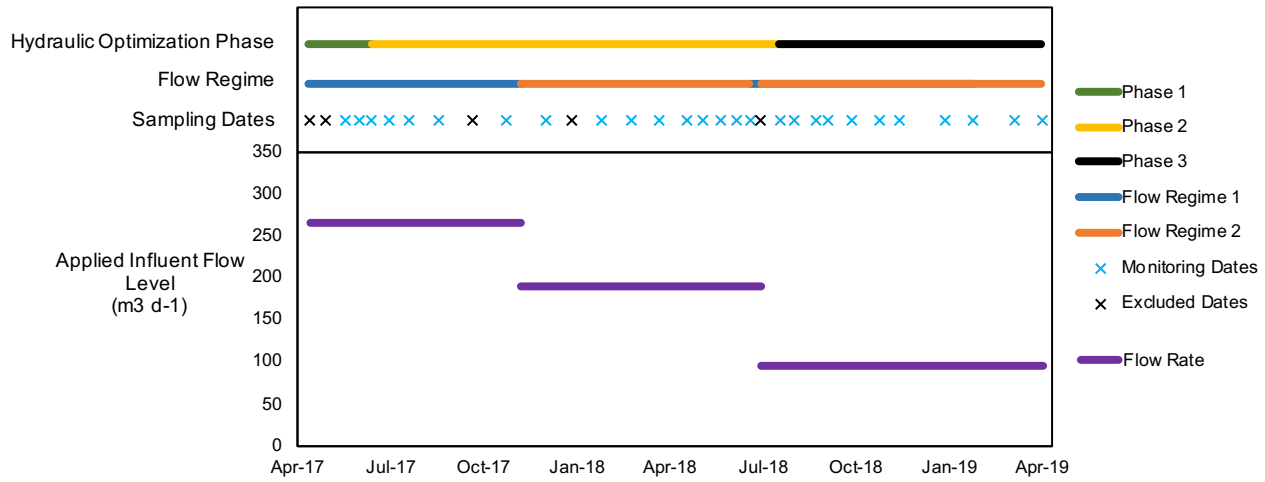

Figure 2-3: A timeline of the operational changes, flow regimes, sampling dates and flow rates applied to the horizontal levee test facility. Excluded sampling dates (dates during which flow to the horizontal levee slope was turned off during and/or directly preceding the collection of monitoring samples) are identified with a black X and were not included in the data analyses performed in this study. Monitoring data from those dates is included in full dataset that can be found on Mendeley Data (Cecchetti et al., 2020b).

2.2.2 Sample collection

Water samples were collected on a monthly or biweekly basis starting in April 2017 (Figure 2-3) from the influent pump station and monitoring wells located at the end of the treatment cells. Additional

samples were collected from the influent and effluent of the surface-flow wetland and periodically from intermediate wells in the subsurface wetland. Samples for chemical analyses were collected using a Masterflex E/S portable water sampler (Cole-Parmer, Vernon Hills, IL, USA) and analyzed in triplicate (between April 2017 and July 2018) or duplicate (between July 2018 and April 2019). At least two well volumes were purged prior to collecting a sample when appropriate. Samples were filtered on-site through 0.7-µm glass fiber filters into 50-mL polypropylene centrifuge tubes and immediately stored on ice prior to analysis, which normally occurred within 24-48 hr. Samples for F+ coliphage analysis were collected in triplicate into acid-washed Nalgene bottles. Bottles were triple rinsed with sample water at the site before collecting samples. Samples were stored on ice during transport to the laboratory. Electrical conductivity and pH were measured at each sampling location in the field using a Ultrameter II (Myron L Company, Carlsbad, CA, USA). Dissolved oxygen and temperature were measured in the field with YSI ProODO Optical Dissolved Oxygen probes (YSI Inc., Yellow Springs, OH, USA).

Porewater samples were collected at depths ranging from 0.1 to 0.9 m into Luer-Lok BD syringes using stainless steel PushPoint sediment porewater samplers (MHE Products, East Tawas, MI, USA). These samples were filtered on-site through 0.7-µm glass-fiber filters or 0.2-µm nylon filters and stored on ice prior to analysis.

2.2.3 Sample processing and analytical methods

Field-filtered samples were stored at 4°C upon returning to the laboratory and were analyzed using established methods.

Within six hours of collection, subsamples for ion chromatography analysis were filtered through 0.2-µm nylon filters into 0.5-mL PolyVials, capped with filter caps, and refrigerated prior to analysis, which normally occurred within 4-36 hours of processing. Samples for cation analyses were acidified to pH<5 to limit volatilization of ammonia prior to analysis. Inorganic anions (Cl^-, NO_2^-, Br^-, NO_3^-, PO_4^{3-} and SO_4^{2-}) and cations (Li^+, Na^+, NH_4^+, K^+, Mg^{2+} and Ca^{2+}) were measured on Dionex Aquion Ion Chromatography systems (Thermo Fisher Scientific, MA, USA). Anion measurements were performed with a Dionex IonPac AS23 column according to U.S. EPA Method 300.0 and cations measurements were performed according to previously described methods (Thomas et al., 2002) by using a 3.0 mM methanesulfonic acid eluent and a Dionex IonPac CS16 column.

15-mL aliquots of each field-filtered sample were transferred for TOC analysis into 24-mL borosilicate glass sample vials that had been rinsed with deionized water and baked at 450°C for 4 hours prior to use. Analysis of non-purgeable organic carbon (NPOC) and total nitrogen (TN) was performed on a Shimadzu TOC-V/CSH analyzer with an attached TN-1 unit according to standard methods (Method 5310B; APHA, 2012). Organic nitrogen concentrations were calculated by subtracting concentrations of nitrate, nitrite and ammonium from total nitrogen measurements.

Concentrations of a suite of trace organic contaminants were quantified according to previously described methods (Jasper et al., 2014a; Prasse et al., 2015; Bear et al., 2017) with minor modifications. Briefly, field-filtered samples were held at 4°C for 24 hours to allow reduced iron to oxidize and precipitate. These samples were filtered through 0.2-µm nylon filters to remove particulates, which mainly consisted of Fe(III)-oxides. To assess potential losses, concentrations of trace organic compounds in filtered samples and samples acidified to approximately pH 2 with HCl were compared. Because acidification could cause artifacts or damage the HPLC/MS-MS system and no significant differences were observed in concentrations measured with the two pre-treatment

methods (p-value > 0.6), the filtration method was used for all analyses. Samples were amended with a mixture containing stable isotope-labeled pharmaceuticals (5 ng of each) and analyzed using isotope dilution liquid chromatography/tandem mass spectrometry (Agilent 1200 series HPLC and Agilent 6460 triple quadrupole mass spectrometer).

F+ coliphage were enumerated using previously published methods (Sinton et al., 1996; EPA Method 1601). Briefly, magnesium chloride was added to 500 mL samples to achieve a final concentration of 0.05 M. Samples were subsequently filtered through a negatively charged 0.45-µm membrane filter (Millipore; HAWP04700) to capture the viruses. Filters were placed gridded-side-down into a 47-mm diameter plastic petri dish containing 300 µL of sterile 1:1 glycerol:PBS solution. The petri dishes containing the filters were frozen at -80°C until further processing (within 6 months). To enumerate the coliphage, the coliphage were eluted from the membrane filters using a solution of 3% beef extract, 3% Tween-80, and 0.3 M sodium chloride. 2 mL of the elution solution was added to each petri dish and the dish was rocked for five minutes on a shaker table at room temperature. The elution liquid was removed from the dish and coliphage was enumerated in the liquid using EPA Method 1601 (DAL method). The filter was placed on solid tryptic soy agar (TSA) media containing the appropriate concentrations of ampicillin and streptomycin antibiotics and the *E. coli* host strain (EPA Method 1601). The numbers of PFU obtained from assaying the liquid media and present on the filter were added together to obtain the concentration of PFU in the assayed water.

2.2.4 Methods for calculating flow rates and fractional load reductions of contaminants

Evapotranspiration. Significant changes in the concentrations of conservative species (i.e., species that pass through the system without reacting or being removed) were observed through the test facility. For example, over the sampling period, changes in conductivity, $[Cl^-]$ and $[Na^+]$ (as C/C_o) averaged 1.5 ± 0.2, 1.7 ± 0.4 and 1.8 ± 0.6. Increasing salinity in the horizontal levee dwarfed what would be expected based on inputs through atmospheric deposition (National Atmospheric Deposition Program, 2019) and was unlikely explained by soil leaching or plant-mediated processes (Öberg and Sandén, 2005; White and Broadley, 2001). It was also unlikely caused by seawater intrusion due to design controls (e.g., the compacted clay liner) and because groundwater collected from the water table onsite had a lower salinity than the influent to the test facility. Rather, increasing salinity through the test facility appeared to be explained primarily by the withdrawal of water via evapotranspiration.

Evapotranspiration (ET) rates were calculated via three methods: (i) a water balance in which available measured effluent flow rates were subtracted from measured influent flow rates (Table A-6) (ET), (ii) using an empirical linear regression model developed based on the assumption that conductivity can be used as a conservative tracer (ET_{obs}) and (iii) using climatic data and the Penman-Monteith equation (ET_v) with an assumed crop coefficient (K_c) of 1.3 (Allen et al, 1998; Howes et al, 2015). Boxplots comparing ET rates calculated over the first two years of monitoring according to the three methods described above are presented in Figure 2-4.

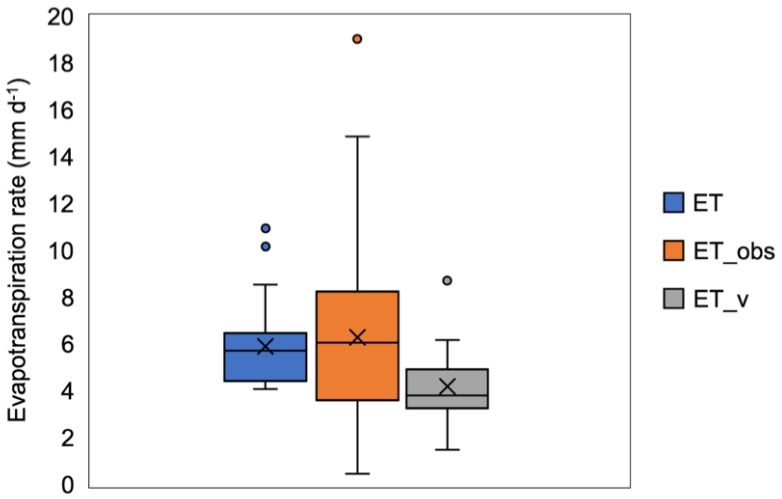

Figure 2-4: Boxplots comparing ET, ET_{obs} and ET_v.

ET values calculated using the first two methods were not significantly different ($p = 0.53$), though ET_{obs} values spanned a much larger range of values. However, flow measurements required to calculate ET values according to the first method were only sparsely available.

The theoretical basis for the regression method (the second method described above) was the mass balance presented in Equation 2-1 through Equation 2-3:

$$Q_{inf}*C_{inf} = Q_{eff}*C_{eff} + Q_{ET}*C_{ET} \quad \textbf{Equation 2-1}$$

$$Q_{inf} = Q_{eff} + Q_{ET} \quad \textbf{Equation 2-2}$$

$$Q_{eff}/Q_{inf} = C_{inf}/C_{eff} = 1 - Q_{ET}/Q_{inf} \quad \textbf{Equation 2-3}$$

where Q_{inf}, Q_{eff}, and Q_{ET} represent the influent, effluent and evapotranspiration flows in the horizontal levee, C_{inf} and C_{eff} represent the concentrations of a conservative species in the influent and the effluent, and C_{ET} – the theoretical concentration of a conservative species in the ET flow – is set equal to zero. Measured ratios of influent and effluent conductivity (C_{inf}/C_{eff}) were significantly different ($p < 0.001$; Wilcoxon signed-rank test) than measured ratios of effluent to influent flows (Q_{eff}/Q_{inf}) on the dates when influent and effluent flow rates were available (Figure 2-5). However, these two variables were strongly correlated ($r^2 = 0.70$; $p < 0.001$). Therefore, we developed an empirical regression to predict Q_{eff}/Q_{inf} on dates when only measurements of C_{inf}/C_{eff} were available (see Figure 2-5). We fit the regression presented in Equation 2-4:

$$Q_{eff}/Q_{inf} = m*(Cond_{inf}/Cond_{eff}) + b \quad \textbf{Equation 2-4}$$

where m and b are empirical slope and intercept constants that had values of 1.05 and 0.08 respectively.

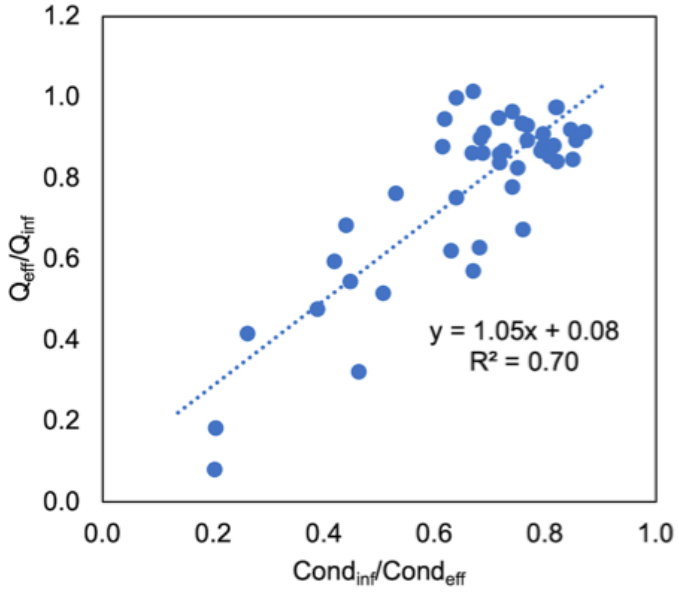

Figure 2-5: Comparison of Q_{eff}/Q_{inf} and to $Cond_{inf}/Cond_{eff}$.

We further verified our ET estimates using the third method described above (e.g., the Penman-Monteith equation) to calculate ET_v values. However, calculated ET_v values were statistically different from ET_{obs} values ($p = 0.0002$) – likely due to our assumption that $K_v = 1.3$, which was based on average literature values reported by Howes et al (2002) for natural wetlands. However, in that study, K_v values ranged from 0.35 to 2.65, suggesting that these values can vary substantially across wetlands and across seasons within the same wetland. K_v values for the test facility (i.e., ET_{obs}/ET_o), range from 1.2 to 3.6. Though these values skew higher than natural wetlands, they are within the range reported for K_c values in the literature (Guerra et al, 2015). However, we should note that K_v values from the test facility are also significantly greater from what has been reported for marshes in the nearby San Joaquin Delta region (0.95 reported by Drexler et al, 2008). These differences may have been influenced to a significant extent by the warm drought-like conditions that dominated much of the monitoring period, which may have led to higher transpiration rates than we might have observed otherwise.

Fractional load reductions of contaminants. Using the ET calculations described above, we estimated the fractional load reductions for contaminants through the test facility based on the Equation 2-5 through Equation 2-7.

$$C/C_o = C_{eff}/C_{inf} \qquad \textbf{Equation 2-5}$$

$$f_{rem} = (Q_{eff}*C_{eff})/(Q_{inf}*C_{inf}) \qquad \textbf{Equation 2-6}$$

$$f_{rem} = [m*(Cond_{inf}/Cond_{eff}) + b]*(C/C_o) \qquad \textbf{Equation 2-7}$$

where f_{rem} represents the fractional load removed. C/C_o represents the ratio of influent to effluent concentrations for a contaminant.

Overland and subsurface flow calculation methods. We calculated the contributions of subsurface and overland flow to the overall effluent flow by manipulating the mass balance presented in Figure

2-6. This method can be simplified by using water constituents that are completely removed in the subsurface in the mass balance (i.e., $C_{ss} = 0$), but are unchanged in the water flowing over the wetland surface (i.e., $C_{OLF} = C_{inf}$). For calculations performed in this study, we used nitrate concentrations for C because we had consistent measurements to confirm that $[NO_3^-]_{ss} = 0$ and $[NO_3^-]_{OLF} = [NO_3^-]_{inf}$. Measurements of nitrate in overland flow water were not statistically distinguishable ($p > 0.05$) from the influent to the wetland across sampling dates. Effluent flow is the combination of subsurface and overland flows. Based on that, we calculated Q_{OLF} and Q_{ss} by first multiplying the effluent flow rate by the multiplier: C_{eff}/C_{inf} (for nitrate) to calculate Q_{OLF} and then subtracted this from Q_{eff} to get Q_{ss}.

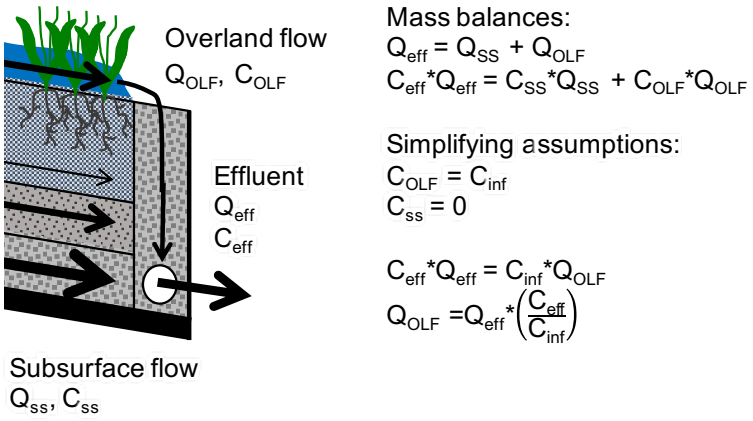

Figure 2-6: Mass balances on water and tracers used to estimate flows in the horizontal levee test facility. Q_{ss}, Q_{eff} and Q_{OLF} are the flow rates in the subsurface, the effluent and the water flowing overland. C_{ss}, C_{eff}, C_{inf} and C_{OLF} are the concentrations of a species C in the subsurface water, the effluent, the influent and the overland flow water.

To validate this method, we used calculated subsurface flow rates and physical information from the field site to estimate hydraulic conductivity and hydraulic retention time for each cell at each sampling time. Hydraulic conductivity values were not shown to be significantly different ($p < 0.05$) from expected values for hydraulic conductivity based on previously conducted constant head permeameter tests using representative soil mixes and *a priori* calculations of hydraulic conductivity conducted based on the media grain sized used for the soils in the test facility and the Carman-Kozeny equation (Kadlec and Wallace, 2009; Benjamin and Lawler, 2013).

2.3 Results and Discussion

During the two-year monitoring period, the horizontal levee processed approximately 126 x 10^3 m^3 of municipal wastewater effluent. To assess water quality improvements that occurred as water passed through the system, we measured contaminants and water quality parameters in over 1000 samples collected from the influent and effluent, as well as over 300 porewater samples. We also measured water flows along with other design and operational variables. The full dataset can be found on Mendeley Data (Cecchetti et al., 2020b).

2.3.1 Water balance

In the experimental wetland system, inflows of municipal wastewater effluent and a small volume of precipitation (which constituted less than 1% of the total volume of water entering the system during the monitoring period and therefore did not have a significant impact on results) were balanced by

outflows through the effluent pipes and evapotranspiration. Water flowed along the ground surface (i.e., overland flow), passed through the subsurface and evaporated or was transpired by the plants (Figure 2-7). Over the 2-year study period, evapotranspiration accounted for the loss of approximately 25% of the water. The remaining water left the system through the outlet pipe. Of this remaining flow, the contributions of overland flow and subsurface flow varied considerably during the three phases of the study (Table 2-2). During phases 1 and 2, overland flow was approximately 2.5 times the magnitude of subsurface flow. During phase 3, swale-type cells continued to have high overland flows (i.e., around 5 times subsurface flows), though overland flow was negligible in most cells (i.e., wet meadow cells with both fine and coarse topsoils, and willow/riparian cells).

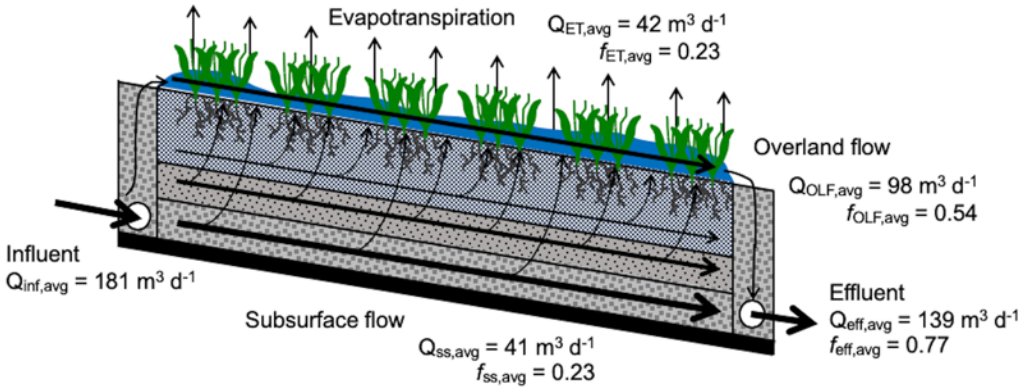

Figure 2-7: Schematic representation of the water balance at the horizontal levee test facility using average values from the monitoring period. Calculated values for the average magnitude of each flow (in m^3 d^{-1}) and the average fraction of the influent flow that each flow represents are included. The figure is not to scale.

Table 2-2: Average flow rates and fractions of the influent flow of the various flows in the test facility during operational phases 1 and 2 and for cells without overland flow during phase 3.

Flow Component	Phases 1 and 2 All Cells		Phase 3 All Cells[a]		Phase 3 Cells without Overland Flow[b]	
	Flow rate, m^{-3} d^{-1}	Fraction, unitless	Flow rate, m^{-3} d^{-1}	Fraction, unitless	Flow rate, m^{-3} d^{-1}	Fraction, unitless
Influent	222	1.0	104	1.0	48	1.0
Evapotranspiration	50	0.22	35	0.34	25	0.53
Overland flow	124	0.56	40	0.38	0.6	0.01
Subsurface flow	49	0.22	30	0.28	22	0.46
Effluent	173	0.78	70	0.67	23	0.47

[a] Average sum of all cells during Phase 3, including swale-type cells.
[b] Average sum of cells during Phase 3, excluding swale-type cells but including all other cells.

Effect of hydrology on contaminant removal. The water balance in the horizontal levee was important due to its influence on contaminant removal. Evapotranspiration removed water from the subsurface, concentrating dissolved species in the remaining water. Subsurface and overland flows mixed together prior to the final sample collection point, but the water experienced different conditions. The very short hydraulic retention times in the overland flow led to little, if any, removal of contaminants, while nearly complete removal of many contaminants was observed in the subsurface flow. Therefore, hydrological variables (e.g., the fraction of subsurface flow) largely determined contaminant removal. Negative correlations ($r^2 > 0.6$) were observed between the fraction of overland

flow and the fractional removal of nitrogen species, pharmaceuticals, and F+ coliphage (Figure 2-8). Using standardized multiple linear regressions, additional variables (e.g., temperature, planting regime) were shown to be less influential on removal of studied contaminants, with the exception of organic nitrogen and acyclovir (Table 2-3). The most significant correlation for most contaminants studied was between subsurface flow and contaminant removal.

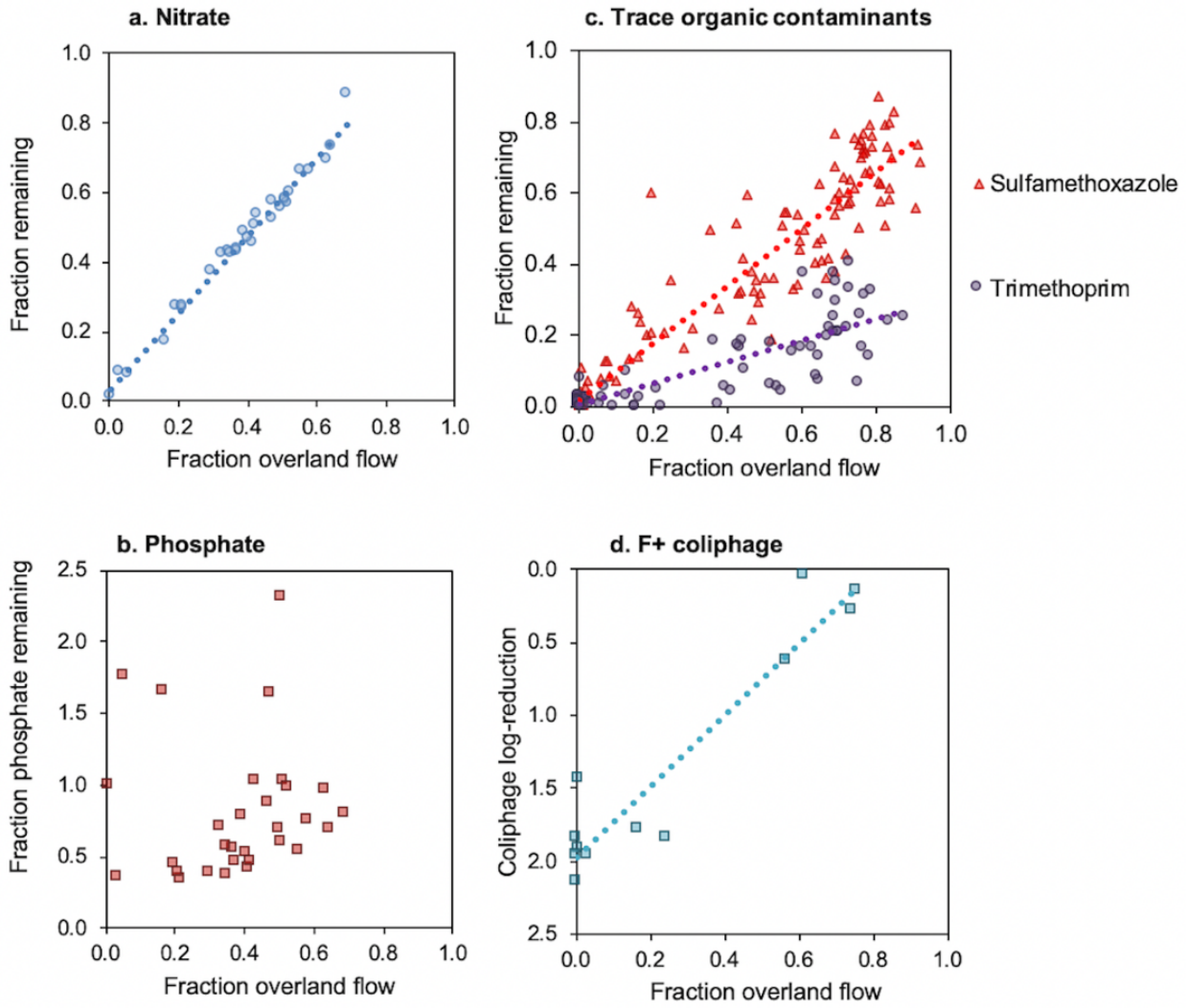

Figure 2-8: The fraction remaining in the effluent of a suite of contaminants, including (a) nitrate (linear regression, r^2 = 0.98), (b) phosphate (linear regression not shown, r^2 = 0.00), and (c) pharmaceuticals (linear regressions, sulfamethoxazole: r^2 = 0.91; trimethoprim: r^2 = 0.73), and the log-reduction of (d) F+ coliphage (log-linear regression, r^2 = 0.89), as a function of overland flow. Values in plot (a) and (b) are flow-weighted averages across the full wetland at each time point. Values in plots (c) and (d) are data from individual wetland cells at each time point.

These observed contaminant removal trends were attributable to efficient removal in the subsurface with little or no contaminant removal in the overland flow. For example, in the case of nitrate, the overland flow experienced short hydraulic residence times (approximately 0.4-1.0 days; tracers are detailed in section A.3 of Appendix A) and aerobic conditions, whereas subsurface flow was

characterized by longer hydraulic residence times (i.e., approximately 12-20 days) and anoxic conditions that are conducive to microbial denitrification. For trace organic contaminants, the lack of contact with biofilms that coat organic matter, plant roots and fluctuating redox conditions in the subsurface reduced contaminant removal in the overland flow. For viruses, we would expect a variety of mechanisms to increase the removal of F+ coliphage in the subsurface. For example, filtration facilitated by attachment to solids, virus inactivation and rhizosphere processes could all contribute to the high levels of removal observed in cells with less overland flow (Vidales et al., 2003; Muerdter et al., 2018). For phosphate, limited contact with phosphate-adsorbing mineral surfaces prevented significant removal in the overland flow. The assumption that little removal of contaminants occurred in overland flow was verified through the collection of samples from the water flowing over the wetland surface (Figure 2-9a), which were consistently statistically indistinguishable ($p > 0.05$) from the influent.

Porewater samples collected deeper than 0.1 m indicated that most contaminants were removed in the subsurface within 5 meters of the inlet to the horizontal levee (Figure 2-9). The subsurface residence time in the first 5 meters of the slope (approximately 0.5-1.0 days) was similar to residence times in the overland flow. The significant and rapid subsurface removal of contaminants was likely due to a combination of mechanisms. Diffusion of oxygen into the subsurface was limited by overlying fine sediments, preventing re-introduction of oxygen and promoting anaerobic processes. The subsurface also provided ample organic matter (i.e., decomposing woodchips, plant roots and exudates) on which microbial communities can obtain energy, promoting microbially-mediated processes such as denitrification (Kadlec and Wallace, 2009).

Consistent with these observations, removal of contaminants was most significant during the third phase of treatment when overland flow was eliminated in most cells (section A.2 of Appendix A). During this period, over 96% of the mass of total nitrogen and nitrate, and 92-99% of trace organic contaminants were removed, compared to 38-48% and 54-86% for the periods with more overland flow (i.e., phases 1 and 2).

In contrast to nitrogen species and trace organic contaminants, hydrologic conditions (e.g., percentage overland flow) did not appear to have a consistent impact on the removal of phosphate (Figure 2-8b). Although removal of phosphate was high during the period when overland flow was eliminated in most cells (averaging 81 ± 23% removal), phosphate removal was poorly explained by hydrological variables in standardized multiple linear regressions, even when combined with other design and operational variables (overall $r^2 = 0.34$ for phosphate compared to $r^2 > 0.75$ for other contaminants).

Standardized multiple linear regressions (Table 2-3) were performed to assess the influence of design and operational variables on performance criteria (e.g., contaminant removal). Tested variables included influent concentrations, temperature, soil texture, planting regime, topography and fraction of total subsurface flow (i.e., the combination of evapotranspiration and subsurface flow). Statistical analyses were performed in Excel (Microsoft Corporation, Redmond, WA, USA) using the Real Statistics Resource Pack software (Release 5.4; Zaiontz, 2018). Removal of dissolved organic nitrogen (DON) appeared to be impacted negatively by temperature, suggesting that DON may form more at higher temperatures, perhaps due to organic matter decomposition. Removal of DON also appeared to be impacted strongly by influent concentration, likely because there were not statistically significant differences between influent and effluent concentrations for organic nitrogen (p-value = 0.09). Both of these variables were more influential than subsurface flow. In the case acyclovir, topography was the most influential variable, suggesting that subsurface flow does not fully explain removal.

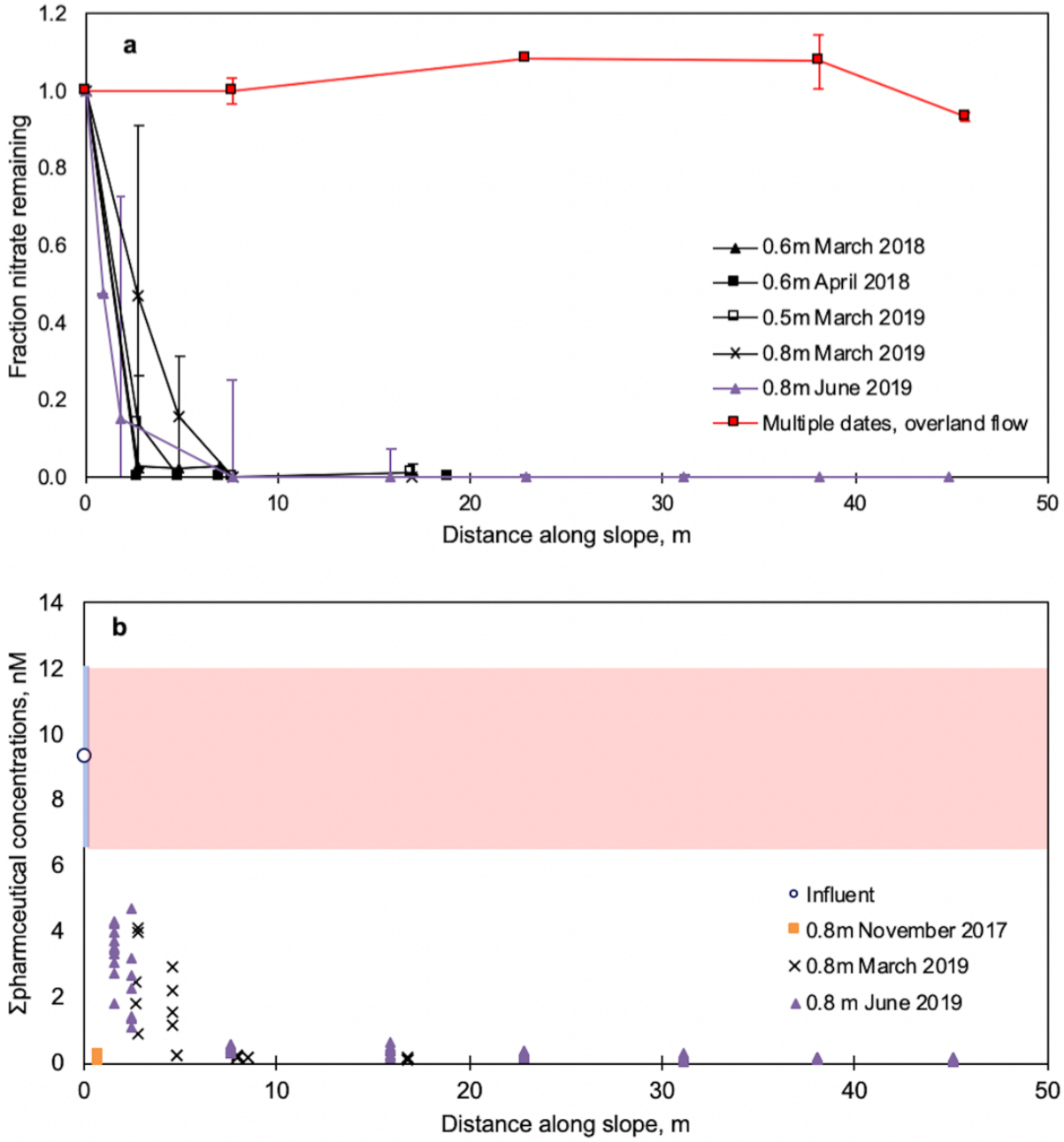

Figure 2-9: Porewater contaminant removal data. (a) Fraction of influent nitrate load remaining in porewater and overland flow samples at various distances along the slope. Error bars show one standard deviation. (b) The combined concentrations of the suite of monitoring pharmaceuticals in porewater samples at various distances along the slope. A red horizontal bar denotes the range of influent pharmaceutical concentrations observed.

Removal of phosphate varied over time, ranging from 74% removal at best to concentrations more than doubling through the full horizontal levee (Figure 2-10). In addition to plant uptake, phosphate exhibits an affinity for a variety of minerals (Holtan et al., 1988; Yao and Millero, 1998) and forms precipitates under certain conditions (Egger et al., 2015; Rothe et al., 2016). Biogeochemical cycling of other elements, such as iron and carbon, can have complex and variable impacts on these

mechanisms in freshwater systems (Caraco et al., 1989; Murray, 1995; Szilas et al., 1998; Lin et al., 2018), which may partly explain the observed variability in phosphate removal.

Table 2-3: Key results from the standardized regression analyses of contaminant fraction remaining. Regression coefficients are presented with p-values for each variable in parentheses. The most influential variable for each contaminant is highlighted and the p-values for variables with statistically significant ($p < 0.05$) relationships are in bold.

Contaminant	Overall r^2	Tested Variables					
		Temperature	Influent Concentration	Planting Regime	Soil Topsoil Type	Topography	Fraction of total subsurface flow[a]
Nitrogen							
Total nitrogen (n=299)	0.97	0.01 (0.37)	-0.08 (**10^{-10}**)	0.08 (**$10^{-7.1}$**)	0.05 (**$10^{-3.3}$**)	-0.02 (0.10)	-0.89 (**10^{-179}**)
Nitrate (n=323)	0.99	-0.04 (**$10^{-6.7}$**)	-0.03 (**$10^{-5.0}$**)	0.02 (0.08)	0.03 (**$10^{-2.6}$**)	-0.02 (**0.05**)	-0.96 (**10^{-256}**)
Nitrite (n=311)	0.85	0.06 (**0.02**)	0.05 (0.08)	-0.06 (**0.05**)	-0.17 (**$10^{-7.0}$**)	0.00 (0.96)	0.84 (**10^{-97}**)
Ammonium (n=227)	0.91	-0.07 (**$10^{-2.9}$**)	-0.04 (**0.04**)	0.00 (0.89)	-0.23 (**10^{-13}**)	-0.00 (0.96)	0.86 (**10^{-90}**)
Organic nitrogen (n=179)	0.41	0.34 (**$10^{-7.1}$**)	-0.41 (**$10^{-9.0}$**)	0.02 (0.81)	0.13 (0.13)	0.01 (0.89)	-0.21 (**$10^{-2.5}$**)
Phosphorus							
Phosphate (n=323)	0.34	0.30 (**$10^{-6.4}$**)	-0.23 (**$10^{-4.3}$**)	-0.06 (0.30)	0.10 (0.14)	-0.35 (**$10^{-7.0}$**)	-0.55 (**10^{-18}**)
Trace organic							
Sulfamethoxazole (n=155)	0.91	-0.05 (**$10^{-1.3}$**)	n.t.	-0.02 (0.43)	-0.02 (0.48)	0.08 (**0.02**)	-0.90 (**10^{-57}**)
Trimethoprim (n=107)	0.78	0.01 (0.91)	n.t.	-0.00 (0.99)	-0.06 (0.34)	0.30 (**$10^{-3.3}$**)	-0.66 (**10^{-13}**)
Acyclovir (n=155)	0.79	-0.09 (**0.05**)	n.t.	-0.02 (0.76)	-0.03 (0.62)	0.56 (**$10^{-9.7}$**)	-0.39 (**$10^{-6.0}$**)
Carboxy-acyclovir (n=155)	0.85	0.11 (**$10^{-3.0}$**)	n.t.	-0.14 (**$10^{-3.1}$**)	-0.26 (**$10^{-7.4}$**)	0.19 (**$10^{-4.1}$**)	-0.86 (**10^{-43}**)
Carboxy-abacavir (n=107)	0.83	0.06 (0.14)	n.t.	-0.04 (0.48)	-0.15 (**0.01**)	0.20 (**$10^{-2.2}$**)	-0.79 (**10^{-19}**)
Propranolol (n=107)	0.75	-0.26 (**$10^{-5.9}$**)	n.t.	0.01 (0.93)	-0.11 (0.12)	-0.24 (**$10^{-2.2}$**)	-1.07 (**10^{-23}**)
Atenolol (n=107)	0.86	-0.02 (0.50)	n.t.	-0.01 (0.79)	-0.03 (0.53)	0.48 (**10^{-10}**)	-0.52 (**10^{-13}**)
Metoprolol (n=107)	0.92	-0.03 (0.22)	n.t.	-0.02 (0.62)	-0.04 (0.27)	0.34 (**$10^{-9.6}$**)	-0.69 (**10^{-27}**)
Carboxy-metoprolol (n=107)	0.34	-0.08 (0.34)	n.t.	0.09 (0.37)	-0.54 (**$10^{-5.1}$**)	0.66 (**$10^{-5.0}$**)	0.00 (0.99)

[a]The fraction of "total subsurface flow" includes all flow that passes through the subsurface (i.e., subsurface flow and evapotranspiration flow). n.t. = variable not tested for selected contaminant.

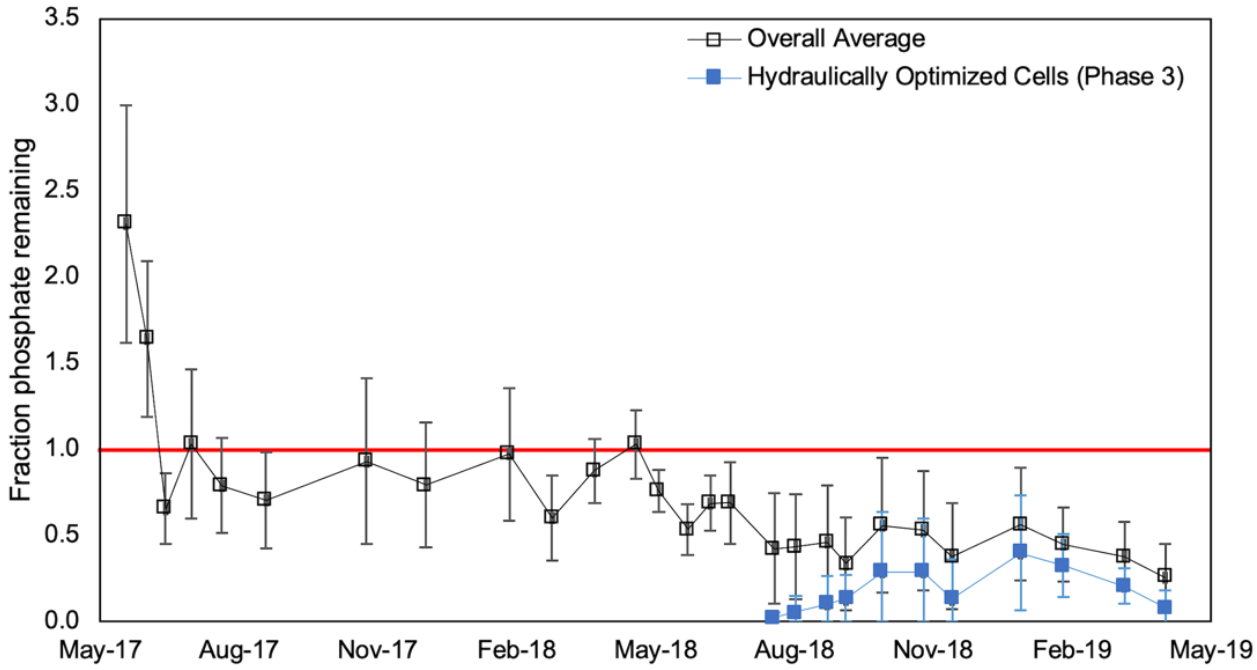

Figure 2-10: Changes in the fraction of influent phosphate remaining in the effluent over time over the entire wetland (all dates) and for hydraulically optimized cells (after July 2018). Values of 1 (denoted by the horizontal red line) signify no removal. Error bars present one standard deviation.

Regardless of the cause of this observed variability, we do not expect long-term phosphate removal in horizontal levees because the mechanisms responsible for phosphate removal are primarily storage

mechanisms that eventually will be exhausted (Chapter 5). For example, following plant uptake, decomposition of plant residues will eventually release a significant portion of assimilated phosphorus back into the subsurface. Additionally, even if the amount of phosphate adsorption sites on minerals in the subsurface remains constant, they will eventually be exhausted without the addition or formation of more mineral surfaces. Further research is required to understand how horizontal levees could be designed and operated to achieve substantial long-term phosphate removal.

2.3.2 Effect of design and operational parameters on hydrology

The interplay between overland flow and subsurface flow was the dominant factor controlling contaminant removal in the horizontal levee, but design and operational parameters (e.g., substrate type, plant species) also had significant impacts on the magnitudes of those flows and therefore on mass removal of contaminants. The impact of cell design on contaminant removal was unclear based on fractional removal of contaminants alone because flows were adjusted in an effort to obtain similar flow distributions. There also were not significant differences in subsurface contaminant removal trends between cells based on porewater observations. However, there were significant differences in the water balance for the different cell treatment types (Figure 2-11a). These differences in flows translated into significant differences in contaminant mass removal rates (Figure 2-11b), suggesting that design decisions, like plant species and soil type, can have a significant impact on the treatment capacity of horizontal levees.

Impacts of cell design on subsurface flows. Over the full monitoring period, there were significant differences in flows based on soil texture. As expected, subsurface flows were significantly higher (i.e., approximately twice as high) in coarse sediment wet meadow cells when compared with those constructed with fine sediments (i.e., 4.6 m^3 d^{-1} versus 2.3 m^3 d^{-1}; p-value < 0.001) because soil texture is correlated with hydraulic conductivity in granular media (Kadlec and Wallace, 2009). However, the magnitude of these differences decreased throughout the monitoring period. In the last monitoring phase, coarse textured cells exhibited flows that were only 54% higher than fine textured cells.

Cells planted with the willow trees, which were constructed with coarse sediments, had the highest subsurface flows and the highest contaminant mass removal rates among tested cell types throughout the full monitoring period. Subsurface flows averaged 4.9 m^3 d^{-1} in these cells, compared with flows of 4.6, 2.3 and 2.4 m^3 d^{-1} in coarse and fine wet meadow cells, and swale-type cells, respectively. Differences in subsurface flows between the willow and the coarse meadow cells were not significant (p-value = 0.92) over the full monitoring period. However, during the third phase of treatment, the differences in subsurface flows between the two coarse-cell planting regimes (willow cells and meadow cells) increased significantly. During the final phase, the willow cells had 59% higher subsurface flows than coarse meadow cells (p-value = <0.001), at 3.6 m^3 d^{-1} versus 2.3 m^3 d^{-1}, corresponding to differences in mass removal of nitrogen on the order of 10 kg N per year per cell (Figure 2-11). The observed impact of riparian planting regimes on subsurface flows was consistent with past research. Willows have extensive rooting zones (Kuzovkina et al., 2009), which lead to greater subsurface flows in stormwater bioinfiltration systems (Read et al., 2008). In the horizontal levee, the willow cells also appeared to play an important role in increasing the volume of water that could be processed by a cell.

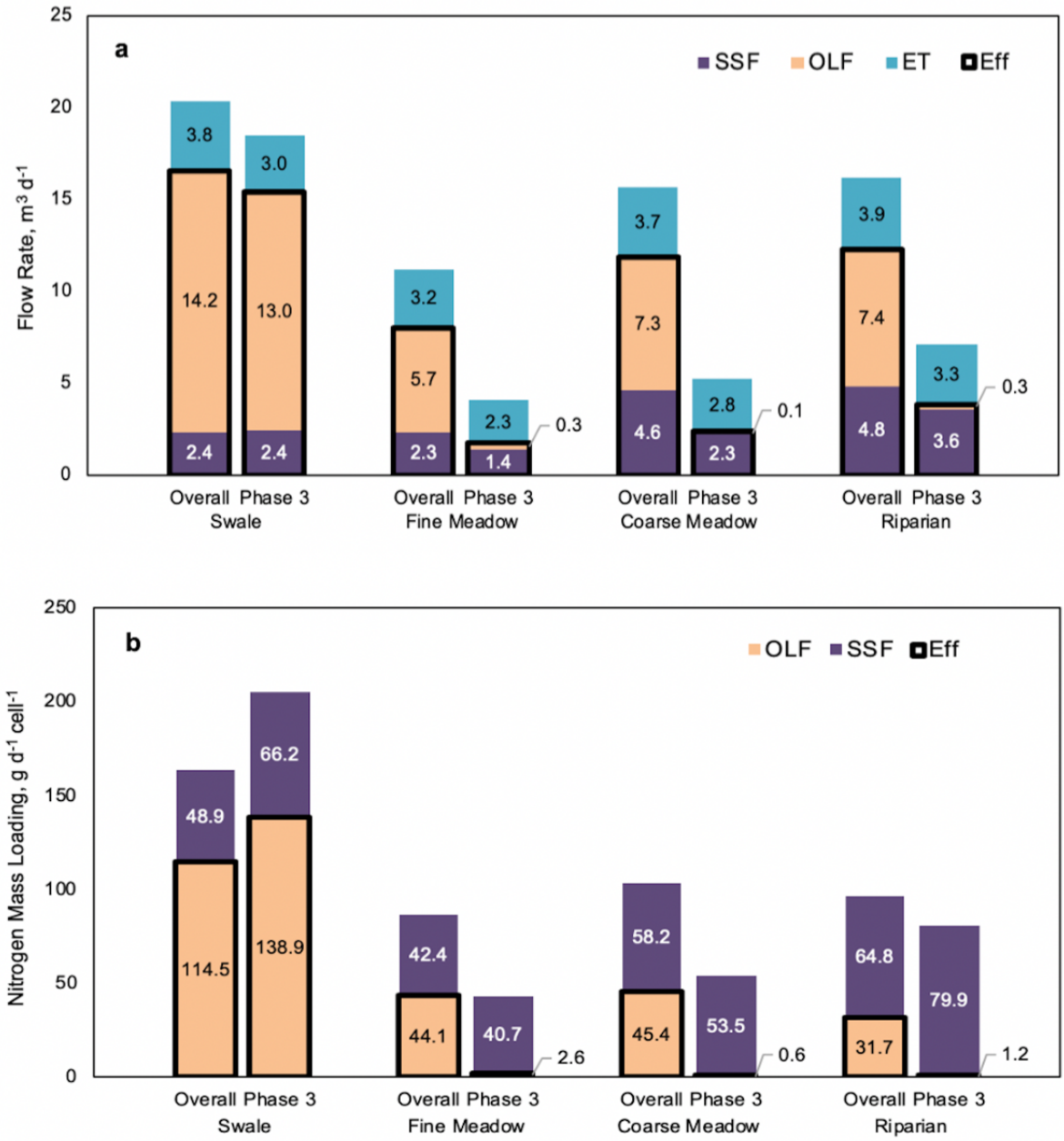

Figure 2-11: (a) Average daily flow rates and (b) nitrate-N mass removed per cell type during the entire monitoring period (bars to the left for each treatment type) and during the third and final phase of the monitoring period (bars to the right). Abbreviations: SSF = subsurface flow; OLF = overland flow; ET = evapotranspiration; and Eff = Effluent flow.

Although subsurface flow in swale-type cells was the lowest throughout phases 1 and 2, these cells had the second highest subsurface flow during the third monitoring phase. There was an average 40% decrease (p-value < 0.001) in the subsurface flow capacity of other cell types, likely due to a variety of clogging mechanisms, whereas subsurface flows of swale cells did not decrease significantly (p-value = 0.85) when compared to earlier monitoring periods. The unique topography of swale-type cells, with swales running down the center of these cells (Figure A-2), may have played a role in the observed subsurface flow conditions. This topography causes senescing plant residues to deposit and

concentrate in the center of the cell, possibly forming an organic episediment layer where microbial activity (e.g., denitrification) could be more significant than in the overland flow of other cells. Additionally, the cross-sectional area of subsurface flow in these cells increases as applied flows increase due to rising water tables. This may explain why subsurface flows remained higher in swale cells during the final monitoring phase, when overland flows were high. During additional monitoring dates, when overland flow was eliminated in swale cells, subsurface flows decreased to 1.3 m^3 d^{-1}, which was comparable to flow rates observed in fine wet meadow cells during the last monitoring period (1.4 m^3 d^{-1})

Declining subsurface flow rates are to be expected in horizontal levees and are likely due to a combination of clogging processes including deposition of particulate matter from the influent, growth of biofilms, and the migration of fine sediments into the pore spaces. These processes are still poorly understood (Knowles et al., 2010), but are particularly important in horizontal levees because removal of contaminants occurs primarily in the subsurface. Decreasing subsurface flow capacities are linked to increasing overland flow rates and decreasing mass removal of contaminants. For long-term decreases in treatment capacity, various mitigation techniques have been suggested for subsurface constructed wetlands to restore higher hydraulic conductivities, such as intermittent application of flow rates, periodic excavation and replacement of subsurface media or the application of chemicals or earthworms to these systems (Nivala et al., 2012). However, many of these mitigation techniques may not be practical at full-scale or could negatively impact co-benefits. Further research is required to understand clogging mechanisms and mitigation techniques better.

Impacts of cell design on evapotranspiration and overland flow. Throughout the monitoring period, evapotranspiration rates were similar among cell types, with average evapotranspiration rates ranging from 3.2 to 3.9 m^3 d^{-1}. Only differences between fine and coarse meadow cells were significant (p-value = 0.02). However, in the third monitoring phase, more significant differences among the cells emerged, with willow cells (3.3 m^3 d^{-1}) exhibiting significantly higher evapotranspiration rates than both coarse (p-value = 0.04) and fine (p-value < 0.001) meadow cells (2.9 and 2.3 m^3 d^{-1}). This observation was consistent with evapotranspiration rates reported in short-rotation coppice forests, which are frequently higher than rates reported for grass-like crops, such as barley and grass ley (Persson and Lindroth, 1994).

Evapotranspiration rates at the field site were significantly higher than rates observed in natural wetlands with similar plant communities. This was consistent with past research, which has also shown that evapotranspiration rates appear to increase in coppice forests when wastewater or sewage sludge are applied as a source of nutrients (Dimitriou and Aronsson, 2011), possibly due to increased biomass growth through nutrient enrichment (Morris et al., 2008). Higher evapotranspiration rates could be beneficial from an operational perspective, because they can drive greater flows of water into the subsurface by lowering the water table, which could increase treatment capacity.

Overland flow correlated strongly with applied flow (Spearman's $\rho = 0.88$) throughout the monitoring period. Swale-type cells had the greatest overland flow, averaging 14.2 m^3 d^{-1} compared to 6.8 m^3 d^{-1} for other cell types, while values were similar (p-values > 0.25) among all other cell types. The significantly higher overland flows in swale-type cells (compared to other cells) during earlier monitoring phases (p-value <0.001) were likely due primarily to topographical differences in the design of those cells. Isolating the impact of topography on overland flows (i.e., comparing cells A-C and cells D-F) yields a Spearman's ρ value of 0.57 – indicating a stronger correlation than observed for temperature (0.05), soil type (-0.02) or planting regime (0.25). Because of these high overland flows, swale-type cells had lower contaminant removal efficiencies than other cells (e.g., over the

entire study period, 31% of applied nitrate was removed in swale-type cells compared to 75% in other cells). However, swale-type cells removed comparable masses of contaminants to other cells because of similar subsurface flows. Swale-type cells removed around 100 kg N $cell^{-1}$ of nitrate-N compared to an average removal of 112 kg of N $cell^{-1}$ in all other cell types. In the final monitoring phase, mass removal of nitrate-N in the subsurface was greatest in swale and riparian type cells with 191 and 242 g N $cell^{-1}$ d^{-1} removed in those cells respectively, compared to 131 and 180 g N $cell^{-1}$ d^{-1} in wet meadow cells with a fine and coarse topsoil type respectively.

2.3.3 Implications for design and operation of horizontal levees

The design of constructed wetlands involves tradeoffs among a variety of considerations, of which construction and operational costs, space requirements, and contaminant removal capabilities are typically most important (Kadlec and Wallace, 2009). Other considerations, such as habitat quality, public benefits (Knight, 1997) and control of disease vectors (Knight et al., 2003) can also drive design decisions. For horizontal levees, subsurface flow capacity appears to have the most significant effect on contaminant mass removal. If sand and gravel needed for the subsurface is not readily available onsite, the purchase and transport of coarse material could increase construction costs, though possibly only marginally. Our research also suggests that other design considerations, such as the plant community composition, can have significant impacts on subsurface flow capacities in these systems, thereby impacting contaminant removal.

Design and operational considerations. In the horizontal levee, contaminant removal was largely confined to subsurface flows at the beginning of the slope, while overland flow affords negligible treatment. Because the amount of treatment achieved is likely to be a critical design objective for these systems, it is essential that they be designed to pass all of the flow through a portion of the subsurface. To achieve this in full-scale systems, appropriate selection of the materials used for subsurface flow is essential. Hydraulic conductivity of potential construction materials can be well approximated using the Carman-Kozeny equation to make *a priori* estimates (Kadlec and Wallace, 2009) or with simple laboratory tests (e.g., constant head permeameter tests). These methods tend to be quite accurate: values approximated for construction materials *a priori* were 0.6-0.9 times observed values in the test facility, while values derived from falling head permeameter tests were not significantly different ($p < 0.05$) from observed values.

Available fill found on a constructed wetland site is often not suitable to provide the needed subsurface flow capacity of these systems. To strike a balance between obtaining the desired subsurface flow capacities and the cost of bringing more permeable materials to the site, engineers could build a narrower treatment zone to achieve treatment within the first few meters of the horizontal levee. Beyond this initial treatment zone, overland flow is not as much of a concern because sufficient treatment will have already been achieved although ponding of surface water should be avoided because it provides potential mosquito breeding grounds. The full sloped wetlands may need to be much longer (50-100 m in length) for geotechnical reasons (e.g., to provide an appropriate level of wave attenuation) and for ecological reasons (to provide sufficient habitat area for wildlife), but the majority of the slope could be constructed using fill found onsite that is appropriate for supporting restored wetland habitat. Additional design features, such as subsurface layers constructed with coarse materials and periodic mixing trenches, could also be included in horizontal levee design to help increase subsurface flow capacities, though it is essential that designers include controls (e.g., geotextile liners) to prevent fine sediments from migrating into the pore spaces in these coarse material zones and clogging them.

In systems where it is critical that horizontal levees meet treatment objectives, continuous real-time monitoring of conductivity can be conducted at the end of the treatment zone (depending on the system configuration) with minimal additional costs or labor requirements (Zhuiykov, 2012). This would allow operators to quickly identify conditions in which overland flow occurs because water flowing over the wetland surface has a lower salinity than water in the subsurface that gets progressively concentrated by evapotranspiration. Flow equalization could precede these systems to ensure that applied flow rates can be temporarily decreased if necessary to prevent overland flow.

Rapid contaminant removal in the subsurface of the experimental system suggests that lower inputs of organic carbon may be sufficient to stimulate contaminant removal, which could reduce material inputs, though further research is needed to understand the requirements for carbon inputs better. horizontal levees may also be ideal for more concentrated wastewater streams, because 80-90% of the length of the slope is effectively unutilized in the experimental system and higher contaminant loads may require more contact time in the subsurface to achieve comparable treatment. Further research is needed to understand how water matrix differences would impact contaminant removal and other co-benefits, but this may be an attractive option for utility managers who are considering water reuse applications and require solutions to deal with concentrated waste streams (i.e. RO concentrate) from advanced water treatment processes.

Comparison to other types of wetlands. Subsurface wetlands that have been built in many locations often do not provide a significant advantage over surface-flow wetlands in terms of space requirements and performance, though they are less susceptible to seasonal variability especially in temperate climates (Kadlec, 2009). Consistent with past research, seasonal climate fluctuations did not have a significant impact on contaminant removal in the horizontal levee. Contaminant removal efficiency was not correlated with ambient or water temperatures during the monitoring period (Figure 2-12). However, the climate in the San Francisco Bay Area is mild and stable: the average daily temperature was 16.4°C at the field site, with 95% of temperatures falling between 11 and 22°C throughout the monitoring period. The relative insensitivity of contaminant removal to seasonal variations in temperature and plant growth may also be partly explained by the asynchronous seasonality of different removal mechanisms. For example, peak activity of plant uptake of nitrate and microbial removal of nitrate occur at different times of year (Kadlec and Wallace, 2009). The mechanisms of contaminant transformation in the subsurface is investigated further in subsequent chapters.

Horizontal levees can offer significant advantages over other types of constructed wetlands used for treating wastewater effluent. Horizontal levees appear to be significantly more efficient in terms of space requirements, provided that water can be directed to the subsurface. To compare area requirements across wetland types, we calculated the wetland area needed for 90% removal (A_{90}^{1}) of nitrate, in hectares per ($m^3\ d^{-1}$), introduced by Jasper et al. (2014b). Open-water and vegetated wetlands have seasonal A_{90}^{1} values ranging from around 1.2 x 10^{-3} ha $(m^3\ d)^{-1}$ and 3.4 x 10^{-3} ha $(m^3\ d)^{-1}$ respectively in the summer and greater than 6 x 10^{-3} ha $(m^3\ d)^{-1}$ in the winter (Jasper et al., 2014b). For comparison, A_{90}^{1} values for horizontal levees were seasonally invariable and ranged from 0.1 to 0.7 x 10^{-3} ha $(m^3\ d)^{-1}$ (Figure 2-13). The median yearly A_{90}^{1} value of 0.2 x 10^{-3} ha $(m^3\ d)^{-1}$ for horizontal levees is significantly lower than even the most efficient summer values for open-water wetlands.

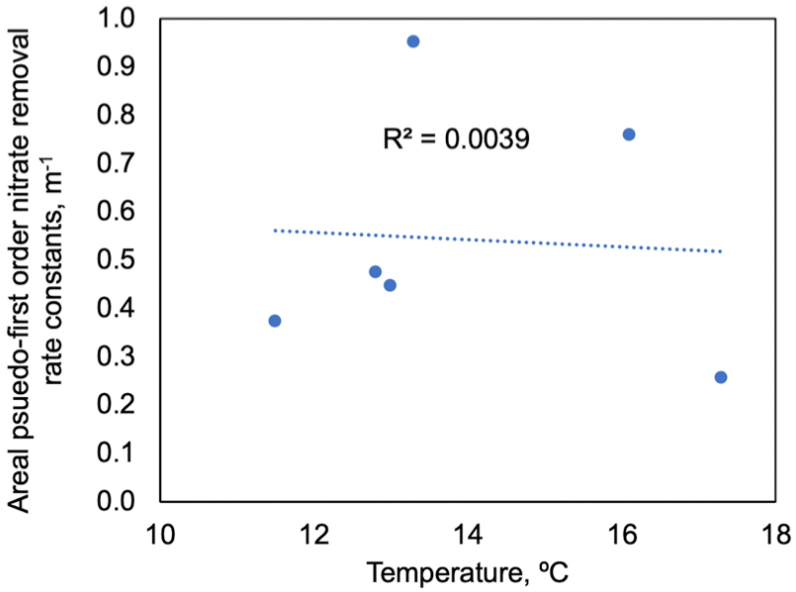

Figure 2-12: Relationship between subsurface contaminant removal rates for nitrate and temperature. Areal pseudo-first order nitrate removal rates constants were calculated using distance along the slope (rather than reaction time) for nitrate measured in porewater samples collected in transects at depths greater than 0.64 m along the subsurface flow path. These values were averaged across all cells sampled on each respective sampling dates. Temperatures are average ambient temperatures over the week leading up to the sampling event.

Additional benefits. Horizontal levees can also provide additional benefits that could make them more attractive than other types of wetlands. For example, coastal wetlands can provide storm surge protection (Shepard et al., 2011), elevation gains to keep pace with sea level rise (Morris et al., 2008), plant and animal biodiversity enhancements, restored habitat, and recreational opportunities (Ghermandi et al., 2010) and increase the resiliency of tidal marshes to sea-level rise (Beagle et al, 2019). Interviews with decision makers in the San Francisco Bay Area, where there is already awareness of the technology, revealed that horizontal levees are viewed more favorably than other nutrient control options because they provide multiple potential benefits, like sustainability and climate change resiliency (Harris-Lovett et al., 2018; Harris-Lovett et al., 2019). Other potential benefits of horizontal levees, such as their ability to provide recreational opportunities, are discussed subsequently.

Growth of native plants was rapid in the test system. Dense vegetation established on the horizontal levee within three years of construction. Native plants rapidly established and outcompeted non-natives (<2% of the surface coverage consisted of non-native plants). In riparian cells, Arroyo willows (*S. lasiolepis*) reached heights above 6 m by mid-2018 (section A.1 of Appendix A). The rapid establishment of dense vegetation observed in this system was likely due to a combination of nutrient enrichment (Morris et al., 2008) and high plant community diversity (Grace et al., 2007), both of which can lead to greater productivity.

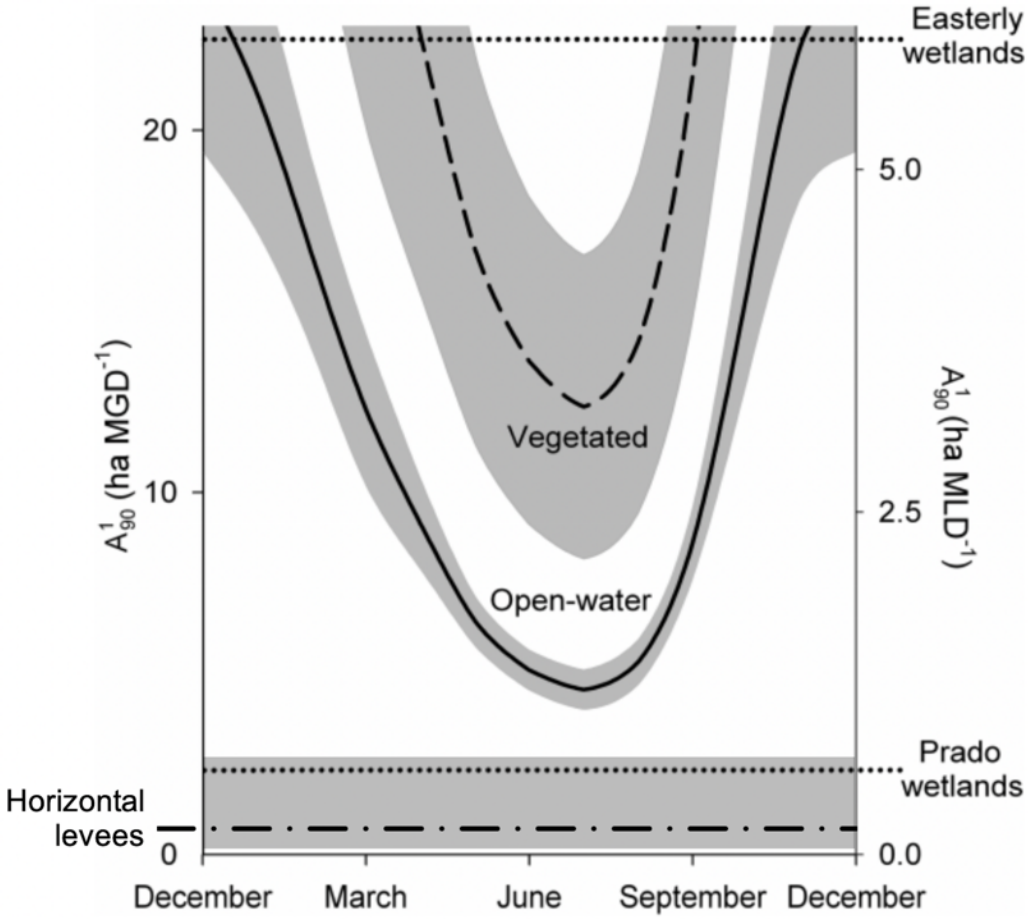

Figure 2-13: A_{90}^{1} of various types of wetlands compared with the horizontal levee as well as the Prado and Easterly wetlands (Jasper et al., 2014b). The range of A_{90}^{1} values for the horizontal levee (0.06-0.72 ha MLD^{-1}; with an average value of 0.23 ha MLD^{-1}) were calculated using the minimum, maximum and median areal pseudo-first order nitrate removal rate constants (Figure 2-12) to determine the wetland length required to remove 90% of nitrate. These distances were adjusted to wetland A_{90}^{1} values using the width of the test facility and subsurface flow rates (minimum, maximum and median) from throughout the monitoring period. The dashed black line represents the median A_{90}^{1} value for horizontal levees while the grey bar around it represents the range of expected values.

Plant biomass growth is strongly linked to climate change resiliency in constructed and natural coastal wetlands through increased accretion, wind wave dissipation and reduced erosion. Specific plants (e.g., willows) have been shown to protect coasts against storm surges (de Oude et al., 2010). Accretion in coastal wetlands is largely driven by organic matter accumulation (Callaway et al., 1997) with primary productivity as a key driver for accretion rates (Morris et al., 2008). Nutrient enrichment appears to have a positive impact on accretion rates in these systems, due to increased biomass growth (Morris et al., 2008). Increasing wetland elevations and dense vegetation growth provided by horizontal levees are essential to combating sea level rise, coastal flooding and storm surges, while stabilizing shorelines (Shepard et al., 2011). Further study is required to quantify these potential benefits fully.

Consistent with past wetlands research (Knight et al., 2001), diverse fauna were also attracted to the test facility, likely due to highly varied habitat and niche complementarity created by the dense

biomass growth (Grace et al., 2007). At full-scale, these benefits would likely increase because habitat diversity and quality tend to increase with wetland size (Hsu et al., 2011). At the horizontal levee, we observed diverse wildlife, including ground squirrels (*Otospermophilus beecheyi*) and other rodents, jackrabbits (*Lepus californicus*), garter snakes (*Thamnophis sirtalis*), gopher snakes (*Pituophis catenifer catenifer*) and other reptiles, amphibians, such as the Pacific tree frog (*Pseudacris regilla*), and a wide array of insects, along with a large and varied community of birds (section A.4 of Appendix A). These observations are in line with past research suggesting that constructed wetlands provide attractive and productive habitats (Kadlec and Wallace, 2009).

An important set of additional benefits in coastal wetlands are the recreational and educational opportunities the provide, as well as aesthetics and benefits related to environmental justice. Meta-analyses have identified nonconsumptive recreation as a valuable benefit of restored and constructed wetlands (Ghermandi et al., 2010) because wetlands can bring "substantial welfare gains" to surrounding communities, and specifically to marginalized communities that typically have limited access to green spaces. In the context of constructed wetlands, this has been largely unexplored, though the distribution of green spaces in urban areas tends to benefit communities that are affluent and predominantly white (Wolch et al., 2014). If sited appropriately, horizontal levees can help combat this. For example, in the San Francisco Bay, horizontal levees could provide recreational opportunities and associated health benefits (Wolch et al., 2014; van den Berg, 2015) to a wide range of geographically, ethnically and socioeconomically diverse communities, while simultaneously protecting those same communities against coastal flooding. This is important because many of the communities that are most threatened by sea level rise consist of marginalized groups (Maantay and Maroko, 2009) who are also at a greater risk during natural disasters due to inequitable distributions of emergency response resources (Qiang, 2019).

2.4 Conclusions

Horizontal levees can achieve significant removal of a wide range of wastewater-derived contaminants, including nutrients, pharmaceuticals and F+ coliphage, while providing other benefits, such as high-quality habitat, and increased shoreline resilience to sea-level rise. At our field site, treatment efficiency was controlled by hydrological conditions, which were the strongest predictors for the removal of a wide range of contaminants removed in these systems. Certain design parameters, such as planting regimes and soil texture, also affected the total mass of contaminants that can be removed based on their influence over maximum subsurface flow rates. Additional research is needed to develop an understanding of the mechanisms behind contaminant removal in this system, as well as how horizontal levees would function under a variety of additional other design and operational conditions, and in more variable climates.

Horizontal levees may also be useful in potable water reuse scenarios, which will likely expand in the future. Currently, there are limited options for disposal of waste streams associated with wastewater reuse (e.g., reverse osmosis concentrate streams), which tend to have low volumes but high concentrations of salts, nutrients and trace organic contaminants. Horizontal levees could be used to treat these waste streams because our results suggest these systems could handle significantly higher contaminant mass loads than we have studied. This application requires testing to ensure that differences in water matrices do not adversely impact treatment capacity, such as through stress to microbial or plant communities caused by higher salinity water. If successful, horizontal levees could continue to be appropriate multi-benefit treatment options even throughout dramatic shifts in water and wastewater management.

Chapter 3. The Fate of Dissolved Nitrogen in a Horizontal Levee: Impacts of Electron Acceptors on Seasonal Nitrate Removal Processes

The following chapter is adapted from a co-authored manuscript with permission from Gonthier, E., Stiegler, A.N., Sedlak, D.L. The fate of dissolved nitrogen in a horizontal levee: impacts of electron acceptors on seasonal nitrate removal processes. *Manuscript submitted for publication*. Reproduced with permission from *Environmental Science & Technology*.

ABSTRACT

Horizontal levees have been proposed as a nature-based approach for removing nitrogen from municipal wastewater effluent that provides additional benefits, such as flood control and terrestrial habitat. However, the performance of this new type of subsurface wetland will depend on biogeochemical conditions. To assess the rates and mechanisms of nitrogen removal, we monitored an experimental horizontal levee that received nitrified wastewater effluent over a 2-year period. In the subsurface, more than 50% of the applied nitrogen was removed by heterotrophic denitrifiers, which consumed labile organic carbon from decaying plants and wood chips that had been added at the time of construction. Fe(III)- and sulfate-reduction during the summer also led to the formation of $FeS_{(s)}$ in the subsurface of the horizontal levee. During cooler winter months when heterotrophic activity slowed down, autotrophic denitrifiers became more important to nitrogen removal. These organisms, which paired oxidation of Fe(II)-sulfides with nitrate reduction, were responsible for up to 30% of the nitrate removed in wetland cells during winter. To predict long-term removal of nitrogen in these systems, we developed an electron transfer model to account for production and consumption of electron donors by various processes. Results indicate that horizontal levees should be capable of removing nitrate from wastewater effluent for more than 50 years before the carbon amended to the system (e.g., wood chips) during construction would be depleted, though the type of wood used may impact organic carbon decomposition rates. After the wood chips are depleted, sulfide minerals, decaying vegetation and root exudates may provide enough electrons to fuel continued nitrogen removal.

3.1 Introduction

Humans have transformed the global nitrogen cycle (Galloway et al., 2008; Seitzinger et al, 2006), more than doubling the natural rate of terrestrial N_2 fixation through the Haber-Bosch process (Gruber and Galloway, 2008). Reactive nitrogen from fertilizers discharged into aquatic ecosystems via runoff or municipal wastewater effluent can stimulate the growth of toxic algae and cause eutrophication in marine and estuarine systems (Anderson et al, 2002). Because increasing global temperatures are predicted to amplify these effects (Xiao et al., 2019), more effective management of nutrient contamination will be needed in coming decades (Heiskanen et al., 2019).

Nutrient removal systems at wastewater treatment plants often require large capital investments (Ko et al, 2015) and are expensive to operate (Tchobanoglous et al., 2013). Nature-based treatment systems can remove nutrients at lower costs while simultaneously providing other benefits (Seifollahi-Aghmiuni et al., 2019). However, they have not been as popular as treatment plant upgrades because they often require larger areas and exhibit diminished performance during cold weather periods (Kadlec and Wallace, 2009). Horizontal levees, a new type of subsurface wetland that builds upon insights from other constructed and riparian wetlands (Hill, 2000) and denitrification walls (Schipper et al., 2004; Schmidt and Clark, 2012), may overcome some of these limitations. A horizontal levee consists of a wedge of sediments that buttresses storm control levees and removes nutrients and trace organic contaminants from wastewater effluent in its subsurface layers in a smaller footprint than most other types of constructed wetlands, as described in Chapter 2 (Cecchetti et al., 2020a). Additionally, horizontal levees provide terrestrial habitat that can protect low-lying urban areas from storm surges (Morris et al, 2013), while providing ancillary benefits (e.g., recreation) that are valued by local stakeholders (Harris-Lovett et al., 2019).

When optimized hydraulically (i.e., in the absence of overland flow), horizontal levees effectively remove nitrogen: 97% of wastewater-derived nitrogen was removed in a pilot-scale horizontal levee without overland flow. This even occurred during the winter, when average water applied temperatures decreased from 21 to 17 °C and plants were senescing as described in Chapter 2 (Cecchetti et al., 2020a). Although plants growing on the surface of the levee took up nitrogen from the wastewater, isotopic analysis indicated that plant uptake was only responsible for about 10% of nitrogen removal, as described in Chapter 4 (Cecchetti et al., *submitted*). Furthermore, due to an absence of plant harvesting, any nitrogen taken up by plants will be released when biomass decays.

We hypothesized that the nitrate removal observed in this pilot system was due to microbial denitrification on the basis of observed anoxic conditions and isotopic fractionation data. However, heterogeneous redox conditions made a range of additional processes possible, such as anammox, Feammox, and dissimilatory nitrate reduction to ammonium (DNRA) (Burgin and Hamilton, 2007; Yang et al., 2012a; Giblin et al., 2013). Additionally, because denitrifiers frequently rely on organic carbon for energy, other microbial processes that result in consumption of organic carbon could impact the denitrification capacity of these systems.

To assess the biogeochemical cycling of nitrogen in these systems, a suite of redox active species were measured in porewater, soils and biomass in a pilot-scale horizontal levee. These data were used to develop a quantitative understanding of elemental cycling in horizontal levees and to elucidate the ways in which subsurface biogeochemistry impacts the long-term removal of nitrogen in those systems.

3.2 Materials and Sampling Methods

3.2.1 Materials

Reagents were purchased from Fisher Scientific (Fairlawn, NJ) at the highest available purity. All solutions were prepared using 18MΩ Milli-Q water from a Millipore system.

3.2.2 Wetland Monitoring

Concentrations of nitrogen species, anions, cations, total organic carbon, and metals, as well as water quality parameters (e.g., temperature and pH) were monitored in the influent, effluent and porewater samples using methods described in Chapter 2 (Cecchetti et al., 2020a). Briefly, the system consisted of twelve hydraulically-separated parallel sloped subsurface wetland cells, which were used to test four treatments: (1) cells planted with willows (in coarse soil); cells planted with wet meadows in (2) coarse or (3) fine soils; and, (4) cells constructed with swales running down their center. Clay loam topsoil was underlain by sand and gravel. All layers were amended with redwood wood chips at approximately 24 g per kg soil. The total depth of these layers was 0.9 m. Below the sand and gravel layers a compacted clay liner prevented infiltration. Nitrified wastewater effluent from the adjacent municipal wastewater treatment plant was delivered to the subsurface via gravel trenches at the top of the slope.

3.2.3 Sample Collection

Porewater, influent and effluent water, as well as soil and plant samples, were collected using previously described in Chapters 2 and 4. Briefly, porewater samples were collected at depths ranging from 0.6 to 0.9 m using stainless steel PushPoint sediment porewater samplers (MHE Products, East Tawas, MI, USA). Influent and effluent samples were collected from the influent pump station and from the 12 effluent monitoring wells at the foot of the wetland slope using a Masterflex E/S portable water sampler (Cole-Parmer, Vernon Hills, IL, USA). All water samples were filtered on-site and stored on ice prior to analysis, which normally occurred within 24-48 hr.

New growth plant leaves were collected from Baltic rushes (*J. balticus*; in wet meadow cells) and Arroyo willows (*S. lasiolepis*; in willow cells) every 3-6 months between August 2016 and June 2019, at various distances along the wetland slope, as described in Chapter 4 (Cecchetti et al., *submitted*). Leaves were separated from their petioles and collected in labeled paper envelopes. Envelopes were placed in plastic bags and stored on ice prior to returning to the lab. Soil samples were collected from the top 10 cm of the soil. In 2016, these soil samples were collected from 9 randomly selected locations per cell. Subsets of additional samples were collected in 2017 and 2018 for comparison. Soil samples were stored on ice prior to returning to the lab where they were frozen prior to analysis.

3.2.4 Sample Processing and Analytical Methods

Sample processing and analytical methods for chemical parameters and isotope measurements in plant, soil and aqueous samples were described in Chapters 2 and 4. Briefly, anions (Cl^-, Br^-, NO_2^-, NO_3^-, PO_4^{3-}, and SO_4^{2-}) were analyzed by ion chromatography according to U.S. EPA Method 300.0. Cations (Li^+, Na^+, K^+, NH_4^+, Mg^{2+}, and Ca^{2+}) were analyzed by ion chromatography according to previously described methods (Thomas et al., 2002). Non-purgeable organic carbon (NPOC), dissolved inorganic carbon and total dissolved nitrogen were measured in 0.7-µm filtered samples using a Shimadzu TOC-V/CSH analyzer with an attached TN-1 unit (Shimadzu Scientific Instruments, Columbia, MD)

according to standard methods (Method 5310B; APHA, 1998). Dissolved transition metals (i.e., $Mn_{(aq)}$ and $Fe_{(aq)}$) were analyzed by inductively coupled plasma mass spectrometry (ICP-MS) according to standard methods (Method 3125; APHA, 1998). Organic nitrogen concentrations were calculated by subtracting concentrations of nitrate, nitrite and ammonium from total nitrogen measurements.

Leaf samples were dried at 65°C for 48 hr immediately upon return to the lab. Soil samples were freeze-dried in a Labconco FreezeZone 12 Freeze Dryer (Labconco, Kansas City, MO). Dried leaf and soil samples were ground to a fine powder (200 mesh) using mortar and pestle, a SPEX SamplePrep 8000 Mill (SPEX SamplePrep, Metuchen, NJ) or a Mini-BeadBeater (Biospec Products, Bartlesville, OK). Soils were analyzed for metals (Fe, Mn and Cu) by inductively coupled plasma atomic emissions spectrometry (ICP-AES) after nitric acid/hydrogen peroxide closed vessel microwave digestion. Dried and powdered soil and plant samples were analyzed simultaneously for carbon, nitrogen and sulfur content (% dry weight). Data for nitrogen, carbon and sulfur stable isotope ratios ($\delta^{15}N$, $\delta^{13}C$ and $\delta^{34}S$) are reported in Chapter 4 (Cecchetti et al., *submitted*).

3.2.5 Statistical Methods

Statistical analyses were performed in Excel (Microsoft Corporation, Redmond, WA, USA) using the Real Statistics Resource Pack software (Release 5.4; Zaiontz, 2018). Reported p-values were derived from non-parametric analyses (i.e., Wilcoxon signed-rank test for paired samples and Mann-Whitney tests for independent samples) unless otherwise specified. When data were normally distributed (i.e., with a p-value > 0.05 for both Shapiro-Wilk and d'Agostino-Pearson tests) parametric analyses (e.g., t tests) were used as specified in the text.

3.3 Mass Balance and Electron Balance Methods and Results

3.3.1 Mass Balances

Methods. Mass balances were conducted to quantify exchanges of redox-active elements between different forms in the subsurface. Mass balances were modeled generally according to Equation 3-1 through Equation 3-4:

$$\text{Storage} = \text{Net advection} + \text{Net Diffusion and Dispersion} + \text{Net chemical reaction} \qquad \textbf{Equation 3-1}$$

$$\frac{\partial}{\partial t}\int c\mathrm{d}V = (Q_{\text{in}}c_{\text{in}} - Q_{\text{out}}c_{\text{out}}) + (D + \in_x)\left\{\left[A\frac{\partial c}{\partial x}\right]_{\text{outlet}} - \left[A\frac{\partial c}{\partial x}\right]_{\text{inlet}}\right\} + \int(r_{\text{v}} + r_{\sigma}a)\mathrm{d}V \qquad \textbf{Equation 3-2}$$

$$\Delta\left(X_{\text{soil}} + X_{\text{plants}} + X_{\text{residual litter}}\right) = Q_{\text{inf}}[X]_{\text{inf}} - Q_{\text{eff}}[X]_{\text{eff}} + J_{diff+disp} + r_{X,rem} \qquad \textbf{Equation 3-3}$$

$$\Delta X_{\text{soil}} + B_{\text{peak}}\theta_{\text{b}}f_X + \Delta X_{\text{residual litter}} = Q_{\text{inf}}[X]_{\text{inf}} - Q_{\text{eff}}[X]_{\text{eff}} + r_{X,rem}V \qquad \textbf{Equation 3-4}$$

where Q_{inf} and Q_{eff} represent the influent and effluent flows in $m^3\ yr^{-1}$, $[X]_{\text{inf}}$ and $[X]_{\text{eff}}$ represent concentrations of species X in kmol m^{-3} in the influent and effluent wastewater respectively, X_{soil}, X_{plants}, and $X_{\text{residual litter}}$ represent the total mass of species X in kmol stored in soil, plant biomass and undecomposed plant residues (litter), respectively, $r_{X,\text{rem}}V$ represents the net chemical or microbial reactions removing element X in kmol yr^{-1}, B_{peak} represents the peak dry weight of total plant biomass in kg DW, θ_{b} represents the plant biomass turnover rate in yr^{-1}, and f_X represents the fraction of species X in plant biomass in kmol X (kg DW)$^{-1}$. Terms in Equation 3-2 have been defined previously (Benjamin and Lawler, 2013). Not all mass balances included all of the terms of every equation above

and some mass balances included additional terms. The diffusion and dispersion term, $J_{diff+disp}$, was assumed negligible in balances on carbon and nitrogen.

X_{soil} measurements were conducted on bulk soil samples and included various solid forms of the elements. With respect to sulfur, nitrogen and organic carbon, this included forms of those elements stored in microbial biomass (e.g., microbial biomass C). As an example, the C_{soil} measurements included microbial biomass C, indigenous organic carbon from construction materials, and decomposing plant roots and litter (see carbon mass balance, below).

The control volume for mass balances included the subsurface soil layers of the wetland and all plant biomass (including both above ground standing biomass and live roots), plant litter deposited on the wetland surface and decaying plant roots. Elements assimilated into plant biomass were largely returned to the soil through litterfall that was deposited and reintegrated into the soil. A large fraction of organic carbon in litter was used for microbial respiration before litterfall mass was reintegrated into the soil, though most other nutrients (e.g., nitrogen, sulfur) remained. 80% of plant residues were considered reintegrated into the wetland for the purposes of the mass balances, based on analyses conducted on depth-resolved soil samples (see section 3.5.3). The system was not assumed to be at steady state and therefore changes in the storage terms over time were not set equal to zero unless they were shown not to change significantly over the monitoring period.

All statistical analyses were conducted using non-parametric analyses because our data rarely met the assumptions required (e.g., a normal distribution of values) for parametric statistical tests.

Overall results. Nitrogen, organic carbon and sulfur content in soil were quantified using elemental analyses performed at the Center for Stable Isotope Biogeochemistry at University of California, Berkeley, as described in Chapter 4 (Cecchetti et al., *submitted*). Manganese and iron content were quantified at the UC Davis Analytical Laboratory using ICP-AES preceded by microwave assisted digestion. Significant differences ($p < 0.05$) were not observed in the iron or nitrogen content of soils collected from the pilot horizontal levee in 2017 and 2018. Significant increases in sulfur ($p < 0.001$) and carbon ($p < 0.05$), and a significant decrease in manganese ($p < 0.01$) were observed over that time (Table 3-1).

Table 3-1: Average solid phase concentrations of redox-active elements in the soil in 2017 and 2018. Statistical comparisons between those dates are presented as p-values derived from two-tail Mann-Whitney tests.

	Mn	Fe	OrgC	N	S
Year of collection	Average solid phase concentration (ppm)				
2017	430 (n=6)	24000 (n=5)	16000 (n=24)	930 (n=24)	240 (n=24)
2018	390 (n=3)	24000 (n=5)	19000 (n=11)	940 (n=11)	320 (n=11)
Statistical comparison	P-values				
2017 v. 2018	**0.01**	0.44	**0.03**	0.80	**<0.001**

To quantify changes in the mass loading of aqueous species of these elements, concentrations were measured in the influent and effluent from each wetland cell on a series of monitoring dates. These values were multiplied by the total flow applied to individual cells, as described in Chapter 2 (Cecchetti et al., 2020a), between those sampling dates to estimate mass loading in the influent and effluent of each cell. Values for individual cells and dates were summed to calculate the total influent and effluent loading to the pilot wetland system. The full dataset is provided on Mendeley Data (Cecchetti et al., 2020b).

Plant uptake measurements were described in Chapter 4 (Cecchetti et al., *submitted*) and estimation methods for production, decomposition and reintegration of plant residues into sediments are presented in section 3.5. The results of the mass balances over the monitoring period are delineated in Table 3-2.

Table 3-2: Mass balances results over the 2-year monitoring period. Values above the dashed line are median measured values whereas those below the dashed line were calculated.

	Mn	Fe	S	N	OrgC
Component	Mass of element (kmol yr^{-1})				
ΔX_{soil}	-8.0	0*	40	0*	780
ΔX_{plants}	0.02	0.2	1.2	9.2	360
$\Delta X_{\text{residual litter}}$	0.002	0.04	0.2	5.2	92
$Q_{\text{inf}}[X]_{\text{inf}}$	0.1	0.1	44	104	64
$Q_{\text{eff}}[X]_{\text{eff}}$	0.7	2.2	24	59	70
$J_{diff+disp} - r_{X,rem}V$	-8.8	-130	62	-81	1200

*Changes in Fe and N content of soil were insignificant over the monitoring period.

Nitrogen mass balances. Two mass balances were conducted on nitrogen. The first mass balance, which was a whole-system mass balance, was performed as described in the preceding section and was used to quantify the amount of nitrogen removed completely via reactions from the system (primarily via denitrification in the spatial reduction sequence). The results of this mass balance are presented in Table 3-2. The second mass balance, which was performed on the ΔN_{soil} component of the overall mass balance, was conducted to quantify the fraction of wastewater-derived nitrogen removed by microbial assimilation.

Overall mass balance. The overall mass balance on nitrogen as detailed in Table 3-2 was performed by applying Equation 3-4 to nitrogen, as in Equation 3-5 below:

$$N_{\text{plants}} + \Delta N_{\text{residual litter}} = Q_{\text{inf}}[N]_{\text{inf}} - Q_{\text{eff}}[N]_{\text{eff}} + r_{N,rem}V \qquad \textbf{Equation 3-5}$$

Because soil nitrogen measurements did not change significantly over the monitoring period, ΔN_{soil} was 0 kmol N. This parameter included not only nitrogen stored in indigenous soil nitrogen forms from the construction materials used in the pilot system, but also nitrogen stored in decaying plant roots and litter reintegrated into the soil (see Equation 3-6 below).

ΔN_{plants} was calculated as the net increase in the amount of nitrogen stored in standing biomass and live plant roots by the end of the monitoring period. Based on median biomass measurements at the beginning (0.4 kg DW m^{-2} and 0.5 kg DW m^{-2} for above and below ground live biomass respectively) and end (1.5 kg DW m^{-2} and 1.0 kg DW m^{-2}) of the monitoring period (Cecchetti et al., *submitted*), the median biomass nitrogen fraction (2.9%) and the size of the site (45.7 m by 110 m; excluding swale-type wetland cells), the net increase in the amount of nitrogen stored in above and below ground biomass throughout the monitoring period was calculated to be 18 kmol N.

$\Delta N_{\text{residual litter}}$ was calculated based on the dry weight of undecomposed litter remaining at the end of the monitoring period, the %C of the litter and its C:N ratio (see section 3.5). Plant litter experienced increasing levels of decomposition and reintegration into wetland soils with time since deposition and the total amount of litter produced had to be adjusted to quantify undecomposed litter. We used values reported in the literature for litter decomposition rates and changes in the %C and C:N of litter over time to do this. Residual litter, i.e., undecomposed litter that had not integrated into the soil, was calculated by multiplying this remaining value by ~20%, which was the fraction of undecomposed

litter we estimated remained unintegrated into the soil or removed by other mechanisms (e.g., consumption by animals) at the end of the monitoring period, based on elemental and isotopic analyses in depth resolved soil samples (described in section 3.5.3). %C of litter was measured in dead biomass. This was adjusted to nitrogen content based on projected C:N ratios based on the amount of litter remaining (section 3.5.2). Based on these models, we calculated that of the 36 kmol N that went to above ground plant litter, nearly 60% (21 kmol N) were reintegrated into the soils and around 15%, or 5.2 kmol N, remained in undecomposed residues on the wetland surface (Figure 3-14b). This is consistent with past research, in which nutrients from litterfall were rapidly released (e.g., up to 50% within the first few days) and 5-20% of litter remained in undecomposed residues long-term (Kadlec and Wallace, 2009). The remaining 9.9 kmol N of litter were largely mineralized and consumed by microorganisms, though some nitrogen was likely lost through consumption by animals and solubilization as DON and export from the system. This final process could explain part of the mass loading of DON in the effluent (i.e., 6.5 kmol N).

Values for $Q_{\mathrm{inf}}[N]_{\mathrm{inf}}$ and $Q_{\mathrm{eff}}[N]_{\mathrm{eff}}$ were calculated as described previously to be 164 kmol N and 59 kmol N over the monitoring period. Using these values, we solved Equation 3-5 for $r_{N,rem}V$, which was approximately -81 kmol N.

Soil nitrogen mass balance. We also conducted a mass balance on the soil nitrogen component of the overall nitrogen mass balance. Soil nitrogen included indigenous soil nitrogen ($\Delta N_{\mathrm{soil,ind}}$) (e.g., nitrogen stored in soil organic matter derived from construction materials), nitrogen stored in microbial biomass (ΔN_{MBC}), nitrogen stored in decaying plant roots ($\Delta N_{\mathrm{BG,decay}}$) and nitrogen reintegrated into the soil stored in decaying plant litter ($\Delta N_{\mathrm{litter,integrated}}$), according to Equation 3-6:

$$\Delta N_{\mathrm{soil}} = \Delta N_{\mathrm{soil,ind}} + \Delta N_{\mathrm{MBC}} + \Delta N_{\mathrm{BG,decay}} + \Delta N_{\mathrm{litter,integrated}} \qquad \textbf{Equation 3-6}$$

Over the monitoring period, the change in soil nitrogen (ΔN_{soil}) was insignificant ($p = 0.80$) and was 0 kmol N in Equation 3-6. Soil nitrogen consisted of nitrogen stored in soil organic matter, microbial biomass and decomposing plant biomass (including decaying plant roots and above ground biomass reintegrated into the soil). Despite insignificant changes in the total amount of soil nitrogen, there were large exchanges between various forms. The significant increase in microbial biomass N (ΔN_{MBC}), which we estimated increased by 49 kmol N based on the geometric mean of microbial biomass N reported in sediments from natural wetlands (Xu et al., 2013) and horizontal subsurface flow constructed wetlands (Truu et al., 2009), was offset by removal of nitrogen from other soil forms. This magnitude of microbial growth is consistent with past research in saturated systems: increasing water content in natural and constructed wetland sediments has been linked to substantial increases (50-300%) in microbial biomass (Witt et al., 2000; McIntyre et al., 2009; Minick et al., 2019). The total mass of nitrogen in decaying roots ($\Delta N_{\mathrm{BG,decay}}$) increased to 6.5 kmol N based on root turnover rates and biomass estimates discussed in Chapter 4 (Cecchetti et al., *submitted*) and Gill et al. (2002). The mass of nitrogen from above ground biomass litter that integrated into the subsurface ($\Delta N_{\mathrm{litter,integrated}}$) was estimated at 21 kmol N. By rearranging Equation 3-6 and solving for $\Delta N_{\mathrm{soil,ind}}$, we estimated that the change in the size of that nitrogen pool was -77 kmol N.

Of the indigenous soil nitrogen exchanged to other forms, approximately 70% (54 kmol N or 27 kmol N yr^{-1}) was taken up into plants. This represented 86% of nitrogen taken up by plants. The remaining 23 kmol N removed from indigenous soil nitrogen was assimilated into microbial biomass. Of N taken into plant biomass, 11 kmol N and 7.2 kmol N (from all sources) were retained in standing above and below ground biomass, with 36 kmol N deposited as litter on the wetland surface and 8.5 kmol N in

decaying plant roots. 27 kmol of microbial biomass nitrogen were left over after loss of indigenous soil nitrogen was accounted for. This nitrogen came from a combination of wastewater nitrogen and nitrogen from decomposing plant litter and roots. We approximated that 2.0 kmol N and 9.9 kmol N were supplied to microbial biomass from the decomposition of below and above ground biomass respectively. The remaining 15 kmol N of microbial biomass N was assimilated from wastewater. This is approximately equivalent to the amount of wastewater-derived ammonium (14 kmol N) removed in the horizontal levee, which is consistent with the preferential use of ammonium by microorganisms for assimilation of nitrogen (Inamori et al., 2008). It is also equivalent to the amount of nitrogen removal unexplained (15 kmol N) when removal due to plant uptake (8.8 kmol N) and denitrification (81 kmol N) are subtracted from the total amount of nitrogen removal observed (104 kmol N).

Carbon mass balance. Soil carbon content increased by approximately 18% over the monitoring period. Using Equation 3-7 below, we assessed the amount of indigenous organic carbon and wood chip carbon consumed by microorganisms:

$$\Delta C_{\text{soil}} = \Delta C_{\text{soil,ind.+WC}} + \Delta C_{\text{MBC}} + \Delta C_{\text{BG,decay}} + \Delta C_{\text{litter,integrated}} \qquad \textbf{Equation 3-7}$$

where $\Delta C_{\text{soil,ind.+WC}}$, ΔC_{MBC} and $\Delta C_{\text{BG,decay}}$ represent changes in kmol yr^{-1} in carbon storage of the indigenous soil carbon pool and wood chips, microbial biomass C and decaying root biomass (BG, decay), respectively.

Over the monitoring period, ΔC_{soil} was measured at +780 kmol (+390 kmol yr^{-1}). Of this increase, a significant fraction was due to microbial biomass C (ΔC_{MBC}), which we estimated increased by +610 kmol based on microbial biomass C reported in sediments from natural wetlands (Xu et al., 2013) and horizontal subsurface flow constructed wetlands (Duncan et al., 1994; Truu et al., 2009) and the assumption that microbial biomass was largely produced during the monitoring period. The total mass of decaying root carbon ($\Delta C_{\text{BG,decay}}$) was calculated at 220 kmol based on root turnover rates and biomass estimates from Chapter 4 (Cecchetti et al., *submitted*) and Gill et al. (2002). The mass of carbon from litter that integrated into the subsurface ($\Delta C_{\text{litter,integrated}}$) was estimated at 180 kmol. By rearranging Equation 3-7 and solving for $\Delta C_{\text{soil,ind.+WC}}$, we estimated that the change in the size of that pool to be -230 kmol. Additional sources of organic carbon are discussed below.

Manganese, iron and sulfur. For manganese and iron, influent and effluent loadings did not reflect the full reduction of Mn(III)/Mn(IV)- and Fe(III)-oxides in this system. We observed significantly higher concentrations of $Mn_{(aq)}$ and $Fe_{(aq)}$ in porewater samples than in effluent measurements, possibly due in part to deposition of carbonate minerals. The results of Visual MINTEQ modeling (section 3.4) suggested that Mn(II)- and Fe(II)-minerals were supersaturated in large portions of the wetland subsurface and were likely precipitating onto sediments. This could partly explain why changes in the Mn and Fe content of soils (-4.0 kmol yr^{-1} and 0 kmol yr^{-1}) were not equivalent to export of those metals from the system. Reductive mobilization followed by deposition of these metals in other forms may have led to heterogeneous spatial distribution throughout within the sediments, which could explain why the term "$J_{diff+disp} - r_{X,rem}V$" in the mass balances in Mn and Fe above did not equal zero, as would have been expected.

However, deposition of these minerals does not appear to explain these discrepancies fully. The increase in loading of these metals ($Q_{\text{inf}}[X]_{\text{inf}} - Q_{\text{eff}}[X]_{\text{eff}}$) was 0.3 kmol yr^{-1} and 1.1 kmol yr^{-1} respectively between the influent and effluent samples, though we would have expected effluent loadings of nearly 100 and 200 kmol yr^{-1} respectively based on porewater samples collected at the end

of the wetland. For these reasons, we concluded that re-oxidation of these species in the gravel effluent collection trench likely occurred prior to the effluent sample collection point.

To produce better estimates of the full extent of iron and manganese reduction, we used porewater concentrations over the first 7.5 m of the slope – prior to the point at which supersaturation of carbonate minerals was predicted to limit concentrations of $Mn_{(aq)}$ and $Fe_{(aq)}$ – to estimate subsurface reduction rates for these species. In the case of Fe(II), these estimates may have been low due to formation of Fe(II)-sulfide minerals, which often occurred within the first 5 m. In the first 7.5 m of the slope there were significant ($p < 0.001$) linear relationships between distance and concentrations of $Mn_{(aq)}$ and $Fe_{(aq)}$ (Figure 3-1). If we extrapolated these relationships to the end of the wetland (45.7 m), we would expect that 0.2 mM $Mn_{(aq)}$ and 0.95 mM $Fe_{(aq)}$ would have been observed in the effluent from the system if precipitation of minerals had not been significant. This is significantly higher than median concentrations of 0.06 and 0.11 that we observed for $Mn_{(aq)}$ and $Fe_{(aq)}$ respectively in porewater samples collected at the end of the wetland slope. The values calculated using the linear relationship discussed above were considered upper bound estimates for iron and manganese reduction because they assumed that reduction of those minerals was uniform across the entire wetland, whereas deposition of sulfide and carbonate minerals onto mineral surfaces may have reduced the reduction rates of Mn(III)/Mn(IV)- and Fe(III)-oxides in latter portions of the wetland.

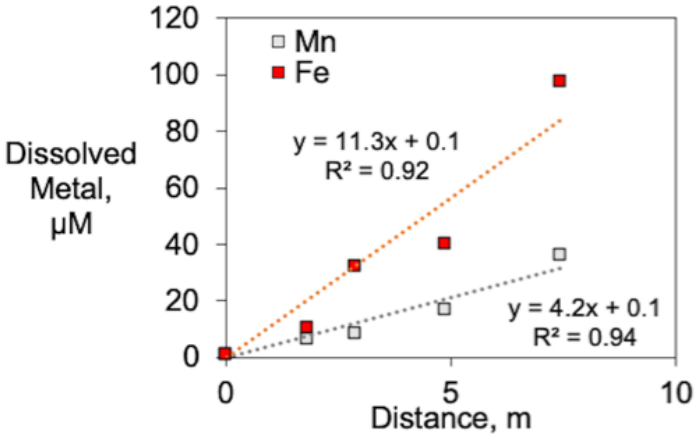

Figure 3-1: Linear relationships between porewater concentrations of $Mn(II)_{(aq)}$ and $Fe(II)_{(aq)}$ and distance along the wetland slope.

The changes in the loading of $Mn_{(aq)}$ and $Fe_{(aq)}$ in the wetland discussed above (0.3 kmol yr^{-1} and 1.1 kmol yr^{-1}) were considered lower bound estimates of manganese and iron reduction. These values were likely lower than actual reduction rates due to mineral deposition discussed above and in section 3.4.

Estimates of manganese and iron reduction were calculated based on the 95th percentile values of observed $Mn_{(aq)}$ and $Fe_{(aq)}$ concentrations in porewater (0.08 and 0.42 mM, respectively) and the median total flow over the monitoring period. These estimates were based on the assumption that the higher end of observations of these species in porewater was reflective of the total amount of reduction of Mn- and Fe-oxides, which was estimated at 4.1 kmol Mn and 22 kmol Fe. While this is our best estimate based on the data collected, it is possible that this value is still lower than actual reduction of those species due to Mn(II)- and Fe(II)-mineral formation.

The sulfur content of the soil increased significantly throughout the monitoring period, likely due in large part to deposition of sulfide minerals and other reduced sulfur species (e.g., elemental sulfur). However, increasing soil sulfur (40 kmol) exceeded the observed decrease in sulfate loading (-19 kmol) by more than double, suggesting that a significant fraction of dissolved sulfur in the influent may have been in forms other than sulfate (e.g., dissolved organic sulfur). However, sulfate reduction appeared to explain the majority of sulfate removal from the aqueous phase and also a significant fraction of the increase in soil sulfur content. Up to 6% of the removal of sulfate could have been attributed to uptake and storage in plant biomass (1.2 kmol).

3.3.2 Balancing Electron Donors and Acceptors

Electron balances were conducted based on the mass balances described above and were used to evaluate how changes in the flows and storages of those elements were related to each other through redox reactions. Electron balances in the horizontal levee pilot facility were modeled according to Equation 3-8 through Equation 3-10:

$$\text{Storage} = \text{Net advection} \qquad \textbf{Equation 3-8}$$

$$\Delta e^-_{\text{donors}} - \Delta e^-_{\text{acceptors}} = (Q_{\text{in}}[\text{EA}]_{\text{in}} - Q_{\text{out}}[\text{EA}]_{\text{out}}) - (Q_{\text{in}}[\text{ED}]_{\text{in}} - Q_{\text{out}}[\text{ED}]_{\text{out}}) \qquad \textbf{Equation 3-9}$$

$$\Delta e^-_{\text{donors}} + (Q_{\text{in}}[\text{ED}]_{\text{in}} - Q_{\text{out}}[\text{ED}]_{\text{out}}) = \Delta e^-_{\text{acceptors}} + (Q_{\text{in}}[\text{EA}]_{\text{in}} - Q_{\text{out}}[\text{EA}]_{\text{out}}) \qquad \textbf{Equation 3-10}$$

where $\Delta e^-_{\text{donors}}$ and $\Delta e^-_{\text{acceptors}}$ represent net changes in storage of electron donors and acceptors in keq yr^{-1}, Q_{in} and Q_{out} represent the influent and effluent flows in m^3 yr^{-1}, $[ED]_{in}$, $[EA]_{in}$, $[ED]_{out}$ and $[EA]_{out}$ represent dissolved concentrations of electron donors and electron acceptors in the influent and the effluent in keq m^{-3}.

We determined that approximately 81 kmol of nitrate and nitrite (of which 76 kmol were nitrate and 5.6 kmol were nitrite), 4.1 kmol manganese (as Mn(III)/Mn(IV)-oxides), 22 kmol iron (as Fe(III)-oxides), and 19 kmol sulfate were reduced through the microbial reduction sequence in the horizontal levee subsurface over the full monitoring period. The mass loading of dissolved oxygen to the subsurface was calculated at 15 kmol based on measured influent dissolved oxygen concentrations and subsurface flow rates (11 kmol), and estimated diffusion of dissolved oxygen into the subsurface (4.4 kmol; see below). Dissolved oxygen was assumed to diffuse into the subsurface with an effective diffusion coefficient of $D_e = 10^{-7}$ m^2 s^{-1} (Shackelford and Daniel, 1991; Kadlec and Wallace, 2009), an assumed porosity (θ) of 0.4 in the clay loam topsoil layer, and a tortuosity factor (τ) of 0.1 (Shackelford and Daniel, 1991). Based on formation of sulfide minerals within the first 5-15 cm of the subsurface, we assumed that dissolved oxygen did not dissolve further than approximately 10 cm into the subsurface before being consumed. Therefore, using the equation: $J = D_e \tau \theta (\partial c/\partial z)$ (Shackelford and Daniel, 1991), we estimated that approximately 4.4 kmol of oxygen diffused into the subsurface and were consumed throughout the monitoring period. It was assumed that all oxygen was consumed in the sediments.

To convert these values to electron equivalents, we used the molar ratios of electrons produced or consumed (eq mol^{-1}) based on the oxidation or reduction half reactions for these species provided in Table 3-3 (Rittmann and McCarty, 2013). Electron acceptor pools were further adjusted to account for the amount of organic carbon that was used for cell synthesis by heterotrophic microorganisms by dividing the total e^- equivalents calculated as described above for oxygen, nitrate, manganese, iron and sulfate by f_e (e^- eq to acceptor/e^- eq to donor) values derived from the literature. f_e values were

assumed to be 0.5, 0.6, 0.6, 0.75 and 0.9 for oxygen, nitrate, Mn(IV), Fe(III) and sulfate respectively (Rittmann and McCarty, 2013). This is reflected in the values presented in the first paragraph of this section and in Table 3-4.

Table 3-3: Oxidation or reduction half reactions for electron donors and acceptors (Rittmann and McCarty, 2013).

Species	Oxidation or Reduction Half Reaction	Ratio, eq mol^{-1}
	Electron Donors	
Wastewater-DOC	$\frac{1}{50}C_{10}H_{19}O_3N + \frac{9}{25}H_2O \leftrightarrow \frac{9}{50}CO_2 + \frac{1}{50}NH_4^+ + \frac{1}{50}HCO_3^- + H^+ + e^-$	1/5
Woodchips, plant residues, plant root exudates	$\frac{1}{4}CH_2O + \frac{1}{4}H_2O \leftrightarrow \frac{1}{4}CO_2 + H^+ + e^-$	1/4
Sulfide	$\frac{1}{8}HS^- + \frac{1}{2}H_2O \leftrightarrow \frac{1}{8}SO_4^{2-} + \frac{9}{8}H^+ + e^-$	1/8
Fe(II)	$Fe^{2+} + 3H_2O \leftrightarrow Fe(OH)_3 + 3H^+ + e^-$	1/1
Mn(II)*	$\frac{1}{2}Mn^{2+} + \frac{1}{2}H_2O \leftrightarrow \frac{1}{2}MnO_2 + H^+ + e^-$	1/2-1/1
	Electron Acceptors	
Oxygen	$\frac{1}{4}O_2 + H^+ + e^- \leftrightarrow \frac{1}{2}H_2O$	1/4
Nitrate	$\frac{1}{5}NO_3^- + \frac{6}{5}H^+ + e^- \leftrightarrow \frac{1}{10}N_2 + \frac{3}{5}H_2O$	1/5
Nitrite	$\frac{1}{3}NO_2^- + \frac{4}{3}H^+ + e^- \leftrightarrow \frac{1}{6}N_2 + \frac{2}{3}H_2O$	1/3
Mn(IV)/Mn(III)-oxides*	$\frac{1}{2}MnO_2 + H^+ + e^- \leftrightarrow \frac{1}{2}Mn^{2+} + \frac{1}{2}H_2O$	1/2-1/1
Fe(III)-oxides	$Fe(OH)_3 + 3H^+ + e^- \leftrightarrow Fe^{2+} + 3H_2O$	1/1
Sulfate	$\frac{1}{8}SO_4^{2-} + \frac{19}{16}H^+ + e^- \leftrightarrow \frac{1}{16}H_2S + \frac{1}{16}HS^- + \frac{1}{2}H_2O$	1/8

*Half-reactions shown for Mn(IV)/Mn(III)-oxides and Mn(II) are specifically for conversion between Mn(IV) and Mn(II). A molar ratio of 1/1.5 was used for Mn to account for the likely presence of Mn(III) in the sediments.

The amount of soil organic carbon (including indigenous organic carbon, decaying roots and wood chip carbon) consumed by microorganisms over the monitoring period was estimated as described in section 3.3.1. The amount of wastewater dissolved organic carbon (DOC) used in microbial processes was estimated based on the difference between influent and effluent mass loading. Plant exudates released from plant roots over the monitoring period were estimated using the range of exudation rates reported by Zhai et al. (2013) for wetland plants (e.g., *J. effusus*) which had a range of 0.2-1.1 mmol kg^{-1} root DM hr^{-1}, with a median value of 0.6 mmol kg^{-1} root DM hr^{-1} (Zhai et al., 2013). Other sources of organic carbon were assumed negligible.

The amount of sulfide minerals available for use as an electron donor was estimated based on the amount of sulfate and iron that were reduced. 19 kmol sulfate were reduced, and 22 kmol iron were reduced. However, for the purposes of this balance, we assumed that only 12 kmol iron were stored in Fe(II)-sulfides as this would constitute a 1:1.5 molar ratio between sulfide and Fe(II), which should

approximately reflect the range of expected molar ratios for sulfides ranging from AVS (Rickard and Morse, 2005) to pyrite (Chen et al., 2016). In total, this constituted 161 keq stored in sulfide minerals. If we take the amount of meq L^{-1} that would have to be transferred from sulfide minerals to nitrate to fuel the amount of autotrophic denitrification that we observed in the winter (3.0 meq L^{-1}) and extrapolate it to the entire wetland, it corresponds to 80 keq, which is approximately 50% of the total 161 keq estimate stored in sulfide minerals.

Table 3-4: Molar and electron changes in electron acceptor and donor pools in the experimental horizontal levee system over the monitoring period. Mass changes are presented in kmol and electrons transferred are presented as keq. Upper and lower bound estimates are presented in brackets (based on 5th and 95th percentiles of measured values or as specified above).

Electron Donors and Acceptors	Change in pool size kmol		Electrons transferred keq	
Organic carbon – Soil organic carbon	230	[72, 350]	930	[290, 1400]
Organic carbon – Plant root exudates	61	[20, 120]	240	[81, 490]
Organic carbon – Wastewater dissolved organic carbon	-6.0	[-28, 22]	-24	[-110, 89]
Sulfide minerals – sulfide	19	[13, 28]	150	[100, 220]
Sulfide minerals – Fe(II)	12	[2.0, 19]	12	[2.0, 19]
Reduced Mn	4.1	[1.2, 5.3]	6.2	[1.8, 7.9]
Total Electron Donors:			**1300**	**[360, 2200]**
Dissolved oxygen	15	[14, 18]	120	[110, 140]
Nitrogen – nitrate	76	[71, 110]	640	[590, 880]
Nitrogen – nitrite	5.6	[5.6, 5.7]	28	[28, 28]
Mn(III/IV)-oxides	4.1	[1.2, 5.3]	14	[3.9, 18]
Fe(III)-oxides	22	[2.0, 26]	30	[2.7, 35]
Sulfate	19	[13, 28]	170	[110, 250]
Total Electron Acceptors:			**1000**	**[850, 1300]**

Reduced manganese was also modeled as a potential electron donor because Mn(II) can be used by microorganisms as an electron donor for reduction of nitrate (Su et al., 2016) and oxygen. The amount of manganese available for this process was estimated to be the same as the amount of manganese reduced as described above.

3.3.3 Estimating System Lifetime Based on the Electron Balance

By manipulating the electron balance model described in Equation 3-8 through Equation 3-10, we made estimates of the system lifetime of horizontal levees. We can use this model, described in Equation 3-11 and Equation 3-12, to predict the amount of organic carbon that needs to be added initially (in the form of wood chips) to ensure sustainable long-term removal of nitrogen.

$$\Delta e^-_{\text{donors}} = \frac{e^-_{\text{donors}}|_{t_{\text{DL}}} - e^-_{\text{donors}}|_{t_o} + V_{\text{in}}[e^-_{\text{donors}}]_{\text{in}} - V_{\text{out}}[e^-_{\text{donors}}]_{\text{out}}}{t_{\text{DL}} - t_o} = \frac{-e^-_{\text{donors}}|_{t_o}}{t_{\text{DL}}} \quad \textbf{Equation 3-11}$$

where $\Delta e^-_{\text{donors}}$ represents the change in electron donating species due to utilization in keq yr^{-1}, t_{DL} and t_o represent the design life and time $t = 0$ in yr, and $e^-_{\text{donors}}|_{t_{\text{DL}}}$ and $e^-_{\text{donors}}|_{t_o}$ represent the total amount of electron equivalents stored in electron donating species at the design life and at $t = 0$ (t_o), respectively, in keq, and $V_{\text{in}}[e^-_{\text{donors}}]_{\text{in}}$ and $V_{\text{out}}[e^-_{\text{donors}}]_{\text{out}}$ represent the total mass of electron donating species applied into and taken out of the horizontal levee throughout its design life in the influent and effluent flows in keq yr^{-1}, respectively. Because dissolved organic carbon loading was equivalent between the influent and the effluent, $V_{\text{in}}[e^-_{\text{donors}}]_{\text{in}}$ and $V_{\text{out}}[e^-_{\text{donors}}]_{\text{out}}$ canceled each other out.

To estimate the design life of the horizontal levee, was set $e^-_{\text{donors}}|_{t_{DL}}$ and t_o to 0, which allows us to model the time at which storage of electron donating species is depleted and could no longer fuel denitrification. This was expanded in Equation 3-12 as follows:

$$t_{DL} = \frac{-(e^-_{\text{soil organic carbon}} + e^-_{\text{wood chips}} + e^-_{\text{Fe(II)}} + e^-_{\text{sulfide}})|_{t_o}}{\Delta e^-_{\text{soil organic carbon}} + \Delta e^-_{\text{wood chips}} + \Delta e^-_{\text{exudates}} + \Delta e^-_{\text{Fe(II)}} + \Delta e^-_{\text{sulfide}}} \qquad \textbf{Equation 3-12}$$

where e^-_i and Δe^-_i represent the amount of electron equivalents (in keq) stored in electron donor pool, *i*, and the annual rate of utilization of electron equivalents from pool *i* (in keq yr^{-1}). We can use this equation and the sets of assumptions provided in Table 3-5 to produce a range of estimates for the horizontal levee design life.

Table 3-5: Set of assumptions and parameters used to estimate the design life of a horizontal levee based on changes in the size and utilization of electron donor pools over a 2 year period.

Electron Donor Pools	Baseline	Condition A	Condition B	Condition C
(A) Indigenous sediment organic matter, keq	15,000	15,000	15,000	15,000
(B) Added wood chips, keq	31,000	31,000	31,000	**18,000**
(C) Wood chip availability, % available	56	56	56	56
(D) Available wood chips, keq (B*C)	17,000	17,000	17,000	10,000
(E) Total soil organic carbon, keq (A+D)	32,000	32,000	32,000	25,000
(F) Sulfide minerals – Fe(II), keq	50	50	50	50
(G) Sulfide minerals – S(-II), keq	440	440	440	440
(H) Total sulfide minerals, keq (F+G)	490	490	490	490
(I) Total electron donor storage, keq (E+H)	**33,000**	**33,000**	**33,000**	**19,000**
Electron Donor Turnover				
(J) Soil organic carbon removal, keq yr^{-1}	-580	-580	-580	-580
(K) Increased Fe(II)-sulfide storage, keq yr^{-1}	0	58	115	115
(L) Total plant biomass turnover, keq yr^{-1}	0	4000	4000	4000
(M) Plant biomass availability, % available	0	4	8	5
(N) Available plant biomass, keq yr^{-1} (L*M)	0	160	320	200
(O) Plant exudates, keq yr^{-1}	0	46	90	90
(P) Total ED turnover, keq yr^{-1} (J+K+N+O)	**-580**	**-310**	**-50**	**-170**
Design life (t_{DL}), yr	**56**	**105**	**660**	150

Beyond the baseline conditions described within the text and in Table 3-5, if we assume condition A, which includes fairly conservative estimates of the availability of plant root exudates, decomposing plant biomass and sulfide minerals, the estimated design life nearly doubles to 105 years. With more optimistic estimates of plant litter carbon availability and production of plant exudates and sulfide minerals, as in condition B, our model yields a much higher estimate of 660 years.

The model can also be used to determine the amount of organic carbon that needs to be added to the system and is customizable based on the availability of organic carbon. If we set a design life objective of 150 years, which is comparable or higher than the design life of many mechanical engineered water treatment systems, we can back-calculate the amount of wood chips needed to denitrify the applied nitrate load over that design life. Using condition C, we estimated that a design engineer would only need to specify the addition of ~4400 kmol C as wood chips to produce a horizontal levee system with the desired design life. To put this in context, this constitutes 43% less wood chips by mass than were added to the experimental system in this study. This approach could lead to significant savings by lowering input requirements.

3.4 Visual MINTEQ Modeling Methods and Results

Mineral saturation indexes and formation were modeled using Visual MINTEQ ver. 3.1 (https://vminteq.lwr.kth.se/visual-minteq-ver-3-1/; downloaded March 2020; Gustafsson, 2014). We used porewater measurements of dissolved metals, conductivity, and other water quality parameters, and estimated values for pH and the concentrations of dissolved inorganic carbon and sulfide as inputs to the model. Saturation indexes of various solid-phases were calculated in porewater to predict the saturation indexes of minerals in the horizontal levee. The MINTEQ database was used for all Visual MINTEQ modeling (Gustafsson, 2014).

3.4.1 Estimates of Dissolved Inorganic Carbon, Sulfide and pH

Measurements of dissolved inorganic carbon (DIC) in the influent and effluent from the horizontal levee were performed on 4 sampling dates. On three of the dates (9/5/18, 9/17/19, and 10/11/18), DIC measurements were performed in influent and effluent samples. On the other date (8/15/18), measurements were also performed on samples from intermediate wells, but from fewer of the effluent samples. Influent DIC values ranged from 0.3-0.5 mM. Effluent DIC measurements averaged 9.6-13 mM with median values ranging from 12-13 mM (excluding Cells A, B, and C). DIC concentrations in the effluent ranged from 9.0 mM to 22 mM (Figure 3-2).

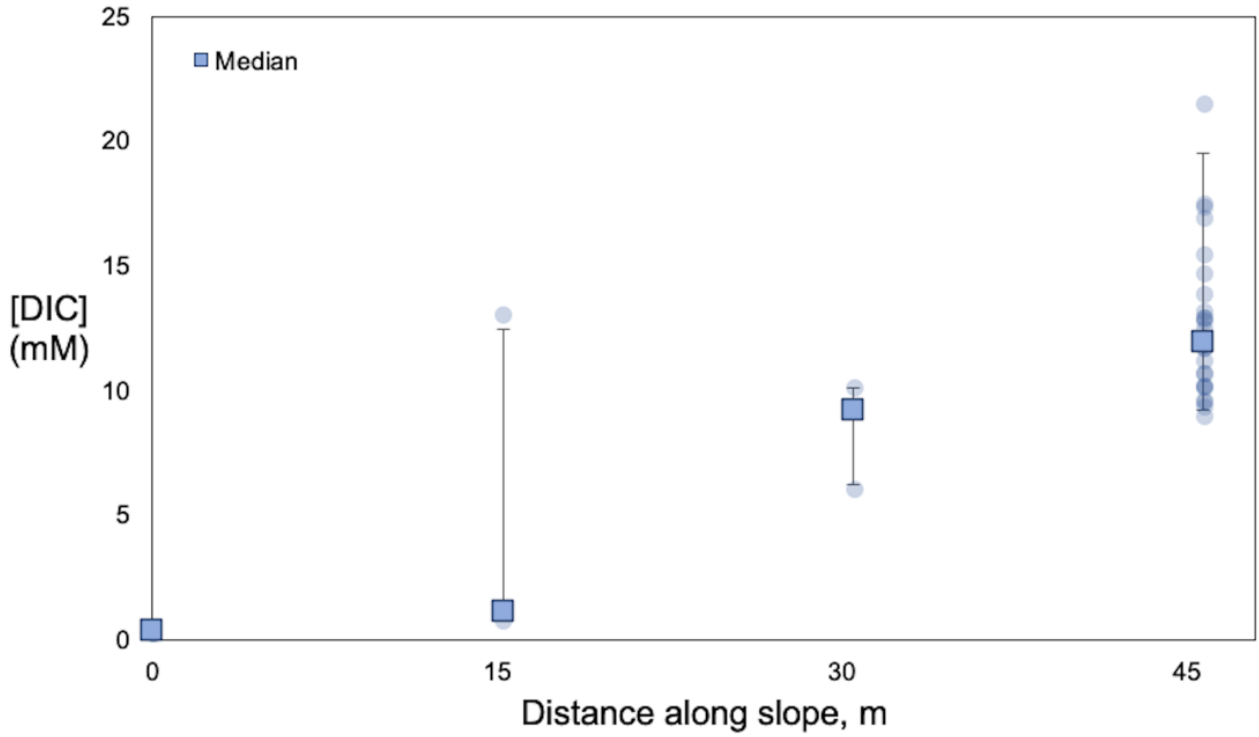

Figure 3-2: Dissolved inorganic carbon measurements in the horizontal levee from the influent, effluent and intermediate wells.

On the date when intermediate well samples were analyzed for DIC (8/15/18), DIC increased with distance along the slope. Influent DIC measurements were 0.5 mM on this date. The first intermediate wells had measurements of 13, 1.1 and 0.8 mM (in E, F and G respectively) and the second intermediate wells had measurements of 9.2, 10, and 6.1 mM of DIC. These corresponded to median

increases of 0.6 mM in the first third of the cell, and 5.3 mM, in the second third of the cell. It is possible that increasing DIC concentrations in the second third of the cell were primarily due to evapotranspiration, i.e., concentrations of inert solutes like Cl^- increased nearly by a factor of 6 in these samples (Figure 3-13).

We estimated the increase in DIC concentrations in porewater samples that was due to organic matter mineralization based on the observed reduction of electron acceptors. This was validated from dates when we had influent and effluent DIC measurements (9/5/18, 9/17/18, and 10/11/18). On those dates, we calculated values using this model that were consistent with the measured effluent DIC measurements. For example, on 9/5/18 in Cell G, we observed the following conditions (Table 3-6).

Table 3-6: Measured and modeled parameters for 9/5/18 in Cell G.

Parameter	O_2	Nitrite	Nitrate	Mn	Fe	Sulfate	DIC
e^-/mol	4	3	5	1.5	1	8	4
Measured Influent (mM)	0.1	0.03	3.0	0*	0*	1.1	0.46
Measured Effluent (mM)	0*	0.001	0.16	0.02*	0.08*	0.56	13
Adjusted Effluent (mM)†	0*	0.000	0.07	0.05*	0.2*	0.23	5.3
Projected ΔDIC (mM)†	0.09	0.02	3.6	0.02	0.05	0.55	**4.8**

*Modeled based on measurements taken on other dates. †Adjusted to account for evapotranspiration rates.

For each species (e.g., DO, nitrate), effluent concentrations were subtracted from the influent and converted to the stoichiometrically appropriate amount of organic carbon converted to DIC. An example for nitrate is shown below:

$$\frac{1}{5}NO_3^- + \frac{6}{5}H^+ + e^- \leftrightarrow \frac{1}{10}N_2 + \frac{3}{5}H_2O$$
$$+ \frac{1}{4}CH_2O + \frac{1}{4}H_2O \leftrightarrow \frac{1}{4}CO_2 + H^+ + e^-$$
$$\frac{1}{5}NO_3^- + \frac{1}{4}CH_2O + \frac{1}{5}H^+ \leftrightarrow \frac{1}{10}N_2 + \frac{1}{4}CO_2 + \frac{7}{20}H_2O$$

We then calculated DIC as: (3.0 – 0.16 mM)*(5 meq (mmol N)$^{-1}$)/(4 meq (mmol C)$^{-1}$) = 3.6 mM.

For Cell G on 9/5/18, we measured effluent DIC concentrations of 13 mM, which corresponds to 5.3 mM when adjusted based on ET (i.e., if the effluent flow were the same as the influent flow, the concentration would have been 5.3 mM, but because ~60% of the water was lost to evapotranspiration, the DIC concentration was additionally "concentrated" to 13 mM). A fraction of DIC may have also been lost to the atmosphere through efflux as CO_2 during evapotranspiration, thought we expect this fraction to be small (Atekwana et al., 2016). Our method yielded an "adjusted" value of 4.8 mM, which would correspond to a measured value of ~12 mM based on that evapotranspiration rate (Figure 3-13). On 9/5/18 and 9/17/18, projected estimates of effluent DIC (DIC produced per electron acceptor process + influent DIC) for individual cells were not statistically different from measured values ($p = 0.68$ and 0.79, paired t-tests) with only a 2-3% difference between measured and projected values. In contrast, projected values on 10/11/18 were ~30% lower than measured values. We note that influent nitrate and sulfate concentrations (2.4 mM and 1.2 mM) were around 15-30% lower than values on other dates, which may explain these discrepancies.

We extrapolated the estimation method above to individual porewater samples by taking the difference in concentrations of electron acceptors between those samples and the influent and translating those

values into DIC produced based on electrons consumed per mole electron acceptor and electrons produced per mol of DIC produced (and organic carbon consumed). Values for individual electron acceptors were then summed to estimate DIC concentration for each sample. These DIC values were adjusted using chloride concentrations in porewater to account for the impact of ET (which increased concentrations of remaining aqueous species by removing water volume). This model was used with median concentrations of DO, nitrate, Mn, Fe and sulfate (and chloride) at various distances and plotted them with measured DIC values for intermediate wells, the influent and the effluent on Figure 3-3.

According to this model, there is a rapid increase in DIC in the first few meters of the slope (where nitrate and sulfate reduction are the most significant) followed by a relatively slow increase in DIC for the remaining portions of the wetland, which is primarily caused by loss of water via evapotranspiration. This model agreed well with the measured values from intermediate wells and the effluent from 8/15/18, especially for latter values. Because there are somewhat wide variations in the parts of the wetland where different microbial processes occur, this model gave more accurate estimates of DIC at various locations throughout the slope than a simple linear model of DIC from the influent to the effluent would have given. Individual outputs for the model based on utilization of electron acceptors differed from a simpler linear model by up to 82% at certain distances along the slope, though these differences were not significant overall ($p = 0.21$; paired t-test). Additionally, our model was used to track shifts in DIC concentrations precisely over small changes in distance.

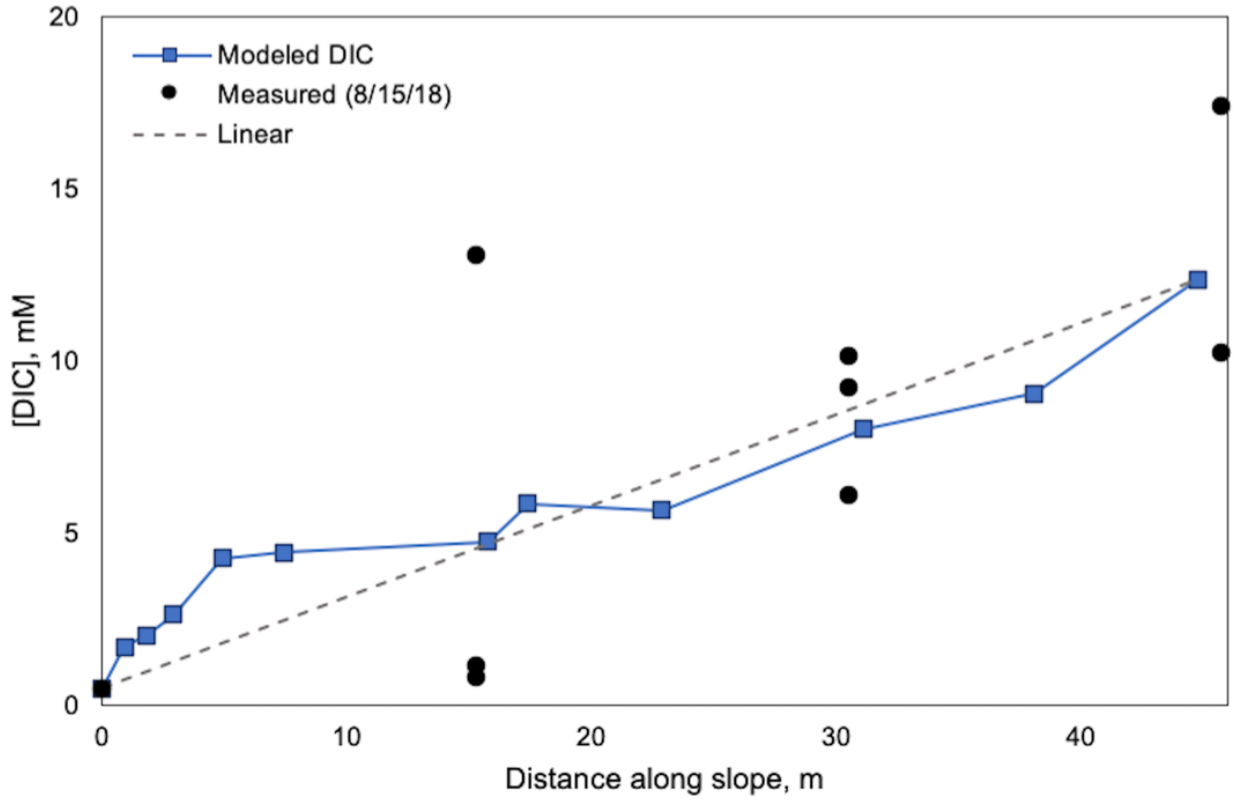

Figure 3-3: Modeled and measured DIC concentrations with distance along the slope compared with a linear DIC model.

pH in porewater samples was modeled using a linear relationship between the influent and effluent. pH values measured throughout the monitoring period are presented in Figure 3-4. This model agreed well with measurements of pH conducted in intermediate wells.

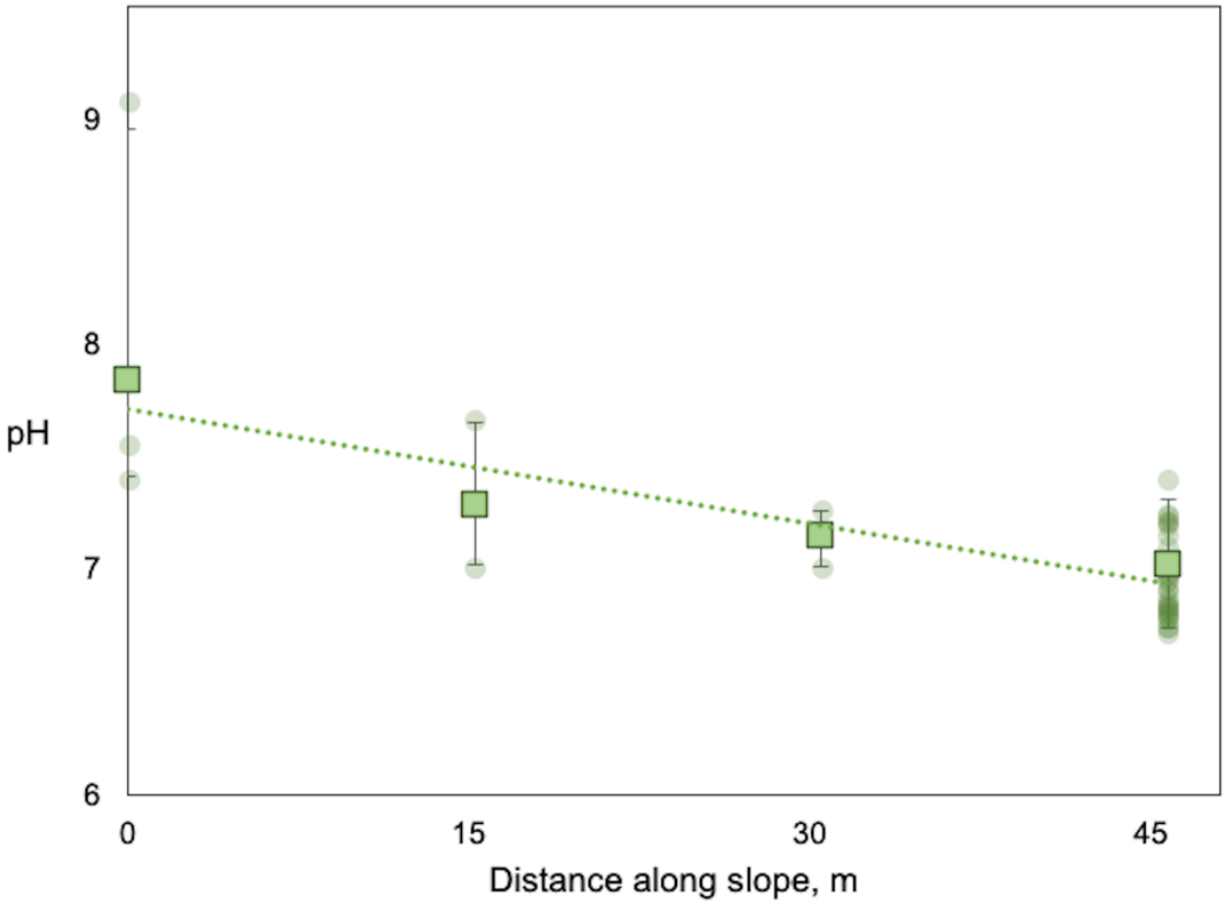

Figure 3-4: Modeled and measured pH throughout the monitoring period.

In Visual MINTEQ, sulfide was modeled with upper and lower bounds. The upper bound for dissolved concentrations was estimated based on the amount of sulfate reduced in the subsurface. This was considered the maximum possible sulfide concentration for the purposes of our modeling. Conversely, the lower bound for sulfide concentrations was modeled as the aqueous concentration of sulfide that would be in equilibrium with the odor threshold for sulfide in air (a partial pressure of approximately 0.3 mPa; Wilby, 1969). We used the odor threshold for sulfide because we consistently detected a sulfide odor in porewater samples collected across the entire wetland. Based on this modeling, we approximated that the lower bound of sulfide concentrations in the subsurface likely ranged between 0.4 and 27 nM depending on the temperature and pH of the individual sample.

3.4.2 Visual MINTEQ Outputs

Modeling in Visual MINTEQ was conducted for each individual porewater sample. Raw data for saturation indexes and speciation of dissolved complexes modeled in Visual MINTEQ are reported on Mendeley Data (Cecchetti et al., 2020b).

First 5 m of the wetland. In the first 5 m after the inlet to the wetland, few mineral phases were supersaturated. Concentrations of both dissolved inorganic carbon (DIC) and sulfide were lower in earlier portions of the wetland because sulfate reduction was not significant in most wetland cells until after approximately 5 m and because the cumulative amount of aqueous Fe(II) and Mn(II) produced and microbial respiration that had occurred increased with distance. Additionally, evapotranspiration concentrated dissolved species as water approached the outlet. Carbonate minerals, such as rhodochrosite (i.e., Mn(II)-carbonate; Figure 3-5a) and siderite (i.e., Fe(II)-carbonate; Figure 3-5b), remained saturated or undersaturated in the early portions of the slope, although calcite was often supersaturated due to high inlet Ca^{2+} concentrations. Sulfide minerals, such as FeS (Figure 3-6a) and Mackinawite (Figure 3-6b), were largely undersaturated at these distances, but the saturation indexes for those minerals increased with distance in early portions of the wetland.

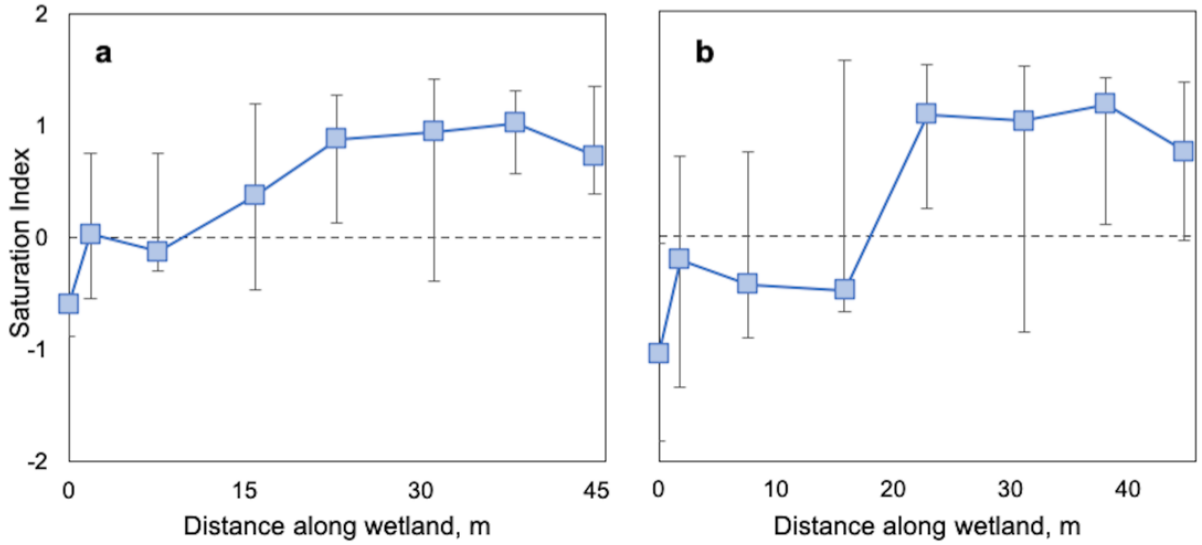

Figure 3-5: Median saturation indexes for (a) rhodochrosite ($MnCO_{3(s)}$) and (b) siderite ($FeCO_{3(s)}$) across the range of conditions modeled with distance along the wetland slope. Error bars represent 95th percentile values.

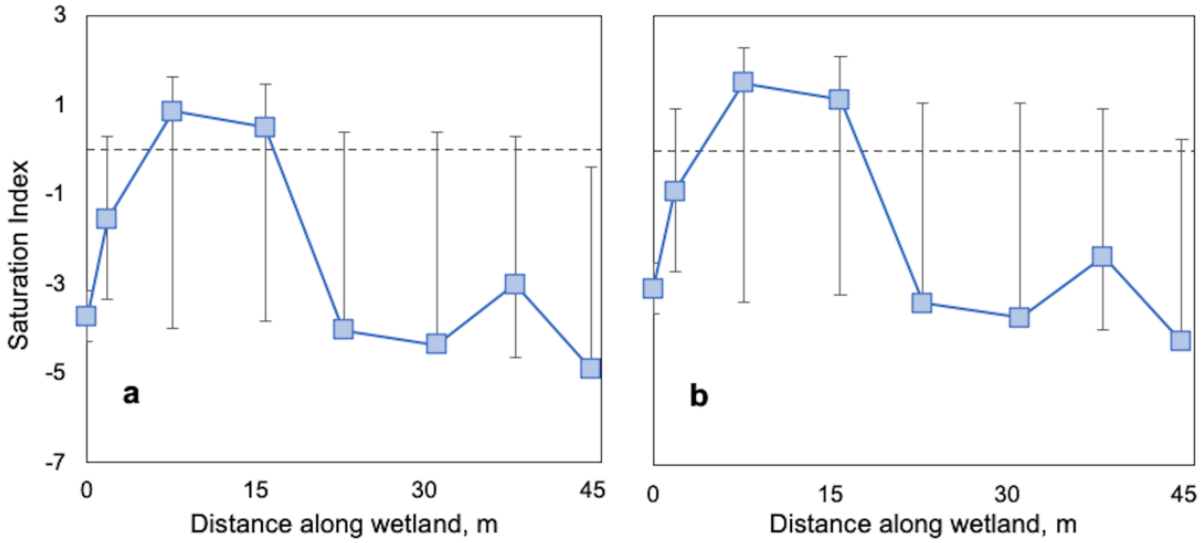

Figure 3-6: Median saturation indexes for (a) amorphous FeS precipitates and (b) Mackinawite (FeS) across the range of conditions modeled. Error bars represent 95th percentile values.

Intermediate portion of the wetland. At intermediate distances along the slope, i.e., approximately between 5 to 20 m, sulfide minerals became supersaturated with median saturation indexes that were approximately 0.5-1.5. Carbonate minerals largely remained at or near saturation.

At these distances, formation of sulfide was significant in most cells due to rapid sulfate reduction. Visual MINTEQ modeling suggested that sulfide minerals would form over these distances, which was supported by other observations at the pilot horizontal levee. For example, samples of sediments collected from the subsurface at distances between 5 and 25 m along the wetland slope were frequently coated with black residues (Figure 3-7). Black residues in reducing sediments are a strong indication of iron sulfide mineral deposition on soils (Cornwell and Morse, 1987) and plant roots (LaFond-Hudson et al., 2018). Additionally, during porewater sampling, mobilized black sediments were frequently observed in porewater that was collected (likely due to agitation during sampling). These black sediments had to be filtered out of aqueous samples.

Figure 3-7: Soil samples stored in 50 mL centrifuge tubes collected from the bottom layer of soil in the horizontal levee. Samples are organized from left to right according to the distance they were collected from along the slope (1.5 m, 6 m, 23 m, and 38 m respectively). Samples collected from 6 and 23 m show visual evidence of high sulfide mineral accumulation (dark sediments).

Latter portions of the wetland. In the final portions of the wetland (between 25 and 45 m), saturation indexes for sulfide minerals decreased significantly (to around -3 to -4) and remained low. Conversely, saturation indexes for rhodochrosite and siderite increased to values around 1 in this portion of the slope. The supersaturation of carbonate minerals combined with the long residence times in the latter portion of the slope, as described in Chapter 2 (Cecchetti et al., 2020a) and section A.3 of Appendix A, suggested that the small changes in $Mn_{(aq)}$ and $Fe_{(aq)}$ concentrations were likely caused by carbonate

mineral precipitation leading to lower aqueous concentrations of those species than we would have expected otherwise.

Seasonality of mineral saturation indexes. Some general seasonal trends were observed in the saturation indexes of sulfide minerals with distance along the slope (Figure 3-8a). In the summer, saturation indexes suggested that sulfide minerals were supersaturated earlier in the slope, becoming supersaturated around 1.5 m from the inlet. In the winter, saturation indexes were significantly lower in the first 5 m of the wetland ($p < 0.02$; one-tailed Wilcoxon sign-rank test) and supersaturation did not occur until after 5 m from the inlet. This suggests that sulfide mineral formation likely occurred earlier in the slope during the summer and possibly within the zone where nitrate reduction also occurred. Significant differences were not observed ($p = 0.64$; Wilcoxon signed-rank test) for siderite saturation indexes between the summer and the winter.

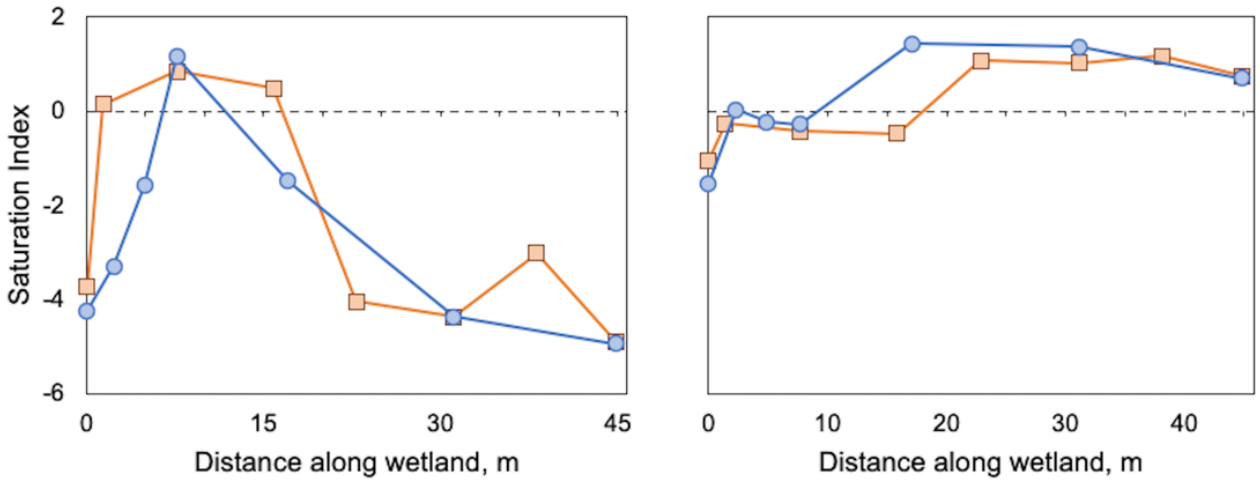

Figure 3-8: Seasonal saturation indexes for (a) amorphous FeS precipitates and (b) siderite ($FeCO_3$). Median values are plotted across cells based on aqueous measurements collected along the wetland slope, modeled using Visual MINTEQ. Blue circles represent winter and spring measurements and orange boxes represent summer and fall measurements.

3.5 Methods for Modeling the Production, Decomposition and Reintegration of Plant Residues

3.5.1 Production of Litterfall and Decaying Plant Roots

Total production of litterfall (kg DW yr^{-1}) in the horizontal levee was modeled by multiplying the peak standing biomass (B_{peak}; kg DW m^{-2}) by the biomass turnover rate (θ_b; yr^{-1}) and the total area of the wetland (6700 m^{-2}), as described in Chapter 4 (Cecchetti et al., *submitted*). This was conducted individually for each cell and then summed over the whole wetland. All litter produced was assumed to deposit onto the wetland surface. Above ground litterfall was modeled separately from below ground decaying plant roots. Values for peak standing biomass and turnover rates are reported in Chapter 4 (Cecchetti et al., *submitted*). Total litterfall produced in each cell over the years modeled are presented in Table 3-7.

Litterfall amounts were further broken down by the month of production according to the fractions of litterfall produced presented in Figure 3-9. These values were estimated based on seasonal litterfall

production presented in the literature (Deghi et al., 1980; Neiff and Poi de Neiff, 1990; Conner and Day, 1992; Ozalp et al., 2007; Kadlec and Wallace, 2009). The greatest fraction of litterfall production occurred between August and November, with 12%, 20%, 27%, and 20% of annual litterfall production occurring in those months, following expected seasonal trends.

Table 3-7: Litterfall production (kg DW) per year and per cell.

	By Cell									
Year	D	E	F	G	H	I	J	K	L	Total
2017*	910	820	950	1100	640	1500	540	1400	600	8500
2018	1300	1400	1400	1900	690	2200	640	2000	620	12000
2019**	470	470	490	600	230	750	240	720	250	4200
Overall	2700	2700	2900	3600	1600	4500	1400	4100	1500	25000

*Litterfall production was included for all of 2017 is presented, though only dates past June 2017 were within the monitoring period. **Litterfall values for 2019 only include up through June 2019.

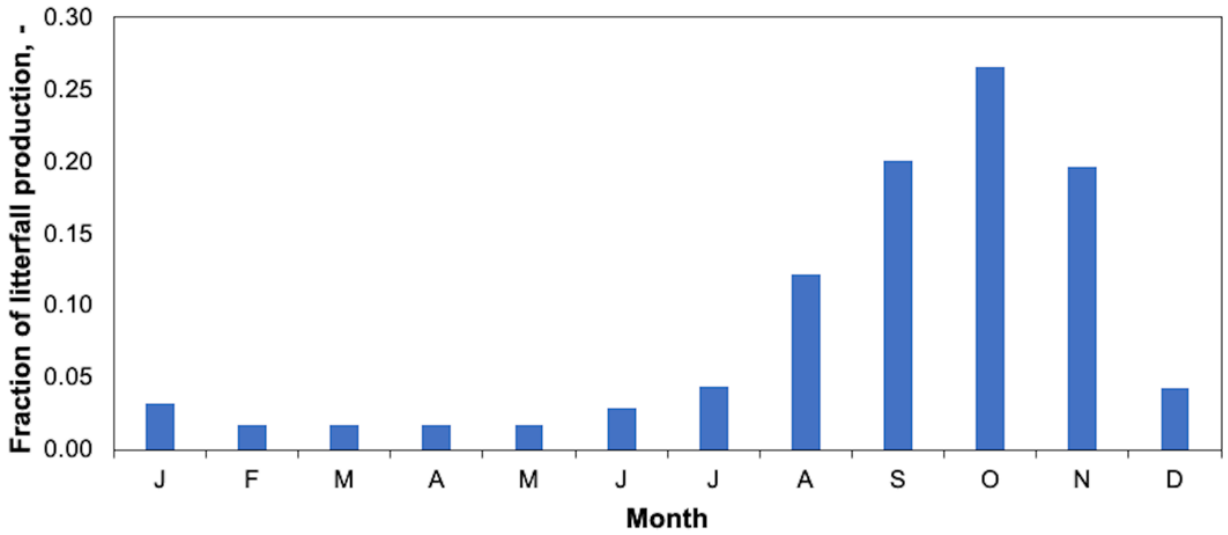

Figure 3-9: Fraction of litterfall produced by month at the horizontal levee.

The mass of senesced plant roots was also modeled according to the method described above, though the plant root senescence by month was assumed to be roughly uniform over the entire year because plant root production and turnover is not as seasonally dependent as above ground biomass is. Root biomass weights and turnover rates were modeled according to relationships presented in the Gill et al. (2002) and as described in Chapter 4 (Cecchetti et al., *submitted*). Senesced root biomass production by cell over the monitoring period is presented in Table 3-8.

Table 3-8: Senesced root biomass production (kg DW) per year and per cell.

	By Cell									
Year	D	E	F	G	H	I	J	K	L	Total
2017*	150	140	150	170	500	190	450	190	480	2400
2018	180	180	190	220	690	240	660	220	640	3200
2019**	150	150	150	180	550	210	570	200	600	2800
Overall	470	480	490	560	1700	640	1700	610	1700	8400

*Litterfall production was included for all of 2017 is presented, though only dates past June 2017 were within the monitoring period. **Litterfall values for 2019 only include up through June 2019.

3.5.2 Decomposition of Litterfall and Senesced Root Biomass

The amount of litterfall remaining over time depended on decomposition rates. In the literature, litterfall decomposition rates are typically modeled according to an exponential model:

$$Y_t/Y_o = e^{-K*t} \qquad \textbf{Equation 3-13}$$

where Y_t/Y_o is the fraction of deposited material remaining at time t (yr) and K is the decay constant with units of yr^{-1} (Mackey and Smail, 1996). Litter decomposition decay rate constants reported in the literature range from 0.7 to 26.4, corresponding to half-lives of 10 days up to a full year. Based on a review of literature values (Deghi et al., 1980; Twilley et al., 1986; Flores-Verdugo et al., 1987; Mackey and Smail, 1996; Twilley et al., 1997; Wafar et al., 1997; Ashton et al., 1999; Tovilla and de la Lanza, 1999; Chimner and Ewel, 2005; Poi de Neiff et al., 2006; Aké-Castillo et al., 2006; Ozalp et al., 2007; Kadlec and Wallace, 2009), we found a median decay constant 3.5 yr^{-1}. However, the sites in those studies varied widely in terms of latitude, climate, site conditions and seasonal temperatures, all of which can affect decomposition.

There are strong relationships between decomposition rates and latitude (Twilley et al., 1997) and between decomposition rates and mean annual temperature (Figure 3-10). Based on latitude (approximately 37.7ºN), we calculated a K value of 3.8 yr^{-1} for the horizontal levee site, whereas based on temperature (with approximately 15 ºC as a mean annual temperature), we estimated a K value of 1.5 yr^{-1}. The latter value was more similar to mean K values reported for *Phragmites* species (1.4 yr^{-1}), *Typha* species (1.4 yr^{-1}), and *Scirpus* species (1.7 yr^{-1}) by Kadlec and Wallace (2009) (reviewing previous studies) for constructed wetlands. For this reason, we used a K value of 1.4 yr^{-1} to model above ground litterfall decomposition in the horizontal levee, which corresponds approximately to a half-life of 150 days. For belowground biomass in constructed wetlands, various studies reviewed by Kadlec and Wallace (2009) found that decaying belowground biomass had a half-life of approximately 1.5-2.0 yr, which corresponds to K = 0.4 yr^{-1}. This value was used to model root decomposition (Kadlec and Wallace, 2009).

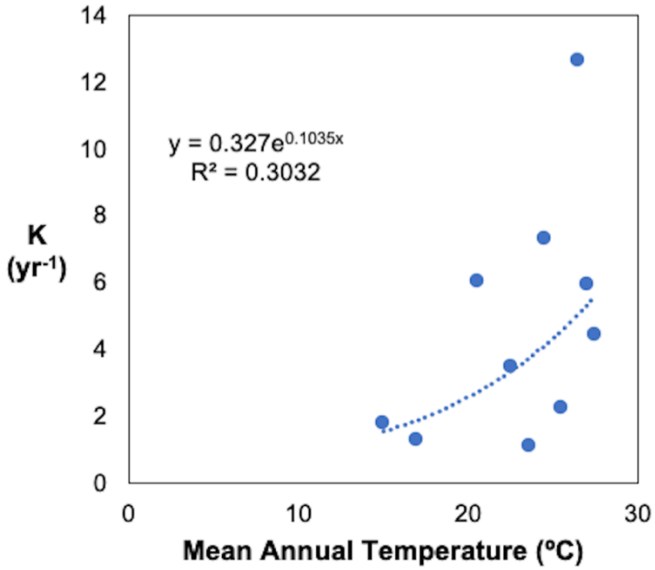

Figure 3-10: Relationship between mean annual temperature (MAT) and litterfall decomposition rate constants (K).

Changes in C:N ratios in litter were modeled using C:N measurements reported by Ozalp et al. (2007) over time. We related fractional changes in C:N measurements to the fraction of biomass remaining using an exponential function as delineated in Figure 3-11. Initial C:N measurements in litterfall at the field site were approximately 26. At the end of 2018, when approximately 49% of the litterfall inputs were remaining, we projected that the C:N ratio in remaining litter had decreased to approximately 12. This approximation method was supported by samples collected in January 2019, when fresh litter had C:N ratios that were already lower on average (median C:N value of 26) than the living biomass collected from the same location (median C:N of 29).

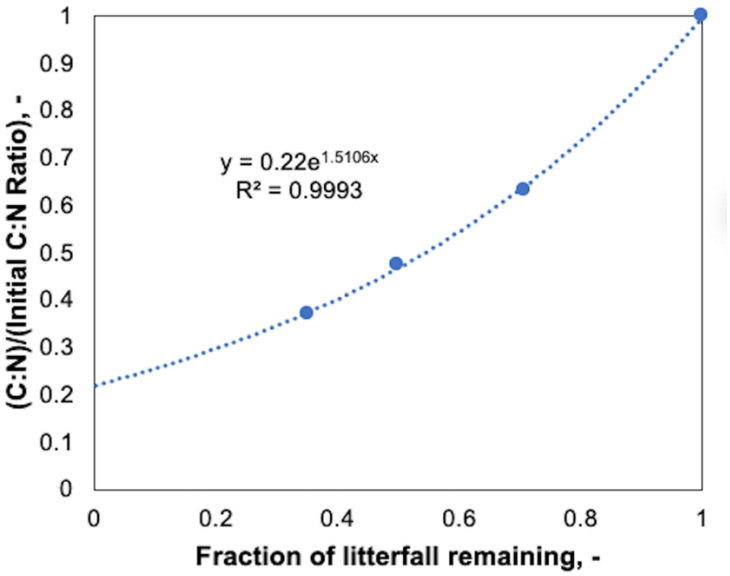

Figure 3-11: Relationship between the fractional change in C:N ratios (C:N at sampling time divided by initial C:N) and the fraction of litterfall remaining at that time.

To model remaining litterfall in the horizontal levee, we multiplied the total litterfall values produced in Table 3-7 and Table 3-8 by the fraction of that litterfall produced each month (using Figure 3-9 for above ground biomass and a uniform distribution for plant roots). Then, we modeled the amount of that litter remaining over the succeeding months by adjusting the initial litterfall mass value according to Equation 3-13 based on the amount of time that had passed. By dividing the total amount of remaining litterfall by the total amount that had been produced up to that point and using the exponential relationship in Figure 3-11, we estimated the C:N ratio at each time point.

At the end of the monitoring period (June 2019), 29000 kg DW of above ground litter and 8400 kg DW of senesced root biomass had been produced over the monitoring period. 9000 kg DW of above ground litter remained undecomposed (32% of initial input) and 5900 kg DW of root biomass remained (70%). The modeled C:N ratios were 9.1 and 16 for remaining above ground biomass litter and senesced root biomass respectively.

3.5.3 Integration of Litterfall and Senesced Root Biomass into Wetland Sediments

Partially decomposed litterfall and senesced root biomass integrated into the wetland sediments at variable rates. All senesced root biomass was assumed to be integrated into the wetland sediment organic matter (as described in section 3.3) regardless of decay rate because decaying roots are located

within the soil matrix and would be measured as a part of soil %C measurements conducted in this study.

Integration of partially decomposed above ground litter was estimated based on depth-resolved measurements of %N, %C, $\delta^{15}N$ and $\delta^{13}C$ conducted in April 2018 (Figure 3-12).

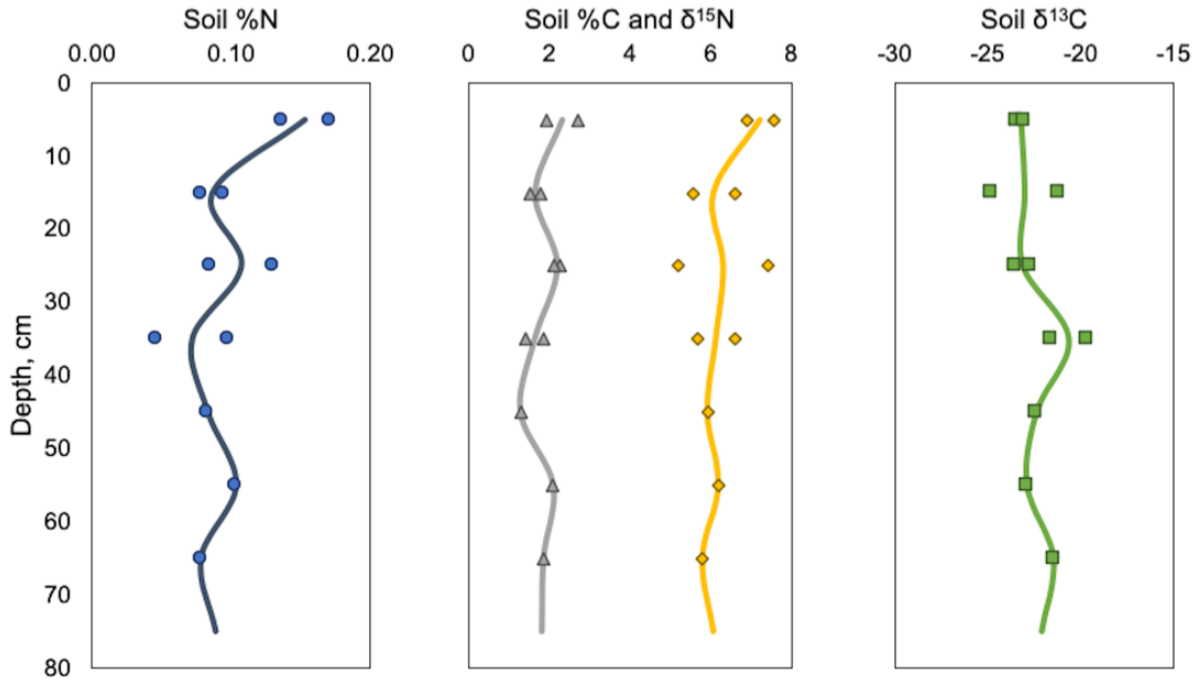

Figure 3-12: Depth-resolved soil measurements of %N (blue circles), %C (grey triangles), $\delta^{15}N$ (yellow diamonds) and $\delta^{13}C$ (green squares). Lines represent moving averages.

Differences were observed between surface soil layers (deaths of 0-10 cm) and deeper layers for all of these measurements. For example, %N was 0.15% on average in surface layers compared to average values of 0.09% in lower layers – a 73% increase in topsoil nitrogen content. Measurements of %C, $\delta^{15}N$ and $\delta^{13}C$ in surfaces soils were 26% higher, 1.1‰ higher and 1‰ lower, respectively. All of these trends matched our expectations based on inputs of organic matter from plant residues. Measurements of %C and %N in deeper layers were not statistically different from samples collected in the previous year ($p = 0.41$ and $p = 0.26$). Using the increased %N and %C values in the top 10 cm of the soil, we estimated that 350 kmol C and 25 kmol N had been added to the topsoil between April 2017 and April 2018. If we assume that this increase in nitrogen and carbon comes from litter carbon (400 kmol C) and nitrogen (35 kmol N) remaining at the end of that period of time, this corresponds to an estimate that 71-87% of partially decomposed litter integrated into wetland surface soils.

Additionally, we conducted mixing models using the $\delta^{15}N$ and $\delta^{13}C$ values in the surface soils (7.2‰ and -23.4‰, respectively), with average plant values (11.0‰ and -29.3‰) and soil values from previous sampling dates (5.8‰ and -22.0‰) as endmembers. From these models, we estimated that 14-17% of carbon and 5-23% of nitrogen in the top 30 cm of the soil came from plant biomass. This corresponds to 300 kmol C (75% of decomposed litter) and 23 kmol N (65% of N from decomposed litter), though these estimates may be low due to differences in $\delta^{15}N$ and $\delta^{13}C$ between plant roots and above ground biomass, which we did not account for in the mixing models.

Based on these values, we estimated that approximately 75-80% of decomposing plant litter and decaying plant roots were integrated into the plant soil carbon and nitrogen components of the mass balances conducted in section 3.3.

3.6 Results and Discussion

In the pilot horizontal levee, the flow of water played a critical role in nitrogen removal, as described in Chapter 2 (Cecchetti et al., 2020a). Applied wastewater effluent either underwent subsurface flow, where nitrogen was efficiently removed as water moved through the subsurface for approximately 10 to 20 days, or overland flow, which resulted in hydraulic residence times on the order of 10 to 24 hours and negligible nitrogen removal. Evapotranspiration concentrated solutes in the remaining water (e.g., porewater chloride concentrations increased by up to a factor of 5 times in the pilot system; Figure 3-13). Because evapotranspiration removed a large volume of water from the subsurface, porewater concentrations were normalized by using conductivity measurements. The swale cells (i.e., cells A-C), illustrated the importance of subsurface flow; less than 35% of the applied nitrogen was removed in these cells due to the fact that approximately 60% of the flow never infiltrated into the subsurface layers. As a result, these cells were excluded from the following analyses. The full dataset is available on Mendeley Data (Cecchetti et al., 2020b).

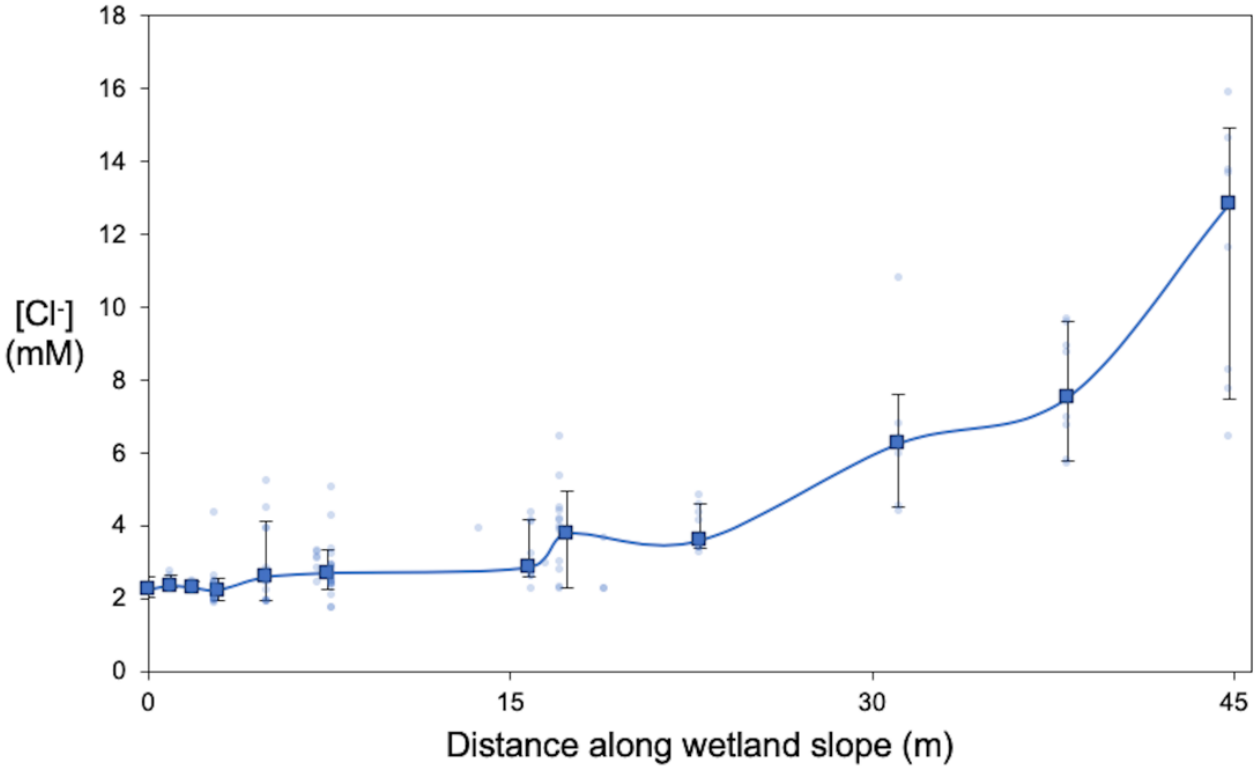

Figure 3-13: Concentrations of chloride in porewater collected from the bottom sediment layer of the horizontal levee subsurface. Samples were collected among cells D-L on a variety of dates.

3.6.1 Nitrogen Cycling in the Horizontal Levee

Throughout the 2-yr monitoring period (June 2017 – June 2019), nitrogen species were removed efficiently in the horizontal levee, particularly when hydraulic conditions were optimized, as described in Chapter 2 (Cecchetti et al., 2020a). Removal of nitrate, ammonium and nitrite exceeded 98% when overland flow was eliminated. However, only about 40% of the dissolved organic nitrogen (DON) was removed under those conditions. Nitrate accounted for the majority of nitrogen lost at over 80% of total influent nitrogen during the two year study (Figure 3-14a). Of the approximately 100 kmol N removed, 77% consisted of nitrate, with ammonium, nitrite and dissolved organic nitrogen (DON) accounting for the remaining 23% (24 kmol N).

Porewater concentrations of dissolved nitrogen species (Figure 3-15) followed consistent trends in the 9 cells studied. Removal of nitrate was rapid and significant ($p < 0.03$) in the first 5 m of the wetland (Figure 3-15). Ammonium and nitrite were also removed in the first 2 m while concentrations of DON did not change significantly ($p = 0.13$) as water passed through the first 15 m of the wetland. After 15 m, nitrogen concentrations did not change significantly ($p > 0.05$). No significant differences ($p > 0.05$) were observed in porewater nitrogen concentrations seasonally or among wetland cell types (cell types are described in Appendix A), except for nitrite, which had significantly lower concentrations ($p < 0.02$) in wet meadow cells with coarse soils.

Mass balance calculations (see section 3.3) indicated that out of the 104 kmol of wastewater-derived nitrogen removed during the monitoring period, approximately 81 kmol N (77%) were removed by conversion to gaseous forms (i.e., presumably $N_{2(g)}$ and $N_2O_{(g)}$) (Figure 3-14b). An additional 15 kmol N (14%) were assimilated into microbial biomass or stored in solid particulate forms in the soil. The remaining 8.8 kmol N (8%) was taken up into above ground plant biomass (6.6 kmol) or plant roots (2.2. kmol), as reported in Chapter 4 (Cecchetti et al., *submitted*). The flows of nitrogen between different compartments were substantial in the horizontal levee (Figure 3-14b). Assuming that soil nitrogen reached a steady state and that plant and litterfall turnover had reached maturity by the end of the monitoring period, these compartments would not represent important long-term sinks of wastewater-derived nitrogen; only denitrification and anammox can explain the observed loss of dissolved nitrogen species.

In constructed wetlands with organic matter-rich water-saturated sediments and plentiful nitrate, denitrification is often the dominant nitrate removal mechanism (Ingersoll and Baker, 1998; Wen et al., 2010; Chen et al., 2014) because oxygen is rapidly consumed (Rivett et al., 2008). We hypothesized that denitrification was the main nitrate removal pathway because there was a substantial source of organic carbon (i.e., wood chips and decaying plants), rapid removal of nitrate was observed in porewater samples and there was clear evidence of reduction of iron and sulfate coincident with the location where nitrate concentrations decreased. Additionally, as reported in Chapter 4 (Cecchetti et al., *submitted*), we observed a strong coupling of $\delta^{18}O$ and $\delta^{15}N$ in nitrate in porewater collected within the first few meters of the inlet. In these samples, the fractionation of oxygen and nitrogen isotopes were strongly correlated (Figure 4-11; Chapter 4) as is typical when denitrification is the dominant removal process affecting nitrate (Kendall, 1998; Dähnke and Thamdrup, 2016). In contrast, if nitrate removal involved anammox, a decoupling of $\delta^{18}O$ and $\delta^{15}N$ caused by re-oxidation of nitrite during carbon fixation (Dähnke and Thamdrup, 2016) would have been expected during nitrate removal.

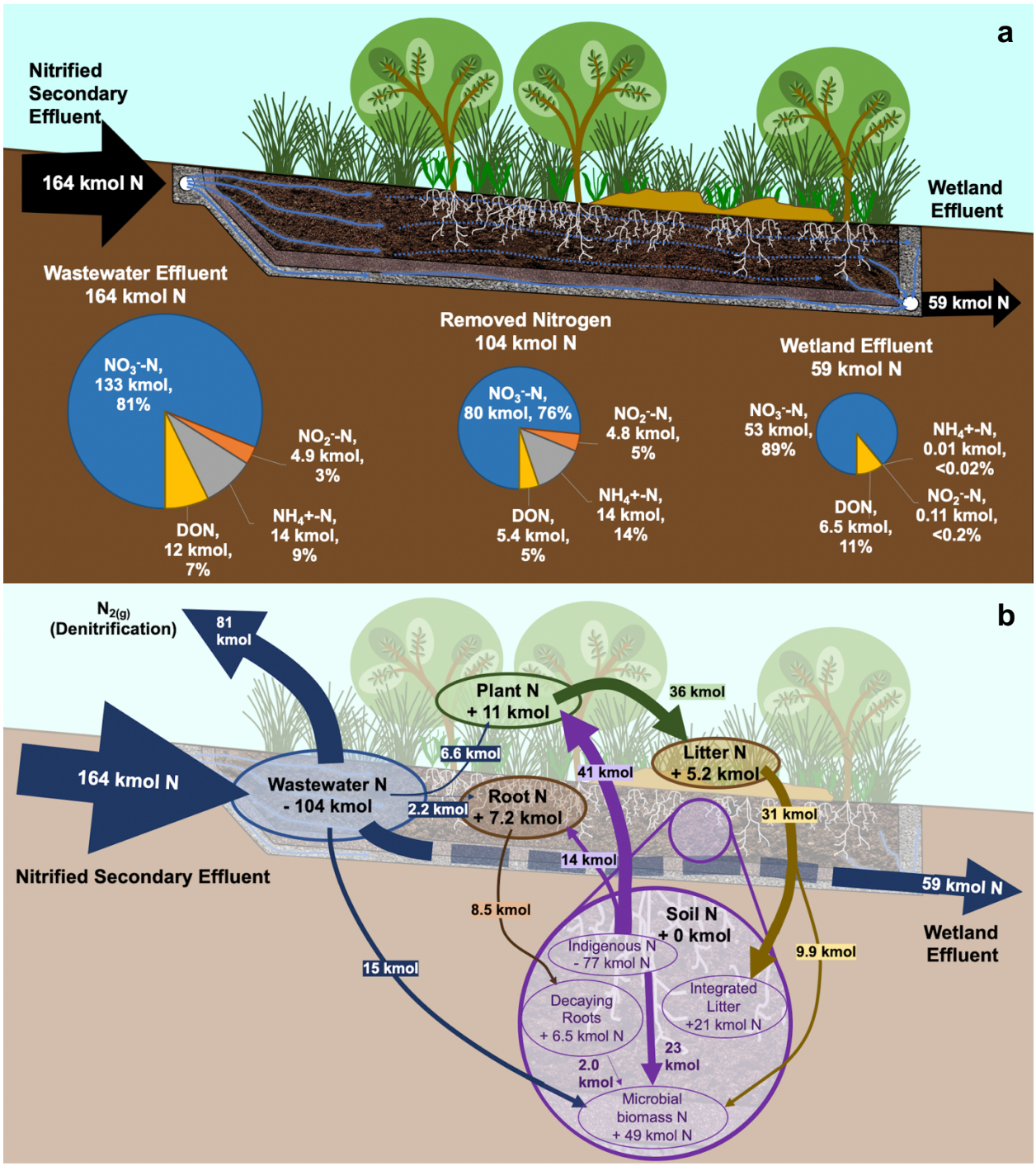

Figure 3-14: Illustrations of nitrogen mass balances over the 2-year monitoring period. (a) Aqueous nitrogen species distributions in the influent, removed nitrogen and effluent. (b) Mass balances conducted on nitrogen. Blue arrows and white text represent wastewater-derived nitrogen flows and their magnitude. Net changes in the size of nitrogen storage pools (e.g., "Plant N") are indicated with black text in the ovals corresponding to each pool; the magnitude of that change is represented by +/– kmol N. Purple arrows, ovals and text represent flows of soil nitrogen, soil nitrogen components, and changes in the size of those components. Green, brown and tan arrows represent flows of nitrogen from above ground plant biomass, plant roots and plant litter.

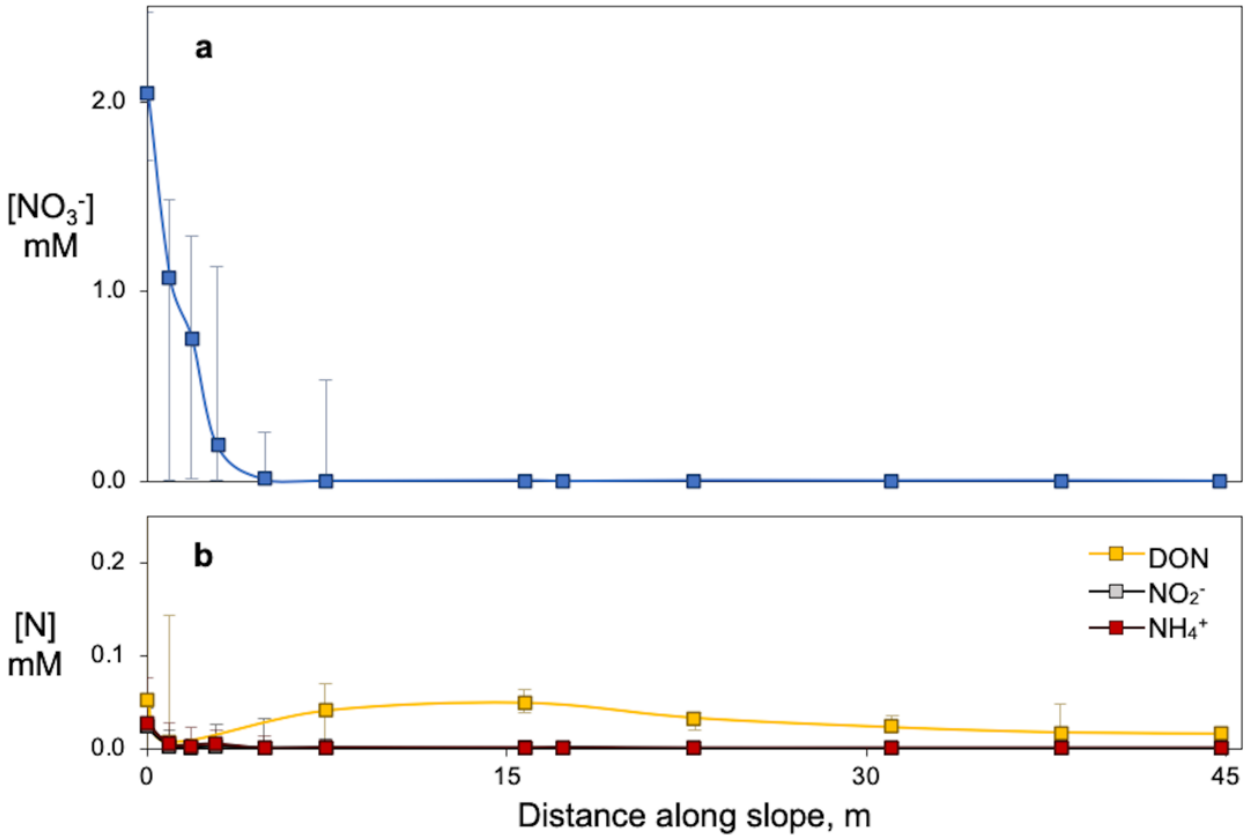

Figure 3-15: Median porewater nitrogen concentrations with 90th and 10th percentile error bars: (a) nitrate; and, (b) other dissolved nitrogen species, collected from the gravel/coarse sand layer of the subsurface. Note the difference in scales. Acronyms: DON = dissolved organic nitrogen.

Other nitrate consumption processes (e.g., DNRA and anammox) can be significant in natural ecosystems (Burgin and Hamilton, 2007) and constructed wetlands (Saeed and Sun, 2012), but we did not observe any biogeochemical evidence to indicate that these processes were significant. Dissimilatory nitrate reduction to ammonium (DNRA) is typically dominant in natural ecosystems when C:N ratios are greater than 12 (Burgin and Hamilton, 2007; Rütting et al., 2011; Murphy et al., 2020). Although C:N ratios greater than 18 were observed just after the inlet to this system, DNRA was not a significant nitrate transformation mechanism, possibly because C:N ratios in the aqueous phase (which ranged from 0.2 to 7.4 in porewater) were lower and not all of the organic carbon in the system was bioavailable (see organic carbon cycling and mass balance).

We only observed evidence of DNRA (i.e., ammonium formation) when nitrate dropped to low levels (e.g., < 10 µM; when >99.5% of nitrate had been removed) (Figure 3-18). DNRA was particularly evident in April 2019, when transient formation of ammonium (an increase of ~10 µM after ~3.5 m along the slope) was observed, but only after the majority (>99.5%) of nitrate had been removed (Figure 3-18). On other dates when similar transient ammonium formation was observed, it only occurred at low nitrate concentrations. Ammonium concentrations rarely exceeded 0.4 mM in the influent to the horizontal levee and decreased rapidly in the subsurface with >99% of porewater ammonium measurements below 24 µM (Figure 3-15). In contrast, in the biomat of open-water treatment wetlands where DNRA can be significant, transient ammonium concentrations up to around

1.8 mM have been observed (Jasper et al., 2014; Jones et al., 2017). It is possible that the products of processes like DNRA were consumed too rapidly in the horizontal levee to be observed (Kappler and Bryce, 2017). The low significance of DNRA in this system is consistent with findings in engineered treatment systems, where denitrification is often dominant at high C:N ratios, especially if there are high inputs of nitrate (Wen et al., 2010; Behrendt et al., 2014).

Ammonium accounted for 14% of nitrogen removed. Its loss was likely explained by microbial assimilation because microorganisms preferentially utilize ammonium (Inamori et al., 2008) over nitrate and DON. A significant fraction of ammonium loading occurred during a period of approximately 6 months between the spring and fall of 2018 when the onsite nitrification facility was not operating efficiently. During that period ammonium frequently comprised up to 20% of the influent nitrogen, compared to approximately 2% over the last 6 months of monitoring. In addition to microbial assimilation, anammox and Feammox can remove ammonium under anoxic conditions in natural systems (Yang et al., 2012a; Li et al., 2015) and constructed wetlands (Shuai and Jaffé, 2019). Anammox requires inputs of nitrite or biological conversion of ammonium or nitrate into nitrite, which we did not observe, possibly due to its rapid consumption. We also did not observe evidence of Feammox, which forms nitrite as a product (Shuai and Jaffé, 2019), despite the large amount of iron stored in the soil (~2200 kmol Fe). However, nitrite is frequently the limiting reactant for anammox and rarely accumulates during denitrification except when there is insufficient labile organic carbon (Kadlec and Wallace, 2009), which was not the case in this system. Based on ammonium removal, we conclude that the maximum contribution of anammox and Feammox to total nitrogen removal in this system was 27 and 14%. To determine the importance of anammox and Feammox more precisely, microbiological (Jones et al., 2017) and/or ^{15}N isotope tracer methods (Erler et al., 2008) would be required.

Partial removal of DON was likely due primarily to ammonification of dissolved organic nitrogen followed by other processes (Kadlec and Wallace, 2009). Despite residence times of more than 12 days in the subsurface (section A.3 of Appendix A), only about 38% of the DON was removed. This finding was consistent with past findings that only about half of wastewater-derived DON was bioavailable to algae in receiving waters in the presence of heterotrophic bacteria (Pehlivanoglu and Sedlak, 2004). Thus, much of the DON in treated wastewater that exited the horizontal levee was likely in a more recalcitrant form that may be less of a concern with respect to coastal eutrophication. However, a fraction of the effluent DON loading may also have been derived from decomposition of plants (van Kessel et al., 2009), leaching from particulate organic nitrogen (Li and Davis, 2014) and release of DON during turnover of microbial biomass (Westerhoff and Mash, 2002). These forms of DON are expected to be more bioavailable than wastewater effluent DON.

Additional discussion is provided in Appendix B.

3.6.2 Biogeochemical Cycles of Redox Active Elements

The biogeochemical cycles that control contaminant removal in the horizontal levee are driven by organic carbon, which was the primary source of electrons for microbial respiration. Heterotrophic microorganisms consumed organic carbon using a cascade of electron acceptors with progressively lower energy yields (i.e., O_2, NO_3^-, Mn- and Fe-oxides, and SO_4^{2-}; Rysgaard et al., 2001). Although other electron donors may have formed in the horizontal levee (e.g., iron sulfides), the majority of long-term reducing power was ultimately due to decomposition of organic matter in wood chips and wetland plants.

Organic carbon cycling and mass balance. Five sources of organic carbon were relevant to biogeochemistry, including three solid forms: (1) organic carbon amendments (i.e., wood chips) mixed into the sediments during construction, (2) plant biomass residues, deposited on the surface of the wetland or from decaying plant roots, and (3) soil organic carbon that was present prior to the planting of the wetland, and two dissolved forms: (4) plant root exudates (Zhai et al., 2013) and (5) wastewater-derived dissolved organic carbon. The largest single source was wood chips (approximately 7800 kmol C), which accounted for approximately 67% of the organic carbon prior to planting. An additional 3700 kmol C were supplied as soil organic carbon that were present in soils prior to the planting of the wetland. If all of the organic carbon from these two sources were bioavailable, it would be equivalent to 46,000 keq of reducing power: enough to denitrify all of the nitrate applied to the experimental system for nearly 70 years. Additionally, the high lignin content of wood chips (Hang et al., 2016) assured that this source of organic carbon would be released slowly (García et al., 2010).

Over the monitoring period, soil carbon increased by approximately 18% ($p < 0.03$; one-tail Mann-Whitney test). This suggests that removal of organic carbon from sediments by oxidation was more than compensated for by organic carbon inputs from plants. Overall, a total of approximately 1400 kmol C (95% CI = 1100 kmol C, 2400 kmol C) of plant biomass were produced in the wetland with approximately 18% stored below ground (Chapter 4). This was consistent with past studies in constructed wetlands (Kadlec and Wallace, 2009) which suggested anywhere from 200 to 7900 kmol C yr^{-1} would be produced above ground and that approximately 25% of plant biomass would be below ground. Due to plant turnover and senescence (see section 3.5), nearly 90% of plant biomass produced during the 2-year study was either deposited as plant residues on the wetland surface or became decaying root biomass. We expect wetland plant residues to be readily assimilable (Stelzer et al., 2014) due to their lower lignin content (<10% of carbon; Moran and Hodson, 1989) relative to wood chips (>25%; Gasparovic et al., 2010). Using measurements of carbon and nitrogen isotopes, organic carbon and nitrogen with depth and a mixing model, we estimated that approximately 80% of carbon in remaining litter residues was integrated into sediments over the monitoring period (see section 3.5.3).

Plant roots also supplied significant amounts of organic carbon to the subsurface through the exudation of labile low molecular weight organic carbon compounds (i.e., exudates), which are utilized by microorganisms. Using root-mass based relationships reported previously for plants used in constructed wetland (Zhai et al., 2013), we estimated that 19 kmol C yr^{-1} (95% CI = 6.3 kmol yr^{-1}, 38 kmol C yr^{-1}) were exuded by plants into the subsurface. Based on these estimates, exudates could supply approximately 16% of the electrons required for the heterotrophic processes observed in this system (Table 3-4).

In contrast, wastewater-derived dissolved organic carbon (DOC) did not appear to be an important source of electrons used in microbial processes. The mass of dissolved organic carbon in the water did not change significantly ($p = 0.11$) between the influent and effluent, consistent with past studies in wood chip amended systems (Schipper et al., 2010; Schmidt and Clark, 2012). Organic carbon in wastewater effluent typically does not appear to be bioavailable. Measurements made at other locations indicate that approximately 10-30% of wastewater DOC consists of biodegradable organic carbon (BDOC; Lai et al., 2011; Wang and Chen, 2018). For this reason, practitioners often add labile forms of organic carbon to wastewater effluent to stimulate denitrification (Zhai et al., 2013; Tchobanoglous et al., 2013). However, it was also not possible to determine if wastewater dissolved organic carbon was consumed in the subsurface and replaced by organic carbon leached from soil organic carbon or plant residues. If we assume based on the upper end of BDOC estimates for wastewater (Lai et al., 2011; Wang and Chen, 2018) that 30% of the wastewater DOC was consumed (29 kmol C), it would account for less than 25% of the electrons required for heterotrophic processes.

Heterotrophic processes and mineral formation. In the first 5 meters of the wetland, nitrate (Figure 3-15) was consumed and there were modest increases in concentrations of $Fe_{(aq)}$ and $Mn_{(aq)}$ (Figure 3-16). The release of Fe and Mn was most likely due to reduction of Fe- and Mn-oxides. The release of trace metals occurred when nitrate was present, likely because reduction of those minerals occurred within anaerobic biofilms where nitrate had already been reduced. In this portion of the slope, dissolved inorganic carbon concentrations began to increase (Figure 3-2 and Figure 3-3), but carbonate minerals remained undersaturated (Figure 3-5). Sulfate reduction began to occur as well, but sulfide minerals also remained undersaturated in the first 5 m of the levee (Figure 3-6).

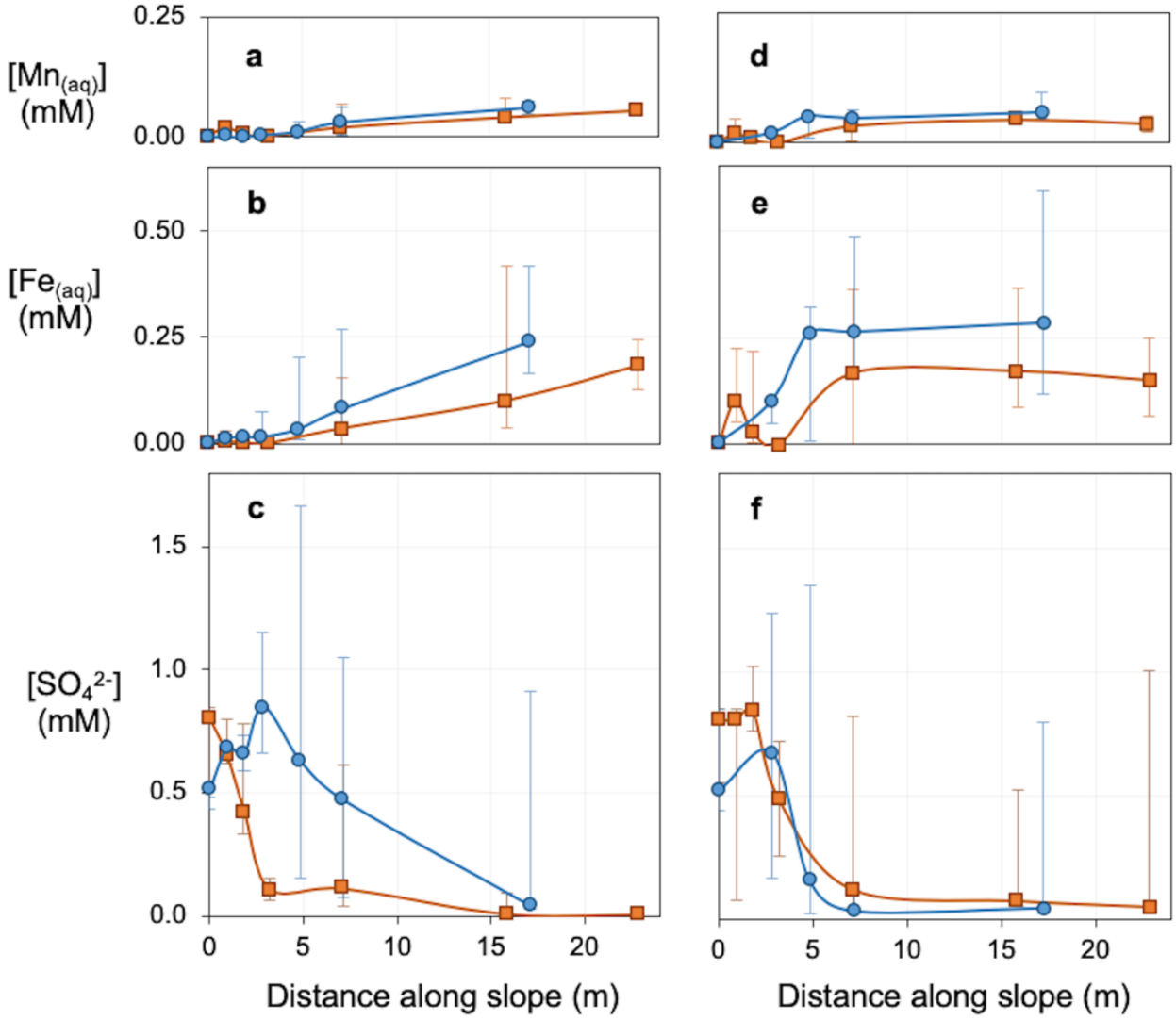

Figure 3-16: Concentrations of $Mn_{(aq)}$, $Fe_{(aq)}$ and sulfate in wet meadow cells with fine topsoils (a, b, and c) and in wet meadow cells with coarse topsoils (d, e, and f). Blue circles represent median concentrations from the winter and spring. Orange squares represent median concentrations in the summer and fall. Error bars represent 90th and 10th percentile values. Note the different scales for each analyte.

After nitrate was depleted, $Fe_{(aq)}$ and $Mn_{(aq)}$ concentrations increased more rapidly before reaching steady concentrations after 5 m at various distances depending on the cell type and the season. Sulfate

reduction was the dominant heterotrophic process after nitrate had been removed until sulfate was depleted around 5 to 20 m from the inlet. We assumed sulfate was converted primarily to sulfide, which should have led to supersaturation with respect to sulfide minerals (Figure 3-6). This was consistent with past findings in organic carbon-amended wetlands, in which the primary fate of sulfate was reduction to sulfide and storage in acid-volatile sulfides (Chen et al., 2016). We hypothesized that these processes resulted in a significant mass of Fe(II) and sulfide – approximately 19 kmol – precipitating out of solution as amorphous iron sulfides, starting around 5 m. This was consistent with black coatings that we observed on sediments collected between 6 and 23 m into the horizontal levee slope (Figure 3-7; Cornwell and Morse, 1987; Wang and Chapman, 1999). The distances at which we observed sulfate reduction varied seasonally (Figure 3-16) and based on cell type (Figure 3-16; Figure 3-17), proceeding most rapidly in cells with a fine topsoil during the summer. Based on these trends, we concluded sulfide mineral were likely forming on sediments even within the first few meters of the cells during the summer (Figure 3-8).

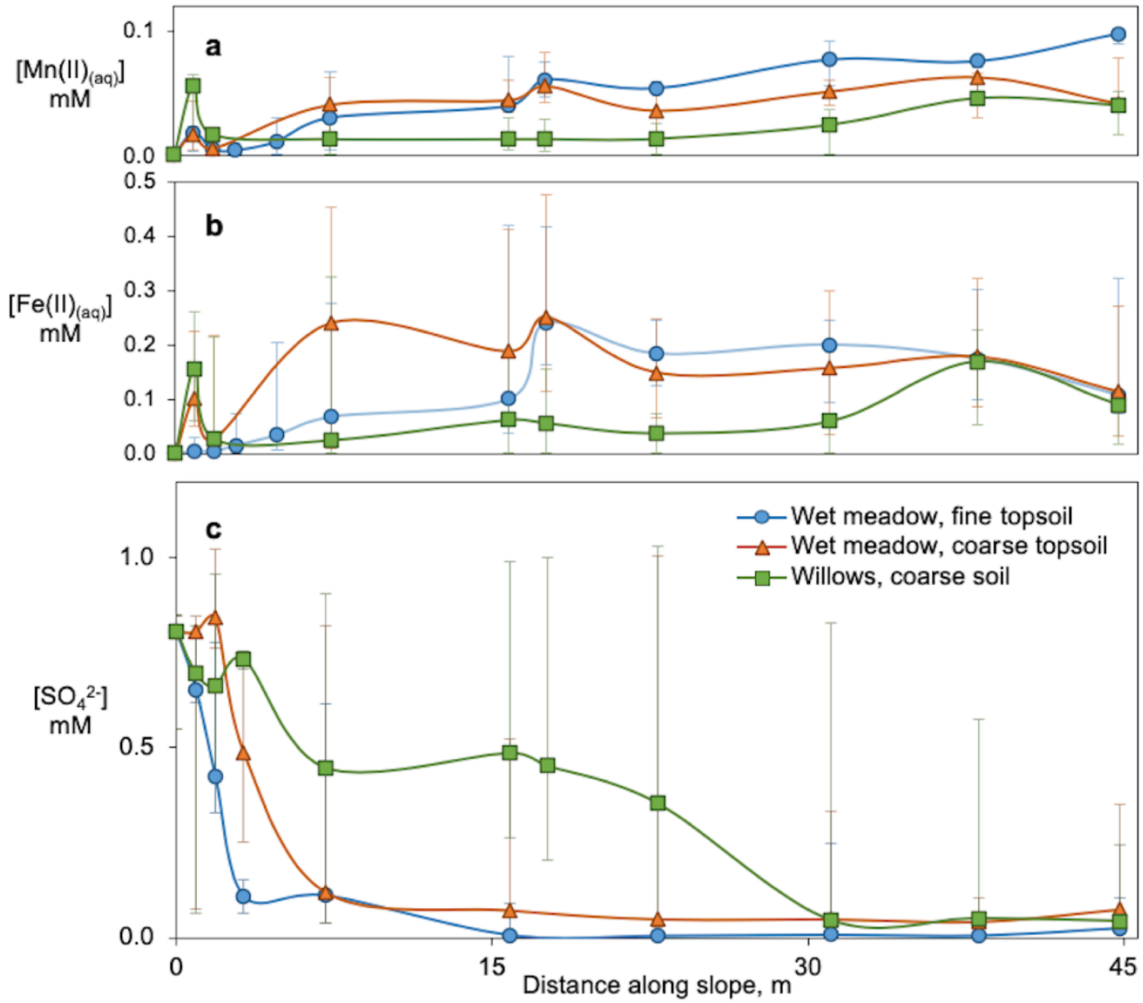

Figure 3-17: Porewater concentrations of: (a)$Mn_{(aq)}$ and (b)$Fe_{(aq)}$ over the full monitoring period, and, (c) sulfate in samples collected during the summer. Wet meadow cells with fine topsoils (blue circles) and coarse topsoils (orange triangles) and from cells planted with willows (green squares). Error bars represent 90th and 10th percentile values.

After sulfate was depleted, we hypothesized that other processes, such as fermentation and methanogenesis, were dominant (see Implications for Horizontal Levee Design). In the final 20 m of the slope, concentrations of dissolved inorganic carbon to increased (Figure 3-2 and Figure 3-3) primarily due to removal of water by evapotranspiration (Figure 3-13). In this portion of the slope, nearly all of the sulfide would have been tied up as $FeS_{(s)}$, $FeS_{2(s)}$ and $S_{(s)}$. Any excess Fe(II) and Mn(II) should have formed carbonate minerals (e.g., $FeCO_{3(s)}$ and $MnCO_{3(s)}$). Estimates based on equilibrium constants indicated saturation indexes were around 1, suggesting that the kinetics of mineral formation were slow or that some other forms of Fe and Mn (e.g. complexes with natural organic matter) were present. Despite having increased by factors of approximately 35 to 110 over the first 15 m of the wetland, $Mn_{(aq)}$ concentrations only increased by an additional 23% ($p < 0.01$; one-tailed t test) between the remaining two-thirds of the wetland and $Fe_{(aq)}$ concentrations did not change significantly ($p = 0.17$; two-tailed Mann-Whitney test) (Figure 3-17), suggesting that $Mn(II)_{(aq)}$ and $Fe(II)_{(aq)}$ produced by heterotrophic processes led to formation of Mn(II)- and Fe(II)-carbonate minerals.

At the start of the experiment, approximately 39 kmol Mn and 2300 kmol Fe were present in the wetland sediments in oxidized forms. Based on porewater concentrations of $Mn_{(aq)}$ and $Fe_{(aq)}$ collected at the end of the wetland, only about 9 and 0.3% of the metals were exported from the wetland, respectively. Porewater $Mn_{(aq)}$, and $Fe_{(aq)}$ concentrations did not vary seasonally ($p > 0.05$; Wilcoxon signed-rank test) but were significantly lower in cells planted with willows (Figure 3-17; Appendix B). Based on these export rates, we would not expect reservoirs of Mn- and Fe-oxides to be exhausted for approximately 20 and 750 years, respectively.

Autotrophic sulfide-driven denitrification. During the monitoring period, we frequently observed increasing sulfate concentrations in the first five meters of the slope coincident with nitrate removal. This trend was more prevalent in the winter and spring (Figure 3-16c and 3-3f, blue circles). For example, in samples collected from cell F in April 2019, nitrate concentrations dropped from 2.1 mM in the influent to less than 0.01 mM in the first 5 m of the subsurface, while sulfate concentrations increased from approximately 0.45 to 1.0 mM before dropping to around 0.25 mM (Figure 3-18). In April 2019 in cell F, a strong inverse correlation ($r^2 = 0.97$; $p = 0.002$) was observed between concentrations of sulfate and nitrate suggesting the occurrence of sulfide-driven autotrophic denitrification or DNRA (Zhang et al., 2012; Jones et al., 2017). This process is typically fueled by sulfide minerals (e.g., acid-volatile sulfides) that deposit on sediments during iron and sulfate reduction (section 3.4.2). These minerals may have formed in the first 5 meters of the subsurface during summer and fall when biological activity was higher.

Unlike past studies in constructed wetlands, in which sulfide-driven DNRA provided a link between nitrate reduction and anammox (Jones et al., 2017), ammonium concentrations did not increase to a significant degree in this system (Figure 3-18b), suggesting that DNRA was not important. These findings were consistent with other studies, in which autotrophic denitrification has been observed in marine (Zhang et al., 2009) and riverine sediments with sulfide mineral deposits (Yang et al., 2012b), and in constructed wetlands with high sulfate loading (Chen et al., 2016; Guo et al., 2020). Sulfide-oxidizing denitrifiers extract electrons not only from sulfide, but also from Fe(II), which can lead to the formation of Fe(III)-oxides as $FeS_{(s)}$ is oxidized (Torrentó et al., 2010).

Sulfide-driven denitrification appeared to be seasonal because increasing sulfate concentrations at the beginning of the wetland were only observed in the winter and spring (Figure 3-16). Additionally, sulfate reduction occurred in the first 3 m of the subsurface during the summer, creating conditions favorable for the formation of Fe(II)-sulfides in parts of the slope where they could fuel denitrification during winter and spring (Figure 3-8).

As a result of this secondary pathway for nitrate removal, there were no significant differences between nitrate removal rates seasonally ($p = 0.78$; Figure 3-19). This contrasts with past research in constructed wetlands, in which nitrate removal rates slowed as temperature decreased ($\theta = 1.11$; Kadlec and Wallace, 2009) in both free-water surface wetlands (Jasper et al., 2014) and subsurface wetlands (Kadlec and Wallace, 2009). On the basis of influent water temperature changes between the summer (21 ± 0.8 ºC) and the winter (17 ± 1.3 ºC) at the pilot-scale wetland, we would have expected nearly a 40% decrease in nitrate removal rates in the winter which would have extended the length of the denitrifying zone of the wetland to approximately 7.0 m. Sulfide-driven denitrification has a much lower temperature dependence ($\theta = 1.06$; Jørgensen et al., 2009) than heterotrophic denitrification, which may explain the lack of seasonality observed in nitrate removal. It has been suggested that sulfide-oxidizing denitrifiers may play a role in stimulating the activity of heterotrophic denitrifiers (Torrentó et al., 2010) possibly through the production of soluble microbial products or cell decay. These processes could all play a role in the insignificant seasonality of subsurface nitrate reduction rates we observed. However, our findings could be complicated by various factors, such as seasonal shifts in the rate of nutrient acquisition by plants (e.g., uptake of nitrogen by wetland plants is often most significant in the spring and early summer; Kadlec and Wallace, 2009).

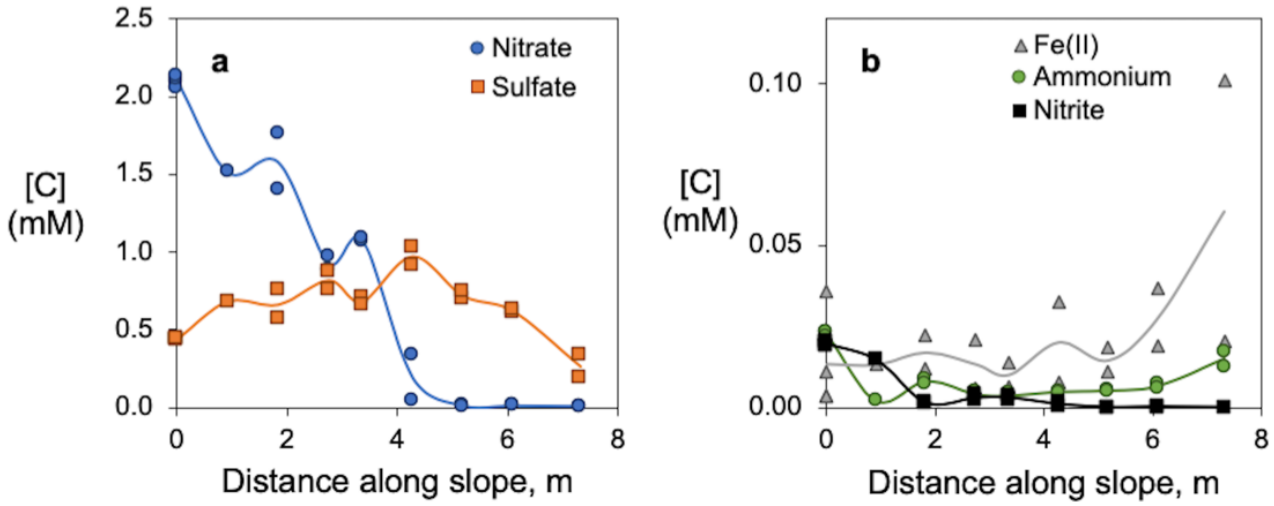

Figure 3-18: Concentrations (i.e., [C]) of dissolved species in porewater samples: (a) nitrate (blue circles) and sulfate (orange squares) and (b) $Fe_{(aq)}$ (grey triangles), ammonium (green circles) and nitrite (black squares) collected from the gravel and coarse sand layers of the subsurface in cell F on April 10, 2019. Note the difference in vertical axes scales. Data points represent individual samples and lines represented moving averages.

The ability of the horizontal levee to avoid decreases in seasonal performance with respect to nitrate removal through sulfide-driven denitrification suggests that horizontal levees may be appropriate in situations where other nature-based solutions have been dismissed in the past because of concerns related to temperature-related diminution in performance. Despite the lower temperature dependence of sulfide-driven denitrification, it is possible that a reduction in nitrate removal would be observed in systems with much colder winter temperatures (e.g., 0 ºC). However, preliminary evidence suggests autotrophic denitrification may be an effective nitrate removal mechanism even at temperatures as low as 3 ºC in engineered systems (Di Capua et al., 2017). More research is needed to assess the function of horizontal levees in more variable climates. Because of the potential for autotrophic denitrification, horizontal levees also may be attractive for nitrate removal in wastewaters with high sulfate

concentrations (e.g., reverse osmosis concentrate from wastewater reuse). Moreover, the amendment of horizontal levee sediments with Fe(III)-oxides or $FeS_{(s)}$ could be a useful way to stimulate sulfide-driven nitrate removal in full-scale systems, as has been reported for other constructed wetland systems (Ge et al., 2019).

Using changes in sulfate and nitrate concentrations in cell F in April 2019 as an example and the stoichiometry of sulfide-driven denitrification (Cardoso et al., 2006; Zhang et al., 2012), we estimate that of the approximately 440 keq required for nitrate reduction during the winter approximately 130 keq were supplied by oxidation of Fe(II)-sulfide. This suggests that nearly a third of the wintertime denitrification in cell F was provided by iron-sulfides. If we extrapolate this to the entire wetland using median changes in nitrate and sulfate, autotrophic denitrification would account for 18% of nitrate removal in the winter, or approximately 10% of total nitrate removal. Additionally, although sulfide deposits may become less reactive as they age and undergo conversion to more stable sulfide minerals (e.g., pyrite; Berner, 1967; Canfield, 1989; Furukawa and Barnes, 1995) it is likely that they will still provide electrons for denitrification, as has been shown previously with pyrite (Torrentó et al., 2011; Ge et al., 2019).

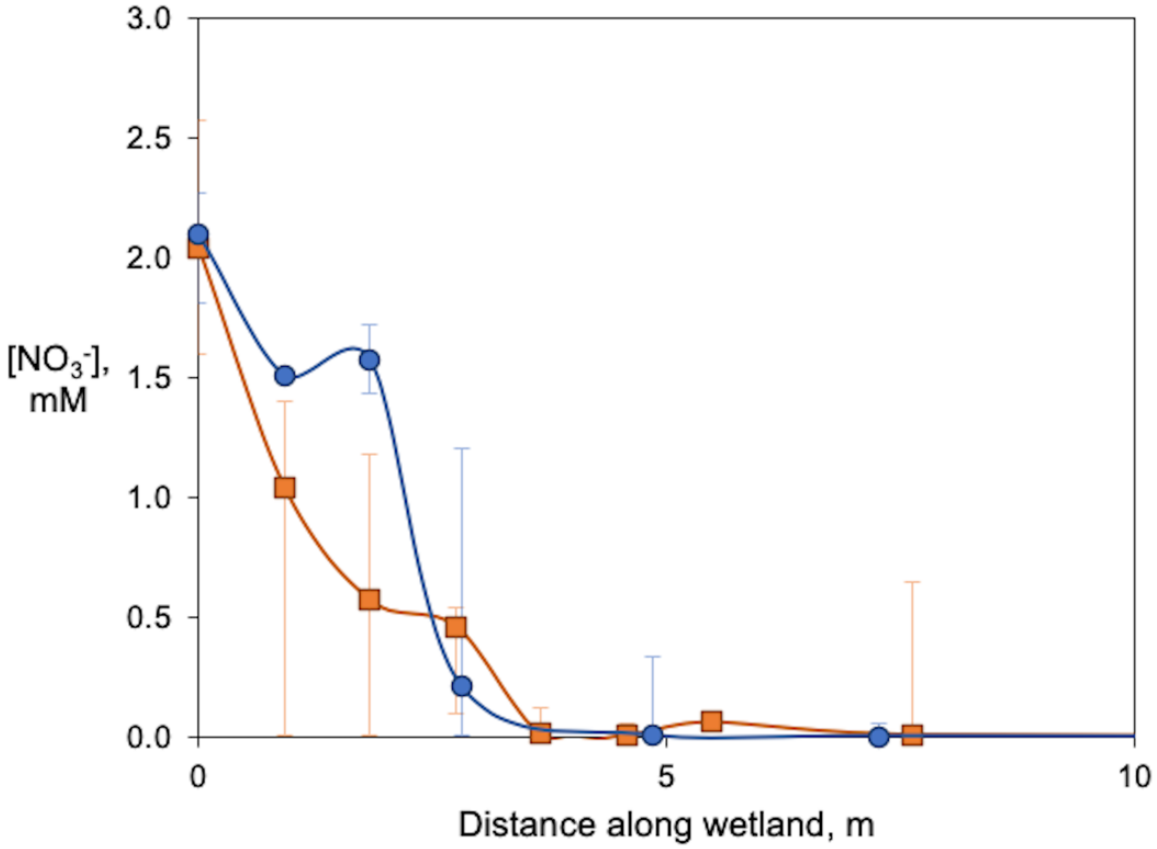

Figure 3-19: Porewater concentrations of nitrate in the first 10 m of the wetland in the summer (orange squares) and the winter (blue circles).

3.6.3 Implications for Horizontal Levee Design

To gain insight into the ways in which understanding biogeochemistry can inform the design of horizontal levees, we used data collected in the pilot system to evaluate the role of different electron

donors and acceptors (described in detail in section 3.3). We estimated that a total of approximately 1000 keq of electrons were required to reduce the electron acceptors in the pilot system over the two-year monitoring period. Electron donors, mainly decaying plants, wood chips and root exudates, provided more than enough reductants to drive this process (Figure 3-20). Within the electron acceptor pool, approximately 670 keq (about 50%) of the electrons were ultimately transferred to convert NO_3^- and NO_2^- into $N_{2(g)}$ and $N_2O_{(g)}$ over the monitoring period. Metal sulfides provided approximately 10% of the electrons needed to reduce the electron acceptors, but they were more important to nitrate removal during colder periods when rates of heterotrophic denitrification decreased. Approximately 20% of organic carbon consumption (54 kmol C) was not accounted for by the monitored electron acceptors (Figure 3-20) and could have contributed to methanogenesis or H_2 production (Conrad, 1996).

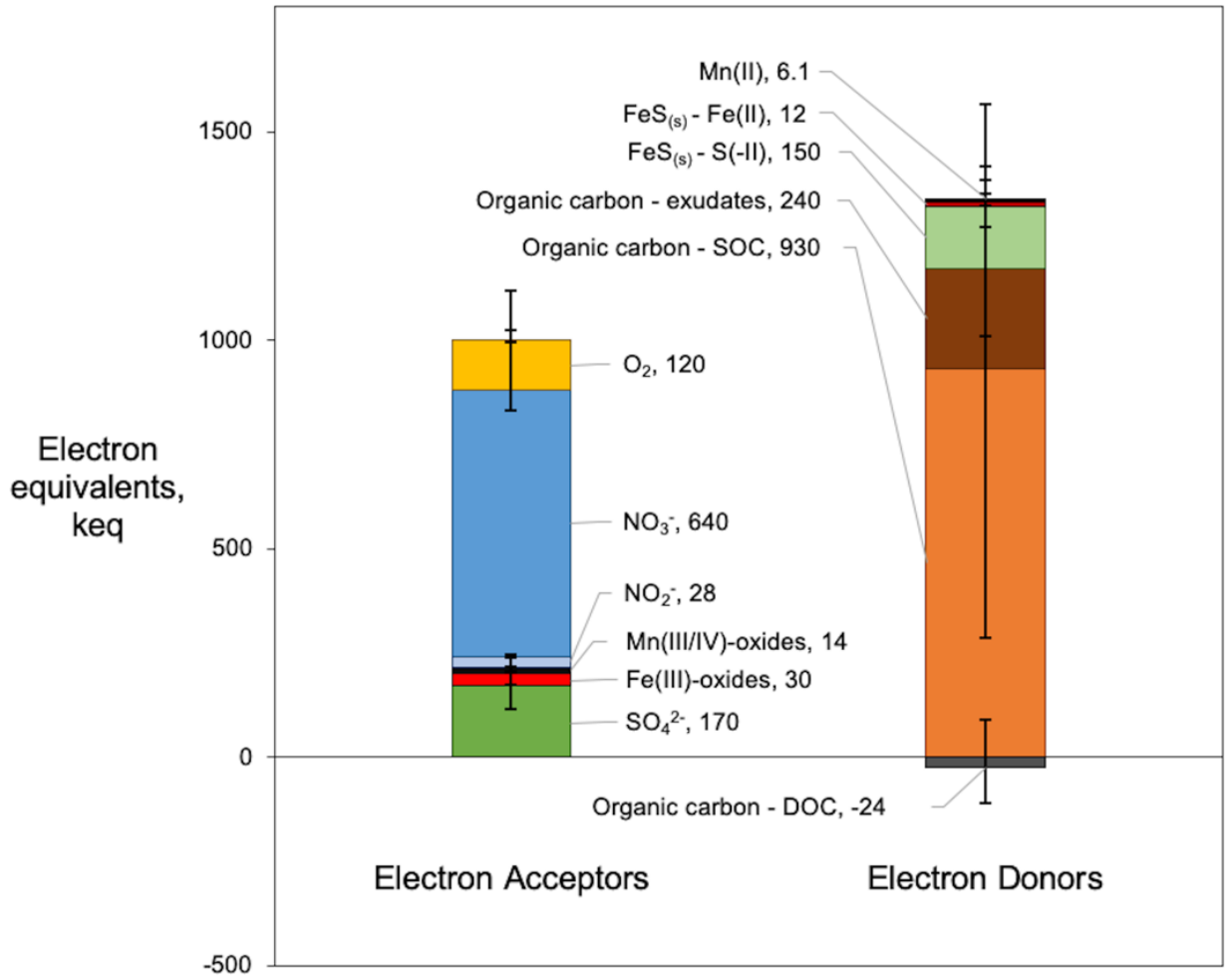

Figure 3-20: Electron equivalents transferred to electron acceptors (EAs) or from electron donors (EDs) in the subsurface of the experimental horizontal levee throughout the monitoring period. Acronyms: SOC = soil organic carbon; DOC = dissolved organic carbon.

If all of this missing carbon was emitted to the atmosphere as methane, average emissions rates over the wetland would have been 5.4 mol CH_4 m^{-2} yr^{-1}, which is lower than emissions rates for more than 90% of subsurface wetlands reported in the literature (e.g., 1.0-20 mol CH_4 m^{-2} yr^{-1} in horizontal subsurface flow wetlands; Kadlec and Wallace, 2009). It is also substantially lower than average

emissions for wetlands and estuaries (39 and 44 mol CH_4 m^{-2} yr^{-1} respectively; Ortiz-Llorente and Alvarez-Cobelas, 2012). This methane emission estimate also may have been lower if the loss of inorganic carbon through formation of carbonate minerals was considered in our calculation. If all organic carbon removed in this system were consumed by heterotrophs, we would predict approximately 290 kmol of dissolved inorganic carbon (DIC) would have been exported from the system, but we only observed 230 kmol (79%) of DIC in the effluent. Based on estimated reduction of manganese and iron, the amount of iron stored in sulfide minerals (section 3.3.2), and export of those metals in the effluent, we estimated that approximately 2.8 and 7.6 kmol of DIC precipitated in rhodochrosite ($MnCO_{3(s)}$) and siderite ($FeCO_{3(s)}$) respectively, accounting for approximately 17% of the missing DIC. For example, of the 22 kmol of iron reduced, 12 kmol were stored in sulfide minerals and approximately 2.3 kmol were exported from the system. The remaining 7.6 kmol was assumed stored in siderite (at a 1:1 molar ratio). Based on these calculations, we hypothesized that hydrogenotrophic methanogenesis explained the majority (~83%) of observed DIC removal (Kao-Kniffin et al., 2010; Lee et al., 2012; Mach et al., 2015).

On the basis of our data, we estimated that wood chips alone could fuel denitrification for approximately 65 years if all of the carbon was available and was ultimately consumed by denitrifiers. However, previous studies of wood chip-amended biological treatment systems have shown that biological activity stimulated by wood chips decreases over decadal time-scales (Schipper et al., 2010), possibly as more easily extracted fractions of wood chip carbon are exhausted. Thus, we expect the rate of organic carbon release from wood chips to decline over time.

Considering the size of the soil organic carbon pool (~8100 kmol C; including woodchips, soil organic matter and decaying root biomass) and the rate of soil organic carbon consumption (~120 kmol yr^{-1}; estimated with the mass balance described in section 3.3.1), we estimate that without contributions from plants soil organic carbon will be depleted in approximately 50 years. However, this pool of organic carbon will be replenished by plants (i.e., roots and litter residues), which produced approximately 2800 kmol C in litter over the two-year monitoring period (Appendix B). Additional reducing power likely came from plant root exudates (Zhai et al., 2013) and iron sulfide deposits. To account for these electron donors, we developed a model for estimating the lifetime with which a horizontal levee can provide efficient nitrogen removal (section 3.3.3; Table 3-4). In this model, we assumed that mature plants would likely stabilize around 1000 kmol C yr^{-1} based on observed biomass production rates. Thus, if approximately 10% of the annual biomass production is ultimately available to microbes in the subsurface, the ability of the system to continue to remove nitrogen will be sustained. Moreover, using this model we determined that lower initial inputs of organic carbon (e.g., wood chips) may have been sufficient to promote long-term denitrification in these systems.

Biogeochemical processes in horizontal levees depend on the electron acceptors present in the soil used for construction of these systems. If construction materials contain high concentrations of reactive Mn(III)/Mn(IV)- and Fe(III)-oxides, reduction of these species could deplete organic carbon that could otherwise be used for denitrification, as has been observed in Mn- and Fe-rich marine sediments (Canfield et al., 1993). Additionally, if the iron content of construction materials is too low, the formation of Fe(II)-sulfide deposits that can store electrons transferred from organic carbon in sediments for later use by autotrophic denitrifiers may be limited. Without autotrophic denitrification in these systems, it is possible that denitrification rates might decrease considerably during winter.

Likewise, an understanding of biogeochemistry can be useful for understanding the effect of changing the composition of the water being treated. In sulfate-rich wastewater streams, such as reverse osmosis concentrate from wastewater reuse applications, sulfate reduction could also deplete the reservoir of

organic carbon. Although a large fraction of the produced sulfide typically forms sulfide mineral deposits, which can serve as a source of electrons for denitrification, Fe(II) is required to form those minerals. Therefore, designers must also consider the iron content of the sediments. If sulfate inputs are too high relative to iron content, $FeS_{(s)}$ might not form. Rather, sulfide could diffuse into root layers where it can cause phytotoxicity (Lamers et al., 2013) or could be exported in the effluent or volatilize, reducing the availability of electron donors in horizontal levees and possibly decreasing the pH of receiving waters (Macdonald et al., 2007). For these reasons, it is essential that designers consider the use of iron amendments or iron-rich sediments (Chen et al., 2016) in horizontal levees receiving sulfate-rich wastewaters.

However, higher inputs of sulfate and iron could also create benefits beyond those related to nitrogen removal discussed in previous sections. Both iron and sulfate inputs have been demonstrated to reduce methane emissions from wetlands (Jäckel et al., 2005; Ali et al., 2008; Bridgham et al., 2012), possibly by poising sediments at higher redox potentials (Easton et al., 2015) or by outcompeting methanogens for organic carbon substrates (Bridgham et al., 2012). Additionally, although sulfate reduction has been shown the stimulate methylmercury production in sulfate-limited systems, high sulfate inputs and porewater sulfide concentrations appear to have an inhibitory effect on methylmercury production and formation potential (Bailey et al., 2017) and iron amendments have also been shown to inhibit methylmercury production in tidal wetland mesocosms (Ulrich and Sedlak, 2010). Sufficiently high loading of sulfate and iron to horizontal levees could expand iron- and sulfate-reducing zones within the subsurface, not only increasing the capacity for storage of electrons in sediments to fuel denitrification, but also limiting the formation of problematic byproducts of wetlands, like methane and methylmercury.

Chapter 4. Use of Stable Nitrogen Isotopes to Track Plant Uptake of Nitrogen in a Nature-Based Treatment System

The following chapter is adapted from a co-authored manuscript with permission from Sytsma, A., Stiegler, A.N., Dawson, T.E., Sedlak, D.L. Use of stable nitrogen isotopes to track plant uptake of nitrogen in an engineered system that improves water quality. *Manuscript submitted for publication*.

ABSTRACT

In nature-based treatment systems, such as constructed treatment wetlands, plant uptake of nutrients can be a significant removal pathway. Current methods for quantifying plant uptake of nitrogen in constructed wetlands, which often involve harvesting biomass and assuming that all nitrogen stored in plants was derived from wastewater, are inappropriate in pilot- and full-scale systems where other sources of nitrogen are available. To improve our understanding of nitrogen cycling in constructed wetlands, we developed a new method to quantify plant uptake of nitrogen by using stable isotopes and a mixing model to distinguish between nitrogen sources. We applied this new method to a pilot-scale horizontal levee system (i.e., a subsurface constructed wetland) over a two-year monitoring period, during which an average of 14% of nitrogen in plants was wastewater-derived and the remaining plant nitrogen was obtained from the soil. Analysis of nitrogen isotopes indicated substantial spatial variability in the wetland: 82% of nitrogen in plants within the first 2 m of the slope came from wastewater while less than 12% of plant nitrogen in the remainder of the wetland originated from wastewater. By combining these source contributions with remote-sensing derived total biomass measurements, we calculated that 150 kg N (95% CI = 50 kg N, 330 kg N) was taken up and retained by plants during the two-year monitoring period, which corresponded to approximately 8% of nitrogen removed in the wetland. Nitrogen uptake followed seasonal trends, increased as plants matured, and varied based on design parameters (e.g., plant types), suggesting that design decisions can impact this removal pathway. This new method can help inform efforts to understand nitrogen cycling and optimize the design of nature-based nutrient control systems.

4.1 Introduction

Humans have extensively modified the nitrogen cycle (Galloway et al., 2008), which has caused widespread damage to aquatic ecosystems, such as eutrophication (Sutton and Bleeker, 2013; Freeman et al., 2019). These impacts have been exacerbated by the loss of coastal wetlands (Li et al., 2018) that historically have reduced the export of nutrients from terrestrial systems (Megonigal and Neubauer, 2019). Despite past attempts to control anthropogenic nutrient inputs using conventional management methods, eutrophication has frequently persisted (Thornton et al., 2013). As an alternative to conventional approaches, engineers have begun to consider the use of constructed wetlands to manage nutrient discharges. Horizontal levees are a new type of subsurface constructed wetland that can protect coastal urban areas against flooding, while treating wastewater effluent in managed wetland habitats. These new types of constructed wetlands can also provide restored habitat and a suite of additional benefits (Kadlec and Wallace, 2009) that were described in greater detail in Chapter 2 (Cecchetti et al., 2020a). Their low cost and resource requirements relative to conventional single-benefit solutions make constructed wetlands particularly attractive to utility managers (Kadlec and Wallace, 2009; Harris-Lovett et al., 2019).

Despite these benefits, there remain many uncertainties about the performance of horizontal levees and the exact processes by which they remove nutrients. In subsurface wetlands, nitrogen is often removed or immobilized by plant uptake as well as a suite of microbial processes, including assimilation, denitrification, and anaerobic ammonium oxidation (Kadlec and Wallace, 2009; Javanaud et al., 2011; Wu et al., 2017). Due to the complex nature of these processes, past assessments of plant uptake in nature-based systems have varied widely, with reported fractions of nitrogen removal attributable to plant uptake spanning three orders of magnitude (i.e., 0.5-90%) (Meers et al., 2008; Saeed and Sun, 2012), though these differences may partly be explained by variations in plant maturation, plant types and nitrogen loading rates.

Rather than attempting to discriminate among mechanisms, researchers often make simplifying assumptions that can lead to large errors when quantifying nitrogen uptake rates. In particular, researchers often assume that all nitrogen in plants is derived from wastewater in these systems (Healy and Cawley, 2002; Geng et al., 2019; Chen et al., 2014; Du et al., 2018). This is a reasonable assumption if other sources of nitrogen (e.g., soil) are absent. However, uptake will be overestimated if wetland plants have access to other nitrogen sources. Differences between nitrogen removal in planted and unplanted (control) wetlands have also been used to estimate plant uptake of nitrogen (Drizo et al., 1997; Kantawanichkul et al., 2009; Paranychianakis et al., 2016), but this comparison ignores the importance of plant roots in stimulating microbial nitrogen removal in the rhizosphere (Zhai et al., 2013). To overcome these limitations, researchers have also quantified plant uptake with ^{15}N-tracer studies in bench-scale wetland microcosms (Zhang et al., 2016; Messer et al., 2017; Hu et al., 2017). However, in pilot-scale to full-scale wetlands, materials costs associated with ^{15}N-tracers alone would be prohibitively expensive.

Stable isotope mixing models provide an alternative approach for estimating plant uptake of nitrogen. Stable isotopes have been widely used to study biogeochemical processes (Dawson et al., 2002; Fry, 2006) and nitrogen cycling in aquatic ecosystems (McClelland and Valiela, 1998; Cole et al., 2004; Reinhardt et al., 2006; Bannon and Roman, 2008; Kohzu et al., 2008; Søvik and Mørkved, 2007; Erler et al., 2010; Kaushal et al., 2011; Chen et al., 2014). However, despite their versatility, the application of stable isotopes to assess nitrogen uptake in constructed wetlands has been limited (Fair and Heikoop, 2006).

In nature-based systems like the horizontal levee, the primary sources of nitrogen are wastewater and soil. With isotope fingerprinting, measurements of nitrogen isotopes in plants can be used to identify their sources of nitrogen, because isotope ratios in plant tissues typically match their source of nitrogen (Craine et al., 2015). Furthermore, wastewater-derived nitrogen is frequently enriched in ^{15}N ($\delta^{15}N \approx$ 25-35‰). As a result, its "isotopic signature" (i.e., $\delta^{15}N$ or nitrogen isotope ratio) is distinguishable from other nitrogen sources, such as soils ($\delta^{15}N \approx$ 0-10‰), the atmosphere ($\delta^{15}N \approx$ -15 to +15‰) or nitrogen fixation ($\delta^{15}N \approx$ 0‰) (Heaton, 1986; Kendall, 1998). The isotopic signatures, which are commonly termed 'end-members', of these different sources can be used in mixing models to determine their relative contribution to the nitrogen found in plants.

In this study, we present a new method for quantifying plant uptake of nitrogen in nature-based treatment systems using a stable isotope mixing model in a pilot-scale horizontal levee. We developed this method in a horizontal levee by coupling: (1) isotopic analysis of plants, wastewater, and soils; (2) remote sensing-derived biomass measurements; and, (3) water quality data. We used this information to assess the contribution of plant uptake to nitrogen removal in this system. This approach is a promising tool for understanding nitrogen fate and managing nitrogen species in both nature-based treatment systems and in natural ecosystems.

4.2 Materials and Methods

4.2.1 Field site

Nitrogen uptake was studied at a demonstration-scale horizontal levee system at the Oro Loma Sanitary District wastewater treatment plant in San Lorenzo, CA as described in Chapter 2 (Cecchetti et al., 2020a) and Appendix A. The subsurface wetland contained 12 gently sloped (1:30) parallel treatment cells (1 m deep, 12 m wide and 46 m long) that were hydraulically isolated from each other. The cells were used to test four treatments (i.e., swale-depression cells, wet meadows with fine and coarse topsoil, and riparian willow cells) that varied in terms of their topography, soil type and native plant community type. Underlaying the 60 cm of topsoil were two 15-cm deep layers of sand and gravel that were amended with organic carbon (i.e., wood chips) to promote microbial denitrification.

Influent samples were collected from a pump station that delivered nitrified secondary municipal wastewater effluent into 12 wetland cells approximately 5 cm below the surface at the top of the slope. The effluent from each cell flowed into a gravel trench spanning the end of the cell and was collected in perforated PVC pipes at the bottom of the trench, from where effluent samples were collected.

Native plants, mainly of the families *Cyperaceae* (sedges), *Juncaceae* (rushes) and *Salicaceae* (willows), were planted between September 2015 and February 2016, approximately 15 months before nitrified wastewater effluent was first introduced into the subsurface. Prior to this time, the cells were irrigated with shallow groundwater obtained from a well located approximately 50 m from the wetland.

Additional details regarding the hydraulics, design, wetland treatments and planting regimes are available in Chapter 2 (Cecchetti et al., 2020a) and Appendix A.

4.2.2 Solid sample collection and processing

$\delta^{15}N$ and $\delta^{34}S$ were measured in foliar and soil samples before and after wastewater effluent was introduced into the horizontal levee to assess isotopic discrimination during uptake (prior to

wastewater introduction) and as inputs for source contribution models (after introduction of wastewater).

Samples of new growth plant leaves were collected from Baltic rushes (*J. balticus*; in cells A-G, I, and K) and Arroyo willows (*S. lasiolepis*; in cells H, J, and L) every 3-6 months between August 2016 and June 2019. These species were chosen due to their dominance in the plant community (*S. lasiolepis*). The $\delta^{15}N$ values for these samples were indistinguishable ($p = 0.71$; Wilcoxon signed-rank test) from composite biomass samples (*J. balticus*) (Figure 4-1). Samples were collected at various distances along the wetland slope. In riparian-type cells, foliar samples from *S. lasiolepis* were collected at 7-10 locations along three transects that were parallel to water flow in each cell. A total of 332 foliar samples of *S. lasiolepis* were collected on 8 sampling dates. In all other cells, samples of *J. balticus* were collected and pooled into 7 distance-resolved samples per cell from transects perpendicular to the direction of flow along the slope. A total of 158 pooled foliar samples of *J. balticus* were collected on 5 sampling dates. Leaves were separated from their petioles at sampling (when appropriate) and placed in paper envelopes. The envelopes were placed inside of plastic bags and stored on ice prior to returning to the lab. Leaf samples were dried at 65°C for 48 hr immediately upon returning to the lab.

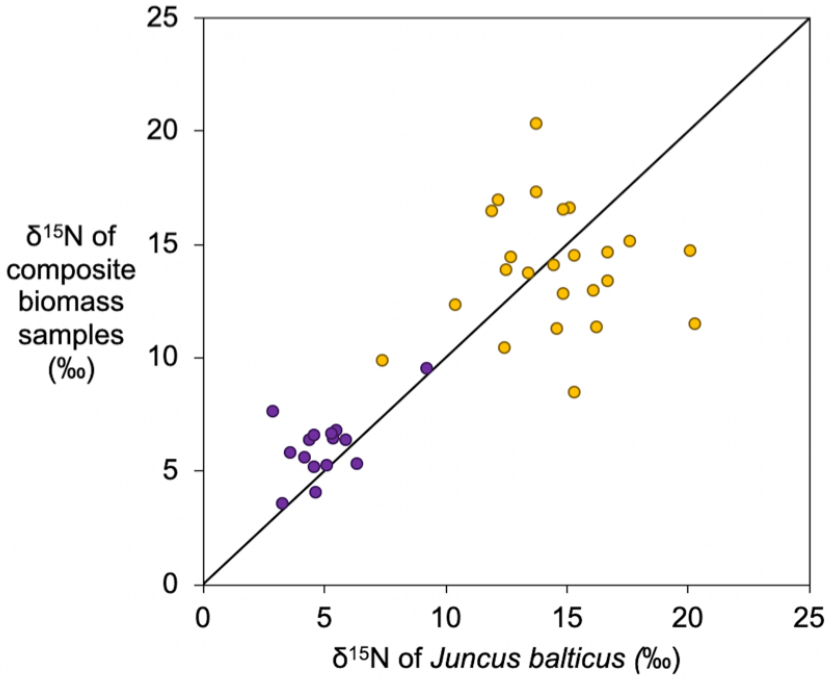

Figure 4-1: Relationship between $\delta^{15}N$ in *Juncus balticus* (Baltic rush) and composite biomass samples collected from the same location. Purple circles correspond to samples were collected in January 2017 (before the application of wastewater) and yellow circles correspond to samples collected in August 2018 (after the application of wastewater). The diagonal line represents a 1:1 relationship. *J. balticus* and composite biomass samples were statistically indistinguishable from each other ($p = 0.71$; Wilcoxon signed-rank test).

Soil samples were collected for isotope analysis from the top 10 cm of the soil. In 2016, these samples were collected from 9 randomly selected locations per cell. Additional soil samples were collected in 2017 and 2018 for comparison. Soil samples were stored on ice prior to returning to the lab. Soil

samples were freeze dried upon returning to the lab using a Labconco FreezeZone 12 Freeze Dryer (Labconco, Kansas City, MO).

Dried leaf and soil samples were ground to a fine powder (200 mesh) using a mortar and pestle, a SPEX SamplePrep 8000 Mill (SPEX SamplePrep, Metuchen, NJ) or a Mini-BeadBeater (Biospec Products, Bartlesville, OK). Ground samples were weighed on a Sartorius microbalance (Sartorius Laboratory Instruments, Goettingen, Germany) and packed into tin capsules (Costech Analytical Technologies, Valencia, CA). Capsules were compressed into spheres and stored in 96-well culture plates prior to analysis.

4.2.3 Water sample collection and processing

Influent and effluent water samples were collected once or twice per month between April 2017 and June 2019 for measurement of water quality parameters (e.g., pH) and concentrations of anions and cations (e.g., NO_3^-) as described in Chapter 2 (Cecchetti et al., 2020a).

To investigate $\delta^{15}N$ and $\delta^{18}O$ in nitrate spatially, porewater samples were collected throughout the entire wetland and on transects along the flow path within the first 10 m of the wetland. Briefly, 25-100 mL samples were collected from depths between 0.1 and 0.9 m into syringes using steel sediment porewater samplers and were filtered directly through 0.2-µm nylon syringe filters into 60-mL or 120-mL polypropylene Nalgene bottles (Sigma-Aldrich, St. Louis, MO, USA). Samples were stored on ice for transport and frozen within 4 hours.

Prior to isotopic analysis, samples were processed according to the procedure detailed by Granger and Sigman (2009) for removing nitrite to limit interferences during nitrate isotope measurements. After thawing, 10-30 mL subsamples were transferred to acid-washed 60-mL HDPE bottles. 20 µL per mL sample of a 5% w/v sulfamic acid solution in 5% v/v HCl were added to convert nitrous acid to N_2 gas. Samples were sealed and left on a shake table at ambient temperature or 30ºC for 20 minutes before being adjusted back to a circumneutral pH with 10 µL of a 2M NaOH solution per mL sample. Nitrate concentrations in processed samples were quantified using ion chromatography. Processed samples were refrozen prior to shipping on ice to the analytical facility.

4.2.4 Analytical methods

The stable isotope composition of soil samples and plant tissue samples was determined according to previously described methods (Mambelli et al., 2016). Briefly, $\delta^{15}N$, $\delta^{13}C$ and $\delta^{34}S$ (as well as %N, %C and %S) were determined by continuous flow (CF) triple isotope analysis using a CHNOS Elemental Analyzer (vario ISOTOPE cube, Elementar, Hanau, Germany) interfaced in line with a gas isotope ratio mass spectrometer (IRMS) (IsoPrime 100, Isoprime Ltd, Cheadle, UK). Isotope abundances are presented in δ notation as deviations from standard references (atmospheric nitrogen (AIR), Vienna PeeDee Belemnite (V-PDB) and Vienna Canyon Diablo Troilite (VCDT) for $\delta^{15}N$, $\delta^{13}C$ and $\delta^{34}S$, respectively) in parts per thousand (‰). Long-term precision for $\delta^{15}N$, $\delta^{13}C$ and $\delta^{34}S$ determinations was ± 0.20‰, ± 0.10‰, and ± 0.40‰.

Concentrations of anions, cations, organic carbon and total nitrogen were measured in water samples according to standard methods (APHA, 2012), as described in Chapter 2 (Cecchetti et al., 2020a). Briefly, nitrate and other anions (e.g., Cl^-, NO_2^-, and SO_4^{2-}) were measured by ion chromatography with an IonPac AS23 column according to U.S. EPA Method 300.0. Cations were measured by ion chromatography as previously described (Thomas et al., 2002). Non-purgeable organic carbon

(NPOC) and total nitrogen (TN) were measured on a Shimadzu TOC-V/CSH analyzer with an attached TN-1 unit according to standard methods (Method 5310B; APHA, 2012).

Measurements of $\delta^{15}N$ and $\delta^{18}O$ in nitrate were made with the bacterial denitrification assay (Sigman et al., 2001) on a Thermo Finnigan GasBench + PreCon trace gas concentration system interfaced to a Thermo Scientific Delta V Plus isotope ratio mass spectrometer (Thermo Electron GmbH, Bremen, Germany). Samples were purged through a double-needle sampler into a helium carrier stream (25 mL min^{-1}). Gas samples passed through a CO_2 scrubber (Ascarite) and N_2O was concentrated in two liquid nitrogen cryo-traps. N_2O was carried by helium to the IRMS via an Agilent GS-Q capillary column (30m x 0.32mm, 40ºC, 1.0 mL min^{-1}). Provisional isotope ratios were adjusted to final values using NIST-certified calibration standards USGS 32, USGS 34 and USGS 35 (National Institute of Standards and Technology, Gaithersburg, MD, USA) and are presented in δ notation as deviations from standard references (atmospheric nitrogen (AIR) and Vienna Standard Mean Ocean Water (SMOW) for $\delta^{15}N$ and $\delta^{18}O$, respectively). The precision for $\delta^{15}N$ and $\delta^{18}O$ measurements was ± 0.4‰ and ± 0.5‰, respectively.

4.2.5 Plant nitrogen source contribution models

We used mixing models to calculate the fraction of nitrogen in plant biomass derived from soil and wastewater nitrogen, respectively. Of mixing model types available, linear and Bayesian mixing models each have their own set of strengths and weaknesses (see section 4.3). We developed both linear and Bayesian mixing models (Evaristo et al., 2017) to test the utility and flexibility of these two methods for calculating plant uptake of nitrogen. Soil nitrogen and wastewater-derived nitrate were the main sources of nitrogen available to wetland plants. Contributions of nitrogen from atmospheric deposition (0.1% of total nitrogen inputs) and fixation of N_2 by wetland plants (0.5% of total nitrogen inputs) were considered negligible based on upper bound estimates found in the literature for similar locations (Schwede and Lear, 2014; NADP, 2019) or natural wetland systems (Bowden, 1987). Discrimination between nitrogen isotopes during plant uptake was assumed to be negligible based on similarities between $\delta^{15}N$ in baseline soil and plant tissue samples (e.g., samples collected prior to the introduction of wastewater to the subsurface in April 2017; Figure 4-6), which was consistent with past findings (Craine et al., 2015). Mixing model assumptions are discussed in section 4.3.

A two-source linear mixing model was applied to our data according to Equation 4-1 and Equation 4-2:

$$\delta^{15}N_{Plants} = (\delta^{15}N_{Soil})(f_{Soil}) + (\delta^{15}N_{ww})(f_{ww}) \quad \textbf{Equation 4-1}$$

$$1 = f_{Soil} + f_{ww} \quad \textbf{Equation 4-2}$$

where $\delta^{15}N_{Plants}$, $\delta^{15}N_{Soil}$, and $\delta^{15}N_{ww}$ are the nitrogen isotope signatures of plants, soil and wastewater nitrogen. The fractional contributions of soil nitrogen and wastewater nitrogen to plants are represented by f_{Soil} and f_{ww}, respectively. This model was applied to individual plant samples, allowing us to calculate means, medians and confidence intervals for f_{Soil} and f_{ww} by cell, cell type and distance along the slope (Phillips and Gregg, 2001).

A two-source Bayesian mixing model was developed using MixSIAR (R package, Stock and Semmens, 2013) with three factors: subsurface concentrations of wastewater-derived nitrate (continuous), distance of sampling locations along the slope (continuous), and wetland cell (random). Soil and wastewater nitrogen were input as model endmembers. A Dirichlet distribution was used as

the prior distribution in all Bayesian mixing models. Iterations of the mixing models are described in section 4.3.

4.2.6 Biomass measurements

Above ground biomass was estimated using a regression developed from temporally resolved high resolution 4-band remote sensing imagery (Planet Team, 2017) and total biomass samples. Over 40 geolocated biomass samples were collected by harvesting all living plant biomass above the ground surface in 0.25 m^2 quadrats. On two dates, dead biomass was collected to facilitate estimates of turnover rates. Biomass samples were stored in plastic bags on ice before returning to the laboratory where they were weighed prior to drying at 65ºC for at least 48 hr. They were re-weighed to calculate moisture content.

On each biomass sampling date, we used remote sensing data to compute three vegetation indices: normalized difference vegetation index (NDVI), green normalized difference vegetation index (GNDVI), and simple ratio (SR) as described in section C.1 of Appendix C. We used these vegetation indices to develop three separate regressions between vegetation index and biomass. The SR-based regression was selected for further analyses because it explained the most variance and had the smallest error. See section C.1 of Appendix C for more details.

Estimation of peak standing biomass was performed on an annual basis for 2017, 2018 and 2019 using standing biomass yielded from the methods described above and polynomial regressions (quadratic) to approximate changes in plant growth and deposition of plant residues between the early spring and late fall. Regressions were performed in Excel and were used to identify the date of peak biomass (ranged from May 27 to August 20, with a median value of June 11). Peak standing biomass values were calculated by solving the polynomial regressions (described here) on those dates. The median peak standing biomass value (by cell) for the monitoring period was 0.8 kg m^{-2} (95% CI = 0.4 kg m^{-2}, 1.8 kg m^{-2}). Dry weights of below ground plant biomass (primarily composed of roots) were calculated using relationships between mean annual temperature and below ground biomass reported in the literature (Gill et al, 2002).

To calculate total above ground and below ground biomass production (i.e., net primary production), peak live biomass measurements were multiplied by biomass turnover rates (separately for above and below ground biomass). Turnover rates of 4.5 yr^{-1}, 4.35 yr^{-1}, and 4.15 yr^{-1} were estimated for aboveground biomass in wet meadow cells (for 2017, 2018 and 2019 respectively) and rates of 2.0 yr^{-1}, 1.5 yr^{-1}, and 1.15 yr^{-1} were assumed for aboveground biomass in willow cells (for 2017, 2018 and 2019 respectively). These were based on values estimated from biomass harvesting campaigns in 2016 and 2019 and from values reported in the literature (Table C-4). From the literature, median aboveground willow turnover rates were 1.15 yr^{-1}. Median aboveground turnover rates for other wetland species were 3.6 yr^{-1}, which was similar to the median rates calculated in this study (4.2 yr^{-1}). Rates determined in this study were calculated by dividing the sum of the weights of dead and live biomass by the weight of standing live biomass in locations where we collected dead and live biomass.

Belowground biomass was assumed to have a consistent turnover rate of 0.6 yr^{-1} in wet meadow cells based on the relationship presented in Gill et al., (2002) ($\theta_b = 0.29e^{0.046*T}$; where T is the mean average annual temperature in deg C). For wet meadows, below ground biomass model outputs were consistent with a review of past literature values (Gill and Jackson, 2000). In willow cells, belowground biomass was assumed to have a turnover rate of 1.4 yr^{-1} based on median literature values (Rytter, 1999; Grogan and Matthew, 2002; Berhongaray et al., 2013).

4.2.7 Plant uptake calculations

Plant uptake of wastewater-derived nitrogen was quantified by multiplying the total production of above and below ground biomass over time by: (1) the elemental composition of biomass (%N), to determine the total amount of nitrogen stored in plant biomass; and, (2) the fraction of biomass nitrogen derived from wastewater (f_{ww}) from the linear mixing model, to determine the mass of that nitrogen obtained from wastewater. These calculations were performed on individual plant samples to produce spatial distributions of plant uptake (total and from wastewater) over the wetland slope. Spatial distributions were then integrated over the length of the wetland in each cell to produce weighted average values of plant uptake over the entire wetland slope for each cell.

4.2.8 Statistical analyses

Statistical analyses were performed in Excel (Microsoft Corporation, Redmond, WA, USA) using the Real Statistics Resource Pack software (Release 5.4; Zaiontz, 2018). Data were not assumed to be distributed normally and reported p-values were derived from non-parametric analyses (i.e., Wilcoxon signed-rank test for paired samples and Mann-Whitney tests for independent samples) unless otherwise specified. When data were normally distributed (i.e., with a p-value > 0.05 for both Shapiro-Wilk and d'Agostino-Pearson tests) parametric analyses (e.g., t tests) were used as specified in the text.

4.3 Mixing Model Method Development

4.3.1 Background on mixing model types

Mixing models have been used widely in ecological studies, largely focusing on food-web interactions and animal diets (Ogle et al., 2014), with many additional applications, such as in pollutant source identification, cross-ecosystem nutrient transfer analyses and assessments of the biogeochemistry of elemental cycles in ecological systems (Phillips, 2001; Stock et al., 2018). These models have been used to estimate the contribution of various sources to a mixture using tracer data collected from both sources and mixtures (Stock et al., 2018). Among the most common mixing model types are linear mixing models, mixing models based on Euclidean distances and Bayesian mixing models, which are discussed in greater detail below and in Stock et al. (2018).

Linear mixing models. Linear stable isotope mixing models are widely accessible because they rely on a simple theoretical framework that is easy to apply, but they have some important drawbacks and limitations. Linear mixing models rely on the assumption that source proportions vary linearly with isotope values and that tissues are uniformly labelled isotopically (Schwarcz, 1991). Furthermore, applications of linear models frequently provide single average estimates of source proportions without quantifying uncertainty though methods for calculating uncertainty for: (1) single isotope two-source mixing models; and, (2) dual isotope, three-source mixing models can be found in the study by Phillips and Gregg, 2001. These models can also be particularly sensitive to endmember values and cannot distinguish accurately between sources when differences in endmember signatures are less than around 2‰ (Phillips and Gregg, 2001), though the latter issue is common for most mixing model types. Furthermore, linear models cannot incorporate mechanistic information or informative data associated with processes they model, and therefore cannot be used predictively (Ogle et al., 2014).

Bayesian mixing models. Bayesian mixing models have been applied with increasing frequency over the past decade because they can provide more robust results than other mixing models (Stock et al.,

2018). An alternative to linear mixing models, Bayesian mixing models are probabilistic and produce a distribution of outputs based on end-member distributions (Phillips et al., 2014). This is one of the key advantages of Bayesian mixing models: they inherently provide estimates of uncertainty. Bayesian mixing models can also incorporate more information about the system being studied, such as concentration dependence and other random, fixed or continuous variables, and can provide estimates of source contributions in systems that are underdetermined for linear mixing models (i.e., an analytical solution cannot be determined) (Stock et al., 2018). However, Bayesian mixing model outputs are frequently more difficult to understand and apply to research, which may lead to inappropriate applications of those models or erroneous interpretations of results by inexperienced researchers. They can also be sensitive to enrichment factors (Bond and Diamond, 2011), though this is not as relevant in plant uptake studies because plants do not discriminate significantly between isotopes during uptake (Craine et al., 2015).

More thorough comparisons of the strengths and weaknesses of types of stable isotope mixing models can be found in Layman et al. (2012), as well as a variety of other publications (Boecklen et al., 2011; Hopkins and Ferguson, 2012; Phillips, 2012; Parnell et al., 2013; Stock et al., 2018). For the purposes of this study, linear and Bayesian mixing models were tested for the estimation of source contributions of soil and wastewater nitrogen to plant biomass nitrogen.

4.3.2 Mixing model assumptions, results and iterations

Linear and Bayesian stable isotope mixing models were applied iteratively to estimate the fraction of nitrogen uptake into plant biomass derived from wastewater. These estimates were compared with information derived from other lines of evidence (e.g., nitrogen concentrations in porewater samples and water quality monitoring data) to produce more robust estimates. Throughout all iterations, a two-source linear mixing model of the form shown in Equation 4-1 and Equation 4-2 was applied to individual plant samples to produce spatially resolved predictions. In some cases, the linear mixing model yielded unrealistic predictions (i.e., $f_{ww} < 0$ or $f_{ww} > 1$). All outputs greater than 1 were assumed to be 1, while outputs less than 0 were assumed to be 0. A two-source Bayesian mixing model in MixSIAR (Package Download: https://github.com/brianstock/MixSIAR; Package User Manual: https://cran.r-project.org/web/packages/MixSIAR/MixSIAR.pdf) was also developed, which produced estimates based on distance along the wetland slope and subsurface nitrate concentration. Bayesian mixing model outputs ranged from 0-1.

First model iteration. In the first set of mixing models, $\delta^{15}N$ measured in solid soil samples (e.g., $\delta^{15}N = 5.7 \pm 0.5‰$) were used as the first end-member. Average $\delta^{15}N_{soil}$ were estimated in each cell based on soil isotope measurements collected in 2016, despite significant shifts in $\delta^{15}N_{soil}$ values that were observed between 2016 and 2017 (section C.2). In these initial models, average values of $\delta^{15}N$ in wastewater over the entire monitoring period (e.g., $\delta^{15}N = 11.8 \pm 6.5‰$) were used for the $\delta^{15}N_{ww}$ endmember. In the linear mixing model, approximately 9% of the model results were not within the range between 0-1.

The results from this initial iteration differed significantly ($p < 0.005$) between linear and Bayesian models, with median fractions of plant nitrogen derived from wastewater of 100% (95% CI = 11%, 100%) and 81% (95% CI = 0%, 100%) over the entire wetland, respectively. Model outputs over the final two-thirds of the slope were inconsistent with collected water quality and porewater data. On dates in cells where overland flow had been eliminated, linear and Bayesian mixing models yielded outputs for the fraction of plant nitrogen derived from wastewater at 70% (95% CI = 0%, 100%) and 92% (95% CI = 0%, 100%) for plants growing in the last third of the slope, despite the fact that

wastewater nitrogen and its isotope signal were not detectable. Without a significant overland flow, from which plants can derive some nitrogen for growth, the outputs of both models appeared to be erroneous in this first iteration. Model outputs were unlikely explained by: (1) intermittent increases in the applied flow rate leading to overland flow that supplied enriched wastewater nitrogen to these farther reaches of the slope; or, (2) internal cycling of wastewater nitrogen that was taken up into plants during early parts of the monitoring period.

Second model iteration – updating the wastewater endmember. To yield estimates that were more consistent with the other monitoring data we collected at the site, wastewater endmembers were adjusted to reflect the measurements most recently taken before a plant sample was collected (i.e., the average influent nitrate $\delta^{15}N$ measurements over the three months prior to sampling). These values should have reflected the wastewater nitrogen that would have been available to plants for the formation of new tissues (e.g., new growth leaves) leading up to each sampling event. Additionally, $\delta^{15}N$ of wastewater-derived nitrate in porewater was calculated with distance along the slope using spatial zero order removal rates and enrichment factors (section 4.3.3) observed in the subsurface. In the linear mixing model, wastewater endmember values were calculated for each sample based on the location that it was collected from to reflect the wastewater $\delta^{15}N$ that would have been observed in wastewater-derived porewater nitrate at each location. There were also consistent trends in nitrate concentrations with depth at the field site, meaning these values could be further weighted based on profiles of nitrate concentration with depth (section 4.3.3). To calculated the wastewater $\delta^{15}N$ experienced at each location, concentration weighted averages of $\delta^{15}N$ were performed with depth. The Bayesian mixing model could not be performed on individual samples in this way. Rather we were forced to use of the overall distribution of wastewater $\delta^{15}N$ values modeled with distance along the slope as the endmember distribution.

The second iteration of the Bayesian mixing model was significantly different from the first ($p < 0.0001$) with median outputs of 56% (rather than 81%). Bayesian outputs were significantly different from the simple linear mixing model as well ($p < 0.0001$). The fraction of plant nitrogen derived from wastewater was estimated at 36% and 56% over the entire wetland, respectively in these models. Model outputs in the final two-thirds of the wetland slope remained inconsistent with collected water quality and porewater data, though linear mixing model outputs came closer to approximating values that would be consistent with other observations. On dates when overland flow had been eliminated from a subset of wetland cells, linear and Bayesian mixing models yielded outputs for the fraction of plant nitrogen derived from wastewater of 25% and 53% (median values) for plants growing in the last third of the slope.

Third model iteration. In the third and final iteration, Bayesian mixing models from MixSIAR were abandoned because they could not be updated with spatially-resolved endmember values to project uptake fractions for individual measurements. Results from the Bayesian model tended to overestimate the contribution of wastewater-nitrate to plant biomass nitrogen. Additionally, these models appeared to be less sensitive to the significant spatial variations in endmember values for wastewater-nitrate, as well as spatial variability in plant isotope measurements, when compared to simple linear mixing models. For example, if we compare average estimates of the contribution of wastewater-derived nitrate to biomass nitrogen over the last third of the slope in cells D through L on February 2019, outputs from MixSIAR models ranged from 39 ± 16% to 71 ± 19% (for optimized and unoptimized iterations respectively) compared to an output of 8 ± 8% from the linear mixing model. Given that overland flow had been eliminated for over a year by this sampling date and that wastewater-nitrate is removed in the subsurface within the first third of the wetland, MixSIAR results presented here appear to be significant ($p < 0.001$) overestimates of uptake compared to the linear mixing model.

We updated the soil endmember values to take into account the porewater "soil-nitrate" measurements that we observed in 2019 (section 4.3.3). Because there were no consistent or significant spatial distributions of soil-nitrate $\delta^{15}N$ values (Figure 4-12), we used the average $\delta^{15}N$ value for these measurements, which was 10.6 ± 2.4‰, as the soil nitrogen endmember, which was more consistent with the values of $\delta^{15}N$ measured in plant leaves (~13‰) in the portions of the slope that did not receive wastewater nitrogen inputs on those dates.

Because the first half of the monitoring period was characterized by extended periods of substantial overland flow (e.g., 40-80% of applied wastewater flowed over the wetland surface; Chapter 1), it is also possible that these plants were enriched in ^{15}N because a fraction of wastewater-derived nitrogen had been taken up into plant biomass at distances beyond 5 m over previous dates and then was cycled back into the subsurface through decomposition of organic matter. If this were the case though, it would further justify the use of soil nitrate measurements described in section 4.3.3 as an endmember as opposed to solid-phase soil $\delta^{15}N$ values. If wastewater-derived nitrogen were taken up into plant biomass that was later deposited onto the wetland surface and decomposed, then the isotope signature of the nitrogen pool in soil and plant residues that was available for plant growth would become progressively enriched in ^{15}N: a phenomenon for which we have evidence. In soil samples collected sequentially with depth in 2018, samples from the first 2 m of the slope and the top 10 cm of the soil were significantly ($p < 0.01$; two-tailed t test) more enriched in ^{15}N (7.0 ± 0.5‰) relative to samples collected in the bottom 80 cm of the soil (5.7 ± 0.3‰). This suggests that, despite evidence that over time the overall soil nitrogen pool became more depleted in ^{15}N (see section C.2.3), the most available fraction of that pool (i.e., the surficial soil and decomposing plant biomass) actually became more enriched compared to the original soil nitrogen pool, possibly due to internal cycling of wastewater nitrogen. Therefore, if the solid-phase soil nitrogen measurements described previously (5.7 ± 0.5‰) had been used as the soil end-member, we would have more than doubled the estimated mass of wastewater nitrogen taken up into biomass (i.e., 380 kg N v. 180 kg N). Based on these combined lines of evidence we determined that using the $\delta^{15}N$ values measured in soil nitrate yields the most robust and accurate representation of what is happening with respect to plant uptake at the field site.

In the final iteration, predictions of the fraction of wastewater derived nitrogen in plant biomass for the linear mixing model were significantly different ($p < 0.0001$) from previous iterations with a median value of 20%. In the first 10 m of the slope, average model outputs remained high at 66 ± 12%, consistent with the high concentrations of wastewater nitrogen in porewater samples collected from that part of the slope. Over the last two-thirds of the slope, results were significantly ($p < 0.0001$) lower than previous results with a median value of 13%, which was more consistent with levels of overland flow observed in this system. Results from this final iteration of our mixing models were consistent with other observations collected at the field site. We performed sensitivity analyses around this final mixing model to test output sensitivity to changes in endmembers and sensitivity to overall plant nitrogen uptake calculations to changes in biomass estimates.

4.3.3 Mixing model endmember values

Variation in wastewater nitrate isotopes. Throughout the monitoring period, $\delta^{15}N$ values for influent wastewater-derived nitrate averaged 11.8 ± 6.5‰. These values varied widely, ranging from 3.5‰ to 35.9‰, but were significantly different than values of $\delta^{15}N$ found in soils ($p < 0.001$) (Figure 4-2). $\delta^{18}O$ values in nitrate in the influent wastewater were similarly variable, averaging 0.71 ± 7.6‰ with a range from -6.0‰ to 24.5‰. Observed $\delta^{18}O$ values fell within the range of values expected for wastewater-derived nitrate (Kendall, 1998; Kaushal et al., 2011).

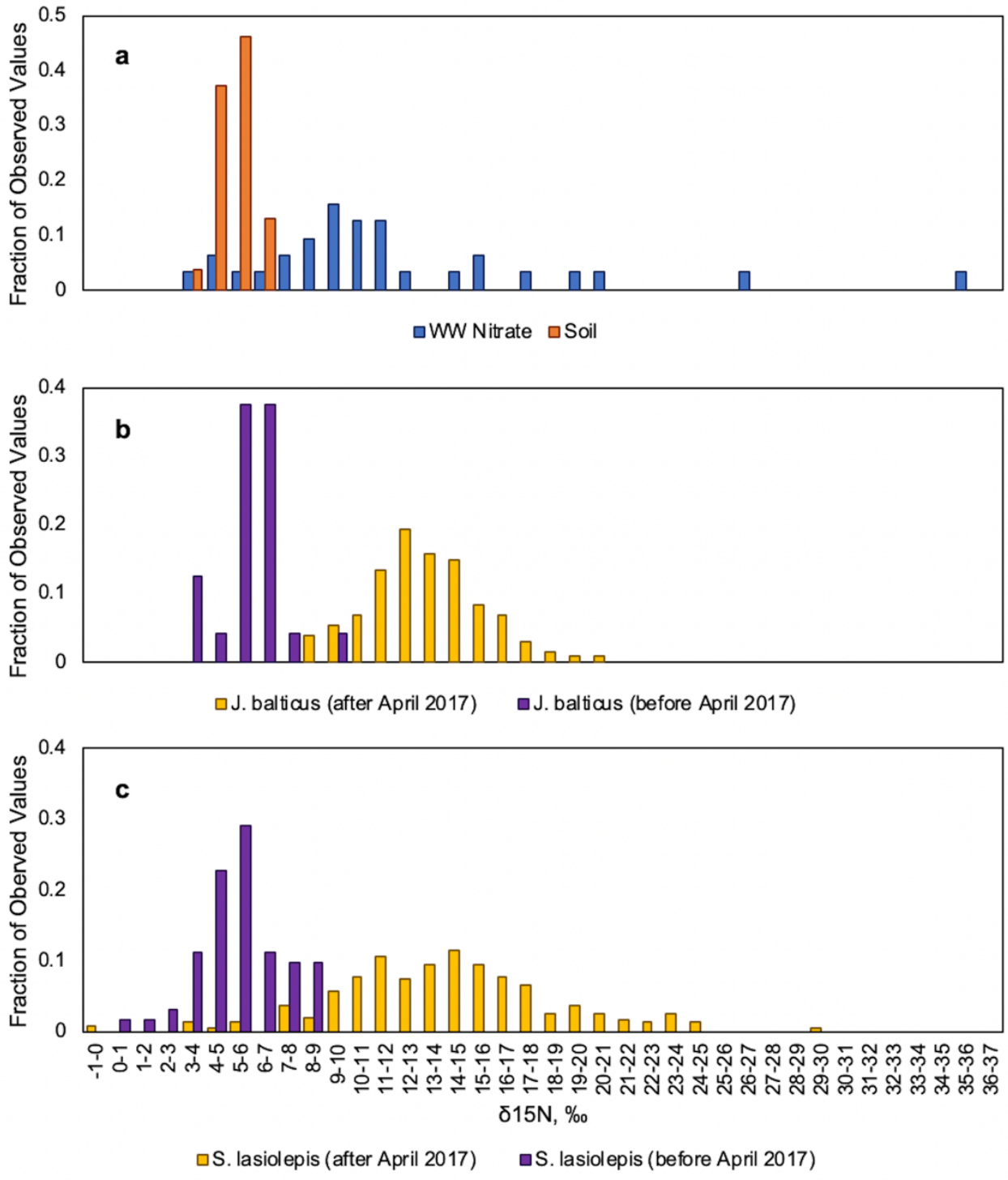

Figure 4-2: Histograms of $\delta^{15}N$ measurements in soils and plants. (a) $\delta^{15}N$ measurements in soil (orange bars) and wastewater nitrate (blue bars); and, foliar $\delta^{15}N$ measurements in: (b) *J. balticus*; and, (c) *S. lasiolepis* before (purple bars) and after (yellow bars) application of wastewater to the experimental system. Over the monitoring period, foliar $\delta^{15}N$ values of *S. lasiolepis* and *J. balticus* samples followed bimodal distributions, with $\delta^{15}N$ values in samples collected prior to April 2017 overlapping with soil $\delta^{15}N$ values and $\delta^{15}N$ values in samples collected after April 2017 overlapping to a greater degree with $\delta^{15}N$ values in influent wastewater nitrate.

There were significant differences in values for both $\delta^{15}N$ ($p < 0.05$; two tailed t test) and $\delta^{18}O$ ($p < 0.001$; two tailed t test) in nitrate before and after an operational change in November 2017 when flows rerouted directly from the nitrification facility onsite to the influent of the subsurface wetland (rather than routing the flow through the surface-flow wetland first). Before November 2017, $\delta^{15}N$ and $\delta^{18}O$ values were 16.8 ± 9.7‰ and 11.1 ± 6.0‰ respectively, whereas these values were 9.9 ± 3.5‰ and -3.4 ± 2.4‰ after the operational change. Lower $\delta^{15}N$ and $\delta^{18}O$ values were to be expected after the operational change because nitrate removal was often significant in the adjacent surface-flow wetland (i.e., nitrate concentrations dropped on average from 2.2 ± 0.2 mM to 0.7 ± 0.4 mM in the surface-flow wetland between June 2017 and November 2017) and microbial processes responsible for nitrate removal (e.g., denitrification) cause residual nitrate pools to become progressively enriched in ^{15}N and ^{18}O (Kendall, 1998).

Subsurface nitrate isotope dynamics. Progressive depletion of wastewater-derived nitrate in the bottom layer of the subsurface (where the majority of subsurface flow occurred) was paired with increasing $\delta^{15}N$ and $\delta^{18}O$ values (Figure 4-8) as distances increased along the wetland slope. $\delta^{15}N$ and $\delta^{18}O$ values were strongly coupled in the first 5 m of the wetland slope, following the trend expected when denitrification is significant (Figure 4-9a) (Kendall, 1998; Kendall et al., 2007). These trends (i.e., depletion of nitrate and enrichment in ^{15}N) were consistent across wetland cells, types and dates (Figure 4-9).

Zero order nitrate removal rate constants (k) were derived from the observed decreases of nitrate concentrations in porewater samples from the bottom layer of the subsurface across various dates according to the following equation:

$$[NO_3^-]/[NO_3^-]_o = 1 - (k)(d) \qquad \textbf{Equation 4-3}$$

where $[NO_3^-]$ is the nitrate concentration in a given porewater sample, $[NO_3^-]_o$ is the influent nitrate concentration, k is the zero order rate constant in m^{-1} and d is the distance in m. Because no obvious trends in seasonality were observed (Figure 4-3), the average k value across all sampling dates was used in modeling concentrations of nitrate and $\delta^{15}N_{ww}$ for dates when porewater samples were not collected. Equation 4-3 was used to model the fraction of nitrate remaining (i.e., $[NO_3^-]/[NO_3^-]_o$), which is equivalent to "f" in Equation 4-4.

Enrichment factors. Enrichment factors for $\delta^{18}O$ and $\delta^{15}N$ during denitrification were calculated according to Equation 4-4 (Mariotti et al., 1981):

$$\varepsilon_i = \frac{\delta_i - \delta_{i,o}}{\ln f} \qquad \textbf{Equation 4-4}$$

where ε_i represents the isotopic enrichment factor and i corresponds to nitrogen or oxygen respectively, $\delta_{i,o}$ represents the influent measured isotopic ratios, δ_i represents the isotopic ratios measured throughout the wetland, and ln(f) corresponds to the fractional extent of the reaction (i.e., the fraction of influent nitrate remaining).

By plotting values of $\ln([NO_3^-]/[NO_3^-]_o)$ versus $(\delta_i - \delta_{i,o})$, we derived average enrichment factors for wastewater-derived porewater nitrate (i.e., -8.1 ± 1.0‰ and -7.2 ± 1.2‰ respectively for nitrogen and oxygen) with an average ratio of enrichment factors (i.e., $\varepsilon_O/\varepsilon_N$) of 0.79 ± 0.06. Values for ε_N and $\varepsilon_O/\varepsilon_N$ were consistent with values measured for denitrification in the environment. Literature values for ε_N range from -5 to -40‰ (Kendall, 1998).

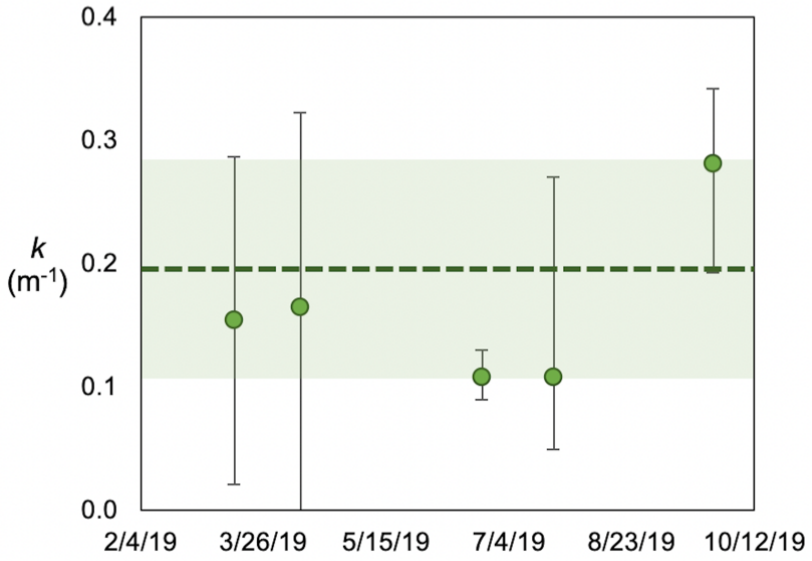

Figure 4-3: Zero order nitrate (*k*) removal rate constants throughout 2019. The overall median rates constant (0.20 m^{-1}) is delineated with the horizontal dashed line with the shaded region shown the 95% confidence interval (95% CI = 0.13 m^{-1}, 0.28 m^{-1}).

Although previously published studies in environmental systems predominantly yielded $\varepsilon_O/\varepsilon_N$ values closer to 0.5 (Kendall, 1998; review of past studies), more recent research has suggested that the range of expected $\varepsilon_O/\varepsilon_N$ values is ~0.5-1 and pure cultures of denitrifiers have been shown to produce $\varepsilon_O/\varepsilon_N$ values close to 1 (Granger et al., 2004). Values of -6.7‰, -12‰ and 1.8 were calculated for ε_N, ε_O and $\varepsilon_O/\varepsilon_N$ in "soil nitrate". Both wastewater nitrate and soil nitrate values followed Rayleigh kinetics closely (Figure 4-4). The decoupling of ε_O and ε_N in "soil nitrate" was likely caused by the more varied set of nitrogen cycle processes, such as anammox and Feammox, that become important at the low nitrate concentrations (Dähnke and Thamdrup, 2016).

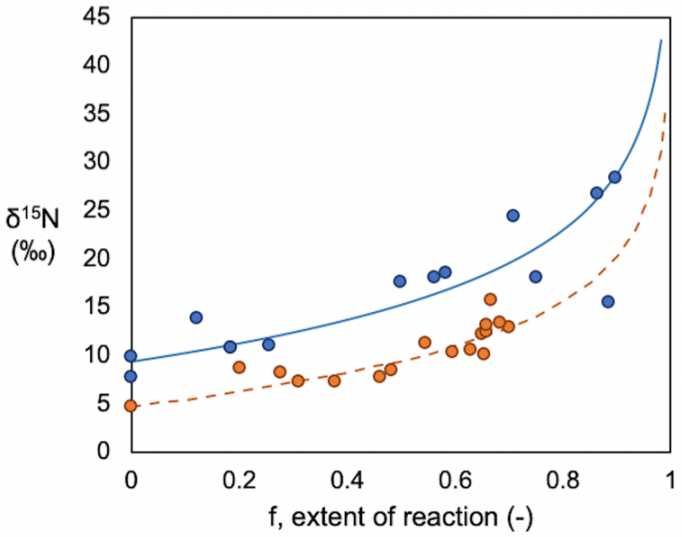

Figure 4-4: Rayleigh kinetics of $\delta^{15}N$ in nitrate for: wastewater-derived nitrate (blue points; blue solid line) and soil-derived nitrate (orange points; orange dashed line) in the subsurface.

Predicting $\delta^{15}N$ in porewater. Combining Equation 4-3 and Equation 4-4, we produced a model that was used to project $\delta^{15}N_{ww}$ values at various distances in the subsurface as follows:

$$\delta_{N,d} = (\varepsilon_N)(1 - k * d) + \delta_{N,o} \qquad \textbf{Equation 4-5}$$

where ε_N is the calculated enrichment factor for nitrate-N during subsurface nitrate removal (see the preceding section), $\delta_{N,o}$ is the $\delta^{15}N$ value for influent wastewater (‰), d is the distance along the slope in m, k is the zero order rate constant in m^{-1} and $\delta_{N,d}$ is the calculated $\delta^{15}N$ value for porewater nitrate at the distance d (‰). An example of modeled nitrate concentrations and $\delta^{15}N$ values, compared to measured values from April 2019 is presented in Figure 4-5.

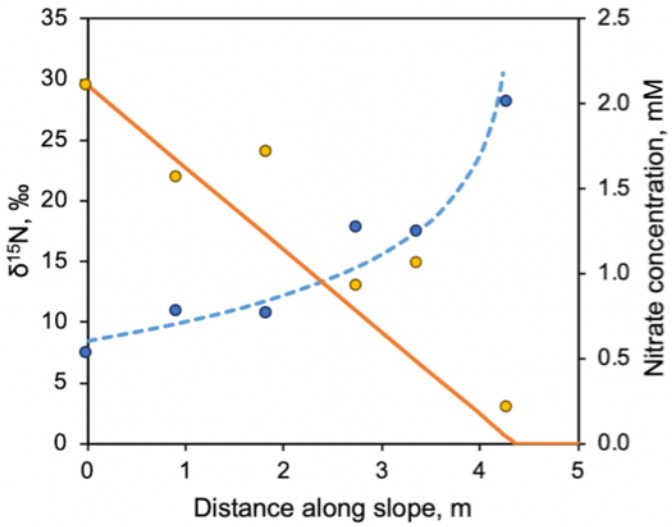

Figure 4-5: Modeled $\delta^{15}N$ values and nitrate concentrations (blue dashed line and orange solid line respectively; left and right vertical axes, respectively) compared with individual measurements (blue and yellow points) from April 2019.

On dates when there was significant overland flow, which was the case for the majority of wetland cells prior to August of 2018, a similar model to the one described above was used to estimate the concentration and $\delta^{15}N$ values of wastewater-derived nitrate in surface layers within the wetland. For this top layer of the wetland soils, it was estimated that removal exhibited zero-order kinetics with depth within the top 10 cm after which nitrate concentrations were not detectable. This was consistent with results from porewater sampling, which revealed that concentrations of nitrate decreased from influent concentrations at the surface to non-detect at depths of ~10-20 cm. Nitrate concentrations at depths between approximately 0.2 and 0.6 m were below the detection limit throughout the majority of the wetland. Nitrate likely diffused into the top layer of the wetland sediment from nitrate-rich water flowing over the wetland surface. Modeled concentrations of nitrate and influent $\delta^{15}N$ values for wastewater nitrate were input to Equation 4-5 to calculate $\delta^{15}N$ values at each depth. The overall average $\delta^{15}N$ values at each distance was then calculated by weighting $\delta^{15}N$ values at various depths by the concentration of nitrate at that depth in a modified Riemann sum according to Equation 4-6.

$$\delta_{N,ave} = \frac{\Sigma([NO_3^-]_h)(\delta_{N,h})}{\Sigma[NO_3^-]_h} \qquad \textbf{Equation 4-6}$$

where $\delta_{\mathrm{N,ave}}$ is the concentration-weight average $\delta^{15}N$ value for wastewater nitrate at each location, $[NO_3^-]_h$ is the concentration of nitrate at each depth h, and $\delta_{\mathrm{N},h}$ is the modeled $\delta^{15}N$ value for wastewater nitrate at each depth h.

Soil-derived porewater nitrate. A second source of nitrate was also identified in porewater samples, which was likely derived from the conversion of soil nitrogen and organic nitrogen to nitrate through ammonification and nitrification. During nitrification, oxygen that is incorporated into produced nitrate comes from water and dissolved oxygen. We would expect dissolved oxygen to be relatively enriched in ^{18}O in a horizontal levee because microbial activity in surface layers can lead to lower dissolved oxygen concentrations and enrichment of the residual dissolved oxygen pool in ^{18}O. High evapotranspiration rates could cause similar enrichment trends to occur in water oxygen (Kendall, 1998).

At distances beyond 4 m in the subsurface, we observed this second nitrate source, "soil-nitrate", in porewater samples from the bottom layers within the wetland subsurface. The tight coupling of $\delta^{15}N$ and $\delta^{18}O$ values observed in the first 4 m no longer held past this point on most sampling dates (Figure 4-10 and Figure 4-11). The two separate nitrate pools are particularly evident in Figure 4-11b with data clustered to the top-left and bottom-right of the chart along diagonal trendlines, which are consistent with past research on pools of nitrate that are being denitrified (i.e., nitrate pools undergoing denitrification become progressively more enriched in ^{18}O and ^{15}N). The $\delta^{15}N$ and $\delta^{18}O$ values in these two pools are significantly different from each other ($p < 0.001$; two-tailed t tests for both), though they follow similar trends.

Nitrate concentrations, $\delta^{18}O$ and $\delta^{15}N$ values in this second nitrate pool followed expected trends. Nitrate concentrations decreased with increasing $\delta^{18}O$ and $\delta^{15}N$ values in this nitrate pool (Figure 4-9d) and followed Rayleigh kinetics (see section on enrichment factors). Additionally, we produced a Keeling plot (Figure 4-13) to identify the original $\delta^{15}N$ value for this source of nitrate. We did not observe significant spatial trends in the concentration or isotope signature of soil-nitrate observations (Figure 4-12), suggesting that this pool of nitrate was being formed throughout the entire wetland.

4.3.4 Sensitivity analyses

Endmember sensitivity analysis. We first performed a sensitivity analysis on model outputs to determine the impact of changes in endmember values on: (1) the fraction of nitrogen in plants derived from wastewater; and, (2) the fraction of wastewater nitrogen removal attributable to plant uptake. The full results of this analysis are provided in Table 4-1. In the sensitivity analysis, we found that a change of 2‰ in the endmember values corresponded to a change in model outputs of up to 61%. A 2‰ change in soil $\delta^{15}N$ values corresponded to average changes of 26% in both the fraction of biomass nitrogen derived from wastewater and the fraction of applied nitrogen removed by plant uptake. Changes of 2‰ in wastewater $\delta^{15}N$ values corresponded to average changes of 8% in both outputs. Based on these results, we concluded that model results were less sensitive to small changes in the wastewater endmember value, but relatively sensitive to changes in the soil endmember value. For example, a shift of ~6‰ in the soil endmember could account for 70% change in model outputs.

Biomass sensitivity analysis. We also evaluated the sensitivity of plant nitrogen uptake calculations to biomass. Changes of 0.1 kg m^{-2} in peak standing biomass (which corresponded to 0.1-0.4 kg m^{-2} more per year when turnover rates are considered, roughly a 10% increase in total biomass production) corresponded to an increase of 1% in the fraction of wastewater nitrogen attributed to plant uptake (e.g., 9% of wastewater nitrogen was removed by uptake as opposed to 8%). This corresponded to

approximately a 10% increase in the mass of nitrogen . Based on these results we concluded that model outputs were sensitive to changes in biomass production and peak biomass, especially for plants with large turnover rates, suggesting that moderate errors (~0.1 kg m^{-2}) in our biomass measurement method would add a significant amount of additional error to our model predictions.

Table 4-1: The impact of changing endmember values on mixing model outputs: (1) the fraction of biomass nitrogen calculated as coming from wastewater, and (2) the fraction of applied nitrogen removed by uptake. Values for "% Change" are relative to the preceding condition.

Change in EM Values		Fraction of biomass N from WW		Fraction of applied N to uptake	
$\delta^{15}N_{ww}$, ‰	$\delta^{15}N_{soil}$, ‰	Average, -	% Change	Average, -	% Change
0	-12	0.41	-	0.24	-
0	-10	0.38	7	0.22	9
0	-8	0.34	11	0.20	10
0	-6	0.30	13	0.18	11
0	-4	0.26	14	0.15	18
0	-2	0.20	26	0.12	22
0	0	0.15	28	0.08	40
0	2	0.08	61	0.05	46
0	4	0.05	46	0.03	50
-4	0	0.16	-	0.09	-
-2	0	0.16	0	0.09	5
0	0	0.15	6	0.08	6
2	0	0.13	14	0.08	6
4	0	0.12	8	0.07	13
6	0	0.11	9	0.06	8
8	0	0.10	10	0.06	5
10	0	0.09	11	0.05	18

4.4 Results and Discussion

Over the two-year monitoring period (6/2017-6/2019), 3570 kg of nitrogen were applied to the horizontal levee. 1660 kg of nitrogen that left the system in wetland effluent was mainly due to overland flow (Figure 4-6). As described in Chapter 2 (Cecchetti et al., 2020a) there were three operational phases during this period (6/2017-11/2017, 11/2017-7/2018, and 7/2018-6/2019), in which flow within the horizontal levee was progressively adjusted to improve system performance. Nitrogen removal increased from 48% of the influent nitrogen mass during the first two monitoring phases to 62% in the final monitoring phase, with >96% removal of nitrogen in the 9 cells operated without overland flow during the final monitoring phase.

Approximately 81% of the applied nitrogen consisted of nitrate. The remainder was comprised of dissolved organic nitrogen (7%), nitrite (3%) and ammonium (9%). Therefore, the most significant nitrogen removal processes in this system were those related to nitrate removal (i.e., microbial assimilation, denitrification, and plant uptake). The full dataset can be found on Mendeley Data (Cecchetti et al., 2020b).

4.4.1 Nitrogen isotope signatures of plants

Data collected throughout the monitoring period were consistent with previous findings that nitrogen in municipal wastewater tends to be enriched isotopically relative to other sources (Heaton, 1986; Kendall, 1998). $\delta^{15}N$ values measured in wastewater had a median value of 9.8‰ (ranging from 3.5‰ to 35.9‰) compared to $\delta^{15}N$ values of 5.7 ± 0.5‰ observed in soil samples.

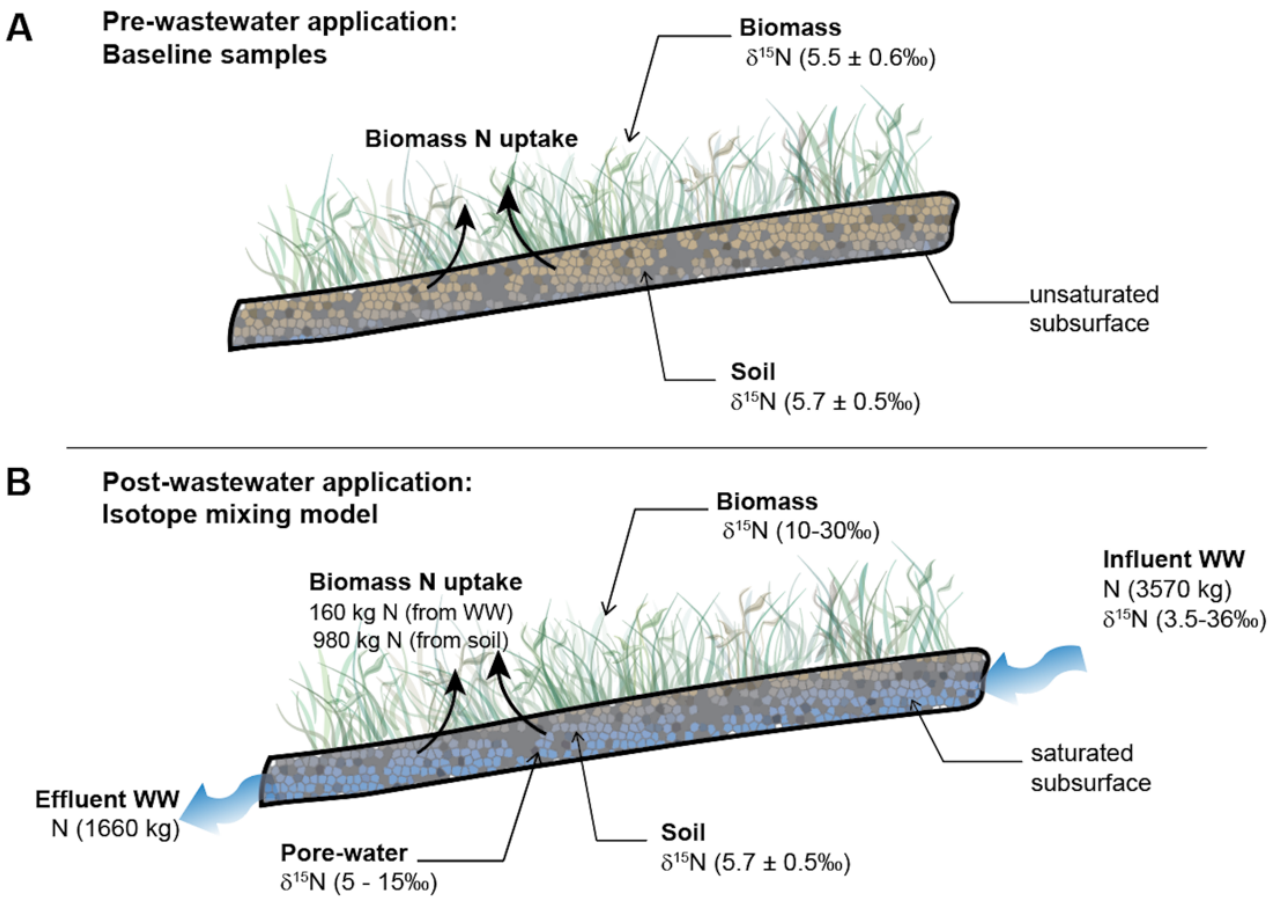

Figure 4-6: Nitrogen mass and isotope flows that were used to evaluated plant uptake of nitrogen. Panel A presents baseline samples, which were collected before the application of wastewater effluent. Panel B presents the isotope mixing model used in this study (post-application). Ranges of $\delta^{15}N$ for porewater, biomass, and influent wastewater in Panel B are approximate. Acronyms: WW = wastewater.

Prior to introduction of wastewater into the subsurface in April 2017 (Figure 4-6a), new-growth foliar plant samples were statistically indistinguishable from soil in terms of $\delta^{15}N$ ($p = 0.59$ and 0.41 from two-tailed t tests for *J. balticus* and *S. lasiolepis*) and also in terms of $\delta^{34}S$ for *J. balticus* ($p = 0.12$) (Figure 4-7), which was consistent with past findings (Tcherkez and Tea, 2013; Craine et al., 2015). In terms of $\delta^{34}S$, *S. lasiolepis* was offset by less than 1‰ ($p < 0.01$) from the soil.

As expected, after wastewater effluent was introduced into the subsurface in April 2017 (Figure 4-6b), shifts in the values of $\delta^{15}N$ were observed in foliar samples (Figure 4-7). After April 2017, $\delta^{15}N$ in foliar samples (of all types) had a median value of 13.8‰ with 95% of measured values falling between 7.4‰ and 23.7‰. This sample distribution was significantly higher ($p < 0.001$) than $\delta^{15}N$ values in plants and soils prior to the introduction of wastewater, despite large variations among individual measurements. More details on the distributions of $\delta^{15}N$ values from different sample types are included in section C.2 and Figure 4-2. $\delta^{34}S$ measured in *J. balticus* did not change significantly ($p = 0.51$) after wastewater was introduced, though $\delta^{34}S$ values in *S. lasiolepis* increased significantly ($p < 0.001$), suggesting these plants were accessing different sources of sulfur.

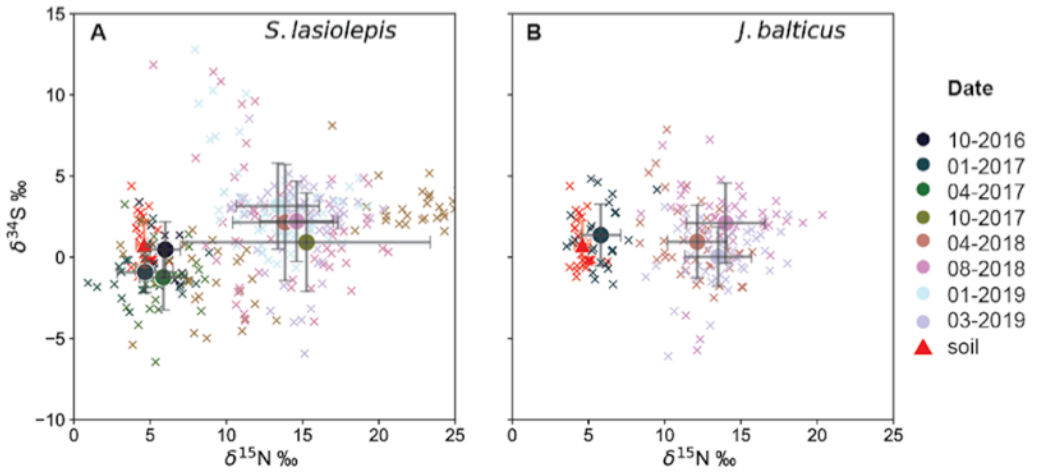

Figure 4-7: $\delta^{15}N$ and $\delta^{34}S$ in new-growth foliar samples from (a) Arroyo willows (*S. lasiolepis*) collected in cells H, J and L and (b) Baltic rushes (*J. balticus*) collected in cells A-G, I and K. Error bars represent the standard deviation of collected samples.

4.4.2 Mixing models

Despite the advantages associated with Bayesian mixing models (section 4.3.1; Phillips et al., 2014), we used a linear mixing model to calculate plant uptake of wastewater-derived nitrogen because it was computationally simpler, could be applied flexibly to individual data points and avoided bias observed in Bayesian models (section 4.3.2) during method development. We progressively optimized our linear mixing models to reflect the conditions at the horizontal levee field site more accurately as described in section 4.3.2.

Endmember values. Throughout the monitoring period, soil nitrogen values were normally distributed with average $\delta^{15}N$ values of 5.7 ± 0.5‰ and a range from 3.8‰ to 6.8‰ (Figure 4-2). Conversely, there were wide variations in $\delta^{15}N$ values in wastewater nitrate applied to the system, which were log-normally distributed with a median value of 9.8‰ and a range from 3.5‰ to 35.9‰. Although there was some overlap, differences in $\delta^{15}N$ from the two sources were significant ($p < 0.001$). The range of observed values for wastewater-derived nitrogen was also consistent with previous findings (Kendall, 1998). Measurements that fell outside of the range of previously reported values likely were caused by operational conditions occurring during the first 6 months of the monitoring period, when influent was passed through a surface flow wetland prior to entering the subsurface as described in Chapter 2 (Cecchetti et al., 2020a) and section A.2 of Appendix A. In the surface flow wetland, nitrate was partially denitrified, and the residual nitrate pool became enriched in ^{15}N.

We also observed progressive enrichment of $\delta^{15}N$ and $\delta^{18}O$ values as nitrate was removed in the subsurface. This phenomenon was consistent with the results of past studies of denitrification (Kendall, 1998; Kendall et al., 2007), suggesting that denitrification was important in the subsurface. Specifically, values of $\delta^{15}N$ and $\delta^{18}O$ increased according to a tightly coupled trend as concentrations of nitrate decreased (section 4.3.3). Additionally, enrichment factors (section 4.3.3) for both $\delta^{15}N$ and $\delta^{18}O$ were consistent with past research on denitrification in subsurface and groundwater systems (Böttcher et al., 1990; Aravena and Robertson, 1998; Mengis et al., 1999). Enrichment of nitrate in

^{15}N due to denitrification likely explains why some foliar $\delta^{15}N$ values were higher than the values of $\delta^{15}N$ measured in wastewater-nitrate collected on preceding sampling dates, which should have reflected the wastewater nitrogen available to those foliar samples (section C.2.2 of Appendix C). Progressive depletion of nitrate and enrichment in ^{15}N was observed consistently across wetland cell types and all four dates when porewater samples were collected (Figure 4-8 and Figure 4-9).

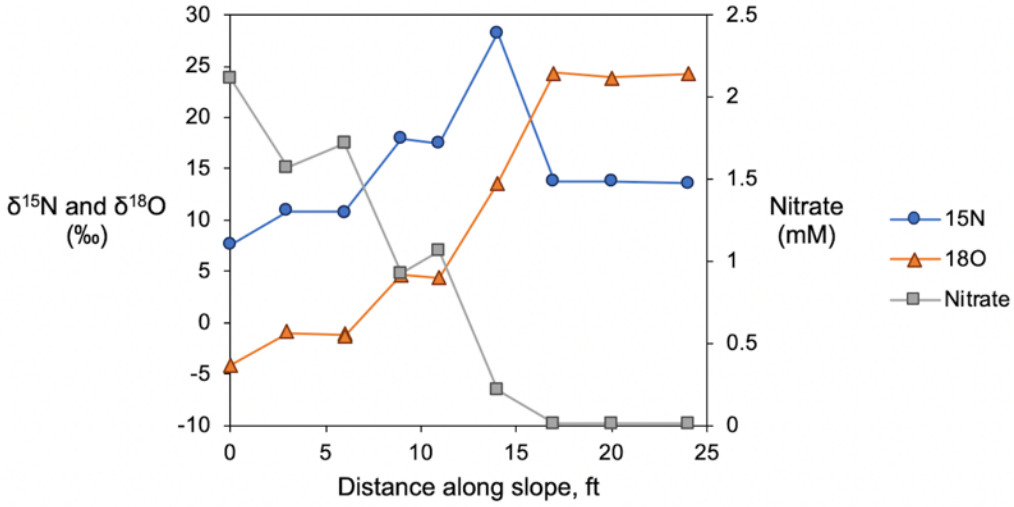

Figure 4-8: Average $\delta^{15}N$ and $\delta^{18}O$ in nitrate and concentrations of nitrate in replicate samples with distance along the slope in cell F in April 2019.

Within the subsurface, wastewater-derived nitrate was denitrified in the first 5 m of the slope. Changes in concentrations of wastewater nitrate in this region were best approximated by a zero-order removal process. Fitted zero-order equations were used to model nitrate concentrations at distances less than 5 m and were paired with enrichment factors (section 4.3.3) to model spatially-resolved wastewater endmember values that could be used to apply the linear mixing model to individual plant samples (section 4.3.3).

At distances beyond 5 m, porewater nitrate concentrations were below 0.4 mg N L^{-1} and did not exhibit significant trends (Figure 4-9e). The coupling of $\delta^{15}N$ and $\delta^{18}O$ values observed in the majority (approximately 75%) of samples collected within the first 5 m was not observed in other parts of the wetland: ratios of $\delta^{18}O$ to $\delta^{15}N$ were significantly ($p < 0.001$) higher ($\delta^{18}O/\delta^{15}N = 1.8$) relative to the first 5 m of the slope ($\delta^{18}O/\delta^{15}N = 0.8$) (Figure 4-10). When porewater nitrate $\delta^{15}N$ and $\delta^{18}O$ were plotted in dual isotope space (i.e. $\delta^{18}O$ v. $\delta^{15}N$; Figure 4-11), values from these two parts of the wetland clustered in distinct regions, suggesting the presence of two sources of nitrate in the porewater.

Porewater nitrate with this second isotopic signature (i.e., higher $\delta^{18}O/\delta^{15}N$ ratios) were considered to be attributable to a separate source of nitrate from wastewater-derived nitrate and were used as the second endmember in the mixing model as described in section 4.3.3. Similar to wastewater-derived nitrate, we observed increasing $\delta^{18}O$ and $\delta^{15}N$ values as nitrate concentrations decreased within this nitrate pool. However, significant spatial trends were not observed, suggesting formation of nitrate from this source occurred across the entire wetland ($r^2 < 0.01$ for all regression types tested; Figure 4-12). Based on their significantly greater $\delta^{18}O$ values, we hypothesized that this second source of nitrate was derived from soil nitrogen and/or decay of plant biomass (see section 4.3.3).

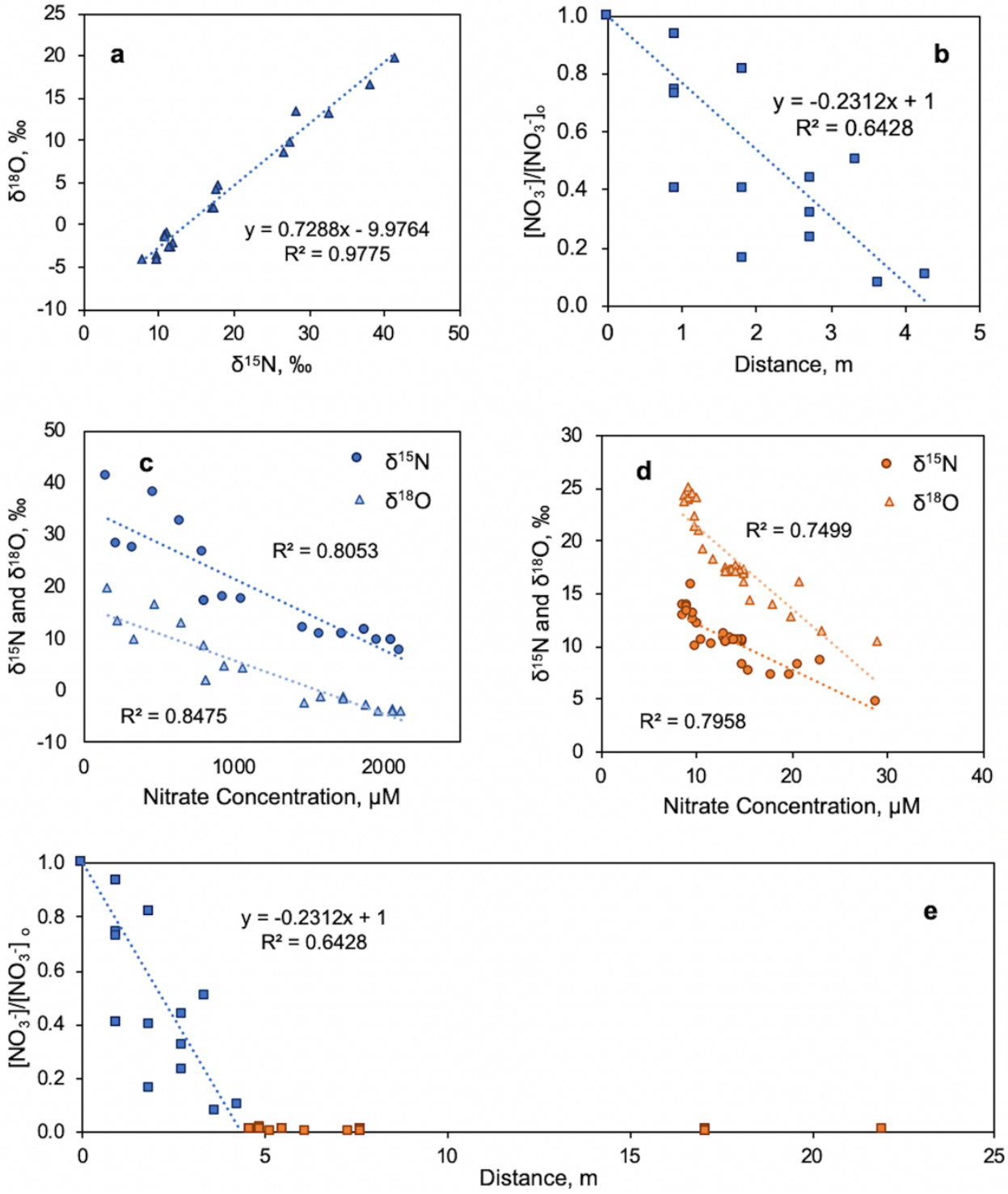

Figure 4-9: Trends in $\delta^{15}N$ and $\delta^{18}O$ of porewater nitrate and porewater nitrate concentrations across sampling dates and cell types. (a) Trend of $\delta^{15}N$ and $\delta^{18}O$ in wastewater-derived porewater nitrate in the first 5 m of the slope. (b) Zero order distance-based nitrate removal reaction relationship (zero order reaction rate constant, k = 0.07 m^{-1}). (c) Trends of increasing $\delta^{15}N$ and $\delta^{18}O$ in wastewater-derived porewater nitrate with decreasing nitrate concentrations. (d) Trends of increasing $\delta^{15}N$ and $\delta^{18}O$ in soil-derived porewater nitrate with decreasing nitrate concentrations. (e) The remaining fraction of influent nitrate in porewater along entire slope (blue boxes represent wastewater-derived nitrate and orange boxes represent soil-derived nitrate).

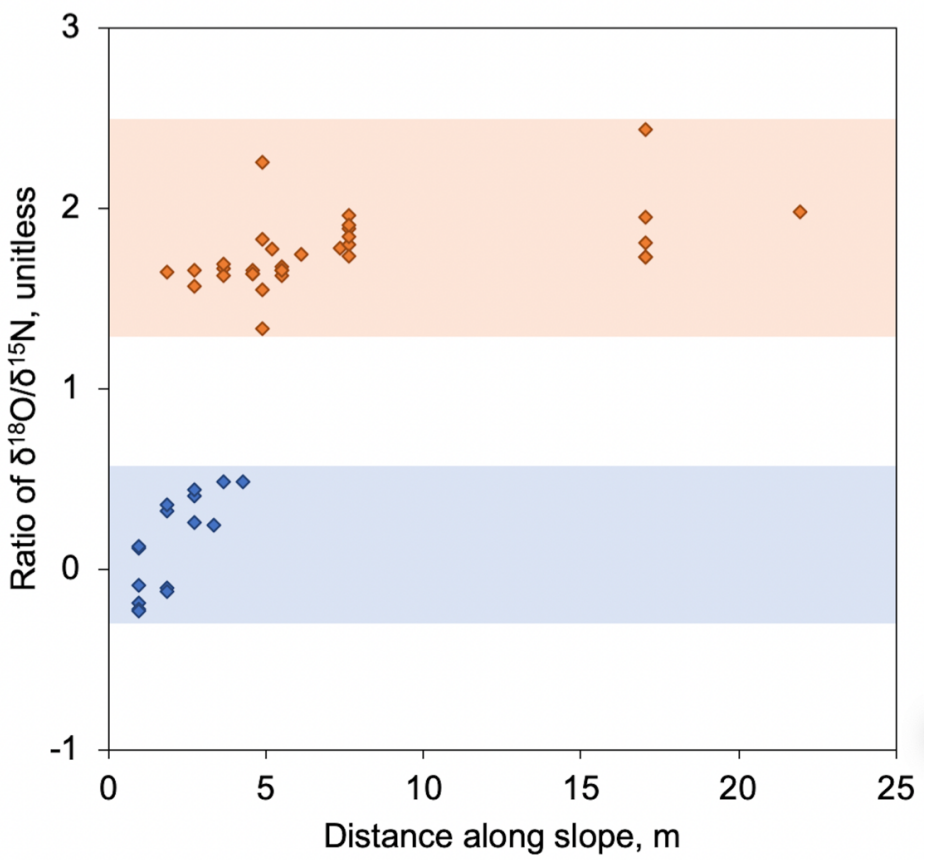

Figure 4-10: Ratios of $\delta^{18}O/\delta^{15}N$ in porewater collected along the horizontal levee slope. The blue shaded region and blue points correspond to wastewater-derived nitrate and the orange shaded region and orange points correspond to soil or plant derived nitrate. The distance at which the soil or plant-derived nitrate signal began to dominate depended on the rate at which denitrification removed wastewater-derived nitrate in the first few meters. For example, on September 25, 2019, samples collected in cell D exhibited the $\delta^{18}O/\delta^{15}N$ signal associated with soil/plant-derived nitrate by 1.8 m from the inlet, whereas the $\delta^{18}O/\delta^{15}N$ signal associated with wastewater-derived nitrate was observed in cell H until after 3.5 m. The variation in the distance at which soil/plant-derived nitrate was observed did not vary significantly ($p > 0.05$) by cell, cell type or seasonally.

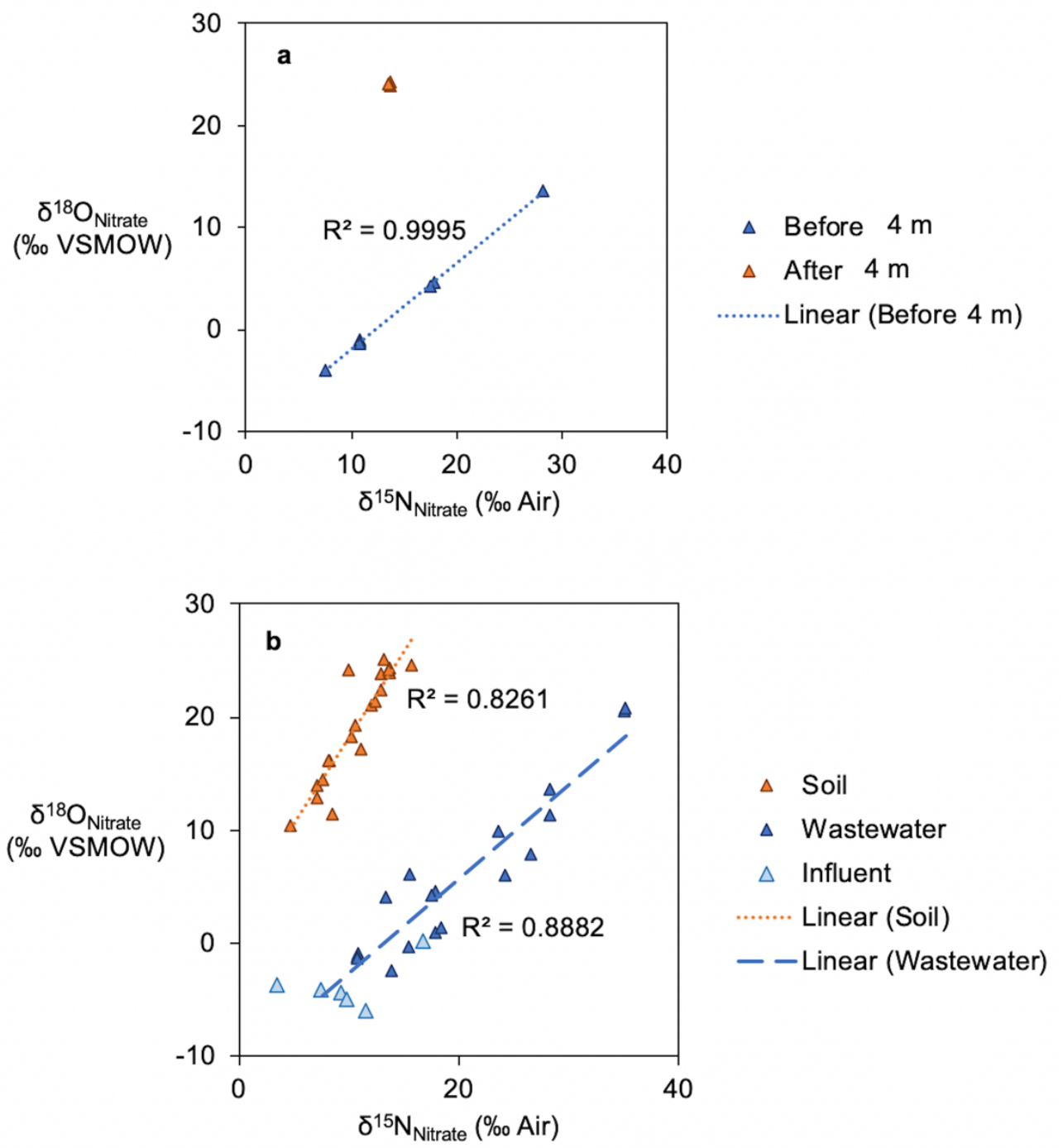

Figure 4-11: Measurements of $\delta^{15}N$ versus $\delta^{18}O$ in porewater samples. (a) Samples collected in April 2019 segregated by those collected before (blue crosses) and after (orange circles) 4 m along the slope. A strong linear relationship ($r^2 = 0.9995$) between $\delta^{15}N$ and $\delta^{18}O$ can be observed for samples collected prior to 4 m. (b) Samples collected over a variety of dates (February, March and April 2019) divided into influent samples (green squares) and porewater samples. The porewater samples are further divided among those derived from wastewater (blue crosses) and those derived from soil (orange circles).

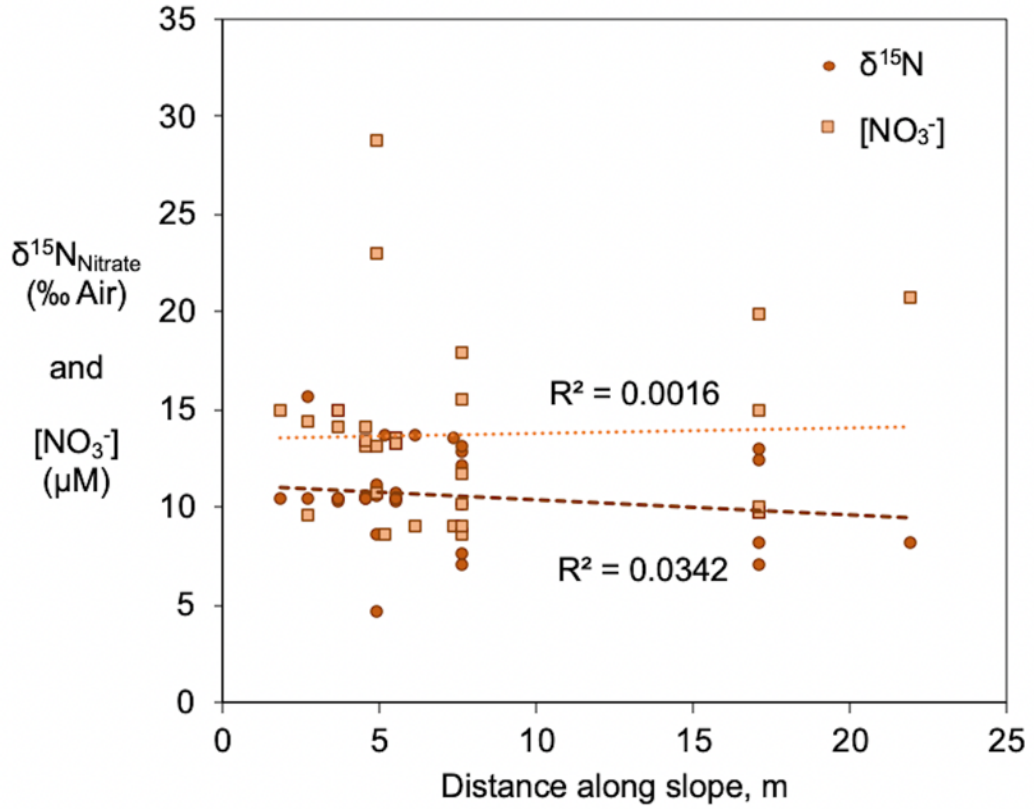

Figure 4-12: Nitrate concentrations and $\delta^{15}N$ in porewater "soil-nitrate" with distance along the wetland slope. Nitrate concentrations are represented by orange squares with a dotted trendline. $\delta^{15}N$ values are represented by orange circles with a brown dashed trendline. Significant spatial trends were not observed.

We used an adapted version of a Keeling plot (Pataki et al., 2003) to identify the source isotope signature of this second nitrate pool, which was approximately 3.2‰ (Figure 4-13). This value was offset by approximately 2‰ from values of $\delta^{15}N$ measured in soil, which was consistent with the expectation that processes that convert soil nitrogen to nitrate (i.e., ammonification and nitrification) discriminate against heavier isotopes. For example, fractionation of -1.4 to -2.3‰ was observed during mineralization of organic nitrogen in saturated sediments (Möbius, 2013). Additionally, this source of nitrate was only observed after wastewater was introduced to the subsurface, which then became saturated with water. Prior to that point, the wetland was only periodically irrigated with well water. Saturated conditions were favorable to denitrifiers that consumed nitrate and enriched the $\delta^{15}N$ values in the residual soil nitrate pool available to plants. This may explain our observation that even plants located in portions of the wetland without contact with wastewater-derived nitrate (i.e., plants located more than 5 m from the inlet to the wetland in cells without overland flow) became enriched in $\delta^{15}N$ after introduction of wastewater. The signal for these plants tended to match this second isotopic signature.

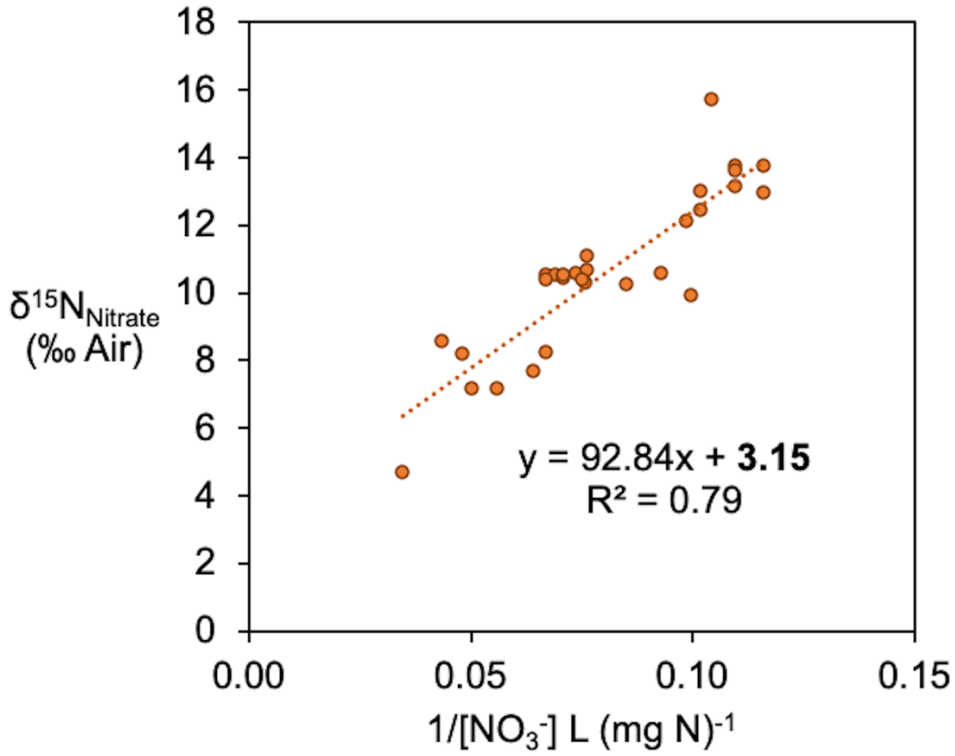

Figure 4-13: Keeling plot used to identify the original isotopic signature of the second nitrate source (i.e., "soil-nitrate") in porewater samples (Pataki et al., 2003).

Alternatively, because the first year of monitoring included extended periods of substantial overland flow (e.g., 40-80% of applied wastewater flowed over the wetland surface), it is also possible that a fraction of the wastewater-derived nitrogen was taken up into plant biomass at distances beyond 5 m and then cycled back into the subsurface through decomposition of organic matter. If so, this would further justify the use of this second nitrate pool as an endmember, as opposed to solid-phase soil $\delta^{15}N$ values, to avoid inflated plant uptake estimates in subsequent years caused by retention of enriched wastewater nitrogen through internal nitrogen cycling.

Mixing model results. According to the model predictions, throughout the monitoring period 14% of nitrogen incorporated into plant biomass came from wastewater. The remaining 86% was mostly likely derived from the soil. The fraction of plant nitrogen coming from wastewater varied with distance along the wetland slope. Approximately 81% of plant nitrogen was derived from wastewater within the first 2 m of the wetland, which was significantly more ($p < 0.001$) than the 13% that was observed in the last two-thirds of the wetland (Figure 4-14). There were no significant differences in the fraction of biomass nitrogen coming from wastewater among cells with different planting regimes ($p = 0.16$) or sediment types ($p = 0.48$) and no seasonal trends in the fraction nitrogen uptake from wastewater, though this may have been partly due to the temporal resolution of sampling (Figure 4-15).

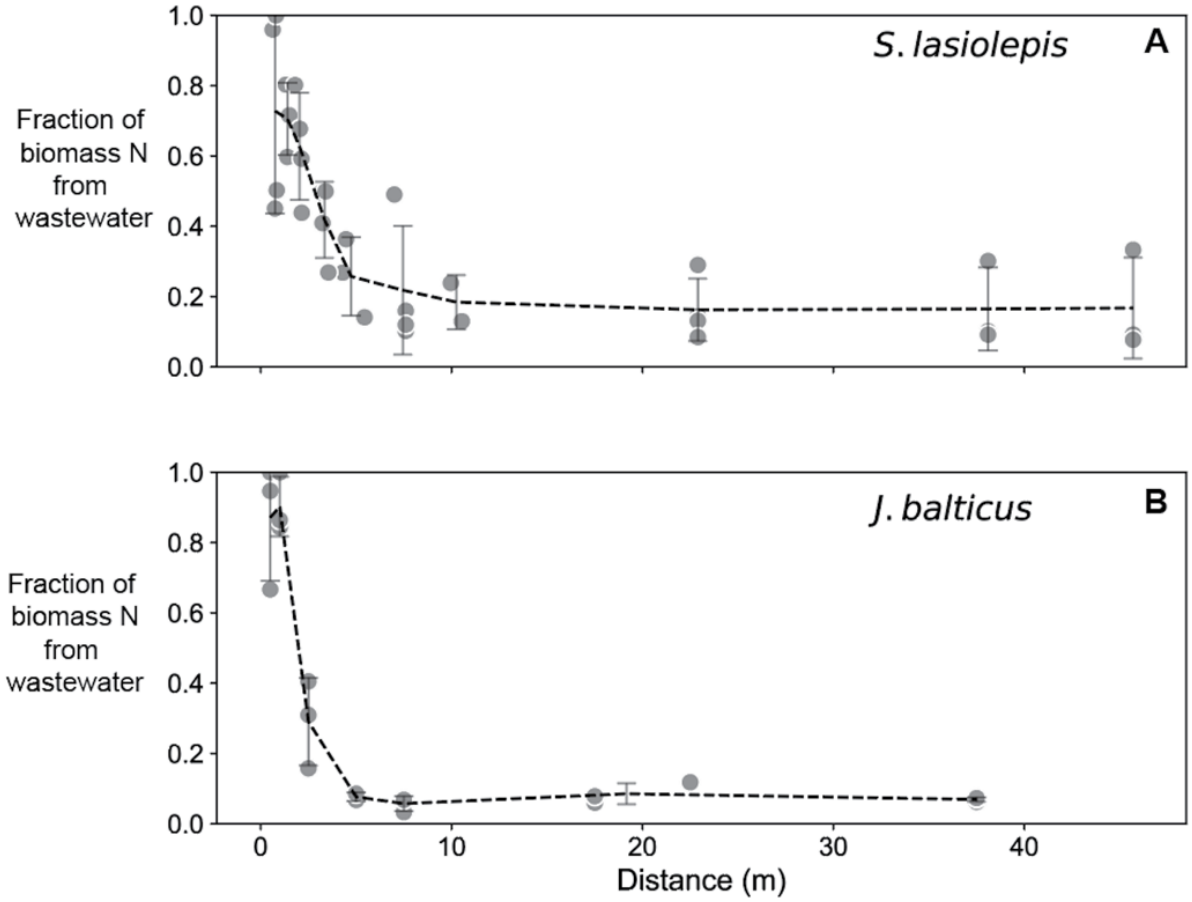

Figure 4-14: The fraction of biomass nitrogen derived from wastewater in (a) wet meadow (*J. balticus*) (n = 6) cells and (b) willow (*S. lasiolepis*) (n = 3) cells. Error bars represent one standard deviation across the monitoring dates when foliar samples were collected. The dotted lines represent moving averages.

We estimated that a low but measurable fraction of plant nitrogen came from wastewater at distances beyond 5 m (approximately 5-10% for wet meadow cells and 10-20% for willow cells) despite the fact that wastewater nitrogen was not detected in porewater beyond the first 10 m of the cells. It is possible that this was caused by: (1) intermittent periods of overland flow that supplied enriched wastewater nitrogen farther along the slopes; or, (2) internal cycling of wastewater nitrogen that had been taken up into biomass beyond 5 m during early parts of the monitoring period.

For these reasons, it is essential to characterize end-member values continuously when applying mixing models to plant uptake calculations in multi-year studies. Because mixing model results were sensitive to small changes in endmember values (e.g., a change of 2‰ in the soil endmember isotope value shifted average model outputs by 25%), using direct measurements of $\delta^{15}N$ from soil (5.7‰), as opposed to the $\delta^{15}N$ from the soil nitrate source in porewater (10.6‰), would have nearly doubled the estimated mass of wastewater nitrogen taken up by biomass (i.e., 300 kg N v. 160 kg N). A detailed comparison of mixing model results, including sensitivity to endmember values and biomass measurements, is provided in section 4.3.

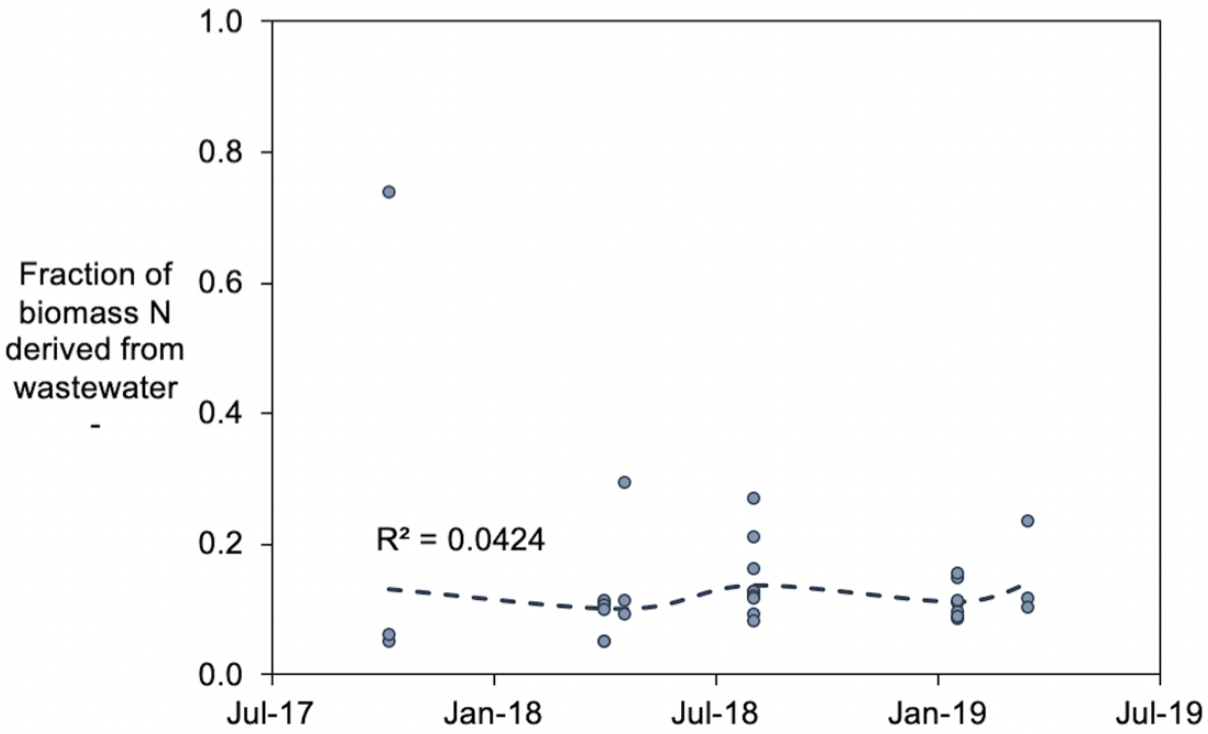

Figure 4-15: The fraction of biomass nitrogen derived from wastewater in individual wetland cells on dates when biomass samples were collected. Data points represent individual cells. The dotted trend line represents the geometric mean of calculated values. Significant seasonal trends were not observed. The r^2 presented is for a linear regression ($r^2 = 0.04$; $p = 0.27$), but other trends (e.g., sinusoidal and polynomial regressions) were not significant either ($r^2 < 0.05$; $p > 0.05$).

4.4.3 Plant uptake measurements

Total above ground biomass in the wetland varied among wetland cells and increased throughout the monitoring period. The median dry weight (DW) of above ground standing biomass was 0.7 kg DW m^{-2} (95% CI = 0.3 kg DW m^{-2}, 1.7 kg DW m^{-2}) for the entire site. The median annual peak above ground biomass, which typically occurred between the middle of May and late July, was 0.7 kg DW m^{-2} throughout the monitoring period, ranging from 0.5 ± 0.1 kg DW m^{-2} in 2017 to 1.5 ± 0.3 kg DW m^{-2} in 2019 – a significant increase ($p < 0.001$). Below ground biomass also increased throughout the monitoring period (Gill et al., 2002), from 0.5 ± 0.1 kg DW m^{-2} in 2017 to 1.0 ± 0.1 kg DW m^{-2} in 2019.

By the end of the monitoring period (June 2019), the peak above ground standing biomass (i.e., the maximum amount of standing biomass observed annually) was significantly ($p < 0.03$) greater in cells planted with willows (i.e., 1.8 ± 0.1 kg DW m^{-2}) than wet meadow cells (i.e., 1.4 ± 0.2 kg DW m^{-2}). However, due to significantly higher turnover rates in wet meadow cells, the annual above ground net primary production (i.e., total mass of plant biomass produced annually) was significantly lower ($p < 0.01$) in cells planted with willows, e.g., 2.0 ± 0.1 kg DW m^{-2} yr^{-1} on average versus 5.7 ± 1.0 kg DW m^{-2} yr^{-1} in those cells planted with wet meadows.

Using peak annual biomass measurements (B_{peak} in kg DW m^{-2}) and turnover rates (θ_{b} in yr^{-1}), the total mass of nitrogen taken up into plant biomass was calculated according to the equation: $N_{\text{uptake}} = B_{\text{peak}}\theta_{\text{b}}f_N$. Over the two year monitoring period, the mass fraction of nitrogen in biomass (f_N; kg N (kg DW)$^{-1}$) had median values of 4.0%, 2.2%, and 2.8% for willows (*S. lasiolepis*), Baltic rush (*J. balticus*) and composite samples from wet meadow cells, respectively. This corresponded to a total mass of nitrogen taken up into plant biomass of 1100 kg N (95% CI = 310 kg N, 2400 kg N) over the monitoring period. Based on the results of the mixing model, this yielded a mass of 150 kg N (95% CI = 40 kg N, 320 kg N) of wastewater-derived nitrate removed via plant uptake over the monitoring period, which corresponded to 10% (95% CI = 3%, 22%) of the nitrate and 8% (95% CI = 2%, 17%) of total nitrogen removed from wastewater during the two-year monitoring period. More than a third of wastewater-derived nitrogen taken up by plants (e.g., 51 kg N or 34%) went into willows, which covered close to a quarter of the site.

Plant uptake calculated using this new method differed significantly from estimates made using the approaches applied in previous studies. For example, if all of the nitrogen stored in plant biomass were assumed to be derived from wastewater in the horizontal levee, plant uptake would have accounted for nearly 60% of the removal of applied wastewater nitrogen, rather than the roughly 8% calculated using the new methods outlined here. Conversely, if increasing fractional nitrogen content (%N) of plant biomass were assumed to be the derived from wastewater, we would have significantly overestimated uptake of nitrogen from wastewater by willows (e.g., 150 kg N v. the 60 kg N calculated by our method), while underestimating uptake of nitrogen by other plants (e.g., 0 kg N, due to insignificant changes in the %N of composite biomass samples during the monitoring period, v. 90 kg N by our method), despite yielding a similar estimate of uptake over the entire pilot system (e.g., 8%).

The amount of wastewater-derived nitrogen taken up by plants only represented a fraction of their total nitrogen requirements. Of the 1100 kg N taken up by plants during the monitoring period, 950 kg N came from the soil. Based on the nitrogen content of the soil at the start of this study (i.e., approximately 10,000 kg N), this rate of extraction would only be sustainable for approximately 10 years assuming all soil nitrogen was accessible and none of the plant biomass nitrogen was returned to the soil. However, a large fraction of the nitrogen taken up into plants was deposited as residues annually. For example, although above ground standing biomass in the wet meadow cells peaked on average around 1.4 kg dry weight m^{-2} in 2019, the total biomass produced was 6.2 kg dry weight m^{-2} with roughly 80% of produced biomass deposited onto the wetland surface or consumed by organisms. If the nitrogen stored within those residues could be accessed by plants during subsequent growth, soils could supply sufficient nitrogen for plant growth to nearly 120 years without nitrogen inputs from other sources. This is more consistent with the nitrogen budgets of natural wetlands, in which internal cycling frequently satisfies the majority plant nitrogen demands (Bowden, 1987; Bowden et al., 1991).

Variations in plant uptake rates. The amount of wastewater-derived nitrate removed through plant uptake increased throughout the monitoring period, varied seasonally and among cell types, and decreased with distance along the wetland. Uptake rates were on average 29% higher in the second year of monitoring (6/2018-6/2019) compared to the first (6/2017-6/2018). For example, average uptake rates were 30 g N d^{-1} $cell^{-1}$ (8% of applied nitrogen) in the spring of 2018 (3/2018-6/2018) versus 46 g N d^{-1} $cell^{-1}$ in the spring of 2019 (3/2019-6/2019). Moreover, the fraction of wastewater N removed by plant uptake was nearly three times higher in the spring of 2019 (23% of removal) than in the preceding spring (8% of removal). This was partly due to lower mass loading rates of wastewater nitrogen in 2019 (which were 50% lower than the preceding year) and also due to higher biomass production, which more than doubled between 2017 and 2019 as plants matured. There were also clear

seasonal trends in both plant uptake and the fraction of wastewater nitrogen removed by uptake (Figure 4-16), which were both highest in the spring when plant growth was the greatest and lowest in the fall when plants were senescing.

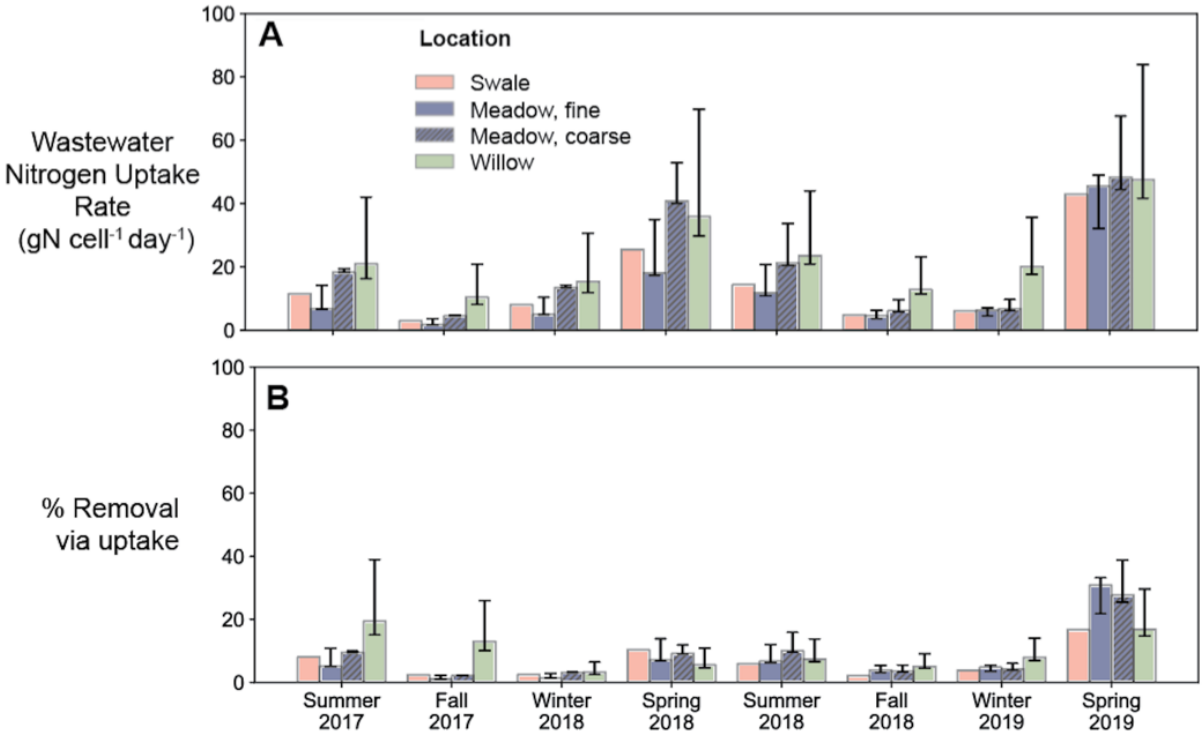

Figure 4-16: Uptake of wastewater-derived nitrogen into plants with time. (a) Uptake rates in g N d^{-1} $cell^{-1}$ and (b) the fraction of nitrogen removal attributed to plant uptake. Error bars represent 95% confidence intervals (n=3). Error bars are not shown for swale cells due to insufficient data.

Cells planted with willows removed a significantly ($p < 0.001$; one-tailed paired t test) greater amount of applied wastewater nitrate by plant uptake (i.e., 23 g N d^{-1} $cell^{-1}$) than wet meadow cells (i.e., 13 g N d^{-1} $cell^{-1}$; Figure 4-16b), despite lower primary production rates in willow cells. The extensive rooting zones of willows likely gave them greater access than other plants to wastewater nitrate that flowed primarily in the deeper subsurface layers, as described in Chapter 2 (Cecchetti et al., 2020a). Additionally, as mentioned in Chapter 2 and Chapter 3, the majority of nitrogen was removed at the beginning of the slope (Cecchetti et al., 2020a; Cecchetti et al., *in prep*). Our mixing model indicated that of the 160 kg of nitrogen removed via plant uptake, 63% (97 kg N) was taken up by plants within the first third (15 m) of the slope, with 45% (70 kg N) removed by plants in the first 2 m alone. These uptake trends were consistent across cells throughout the monitoring period.

4.4.4 Implications for horizontal levee design

There are a variety of design features that could be incorporated into horizontal levees to optimize both nutrient removal and plant uptake of nitrogen. In the pilot-scale horizontal levee, the majority of applied nitrogen (>96%) was removed at the beginning of the wetland before wastewater effluent came

into contact with the plants that occupied the remaining 90% of the levee slope. If cells were constructed to increase contact of wastewater nitrogen with plant roots along the entire horizontal levee, the fraction of wastewater nitrogen taken up by plants could increase substantially. Some of the design features proposed in Chapter 2 for optimizing hydraulics (Cecchetti et al., 2020a), such as using granular media with a higher hydraulic conductivity, could also increase contact of wastewater nitrate with plant roots by spreading nitrate from wastewater throughout the subsurface. However, rapid denitrification rates still might limit plant uptake.

Alternatively, designers could consider using multiple water inlet points with subsurface piping manifolds located at regular intervals along the slope to increase the fraction wastewater nitrogen taken up by biomass. Despite significant denitrification rates, this design feature would increase average subsurface nitrate concentrations further along the slope, increasing the potential for plant uptake in portions of horizontal levees that would not be exposed to wastewater nitrogen loads in systems with a single inlet. Ideally, these manifolds would be spaced every 10-20 m to achieve the greatest possible contact between wastewater nitrogen and plant roots. Other applications, such as batch application of wastewater or systems relying on percolation via surface application of water may also be useful in increasing plant uptake of effluent nitrogen.

Additionally, our research in Chapter 2 showed that willows increase the subsurface flow capacity of horizontal levees, which could increase the mass of solutes removed by uptake (Cecchetti et al., 2020a). When combined with our findings that willows have higher nitrogen uptake rates than other wetland plants, it is clear that willows have a significant capacity to promote nitrogen removal in horizontal levees through multiple mechanisms.

It is important to note that nitrogen uptake into plant biomass constitutes a storage mechanism, rather than a permanent sink. However, it is likely that the release of nitrogen into the subsurface from decaying plant residues will either be: (1) taken up by plants again; or, (2) denitrified by microorganisms using organic carbon from plant residues as an electron donor before nitrogen leaves in the system effluent. For example, if just 10% of the approximately 18,000 kg yr^{-1} of organic carbon from plant biomass decomposed each year – a conservative estimate based on reported litter decomposition rates (Aké-Castillo et al., 2006, review of past studies) – this additional input of organic carbon would be sufficient to denitrify 1600 kg N yr^{-1}, which is greater than annual uptake of nitrogen from all sources in this system and more than 10 times the amount of nitrogen taken up from wastewater specifically (160 kg N).

4.5 Conclusions

In this study, isotope fingerprinting and mixing models were used to evaluate the uptake of nitrogen in a horizontal levee – a new nature-based system for improving water quality which also protects coastal infrastructure from the effects of sea-level rise. Our findings indicate that plant uptake is responsible for removal of a significant fraction of nitrogen entering the system, with more than 20% of nitrogen removed by plant uptake in the spring of 2019. The exact mechanisms by which the remainder of nitrogen was removed is still unknown. However, on the basis of the site biogeochemistry described in Chapter 3 (Cecchetti et al., *in prep*) and isotope fractionation observed in porewater in the first 5 m of the system it appears that a majority of this remaining nitrogen was removed by microbial denitrification.

The new isotope methods detailed in this study are promising techniques for quantifying plant uptake of wastewater-derived nitrogen in natural treatment systems. Mixing models based on isotope

fingerprinting provide a more robust means of measuring plant uptake because they do not rely on assumptions that were necessary in previous methods. Isotope methods can improve understanding of nitrogen uptake mechanisms and resolve the wide discrepancies in reported values of nitrogen uptake by plants in other nature-based treatment systems.

More precise estimates of the relative contribution of plant uptake to nitrogen removal is important in multi-benefit treatment systems because it can help designers to prioritize objectives. For example, if plant uptake were found to be insignificant, designers could consider objectives related to habitat creation and planting regimes separately from water quality improvement objectives. Additionally, our results demonstrate that willows have a significant capacity through multiple mechanisms to promote nitrogen removal in horizontal levees. Finally, although plant uptake constitutes a storage mechanism rather than an ultimate removal in systems like the horizontal levee (i.e., where plants are not harvested and removed) labile organic carbon inputs from decaying biomass appear to be sufficient to denitrify the amount of nitrogen reintegrated in the subsurface from senesced biomass.

Chapter 5. The Cycling of Phosphorus in a Horizontal Levee

5.1 Introduction

Extraction of mineral phosphorus for agricultural fertilizers has led to a fourfold increase in its mobilization worldwide (Childers et al., 2011) accompanied by elevated concentrations in runoff and municipal wastewater. Phosphorus is often the limiting nutrient for algal growth in freshwater systems, where oxic conditions favor its partitioning to metal oxides in sediments (Caraco et al., 1989). As the trophic status of lakes transition to eutrophic conditions, phosphorus tends to be mobilized as reducing conditions in sediments release phosphate that was associated with Fe(III)- and Mn(III)/Mn(IV)-oxides. To reduce the impact of phosphorus on freshwater ecosystems, sources associated with both agricultural land and municipal wastewater treatment plants will need to be controlled.

Removal of phosphorus from wastewater is technically challenging. Enhanced biological phosphorus removal requires careful control of operational conditions and large capital investments (Oehmen et al., 2007; Le Corre et al., 2009; Zheng et al., 2014), while chemical removal by adsorption or precipitation can be expensive due to chemical use (Kumar and Pal, 2015). In contrast, nature-based systems, like the horizontal levee, are attractive because of their low costs and small input requirements (Kadlec and Wallace, 2009). These systems may be even more attractive if phosphorus removal occurs along with removal of other contaminants, such as nitrogen, trace organic contaminants and waterborne pathogens, as described in Chapter 2 (Cecchetti et al., 2020a).

In constructed wetlands, the removal of dissolved phosphorus is dominated by chemical processes that are linked to microbial activity. Phosphate is frequently the dominant form of phosphorus in wastewater although dissolved organic phosphorus can account for up to 81% of total phosphorus (Qin et al., 2015). In aerobic sediments, phosphate tends to adsorb onto Fe(III)-oxide minerals (Holtan et al., 1988). In addition to its affinity for Fe(III)-oxides, phosphate can adsorb onto mixed valence minerals (e.g., magnetite). For example, vivianite (i.e., $Fe_3(PO_4)_{2(s)}$) formation may also play a role in anaerobic soils when Fe(III)-oxides are reduced by microorganisms to release Fe(II) (Lin et al., 2020). Biological assimilation processes (i.e., into plants and microbial biomass) usually play a limited role in immobilization of phosphorus, although cyclical uptake and release of phosphorus during decomposition can impact its distribution among different forms (Wild, 1950). Due to the high N:P ratio in wastewater and the presence of phosphorus in many native soils where horizontal levees would be built, we do not expect uptake of phosphorus by plants or microbes to represent a removal pathway. Furthermore, plants are not harvested in the horizontal levee, which means that plant phosphorus will be recycled back to horizontal levee sediments during senescence when these processes achieve a steady state.

Although the sediments in the pilot-scale wetland described in previous chapters consisted of about 2.5% iron by weight, monitoring of influent and effluent from the system indicated that phosphate removal was limited, as described in Chapter 2 (Cecchetti et al., 2020a). The presence of dissolved Fe in porewater samples (see Chapter 3; Cecchetti et al., *in prep*) suggested that Fe(III)-oxides were being reduced, potentially leading to lower capacity for adsorption of phosphate onto surfaces. Fe(II) released by this process also can immobilize phosphate through formation of vivianite or can form other minerals (e.g., $FeS_{(s)}$, $FeCO_{3(s)}$). After it is discharged, the $Fe(II)_{(aq)}$ in the wetland effluent is

rapidly oxidized by oxygen to form Fe(III)-oxides that are expected to have a high affinity for phosphate. Therefore, phosphate released by the wetland might be immobilized immediately after it is discharged.

To understand the fate of phosphorus in horizontal levees, a pilot-scale horizontal levee was monitored over a two year period. Analysis of water, soils and plants, was used to assess mass balance on phosphorus to gain insight into ways in which system operation could be improved to enhance phosphorus removal. We also investigated interactions between phosphorus and the cycling of metals, with a focus on iron, which tends to have the largest impact on phosphate cycling in similar systems. Preliminary experiments also were conducted to assess the potential for phosphorus removal on Fe(III)-oxides formed when effluent from the wetland is aerated.

5.2 Materials and Methods

5.2.1 Field site

Phosphorus cycling was studied at a demonstration-scale horizontal levee at the Oro Loma Sanitary District wastewater treatment plant in San Lorenzo, CA that was described in Chapter 2 (Cecchetti et al., 2020a). Briefly, this system consisted of 12 parallel sloped treatment cells that varied in topography, soil type and plant community composition. Cells were gently sloped (1:30) and consisted of a topsoil layer underlain with gravel and coarse sand, amended with wood chips.

Details regarding the hydraulics, design, operating conditions and planting regimes are described in Chapter 2 (Cecchetti et al., 2020a) and Appendix A.

5.2.2 Sample collection

Samples of influent and effluent water, porewater, soils and plant biomass were collected from the field site to quantify mass loading of solutes and to assess mechanisms responsible for phosphorus removal. Detailed descriptions of water sampling methods, mass balances on contaminants and redox-active species, and plant uptake measurements of nitrogen are provided in Chapter 2 (Cecchetti et al., 2020a), Chapter 3 (Cecchetti et al., *in prep*), and Chapter 4 (Cecchetti et al., *submitted*), respectively. A brief overview is included below.

Influent and effluent water samples were collected on a monthly or biweekly basis throughout the 2-yr monitoring period (April 2017-June 2019). Porewater samples were collected on nine dates at depths ranging from 0.1 to 0.9 m into Luer-Lok BD syringes using stainless steel PushPoint sediment porewater samplers (MHE Products, East Tawas, MI, USA). Water samples were filtered on-site and stored on ice prior to analysis (within 48 hr), as described in Chapter 2 (Cecchetti et al., 2020a). As described in Chapter 4 (Cecchetti et al., *submitted*), plant samples were collected every 3-6 months in paper envelopes that were stored in plastic bags on ice prior to returning to the lab. Soil samples were collected from the top 10 cm of the soil and stored on ice prior to returning to the lab (Cecchetti et al., *submitted*).

5.2.3 Sample processing and analytical methods

Sample processing methods and analyses of water samples (anions, cations, TOC and metals), soils (content of N, C, S, Mn, Fe, and P) and plant tissues were described in previous chapters (Cecchetti et al., 2020a; Cecchetti et al., *submitted*; Cecchetti et al., *in prep*). Water samples were filtered in the field through 0.7-μm glass fiber filters and stored on ice prior to analysis. Phosphate was measured by

ion chromatography according to U.S. EPA Method 300.0 and cations were analyzed by ion chromatography as described previously (Thomas et al., 2002; Cecchetti et al., 2020a). Dissolved organic carbon was measured using a Shimadzu TOC-V/CSH analyzer according to standard methods (Method 5310B; APHA, 1998; Cecchetti et al., 2020a).

Dissolved transition metals (i.e., Mn and Fe), trace metals/metalloids (i.e., Cu, Ni, As, Se, Cd, Cr, Pb, and Zn), and total phosphorus were analyzed by inductively coupled plasma mass spectrometry (ICP-MS) on undigested samples using standard methods (Method 3125; APHA, 1998; for metals and trace metals) and previously described methods (Dayton et al., 2017). Dissolved organic phosphorus was calculated by subtracting concentrations of phosphate from total phosphorus measurements. Field-filtered samples were stored at 4°C upon returning to the laboratory prior to preparation for analysis by ICP-MS. Samples collected prior to October 2018 were stored at 4°C for 6-12 months prior to sample preparation. These samples were shaken vigorously (to resuspend any particles) and were diluted with nitric acid without additional filtration. Samples collected after October 2018 were prepared for ICP-MS within 6 hours of sampling and were shaken vigorously and filtered through 0.2-μm nylon filters prior to dilution with nitric acid. In all cases, 0.1 mL aliquots of samples were diluted into a 1% nitric acid solution and stored at room temperature on the bench-top before analysis by ICP-MS, which typically occurred within 7 days of preparation.

Leaf samples were dried at 65°C for 48 hr immediately upon return to the lab. Soil samples were frozen immediately upon return to the lab and then freeze-dried. Dried leaf and soil samples were ground into a fine powder (200 mesh) and analyzed for metals (Fe, Mn and Cu) and total phosphorus using inductively coupled plasma atomic emissions spectrometry (ICP-AES) preceded by a nitric acid/hydrogen peroxide closed vessel microwave digestion. Powdered soil and plant samples were analyzed for content and stable isotope ratios of carbon, nitrogen and sulfur (Mambelli et al., 2016; Cecchetti et al., *submitted*).

5.2.4 Measurements of total phosphorus and trace metals by ICP-MS

For total phosphorus measurements, ICP-MS was chosen over colorimetric techniques because it is rapid and easily automated and colorimetric analysis is susceptible to bias if digestion does not completely convert organic phosphorus and polyphosphates into phosphate (Dayton et al., 2017). Previous research (Gallagher and Scholes, 2017, unpublished results) identified acid-persulfate digestion methods as the most effective pre-treatment for conversion of phosphorus to dissolved forms prior to total phosphorus measurements (Dayton et al., 2017). Therefore, we compared measurements of phosphorus by ICP-MS between acid-persulfate digested and undigested samples (Figure 5-1) from water samples relevant to this study (i.e., influent, effluent and porewater samples) to determine the utility of digestion prior to ICP-MS for our samples.

Samples were digested using the autoclave-assisted acid-persulfate digestion method described by Dayton et al. (2017) with minor modifications. Briefly, 5 mL of sample were diluted to 50 mL of Milli-Q water in 100-mL acid-washed glass bottles. 1 mL of 30% sulfuric acid solution and 0.5 g potassium persulfate were added to each sample and lightly mixed. Samples were digested for 60 minutes in the autoclave at 121°C and 120 kPa. After digestion, samples were neutralized with NaOH and diluted to 100 mL with Milli-Q water. 1 mL aliquots of digested samples were then diluted into a 1% nitric acid solution and stored on the benchtop prior to analysis.

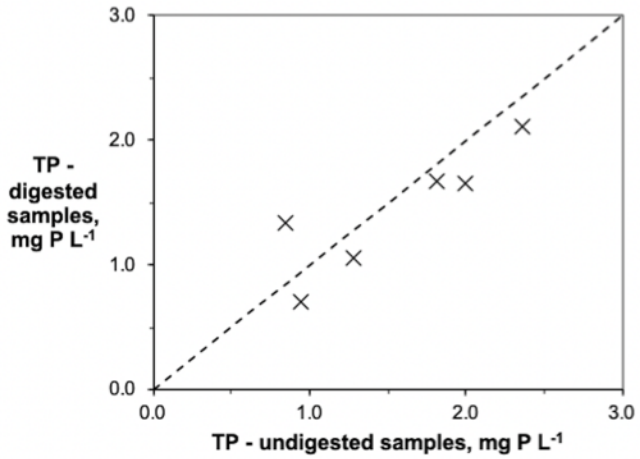

Figure 5-1: Comparison of measurements of total phosphorus in digested and undigested samples. Analysis was conducted by ICP-MS.

Measurements of total phosphorus were not statistically different ($p = 0.35$; Wilconox signed rank test) between digested and undigested samples, suggesting that digestion was not necessary to quantify total phosphorus by ICP-MS in the samples collected from the horizontal levee. Additionally, significant differences were not observed between measurements of Mn ($p = 0.25$), Fe ($p = 0.75$), As ($p = 0.35$), Si ($p = 0.07$) Cu ($p = 0.12$), Zn ($p = 0.05$), Cd ($p = 0.12$) or Pb ($p = 0.22$) between digested and undigested samples using two-tailed paired t-tests. Concentrations of Ni and Cr measured in undigested samples were significantly lower ($p < 0.05$ for both species; Wilconox signed rank test) than those measured in digested samples (i.e., differences of 72-97% and 9-91% respectively) demonstrating that these metals are not fully recovered without digestion. However, the ratios of influent to effluent measurements were not significantly different between digested and undigested samples ($p = 0.28$ and 0.83, respectively) for Ni and Cr (e.g., concentrations of Ni in effluent samples were 97% and 99.6% of those measured in influent samples for digested and undigested samples, respectively).

5.2.5 Visual MINTEQ modeling and statistical analyses

To assess the fate of phosphate in the subsurface, we predicted saturation indexes of mineral phases in the horizontal levee with Visual MINTEQ (ver. 3.1; Gustafsson, 2014) using measured porewater concentrations of aqueous species, as well as parameters and assumptions detailed in Chapter 3 (Cecchetti et al., *in prep*). A significant fraction of phosphate measurements were below the limit of quantitation (LOQ = 0.061 mg P L^{-1}), but were above the limit of detection (i.e., LOD = 0.014 mg P L^{-1}). For modeling in Visual MINTEQ, samples with concentrations between the limits of quantitation and detection were assumed to have concentrations that were half of the LOQ (i.e., 0.031 mg P L^{-1}). For samples in which the phosphate signal was below the detection limit, phosphate concentrations were assumed to be zero.

Statistical analyses were performed in Excel (Microsoft Corporation, Redmond, WA, USA) using the Real Statistics Resource Pack software (Release 5.4; Zaiontz, 2018). Unless specified otherwise, all reported p-values were derived from non-parametric tests (i.e., Wilcoxon signed-rank test for paired samples and Wilconox-Mann-Whitney tests for independent samples) because collected data were not normally distributed.

5.3 Results and Discussion

The 2-year monitoring period (6/2017-6/2019) was split into three operational phases as described in Chapter 2 (Cecchetti et al., 2020a). Briefly, in the first monitoring phase (6/2017-11/2017), wastewater was pretreated in a surface flow wetland prior to application to the subsurface. During this period, approximately half of the applied water flowed over the wetland surface, short-circuiting the system. More than 75% of the phosphate released in the effluent over the entire monitoring period was due to overland flow occurring during this first six-month phase. During the second monitoring phase (12/2017-7/2018), wastewater was no longer pretreated in the surface flow wetland, but the fraction of overland flow remained high (i.e., it accounted for 64% of the total flow). During the final monitoring phase (8/2018-6/2019), the applied flow rate was reduced significantly (by nearly 60%) and overland flow was eliminated in 9 of the 12 cells (cells D-L). Because cells A-C were difficult to optimize hydraulically, due to swales running down their center, data from those cells were not included in this study. More details are provided in Chapter 2 (Cecchetti et al., 2020a).

5.3.1 Phosphorus cycling in the horizontal levee

Overall, phosphorus was not removed in the nine wetland cells throughout the two-year monitoring period. Rather, a small but statistically significant increase ($p < 0.05$) in the mass of phosphorus in the effluent was observed. The release of phosphorus was largest during the first monitoring phase, when the mass of phosphorus leaving the wetland was 24% higher than the mass entering the system. During the final two monitoring phases, differences between the influent and effluent loading of total phosphorus were not significant ($p > 0.46$). Of the 210 kg of wastewater-derived phosphorus applied to the horizontal levee, 200 kg P (94%) was in the form of phosphate and 11 kg (6%) was in organic forms (mainly dissolved organic phosphorus). In the wetland effluent 33% of the phosphorus consisted of organic forms over the full monitoring period, although this fraction accounted for more than 89% of effluent phosphorus during the final monitoring phase.

During the first monitoring phase (6/2017-12/2017), there was significant variability in the loading of phosphate to the horizontal levee. This was partly because water was pre-treated in a surface flow wetland where seasonally variable evapotranspiration rates concentrated solutes that were not removed. For example, during the summer and fall of 2017, when evapotranspiration rates were the highest, influent phosphate concentrations to the horizontal levee (i.e., median value were 4.2 mg P L^{-1}) were significantly ($p < 0.01$) higher than those measured during the winter and spring of 2017 and 2018 (e.g., median values were 0.7 mg P L^{-1}). Additionally, phosphate loading to the surface flow wetland was more variable at this time (i.e., median phosphate concentrations in the influent to the surface flow wetland were 2.9 mg P L^{-1} with a range from 1.0 to 11 mg P L^{-1}). Overall, influent phosphate concentrations to the horizontal levee during the first monitoring phase had a median value of 2.8 mg P L^{-1} and were significantly higher ($p < 0.01$) than concentrations applied to the wetland during the final monitoring phase (8/2018-6/2019), when a median value of 0.8 mg P L^{-1} was observed.

Phosphate removal increased significantly ($p < 0.01$) during the monitoring period. During the first phase, only 11% of the applied phosphate (18 kg P) was removed. This occurred because a significant fraction of the applied wastewater short-circuited the subsurface treatment zone of the wetland by flowing over the wetland surface, leading to little removal of phosphate (or other contaminants) in the wetland (see Chapter 2; Cecchetti et al., 2020a). In contrast, during the last two phases, phosphate removal increased significantly ($p < 0.001$) to nearly 33% and greater than 84%, respectively. Removal of phosphate increased because decreasing flows of wastewater (i.e., from 7.6 m^3 d^{-1} during the first

year to 3.4 m^3 d^{-1} in the final monitoring phase) caused a significantly ($p < 0.001$) greater fraction of the applied wastewater to pass through the subsurface (99% compared to 68% in the first operational phase) (Cecchetti et al., 2020a). When combined with the changes in operational conditions discussed above (i.e., re-routing nitrified effluent directly to the horizontal levee), decreasing flows caused the loading of phosphate to be more than 90% lower during the final phase (13 kg P) compared to the first monitoring phase (160 kg P).

After phosphate was removed in the subsurface, organic phosphorus concentrations increased. For example, although the mass of phosphate dropped significantly ($p < 0.01$) between the influent and the effluent of the wetland during the last monitoring phase (i.e., from 13 kg P to 2.1 kg P), it was largely counterbalanced by dissolved organic phosphorus, which increased from 3.8 kg P in the influent to 13 kg P in the effluent. A strong inverse correlation (Spearman's $\rho = -0.57$) was observed between concentrations of phosphate and dissolved organic phosphorus in the influent, effluent and porewater samples. The observed shift in the speciation of phosphorus suggests that the system reached a steady state with respect to phosphorus turnover, possibly because removal phosphate, which was mostly removed on minerals, was balanced by the release of organic forms of phosphorus from decaying organic matter.

Porewater concentrations of phosphorus species provide some insight into the processes that resulted in this change in phosphorus speciation in the subsurface. Data from the three wet meadow cells with fine topsoil and the three cells planted with willows to demonstrate differences observed between treatments that are illustrative of all 9 cells (Figure 5-2). In wet meadow cells with a fine topsoil, concentrations of total phosphorus did not change significantly along the wetland slope ($p = 0.38$) (Figure 5-2; blue circles), but phosphate concentrations decreased rapidly in the subsurface, with median concentrations dropping from 1.1 ± 0.5 mg P L^{-1} in the influent to below the quantitation limit (0.061 mg P L^{-1}) in most samples collected beyond 3 m. Similar changes in the concentration of phosphate ($p > 0.05$) were observed in wet meadow cells with a coarse topsoil and in cells planted with willows.

Phosphate removal was likely explained by a combination of processes, including adsorption onto Fe(III)-oxides, precipitation of phosphate minerals and uptake into plant and microbial biomass. Adsorption and mineral precipitation likely explained the majority of observed phosphate removal (see fate of phosphate in a horizontal levee). Phosphorus requirements during growth of microbial biomass in the subsurface were also substantial during the first phase, when the introduction of wastewater to the subsurface created saturated conditions. The increased water content in the subsurface likely led to growth of microbial biomass (McIntyre et al., 2009), which we estimated increased by approximately 30%, or 2000 kg dry weight, of which approximately 90 kg were estimated to be phosphorus. Additionally, uptake of phosphorus into plant biomass during this phase (20 kg P) was comparable in magnitude to the observed phosphate removal. Despite the uptake of phosphorus by these processes, we do not believe that these were responsible for the observed phosphate removal because phosphate removal was nearly complete within the first 2.5 m of the wetland. Furthermore, although plant uptake of phosphorus increased significantly in the last monitoring phase (with 90 kg P taken into plant biomass) we did not observe an increase in the mass removal of phosphorus from the aqueous phase, suggesting that plant uptake was not driving the observed wastewater-phosphorus removal. Thus, the majority of phosphorus taken up by plants and microbes was likely derived from the soil, which contained approximately 3400 kg P at the beginning of the monitoring period. This is consistent with observations for nitrogen uptake in horizontal levees described in Chapter 4 (Cecchetti et al., *submitted*).

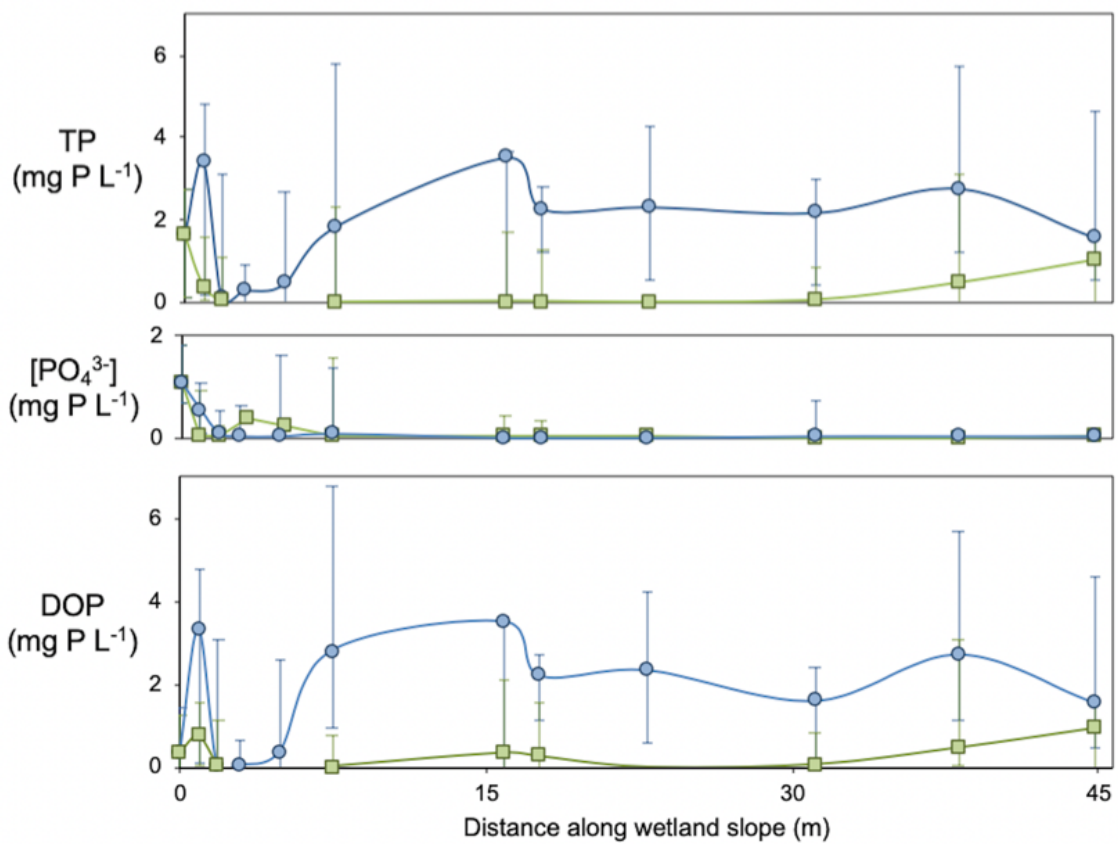

Figure 5-2: Concentrations of dissolved phosphorus species in porewater samples collected from the gravel/coarse sand layer of the subsurface at various distances along the slope in wet meadow cells with a fine topsoil (blue circles) and cells planted with willows (green squares). Data points represent median values with vertical error bars representing 90th and 10th percentile values.

In contrast to the decreasing phosphate concentrations we observed, concentrations of organic phosphorus increased ($p < 0.05$) between the influent (i.e., median concentrations were 0.3 mg P L^{-1}) and the effluent (i.e., 1.6 mg P L^{-1}) in wet meadow cells with a fine topsoil. Taking evapotranspiration into account, which removed approximately 50% of the water flowing through the subsurface (Cecchetti et al, 2020a; Cecchetti et al., *in prep*), the increased loading of dissolved organic phosphorus in the effluent (approximately 4.4 g P d^{-1} $cell^{-1}$) was similar to the loss of phosphate removed in the subsurface (approximately 6.0 g P d^{-1} $cell^{-1}$). Similar trends were observed in the wet meadow cells with coarse soils ($p > 0.05$). However, dissolved organic phosphorus was significantly ($p < 0.01$) lower in porewater samples collected from cells planted with willows (Figure 5-2; green squares). Concentrations of organic phosphorus only increased significantly ($p < 0.01$) in the last 15 m of those cells (from 0.05 to 1.0 mg P L^{-1} at 30 and 45 m respectively), with median values of 2.1 mg P L^{-1} in the effluent, suggesting that production of dissolved organic phosphorus was substantial in the last few meters prior to the effluent and may not have been significant if the wetland were shortened by 5 to 10 m.

The cause of these differences in dissolved organic phosphorus production between the willow and wet meadow cell types is unclear, but it may be related to sulfate reduction, as described in Chapter 3 (Cecchetti et al., *in prep*). The distances at which organic phosphorus concentrations increased in wet meadow cells with a fine topsoil (between approximately 5 and 7.5 m) and cells planted with willows

(between approximately 30 and 45 m) closely match the distances at which sulfate reduction occurred within those cells (Cecchetti et al., *in prep*). Thus, some phenomenon whereby production of sulfide (via sulfate reduction) promotes the release of organic phosphate from sediments (Caraco et al., 1989) may be important. Sulfide production may also play a role in the mobilization of organic phosphorus compounds that adsorb to surfaces if sulfide competes for those surfaces or alters mineral properties. Alternatively, the microbial communities that become dominant when sulfate is no longer available (e.g., fermenters and methanogens) may release organic phosphorus through the breakdown of complex organic matter or may release microbial products containing phosphorus. Further research is required to understand the mechanisms responsible for these apparent discrepancies.

It is unlikely that most of the dissolved organic phosphorus export was attributable to leaching of organic matter from decomposing residues from plants growing on the wetland. As reported in Chapter 3 (Cecchetti et al., *in prep*), the loading of dissolved organic carbon did not change significantly between the influent and the effluent of the wetland. There was a significant decrease ($p < 0.005$) in the DOC:DOP molar ratios in the wetland from a median value of 56 in the influent, to a median value of 13 in the effluent. The DOC:DOP ratio observed in the porewater samples was substantially lower than reported in past studies of wastewater effluent (e.g., approximately 100-1000; Qin et al., 2015). Because leachates from plant residues frequently have much higher molar C:P ratios than those observed in the horizontal levee (e.g., median values of 360 are reported in the literature with a range from 20 to 2700; Yavitt and Fahey, 1986; Turner, 1993; Uselman et al., 2012; Duan et al., 2014), we would expect the DOC:DOP in the effluent to be substantially higher if organic phosphorus export were mainly caused by leaching of organic matter from plants. Rather, the decreasing DOC:DOP ratios may have been due to release of protein-like soluble microbial products with low C:P ratios as water passed through the system (Shin and Kang, 2003).

Changes in aqueous phosphorus speciation have important implications for efforts to assess the impacts of nature-based treatment systems. Our data indicate that monitoring of phosphate loads alone can miss a significant fraction of total phosphorus being exported to the environment. This is relevant for wastewater treatment plants because National Pollutant Discharge Elimination System (NPDES) permits for wastewater dischargers are typically based on total phosphorus (epa.gov/npdes). Past research on phosphorus removal from wastewater that focused on phosphate removal without considering the potential for organic phosphorus formation in nature-based systems may fail to address the needs of users of the technology. Additionally, a large fraction of dissolved organic phosphorus may be bioavailable, meaning that the removal of phosphate in the horizontal levee would offer little benefit with respect to protecting and estuary from the effects of phosphorus-induced eutrophication (Qin et al., 2015).

Fate of phosphate in a horizontal levee. In the horizontal levee subsurface, concentrations of phosphate decreased significantly at the beginning of the slope (i.e., 0 to 3 m; Figure 5-2). In this region, median dissolved Fe concentrations were approximately 40 μM due to the presence of nitrate, which limited reduction of Fe(III)-oxides, as detailed in Chapter 3 (Cecchetti et al., *in prep*). For these reasons, we hypothesized that the decreasing porewater concentrations of phosphate in this part of the slope were likely caused in part by adsorption of phosphate onto Fe(III)-oxides. Despite the relatively low concentrations of Fe(II) in this region, phosphate minerals including vivianite ($Fe_3(PO_4)_{2(s)}$) and amorphous calcium phosphate ($Ca_3(PO_4)_{2(s)}$) were supersaturated, with saturation indexes ranging from 0.5 to 3.5. Vivianite formation has been suggested as a potentially important sink of phosphate in iron-rich sediments (Baken et al., 2015) and in anoxic wetlands soils (Walpersdorf et al., 2013). Thus, formation of phosphate minerals may also explain the decreasing phosphate concentrations observed in porewater samples (Figure 5-2).

Moreover, a composite soil sample from this portion of the slope in cell F had a higher phosphorus content (0.08%) in 2018 than soil samples collected beyond 5 m along the slope on that same date and from the preceding year, which had a median phosphorus content of 0.06%. Although these data are limited, this specific observation suggests that mineral forms of phosphorus may be accumulating in the first 3 m of the wetland. If this 30% difference in phosphorus content were consistent across the whole first portion of the wetland, it would correspond to an increase of 50 kg P stored in soils in the first 3 m, which is approximately equivalent to the decrease in phosphate mass observed in the aqueous phase over the monitoring period (40 kg P). However, additional analyses (e.g., characterization of minerals formed on sediments) are needed to determine the relative contribution of adsorption and mineral precipitation to increased storage and as removal mechanisms. The contribution of these mechanisms to removal has important implications for long-term phosphate removal in these systems because the saturation of available adsorption sites will ultimately limit the capacity for phosphate removal by adsorption onto Fe(III)-oxides and the reduction of Fe(III) will ultimately decrease concentrations of dissolved metals (e.g., $Fe(II)_{(aq)}$) needed for vivianite formation.

In the remainder of the wetland slope (i.e., 3 to 45 m), phosphate concentrations remained low, with two-thirds of porewater samples containing phosphate concentrations below the limit of quantitation and 33% exhibiting concentrations below the detection limit. At these distances, most phosphate minerals were undersaturated, although increasing aqueous iron concentrations (Cecchetti et al., *in* prep) caused vivianite to become supersaturated in the majority of samples collected beyond 20 m. However, because more than 97% of wastewater-phosphate had already been removed prior to reaching this portion of the slope, vivianite formation in latter portions of the wetland did not contribute significantly to the observed phosphate removal. It is worth noting that adsorption of phosphate onto iron-oxides and vivianite formation may have limited the mobility of any phosphate released by native soils or decomposing organic matter. More research is needed to understand these processes in the horizontal levee, as well as the potentially complex impacts of iron and sulfur cycling on these processes.

Phosphorus mass balance. Although removal of phosphorus did not occur in the horizontal levee, it is evident that changes in the phosphorus speciation occurred and that different pools of phosphorus grew and shrank as the plant community continued to mature during the two-year study. A conceptual model of phosphorus cycling in horizontal levees is presented in Figure 5-3. At the beginning of the monitoring period, analysis of representative soil samples indicated that 3400 kg P (95% CI = 3100 kg P, 4000 kg P) was present in the horizontal levee with greater than 98% consisting of phosphate and organic phosphorus in soil used to construct the levee slope. As expected, soil phosphorus content did not change significantly ($p = 0.57$) during the monitoring period because the total mass of phosphorus entering the system accounted for less than 10% of the phosphorus already in the system.

Soil C:P ratios in horizontal levee soils also did not change significantly during the monitoring period ($p > 0.99$). Mean soil C:P ratios were 21, which is substantially lower than the range of ratios reported for soil organic matter (i.e., 919 and 61; Tipping et al., 2016), suggesting that a large fraction of soil phosphorus was stored in mineral forms. Using the mixing model described by Tipping et al. (2016), we estimated that approximately 10% of the phosphorus stored in the soil was in organic forms, which corresponds to approximately 340 kg P. This was consistent with the 290 kg P (95% CI = 30 kg P, 1500 kg P) that we estimated were stored in microbial biomass based on past studies of soil microbial P in natural and constructed wetlands (Olila et al., 1997; Qualls and Richardson, 2000; Baum et al., 2003; Xu et al., 2012). The remaining 3100 kg was likely stored primarily in mineral forms in the soil.

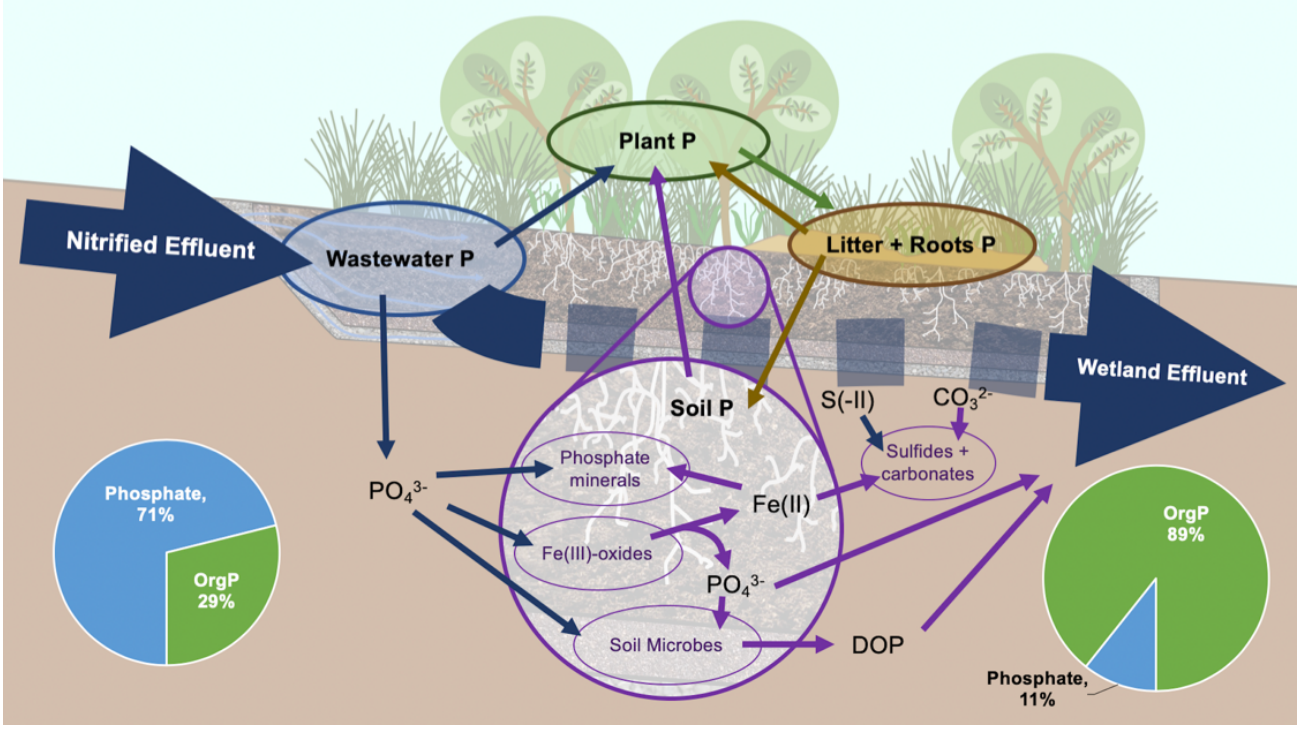

Figure 5-3: Conceptual model of phosphorus cycling in the horizontal levee during the two-year monitoring period. Pie charts show the speciation of phosphorus among phosphate and dissolved organic phosphorus (OrgP) in the influent and the effluent from the wetland during the third monitoring phase.

Using data on plant growth, we estimate that 150 kg P (95% CI = 100 kg P, 230 kg P) from all sources were taken up into plant biomass during the monitoring period. This was calculated based on uptake rates of nitrogen calculated in Chapter 4 (Cecchetti et al., *submitted*) and the assumption of a N:P ratio in plants of 15, which is a typical value when neither nitrogen nor phosphorus limitation are significant (Koerselman and Meuleman, 1996). Because plant biomass was not harvested from the horizontal levee, any phosphorus incorporated into plant biomass will eventually be returned to the subsurface in decomposing plant residues, suggesting internal cycling of phosphorus could sustain plant growth without inputs from wastewater. Because we observed no significant differences in the total mass of phosphorus between influent and effluent over the monitoring period, we inferred that plant and microbial biomass obtained phosphorus primarily from sources other than wastewater (e.g., from phosphorus in the soil).

It is possible that microorganisms assimilated phosphate from wastewater effluent, which was subsequently released as organic phosphorus during decay. This would be consistent with past research in which microbial uptake has only been a temporary sink for wastewater-derived phosphorus (Kadlec and Wallace, 2009). However, in wet meadow cells with a fine topsoil dissolved organic phosphorus concentrations in porewater did not increase until after approximately 5 m along the slope, despite wastewater-phosphate being removed within the first 3 meters (Figure 5-2). This suggests an alternative explanation for the observed shifts in phosphorus speciation is needed. Rather, it appears that wastewater-phosphate was removed in the first few meters of the subsurface by a combination of methods discussed above and that dissolved organic phosphorus export in latter parts of the slope was due to microbial turnover of phosphorus derived from the soil materials used during construction. This export would constitute a loss of less than 1% of the phosphorus in the horizontal levee annually, which could explain why we did not observe significant changes in the phosphorus content of the soils.

It is possible that this export of dissolved organic phosphorus would not be as significant if horizontal levees were constructed with sediments with lower phosphorus content, though it is unclear how this would impact plant growth and acquisition of plant phosphorus from different sources (i.e., the soil and wastewater). Further research is needed to understand these mechanisms and the impact of phosphorus content of the soil on them.

5.3.2 Post-treatment ponds for phosphorus recovery

In horizontal levees constructed with iron-containing sediments, relatively high concentrations of dissolved $Fe(II)_{(aq)}$ are likely to be present in the effluent. For example, in the pilot-scale horizontal levee, dissolved Fe had a median value of 5.7 mg Fe L^{-1} and ranged from 1.3 to 23 mg Fe L^{-1} in the effluent despite being at supersaturation with respect to siderite (see Chapter 3; Cecchetti et al., *in prep*). When exposed to dissolved oxygen, $Fe(II)_{(aq)}$ is oxidized to Fe(III) on the timescale of less than an hour (Davison and Seed, 1982). Fe(III)-oxides produced from Fe(II) oxidation often have a high affinity for phosphate, and this is especially true of the poorly crystalline iron oxides that typically form during oxidation by oxygen under circumneutral pH conditions (Slomp et al., 1996). The affinity of iron particles for phosphate is the basis for the coagulation-flocculation process used in wastewater treatment plants practicing chemical phosphorus removal (Zhou et al., 2008; Wilfert et al., 2015). In general, removal increases at lower pH values (Smith et al., 2008). It is not uncommon for iron-amended flocculation systems to achieve residual concentrations of total phosphorus below 0.1 mg P L^{-1} at circumneutral pH with iron dosed to around 10 mg L^{-1}. This would constitute >90% removal of applied phosphorus at the field site described in this study. However, unlike municipal wastewater effluent, much of the dissolved phosphorus in the effluent from the horizontal levee is in an organic form.

Organic phosphorus compounds also can be absorbed by iron oxides (Shang et al., 1992; Berg and Joern, 2006; Ruttenberg and Sulak, 2011; Lü et al., 2017). In fact, a variety of organic phosphorus compounds exhibit a relatively high affinity for iron-oxides (Ruttenberg and Sulak, 2011). However, we expect the phosphorus exported in organic forms from horizontal levees to be associated with polymeric natural organic matter. Although this organic phosphorus fraction will likely adsorb to iron oxides, we expect the organic phosphorus in the effluent from the horizontal levee to have a lower affinity for iron oxides than phosphate and the relatively simple organic phosphorus compounds (e.g., glucose 6-phosphate) that have been studied in the past (Lü et al., 2017). More research is needed to characterize the forms of organic phosphorus exported in horizontal levee effluent and their affinity for iron oxides.

Despite these potential limitations, relatively minor modifications to a horizontal levee system could be employed to facilitate oxidation of Fe(II) and immobilize phosphorus. For example, horizontal levees could be followed by a small hydraulic jump to aerate the effluent before discharging it into a post-treatment shallow open pond (Kucukali and Cokgor, 2009). A quiescent shallow pond would allow for phosphate adsorption and the settling of the flocs prior to discharge of water from the system. Periodic collection of the Fe(III)-oxide flocs deposited in this system could be performed to recover phosphorus as a potentially valuable product.

In water flowing out of the subsurface of horizontal levees, dissolved iron concentrations typically ranged from 10-25 mg Fe L^{-1}. This is comparable to the doses of Fe(III) that have produced substantial removal of phosphorus in past research on chemical phosphorus removal from wastewater (Smith et al., 2008) and would consume approximately 4 mg O_2 L^{-1} to oxidize to Fe(III)-oxides. Because $Fe(II)_{(aq)}$ oxidizes rapidly in the presence of oxygen – Davison and Seed (1982) reported half-lives for

Fe(II) oxidation in freshwaters on the order of 4 minutes to 6 hours in waters at circumneutral pH and 20ºC – this process is not limited by oxidation kinetics. Finally, because ~90% of iron-oxide particles formed in a typical particle size distribution settle within 15 hours (Benjamin and Lawler, 2013), it is also unlikely that sedimentation kinetics in these systems would limit their ability to remove forms of phosphorus that exhibit affinity for iron oxides. However, the removal of phosphorus in these systems will likely also depend on other factors, such as concentrations of natural organic matter (Zhou et al., 2008) and other metals (Li et al., 2014).

To assess the potential for using the formation of Fe(III)-oxides to remove phosphorus from the effluent of the horizontal levee, effluent samples were amended with Fe(II) and Fe(III) salts at concentrations representative of horizontal levee effluent (10 to 30 mg Fe L^{-1}). In these experiments, samples were amended with iron because effluent collected from the wetland at the time of the experiment was impacted by overland flow and had lower $Fe_{(aq)}$ concentrations (approximately 0.05 mg Fe L^{-1}) than typically observed after flow had been adjusted to minimize overland flow. Thus, iron had to be added to these experiments to reflect typical $Fe_{(aq)}$ concentrations in the effluent. In these experiments, concentrations of dissolved iron and total phosphorus in the supernatant dropped by >50% within 2 hours (Figure 5-4a/b; Wallis et al., 2015). A visible Fe(III)-oxide floc formed and settled rapidly out of the water column (Figure 5-5). Negligible additional removal of dissolved phosphorus was observed in these experiments between 2 and 24 hr. However, the pH of these experiments (7.9-8.9) was higher than the typical pH observed in horizontal levee effluent (pH ~ 6.5) and lower pH often promotes removal of phosphorus by iron-oxides (Smith et al., 2008). Additional experiments are needed to characterize this process under more representative conditions and to understand better the formation of iron flocs from native dissolved iron.

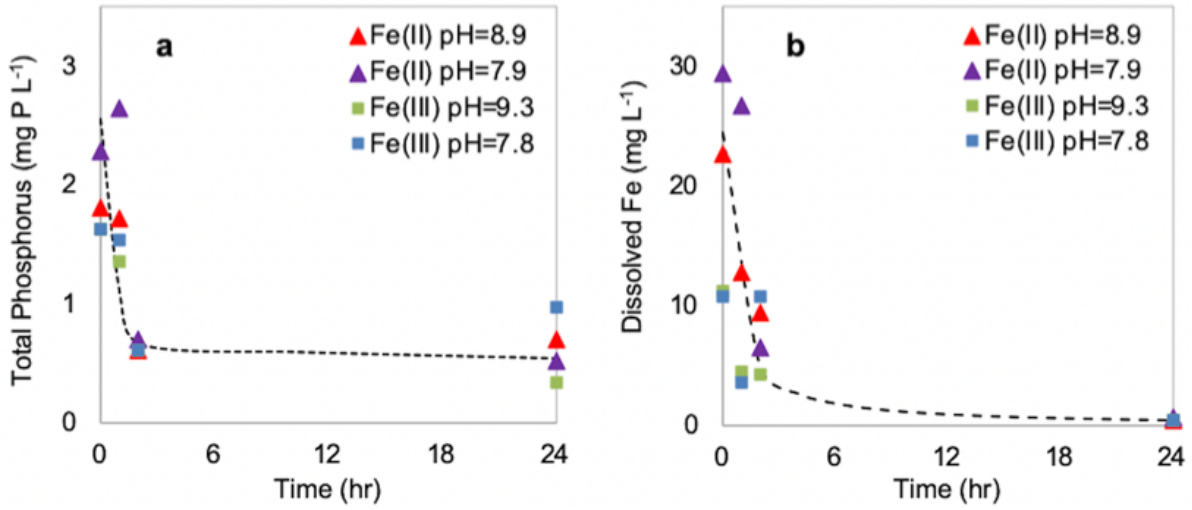

Figure 5-4: Concentrations of (a) total phosphorus and (b) dissolved iron in the supernatant of samples of wastewater amended with 10 to 30 mg Fe L^{-1} to test the removal of phosphorus by iron oxide flocs. All measurements were approximately an order of magnitude above the limits of quantitation (LOQ) for total phosphorus (LOQ = 0.003 mg P L^{-1}) and $Fe_{(aq)}$ (LOQ = 0.005 mg P L^{-1}), respectively.

Although phosphate and dissolved organic phosphorus concentrations were not measured in these experiments, approximately 50% of the phosphorus in the effluent from the horizontal levee was typically in organic forms at the time this experiment was conducted. Because total phosphorus concentrations decreased in these experiments by approximately 50-80%, it appears that some fraction of the organic phosphorus in horizontal levee effluent adsorbed onto iron oxides. More experiments

are required to assess changes in the aqueous speciation of phosphorus during Fe(III)-oxide formation and to characterize the phosphorus fractions that adsorb onto iron oxides in these experiments.

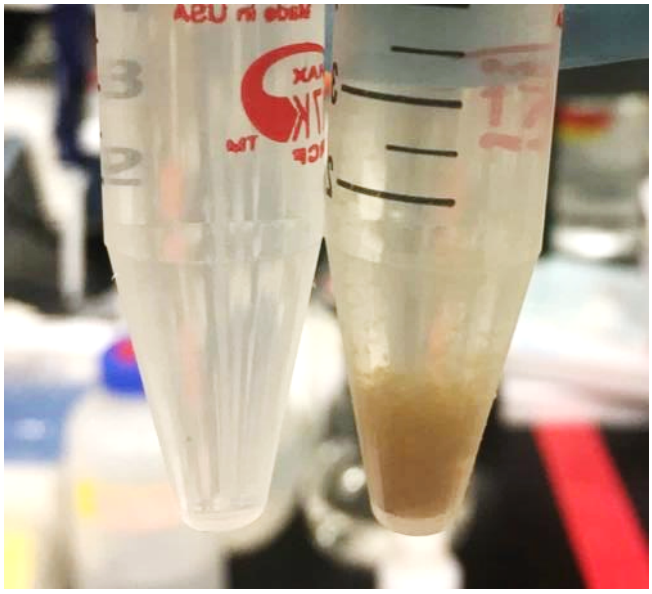

Figure 5-5: Formation of iron-oxide flocs in wastewater collected from the horizontal levee. The tube to the left is an acidified sample (pH ~ 2) and the tube to the right is unacidified. Samples were left exposed to the atmosphere at ambient temperature overnight.

Assuming that Fe(II) oxidation and flocculation and sedimentation of Fe(III)-oxide flocs would occur within 15 hr, we calculated that an additional aerated pond with a surface area of approximately 400 m^2 and depth of 0.3 m could accommodate the typical daily flow to the horizontal levee (i.e., 190 $m^3\ d^{-1}$) with a residence time of 15 hr that would allow for phosphorus removal by this mechanism. If added onto the end of the horizontal levee, this additional system would increase the length of horizontal levees by approximately 6%. Because horizontal levees are intended to be a part of coastal wetland gradients, it is possible that this additional process could be integrated easily into the current system, though it is unclear how tidal action might impact the aerated ponds.

If 15 mg Fe L^{-1} were transferred from the horizontal levee subsurface to these aerated ponds, this would constitute around 500 kg Fe yr^{-1}, which could be sustained for up to 300 years based on the iron content of the pilot-system. Each year, a total volume of 0.5 m^3 of iron oxides would be produced. Assuming a bulk density of the produced iron-oxide flocs of 1.15 g cm^{-3} (Benjamin and Lawler, 2013), we predict that the iron oxide floc would form an layer that would grow by approximately 1 mm annually at the base of the pond described above (i.e., with a 400 m^2 surface area). If 90% of the phosphorus in the effluent was removed, we would expect approximately 40 kg P yr^{-1} to be deposited in Fe(III)-oxide flocs. Because Fe(III)-oxides have a high affinity for phosphorus, it is likely that these flocs would release phosphorus slowly if applied as fertilizers (Zhou et al., 2008).

Addition of a pond after the horizontal levee to facilitate phosphorus removal holds promise as a means of removing and recovering phosphorus. However, more research is required to understand the kinetics and capacity for phosphorus removal in these systems under conditions that better reflect an aerated post-treatment pond. Additionally, it is possible that iron-oxide flocs could also act as a sink for toxic trace metals, such as lead and copper, that also have high affinities for iron-oxides and are found in

wastewater effluent (Amann et al., 2018). Depending on the concentrations, the presence of these metals could limit the applicability of the collection and use of iron-oxide sludges from these systems as fertilizers in agriculture.

5.4 Conclusions

Phosphorus removal is important in freshwater ecosystems because it can stimulate algal blooms. Data collected at a pilot-scale horizontal levee indicates that these systems do not remove phosphorus as currently designed. The decrease in phosphate observed within the first three meters of the wetland was balanced by the formation and release of dissolved organic phosphorus in the subsurface. Despite minimal removal of phosphorus in horizontal levees as currently designed, it may be possible to enhance the removal by adding an aerated pond after water is released from the subsurface. By stimulating rapid oxidation of $Fe(II)_{(aq)}$ to form Fe(III)-oxide flocs that have a high affinity for phosphorus, aerated ponds could create conditions that promote the sedimentation and removal of phosphorus-rich iron-oxide sludges. If collected periodically, these sludges could be used as an agricultural fertilizer. Without significant additional maintenance or operational complexity, this post-treatment addition could provide another important benefit to those already described in the previous chapters. Additional research is needed to assess the affinity of dissolved organic phosphorus for the flocs produced when horizontal levee effluent encounters oxygen and to determine the mechanism through which phosphate is removed at the beginning of the horizontal levee.

Chapter 6. Conclusions and Future Directions

6.1 Summary

The ability of horizontal levees to remove contaminants from wastewater effluent was evaluated in a pilot-scale facility. Horizontal levees are nature-based constructed subsurface treatment wetlands located along the seaward side of storm control levees in coastal areas. These systems can provide simultaneous benefits including treatment of wastewater-derived contaminants in their subsurface layers, protection of storm control levees by attenuating wave action, restoration of valuable wetland habitat, and many ancillary benefits (e.g., recreational opportunities). The subsurface layers of horizontal levees provide ideal conditions for the promotion nutrient removal processes, such as denitrification and plant uptake of nutrients, and also promote a variety of other processes, such as adsorption, mineral precipitation and anaerobic processes, that can remove trace metals, trace organic contaminants (e.g., pharmaceuticals) and pathogen indicators (e.g., F+ coliphage).

To evaluate the ability of horizontal levees to remove nutrients from wastewater effluent, we studied a pilot-scale horizontal levee facility over a 2-year monitoring period. Monitoring of water quality conditions and contaminant concentrations was conducted on a bi-weekly to monthly basis over this period of time to track changes in the loading of contaminants between the influent and effluent of the pilot system. These measurements were paired with flow monitoring and a set of mass balances to evaluate the impact of hydrological conditions on contaminant removal in the pilot system and to optimize the system progressively. Samples of porewater were also collected to evaluate the impact of redox conditions on contaminant removal and to develop a model for projecting the long-term ability of these systems remove nitrogen via denitrification. The removal of nutrients by plant uptake was evaluated by tracking natural abundance levels of ^{15}N in plants, soils and the influent wastewater. we then employed an isotope mixing model to determine the contribution of different nitrogen sources (primarily soil and wastewater) to the nitrogen stored in plant biomass. Finally, the mechanisms responsible for phosphorus removal in these systems were evaluated by tracking changes in the speciation of phosphorus between various forms and by using mass balances on phosphorus and other elements that are related to the mobility of phosphorus in sediments (e.g., iron).

In the following sections, we summarize the key findings of these studies and discuss their implications for the design of future horizontal levee systems and similar nature-based systems, such as riparian treatment zones along rivers. Additionally, we will discuss the utility of the methods that were developed for investigating contaminant removal in nature-based treatment systems and how these can be used to improve our understanding of the mechanisms responsible for that removal. Finally, we will present some of the critical research questions that remain unanswered by my research and should be addressed in future studies.

6.2 Optimization of Horizontal Levees for the Removal of Nutrients

In Chapter 2, we presented our research on the progressive optimization of a pilot-scale horizontal levee for contaminant removal. To do this, we used a combination of water quality monitoring and hydrological data to identify the ideal operational conditions for maintaining efficient removal of contaminants. Once identified, we adjusted the operation to match those conditions. We determined that hydrological conditions, and in particular the fraction of flow in the subsurface (versus running

over the wetland surface), were the most important factors controlling contaminant removal. This was true across various classes of contaminants, including nitrogen species, a suite of trace organic contaminants, and pathogen indicators (e.g., F+ coliphage), with strong correlations ($r^2 > 0.73$) observed between the fraction of water flowing through the subsurface and fractional removal of tested contaminants. Additionally, using samples of porewater collected along transects within the pilot horizontal levee cells, we identified that contaminant removal occurred rapidly at the beginning of the wetland slope, with most contaminants removed by greater than 90% within the first 5 m of the subsurface.

We observed that other design parameters, specifically the types of construction materials (e.g., soils) and plant communities used on horizontal levees, can have a significant impact on the maximum flow that can be applied to the subsurface before water begins to flow over the surface of the wetland. This impacts the total mass of contaminants that can be removed in horizontal levees because cells with different subsurface flow capacities achieved comparable fractional removal of contaminants.

From our findings, we identified a few design features that could be used to promote efficient removal of contaminants in future horizontal levees. First, horizontal levees require subsurface flow to achieve efficient contaminant removal and should therefore be designed to promote subsurface flow. This could be achieved by using construction materials with a high hydraulic conductivity (e.g., gravel) or with spaced inlet trenches along the horizontal levee slope to ensure that all of the flow passes through a portion of the subsurface. Additionally, because contaminant removal was primarily achieved in a small portion of the subsurface at the top of horizontal levee, higher hydraulic conductivity sediments could be strategically placed at the beginning of those wetlands (e.g., in the first 5-10 m) to allow for greater subsurface flow rates where contaminant removal is significant, without concern about water flowing over the surface once it has received an appropriate amount of treatment in the subsurface. It is important to note that higher hydraulic conductivity sediments may inadvertently decrease areal removal rates. This could be caused by the higher velocity of water flow through pore spaces that can be achieved with higher hydraulic conductivity materials, as well as the larger cross-sectional area of pores relative to the biofilms in which denitrifiers are active. Lastly, our results suggested that planting willows (*Salix* sp.) on horizontal levees may be useful because their extensive rooting zones appear to create higher subsurface flow rates in horizontal levees, leading to greater mass removal of contaminants.

6.3 Using New Methods to Develop a Mechanistic Understanding of Contaminant Removal in Nature-Based Systems

In Chapter 3 and Chapter 4, we used a variety of methods, including extensive porewater sampling paired with mass balances and tracking of ^{15}N in the horizontal levee, to identify the mechanisms responsible for nitrogen removal. In Chapter 5, we identified the mechanisms responsible for removal of phosphorus by tracking changes in the phosphorus speciation in samples collected throughout the horizontal levee subsurface and using mass balance methods.

Denitrification was identified as the primary nitrate removal mechanism in the horizontal levee and was responsible for 1100 kg N removed over the two-year monitoring period: approximately 75% of the 1470 kg N applied to the subsurface of the pilot system (in cells D through L). We used evidence from a combination of sources, including coupled trends in ^{15}N and ^{18}O isotopes in porewater nitrate, to identify this as the primary removal mechanism. An additional 210 kg N (14% of removal) were assimilated into microbial biomass, though we do not expect this mechanism to be responsible for long-term nitrogen removal because internal turnover of microbial biomass nitrogen produces the

nitrogen required for microbial assimilation at steady state conditions. The remaining 150 kg N were removed by plant uptake (discussed below). By tracking speciation of dissolved nitrogen and concentrations of other redox-active species ($Mn(II)_{(aq)}$, $Fe(II)_{(aq)}$, and sulfate) in the subsurface, we mapped a spatial oxidation-reduction sequence. Evaluating biogeochemical processes was essential to developing an understanding of the long-term nitrogen removal capability of horizontal levees because organic carbon drives many of these processes and is also required for denitrification as an electron donor and energy source. The electrons required to fuel denitrification over the monitoring period (630 keq) were equivalent to more than 50% of the electrons transferred from organic carbon in sediments (1150 keq). However, not all reductants required for denitrification were supplied by organic carbon and more than 60% of the electrons transferred from electron donors went to species other than nitrate.

A significant portion of the electrons transferred from organic carbon species (approximately 17%) were utilized in the reduction of Fe(III)-oxides and sulfate. Accumulation of the products of these processes ($Fe(II)_{(aq)}$ and sulfide) in the aqueous phase created supersaturated conditions for iron-sulfide minerals in the subsurface, leading to the formation of sulfide mineral deposits that were observed on collected sediments. This process appeared to be significant during the summer with rapid removal of applied sulfate in the subsurface. In the winter, we observed strong correlations between increasing sulfate and decreasing nitrate concentrations, likely due to the utilization of iron sulfide deposits as an electron donor by autotrophic denitrifiers. This process appeared to account for nearly 20% of the nitrate reduction observed in the winter. To produce a better understanding of the interactions between these biogeochemical cycles, we integrated these electron transfers into an overall electron transfer model through which we could estimate the lifetime over which a horizontal levee could remove nitrate from wastewater effluent. Based on the conditions observed in the pilot-system, we estimated that if just 10% of the carbon stored in plant biomass produced in the pilot system became available to fuel microbial processes, nitrogen removal in horizontal levees would become self-sustaining. Using this model, we determined that significantly lower additions of wood chip carbon may be necessary to stimulate long-term nitrogen removal.

To evaluate the magnitude of plant uptake in these systems, we applied an isotope mixing model. We developed this new method for quantifying plant uptake because past research has had to rely on assumptions that would not be valid in a full-scale horizontal levee system, such as that all nitrogen taken up into plants was derived from wastewater. In horizontal levees, nitrogen is available from multiple sources, with the primary sources being wastewater and indigenous soil nitrogen. To measure plant uptake, we analyzed $\delta^{15}N$ in samples of plant biomass (i.e., new growth leaves) and used measurements of $\delta^{15}N$ in soils and wastewater as endmembers. Using a linear mixing model, we identified that 14% of nitrogen in plants (approximately 120 kg N in cells D through L, with an additional 30 kg N in swale-type cells) was taken up from wastewater derived nitrogen, with the remaining 86% (approximately 880 kg N in cells D through L with an additional 250 kg N in swale-type cells) derived from soil. There were significant spatial and seasonal trends in plant uptake of wastewater nitrogen, with a larger fraction of biomass nitrogen derived from wastewater at the beginning of the wetland and higher uptake rates observed in the spring and summer.

Plant uptake accounted for 8% of the wastewater nitrogen applied to the horizontal levee. Alternative methods for quantifying this pathway would have yielded values ranging from 0-4% to nearly 60% of wastewater-nitrogen removal attributed to plant uptake. This new method is a more precise tool for quantifying nitrogen uptake by plants in nature-based treatment systems or natural ecosystems receiving wastewater nitrogen. This method could also be applied in any system where multiple nitrogen sources with distinct isotope signatures are available to plants. In systems where 3 or more

sources of nitrogen are available, the contribution of sources cannot be solved analytically using a linear mixing model, but Bayesian mixing model approaches may be applicable to produce similar estimates of plant uptake rates in those systems. By quantifying plant uptake of nitrogen more precisely, researchers can help resolve the large variation in nitrogen uptake rates that have been reported in the literature. Additional research would be useful to resolve variations in uptake of nitrogen among different plant species and communities selected based on past knowledge regarding rooting depths, nutrient demands and uptake phenologies.

Phosphorus was not removed in the horizontal levee. Approximately 210 kg P (in all forms) was applied to the horizontal levee and the effluent load (250 kg P) was approximately 17% higher during the 2-yr monitoring period. Total phosphorus removal did not improve over the monitoring period. Conversely, removal of phosphate increased from only 11% of applied phosphate during the first monitoring phase to greater than 84% during the last phase. The 40 kg reduction in phosphate was likely removed by a combination of adsorption onto Fe(III)-oxides and vivianite ($Fe_3(PO_4)_{2(s)}$) formation at the beginning of the levee slope, and to a lesser extent through uptake into plant and microbial biomass. Production of organic phosphorus was likely due to microbial turnover and export of the soil phosphorus pool. Despite observing little removal of phosphorus within the horizontal levee, microcosms performed with effluent from the horizontal levee suggest that removal of phosphorus could be achieved in post-treatment aerated systems. This could occur through the adsorption of phosphorus onto Fe(III)-oxide precipitates that form during abiotic oxidation of $Fe(II)_{(aq)}$, which is rapid in the presence of oxygen. Because $Fe(II)_{(aq)}$ is abundant in effluent from the horizontal levee subsurface (with concentrations often around 10-15 mg L^{-1}) this presents a promising option for enhancing phosphorus removal prior to discharging effluent to aquatic systems that may be sensitive to phosphorus inputs.

6.4 Future Research Directions

With the studies detailed in this dissertation, we have tested the impact of design and operational variables on contaminant removal in horizontal levees and provided a mechanistic interpretation of nitrogen removal in those systems. We also developed tools for measuring plant uptake of nitrogen and for projecting the design life of horizontal levees with respect to nitrogen removal based on the biogeochemistry of nitrogen, carbon and other redox-active species in the subsurface of horizontal levees. These studies include important findings that can be used to inform the design of future horizontal levee systems by practitioners and can aid future researchers in the development of monitoring methods for studying water quality improvements in similar nature-based treatment systems. However, there remain large gaps in our understanding of how these systems function, specifically with respect to the removal of a suite of additional contaminants that are commonly found in wastewater, such as trace organic contaminants (e.g., pharmaceuticals), trace metals, per- and polyfluoroalkyl substances (PFASs), and organophosphorus esters.

Past research suggests that subsurface constructed wetlands may be effective at removing many trace organic contaminants from wastewater (García et al., 2010; Matamoros and Bayona, 2006). For example, 50-96% removal of PFASs has been observed in a constructed wetland system by previous researchers (Yin et al., 2017). Conversely, there appears to be some uncertainty regarding the ability of constructed wetland systems to remove trace metals (Vymazal et al., 2007; García et al., 2010; Galletti et al., 2010). Despite evidence of significant removal of trace organic contaminants (e.g., pharmaceuticals) in horizontal levees (presented in Chapter 2), we do not currently understand the mechanisms responsible for that removal, and we have yet to investigate the potential formation of transformation products (e.g., pharmaceutical metabolites) during treatment. Moreover, it is not fully

clear how treatment of wastewater-derived contaminants in horizontal levees would be impacted by the application of alternative water matrixes, such as the concentrate stream from reverse osmosis processes at wastewater reclamation facilities, though a growing body of literatures suggests that constructed wetlands can be effective at removing contaminants from higher salinity water sources (Liang et al., 2017; review of past studies). Additionally, because wastewater treatment facilities have recently been identified as an important source of microplastics to the environment (Ziajahromi et al., 2017), the fate of microplastics in horizontal levees should also be evaluated. More research is clearly required to answer the important questions we have about the fate, transport and removal of these additional contaminants in horizontal levees.

Research is already being conducted at the horizontal levee pilot facility to answer some of the questions discussed above regarding removal of different classes of contaminants (Stiegler et al., *in prep*; Rodgers et al., *in prep*). For example, preliminary evidence suggests that a combination of biological, chemical and physical processes, such as plant uptake, biotransformation, and adsorption, are responsible for the removal of pharmaceuticals observed in this system (Stiegler et al., *in prep*). Mass balances and reactive transport models have also been developed and validated through field measurements to assess the fate and transport of organophosphorus esters in these systems (Rodgers et al., *in prep*). Furthermore, reverse osmosis concentrate from wastewater reclamation systems is currently being tested as a source water at the horizontal levee test facility. Research is planned to evaluate the removal of a broad range of contaminants, including trace organic contaminants and trace metals, from concentrated wastewater streams applied to horizontal levee systems.

Despite characterizing the mechanisms responsible for nutrient removal, we have not investigated the microbial interactions that drive these processes in horizontal levees. Microbial processes are responsible for the majority of removal of nitrogen, with greater than 90% of nitrogen removed by microbial denitrification or assimilation into microbial biomass, as detailed in Chapter 3. In aquatic systems and soils, these processes are frequently driven by complex metabolic handoffs between microorganisms (Hug and Co, 2017). However, the application of new high-throughput sequencing approaches to the study of constructed wetland systems has been limited thus far (Bulseco et al., 2020). To evaluate the microbial interactions driving the cycling and removal of contaminants in horizontal levees, metagenomics and metatranscriptomics analyses are currently being conducted on samples collected at the pilot system. The results of these studies will be used to provide greater detail regarding the microbial processes that are occurring in the horizontal levee, as well as the metabolic capabilities of those communities that are not currently being expressed but might be useful from an engineering perspective. Because microbial processes often occur in cryptic cycles in the environment (Kappler and Bryce, 2017), the greater mechanistic resolution of these studies can provide important details to inform the design and optimization of future systems. There are also concerns regarding greenhouse gas emissions from horizontal levees based on past research suggesting that emissions of these gases can be significant in subsurface constructed wetlands (Mander et al., 2014). Because microbes control the production and consumption of these trace gases (Conrad, 1996), research is planned to evaluate greenhouse gas emissions and the microbial communities that control them in the horizontal levee pilot system.

Questions also remain regarding the ability of these systems to adapt to a changing climate, though they have been designed specifically to serve that purpose. For example, it is not clear how changes in the hydraulic conditions in tidally-influenced horizontal levees will impact contaminant removal. However, based on our research detailed in Chapter 3, it seems clear that any increase in water flow over the surface of the wetland will lead to decreased contaminant removal efficiency. This might be expected if rising tides lead to higher water tables in full-scale systems.

It is critical that horizontal levees be investigated further to understand the processes responsible for contaminant removal within them. Identifying these processes is essential to the design and optimization of these systems because ideal conditions to promote removal often are not consistent across different classes of contaminants and the processes that remove them. Future research should focus on identifying the contaminant removal mechanisms for the suite of additional contaminants discussed above and how contaminant removal is impacted by changing climatic conditions. The design of horizontal levees to remove these contaminants efficiently is critical if we want to reduce the loading of these contaminants to the environment to protect sensitive aquatic ecosystems and all of us that rely on them.

References

1. Aké-Castillo, J.A., Vázquez, G., López-Portillo, J., 2006. Litterfall and decomposition of *Rhizophora mangle* L. in a coastal lagoon in the southern Gulf of Mexico. Hydrobiologia 559, 101-111.

2. Ali, M.A., Oh, J.H., Kim, P.J., 2008. Evaluation of silicate iron slag amendment on reducing methane emission from flood water rice farming. Agriculture, Ecosystems & Environment 128 (1-2), 21-26, https://doi.org/10.1016/j.agee.2008.04.014.

3. Allen, R.G., Pereira, L.S., Raes, D., Smith, M., 1998. Crop evapotranspiration – guidelines for computing crop water requirements. FAO Irrigation and Drainage Paper 56, ISBN 92-5-104219-5.

4. Amann, A., Zoboli, O., Krampe, J., Rechberger, H., Zessner, M., Egle, L. 2018. Environmental impacts of phosphorus recovery from municipal wastewater. Resources, Conservation & Recycling 130, 127-139, https://doi.org/10.1016/j.resconrec.2017.11.002

5. American Public Health Association (APHA). *Standard Methods for the Examination of Water and Wastewater,* 22nd Ed. American Public Health Association, American Water Works Association, Water Environment Foundation: Washington, DC, 2012.

6. Amichev, B.Y., Kurz, W.A., Smyth, C., van Rees, K.C.J., 2012. The carbon implications of large-scale afforestation of agriculturally marginal land with short-rotation willow in Saskatchewan. Global Change Biology: Bioenergy 4, 70-87, https://doi.org/10.1111/j.1757-1707.2011.01110.x.

7. Anderson, D.M., Glibert, P.M., Burkholder, J.M., 2002. Harmful algal blooms and eutrophication: nutrient sources, composition and consequences. Estuaries 25 (4b), 704-726, https://doi.org/10.1007/BF02804901.

8. Aravena, R., Robertson, W.D., 1998. Use of multiple isotope tracers to evaluate denitrification in ground water: study of nitrate from a large-flux septic system plume. Ground Water 36 (6), 975-982, https://doi.org/10.1111/j.1745-6584.1998.tb02104.x.

9. Armstrong, W., 1968. Oxygen diffusion from the roots of woody species. Physiologia Plantarum 21, 539-543.

10. Ashton, E.C., Hogarth, P.J., Ormond, R., 1999. Breakdown of mangrove leaf litter in a managed mangrove forest in Peninsular Malaysia. Hydrobiologia 413, 77-88.

11. Atekwana, E.A., Molwalefhe, L., Kgaodi, O., Cruse, A.M., 2016. Effect of evapotranspiration on dissolved inorganic carbon and stable carbon isotopic evolution in rivers in semi-arid climates: the Okavango Delta in north west Botswana. Journal of Hydrology: Regional Studies 7, 1-13, https://doi.org/10.1016/j.ejrh.2016.05.003.

12. Aulenbach, B.T., Buxton, H.T., Battaglin, W.A., and Coupe, R.H., 2007, Streamflow and nutrient fluxes of the Mississippi-Atchafalaya River Basin and subbasins for the period of record through 2005: U.S. Geological Survey Open-File Report 2007-1080, https://toxics.usgs.gov/pubs/of-2007-1080/index.html.

13. Bailey, L.T., Mitchell, C.P.J., Engstrom, D.R., Berndt, M.E., Coleman Wasik, J.K., Johnson, N.W., 2017. Influence of porewater sulfide on methylmercury production and partitioning in sulfate-impacted lake sediments. Science of the Total Environment 580, 1197-1204, https://doi.org/10.1016/j.scitotenv.2016.12.078.

14. Baken, S., Verbeeck, M., Verheyen D., Diels, J., Smolders, E., 2015. Phosphorus losses from agricultural land to natural waters reduced by immobilization in iron-rich sediments of drainage ditches. Water Research 71, 160-170.

15. Bannon, R.O., Roman, C.T., 2008. Using stable isotopes to monitor anthropogenic nitrogen inputs to estuaries. Ecological Applications 18 (1), 22-30, https://www.jstor.org/stable/40062108.

16. Baum, C., Leinweber, P., Shlichting, A., 2003. Effects of chemical conditions in re-wetted peats on temporal variation in microbial biomass and acid phosphatase activity within growing season. Applied Soil Ecology 22, 167-174.

17. Baye, P., ESA, 2012. *Oro Loma Wet Weather Equalization, Treatment Wetland and Ecotone Demonstration Project: Initial Feasibility Study*. Oro Loma Sanitary District, San Lorenzo, CA.

18. Beagle, J., Lowe, J., McKnight, K., Safran, S.M., Tam, L., Szambelan, S.J., 2019. *San Francisco Bay Shoreline Adaptation Atlas: Working with Nature to Plan for Sea Level Rise Using Operational Landscape Units*. SFEI Contribution No. 915. SFEI & SPUR: Richmond, CA. p 255, https://www.sfei.org/documents/adaptationatlas.

19. Behrendt, A., Tarre, S., Beliavski, M., Green, M., Klatt, J., de Beer, D., Stief, P., 2014. Effect of high electron donor supply on dissimilatory nitrate reduction pathways in a bioreactor for nitrate removal. Bioresource Technology 171, 291-297, https://doi.org/10.1016/j.biortech.2014.08.073.

20. Benjamin, M.M., Lawler, D.F., 2013. *Water Quality Engineering: Physical/Chemical Treatment Processes*. 1st Ed. John Wiley & Sons, Inc.: Hoboken, NJ.

21. Berg, A.S., Joern, B.C., 2006. Sorption dynamics of organic and inorganic phosphorus compounds in soil. Journal of Environmental Quality 35, 1855-1862, https://doi.org/10.2134/jeq2005.0420.

22. Berhongaray, G., Janssens, I.A., King, J.S., Ceulemans, R., 2013. Fine root biomass and turnover of two fast-growing poplar genotypes in a short-rotation coppice culture. Plant Soil 373, 269-283, https://doi.org/10.1007/s11104-013-1778-x.

23. Berner, R.A., 1967. Thermodynamic stabilities of sedimentary iron sulfides. American Journal of Science 265, 773-785.

24. Boecklen, W.J., Yarnes, C.T., Cook, B.A., James, A.C., 2011. On the use of stable isotopes in trophic ecology. Annual Review of Ecology, Evolution, and Systematics 42, 411-440, https://doi.org/10.1146/annurev-ecolsys-102209-144726.

25. Bond, A.L., Diamond, A.W., 2011. Recent Bayesian stable-isotope mixing models are highly sensitive to variation in discrimination factors. Ecological Applications 21 (4), 1017-1023, https://doi.org/10.1890/09-2409.1.

26. Bowden, W.B., 1987. The biogeochemistry of nitrogen in freshwater wetlands. Biogeochemistry 4 (3), 313-348, https://www.jstor.org/stable/1468671.

27. Bowden, W.B., Vörösmarty, C.J., Morris, J.T., Peterson, B.J., Hobbie, J.E., Steudler, P.A., Moore III, B., 1991. Transport and processing of nitrogen in a tidal freshwater wetland. Water Resources Research 27 (3), 389-408, https://doi.org/10.1029/90WR02614.

28. Boyer, E.W., Alexander, R.B., Parton, W.J., Li, C., Butterbach-Bahl, K., Donner, S.D., Skaggs, R.W., Del Gross, S.J. 2006. Modeling denitrification in terrestrial and aquatic ecosystems at regional scales. Ecological Applications 16 (6), 2123-2142.

29. Böttcher, J., Strebel, O., Voerkelius, S., Schmidt, H.-L., 1990. Using isotope fractionation of nitrate-nitrogen and nitrate-oxygen for evaluation of microbial denitrification in a sandy aquifer. Journal of Hydrology 114, 413-424, https://doi.org/10.1016/0022-1694(90)90068-9.

30. Breusch, T. S., Pagan, A. R., 1979. A Simple Test for Heteroscedasticity and Random Coefficient Variation. Econometrica 47 (5), 1287–1294. JSTOR. https://doi.org/10.2307/1911963.

31. Bricker, S.B., Longstaff, B., Dennison, W., Jones, A., Boicourt, K., Wicks, C., Woerner, J., 2008. Effects of nutrient enrichment in the nation's estuaries: a decade of change. Harmful Algae 8, 21-32.

32. Bridgham, S.D., Cadillo-Quiroz, H., Keller, J.K., Zhuang, Q., 2013. Methane emissions from wetlands: biogeochemical, microbial, and modeling perspectives from local to global scales. Global Change Biology 19, 1325-1346.

33. Bulseco, A.N., Vineis, J.H., Murphy, A.E., Spivak, A.C., Giblin, A.E., Tucker, J., Bowen, J.L. Metagenomics coupled with biogeochemical rates measurements provide evidence that nitrate addition stimulates respiration in salt marsh sediment. Limnology and Oceanography 65, 2020, S321-S339, https://doi.org/10.1002/lno.11326.

34. Burgin, A.J., Hamilton, S.K., 2007. Have we overemphasized the role of denitrification in aquatic ecosystems? a review of nitrate removal pathways. Frontiers in Ecology and the Environment 5 (2), 89-96, https://doi.org/10.1890/1540-9295(2007)5[89:HWOTRO]2.0.CO;2.

35. Burgin, A.J., Yang, W.H., Hamilton, S.K., Silver, W.L., 2011. Beyond carbon and nitrogen: how the microbial energy economy couples elemental cycles in diverse ecosystems. Frontiers in Ecology and the Environment 9 (1), 44-52, https://doi.org/10.1890/090227.

36. Callaway, J.C., DeLaune, R.D., Patrick, W.H., Jr., 1997. Sediment accretion rates from four coastal wetlands along the Gulf of Mexico. Journal of Coastal Research 13 (1), 181-191, https://www.jstor.org/stable/4298603.

37. Canfield, D.E., 1989. Reactive iron in marine sediments. Geochimica et Cosmochimica Acta 53, 619-632.

38. Canfield, D.E., Thamdrup, B., Hansen, H.W., 1993. The anaerobic degradation of organic matter in Danish coastal sediments: iron reduction, manganese reduction, and sulfate reduction. Geochimica et Cosmochimica Acta 57, 3867-3883.

39. Caraco, N.F., Cole, J.J., Likens, G.E., 1989. Evidence for sulphate-controlled phosphorus release from sediments of aquatic systems. Nature 341, 316-318, https://doi.org/10.1038/341316a0.

40. Cardoso, R.B., Sierra-Alvarez, R., Rowlette, P., Flores, E.R., Gómez, J., Field, J.A., 2006. Sulfide oxidation under chemolithoautotrophic denitrifying conditions. Biotechnology and Bioengineering 95 (6), 1148-1157, https://doi.org/10.1002/bit.21084.

41. Cayan, D.R., Bromirski, P.D., Hayhoe, K., Tyree, M., Dettinger, M.D., Flick, R.E., 2008. Climate change projections of sea level extremes along the California coast. Climate Change 87, S57-S73.

42. Cecchetti, A.R., Stiegler, A.N., Graham, K.E., Sedlak, D.L., 2020a. The horizontal levee: a multi-benefit nature-based treatment system that improves water quality and protects coastal levees from the effects of sea level rise. Water Research X 7, 100052, https://doi.org/10.1016/j.wroa.2020.100052.

43. Cecchetti, A., Stiegler, A., Sytsma, A., Gonthier, E., Graham, K., Boehm, A.B., Dawson, T., Sedlak, D., 2020b. Monitoring Data from a Pilot-Scale Horizontal Levee System, Mendeley Data, v2, https://doi.org/10.17632/xwx83vzmf6.2.

44. Cecchetti, A.R., Sytsma, A., Stiegler, A.N., Dawson, T.E., Sedlak, D.L., Use of stable nitrogen isotopes to track plant uptake of nitrogen in a nature-based treatment system. *Manuscript submitted for publication*.

45. Cecchetti, A.R., Stiegler, A.N., Gonthier, E., Sedlak, D.L., The fate of dissolved nitrogen species in a horizontal levee: impacts of electron acceptors on seasonal nitrate removal processes. *Manuscript in preparation*.

46. Chacón, N., Dezzeo, N., Muñoz, B., Rodríguez, J.M., 2005. Implications of soil organic carbon and the biogeochemistry of iron and aluminum on soil phosphorus distribution in flooded forests of the lower Orinoco River, Venezuela. Biogeochemistry 73, 555-566.

47. Chen, Y., Wen, Y., Zhou, Q., Vymazal, J., 2014. Effects of plant biomass on nitrogen transformation in subsurface-batch constructed wetlands: a stable isotope and mass balance assessment. Water Research 63, 158-167, https://doi.org/10.1016/j.watres.2014.06.015.

48. Chen, Y., Wen, Y., Zhou, Q., Huang, J., Vymazal, J., Kuschk, P., 2016. Sulfate removal and sulfur transformation in constructed wetlands: the role of filling material and plant biomass. Water Research 102, 572-581.

49. Childers, D.L., Corman, J., Edwards, M., Elser, J.J., 2011. Sustainability challenges of phosphorus and food: solutions from closing the human phosphorus cycle. BioScience 61(2), 117-124, https://doi.org/10.1525/bio.2011.61.2.6.

50. Chimner, R.A., Ewel, K.C., 2005. A tropical freshwater wetland: II. production, decomposition, and peat formation. Wetlands Ecology and Management 13, 671-684.

51. Cloern, J.E., 1999. The relative importance of light and nutrient limitation of phytoplankton growth: a simple index of coastal ecosystem sensitivity to nutrient enrichment. Aquatic Ecology 33, 3-16.

52. Cloern, J.E., 2005. Heat wave brings an unprecedented red tide to San Francisco Bay. Eos, Earth and Space Science News 86 (7), 15.

53. Cloern, J.E., Jassby, A.D., 2012. Drivers of change in estuarine-coastal ecosystems: discoveries from four decades of study in San Francisco Bay. Geophysics Reviews 50, 2-33.

54. Cole, M.L., Valiela, I., Kroeger, K.D., Tomasky, G.L., Cebrian, J., Wigand, C., McKinney, R.A., Grady, S.P., da Silva, M.H.C., 2004. Assessment of $\delta^{15}N$ isotopic method to indicate anthropogenic eutrophication in aquatic ecosystems. Journal of Environmental Quality 33, 124-132, https://doi.org/10.2134/jeq2004.1240.

55. Conner, W.H., Day Jr., J.W., 1992. Water level variability and litterfall productivity of forested freshwater wetlands in Louisiana. The American Midland Naturalist 128 (2), 237-245.

56. Conrad, R., 1996. Soil microorganisms as controllers of atmospheric trace gases (H_2, CO, CH_4, OCS, N_2O, and NO). Microbiology Reviews 60 (4), 609-640, https://www.ncbi.nlm.nih.gov/pmc/articles/PMC239458/pdf/600609.pdf.

57. Cordell, D., Drangert, J.O., White, S., 2009. The story of phosphorus: global food security and food for thought. Global Environmental Change 19, 292-305.

58. Cornwell, J.C., Morse, J.W., 1987. The characterization of iron sulfide minerals in anoxic marine sediments. Marine Chemistry 22 (2-4), 193-206.

59. Craine, J.M., Brookshire, E.N.J., Cramer, M.D., Hasselquist, N.J., Koba, K., Marin-Spiotta, E., Wang, L., 2015. Ecological interpretations of nitrogen isotope ratios of terrestrial plants and soils. Plant and Soil 396, 1-26, https://doi.org/10.1007/s11104-015-2542-1.

60. Darke, A.K., Walbridge, M.R., 2000. Al and Fe biogeochemistry in a floodplain forest: implications for P retention. Biogeochemistry 51, 1-32.

61. Davis, S.M., 1989. *Sawgrass and cattail production in relation to nutrient supply in the Everglades.* Sharitz R.R., Gibbons J.W. (eds.) U.S. Department of Energy Conference No.

8603101, held in Charleston, South Carolina; National Technical Information Service: Springfield, Virginia, 325–341.

62. Davis, S.M., 1994. Phosphorus inputs and vegetation sensitivity in the Everglades. In: *Everglades: The Ecosystem and Its Restoration*, Davis S.M., Ogden J.C. (eds.) St. Lucie Press: Delray Beach, Florida, 357–378.

63. Davison, W., Seed, G., 1983. The kinetics of the oxidation of ferrous iron in synthetic and natural waters. Geochimica et Cosmochimica Acta 47(*1*), 67-79, https://doi.org/10.1016/0016-7037(83)90091-1.

64. Dawson, T.E., Mambelli, S., Plamboeck, A.H., Templer, P.H., Tu, K.P., 2002. Stable isotopes in plant ecology. Annual Reviews of Ecology and Systematics 33, 507-559, https://doi.org/annurev.ecolsys.33.020602.095451.

65. Dayton, E.A., Whitacre, S., Holloman, C., 2017. Comparison of three persulfate digestion methods for total phosphorus analysis and estimation of suspended solids. Applied Geochemistry 78, 357-362, https://doi.org/10.1016/j.apgeochem.2017.01.011.

66. Dähnke, K., Thamdrup, B., 2016. Isotope fractionation and isotope decoupling during anammox and denitrification in marine sediments. Limnology and Oceanography 61, 610-624.

67. Deghi, G.S., Ewel, K.C., Mitsch, W.J., 1980. Effects of sewage effluent application on litter fall and litter decomposition in cypress swamps. Journal of Applied Ecology 17 (2), 397-408.

68. de Oude, R., Augustijn, D.C.M., Wijnberg, K.M., Dekker, F., de Vries, M.B., Suzuki, T. Bioengineering in front of a river dike: wave attenuation by vegetation. In: Christodoulou, G.C., Stamou, A.I. (Eds.), *Environmental Hydraulics: Proceedings of the 6th International Symposium on Environmental Hydraulics, Athens, Greece, 23-25 June 2010* (pp. 253-258). Boca Raton: CRC Press, 2010.

69. Di Capua, F., Milone, I., Lakaniemi, A-M., Lens, P.N.L., Esposito, G., 2017. High-rate autotrophic denitrification in a fluidized-bed reactor at psychrophilic temperatures. Chemical Engineering Journal 313, 591-598, https://doi.org/10.1016/j.cej.2016.12.106.

70. Dimitriou, I., Aronsson, P., 2011. Wastewater and sewage sludge application to willows and poplars grown in lysimeters – Plant response and treatment efficiency. Biomass and Bioenergy 35 (1), 161-170, https://doi.org/10.1016/j.biombioe.2010.08.019.

71. Drexler, J.Z., Anderson, F.E., Snyder, R.L, 2008. Evapotranspiration rates and crop coefficients for a restored marsh in the Sacramento-San Joaquin Delta, California, USA. Hydrological Processes 22, 725-735, https://doi.org/10.1002/hyp.6650.

72. Drizo, A., Frost, C.A., Smith, K.A., Grace, J. 1997. Phosphate and ammonium removal by constructed wetlands with horizontal subsurface flow, using shale as a substrate. Water Science & Technology 35 (5), 95-102.

73. Du, L., Trinh, X., Chen, Q., Wang, C., Wang, H., Xia, X., Zhou, Q., Xu, D., Wu, Z., 2018. Enhancement of microbial nitrogen removal pathway by vegetation in Integrated Vertical-Flow Constructed Wetlands (IVCWs) for treating reclaimed water. Bioresource Technology 249, 644-651, https://doi.org/10.1016/j.biortech.2017.10.074.

74. Duan, S., Delaney-Newcomb, K., Kaushal, S.S., Findlay, S.E.G., Belt, K.T., 2014. Potential effects of leaf litter on water quality in urban watersheds. Biogeochemistry 121, 61-80, https://doi.org/10.1007/s10533-014-0016-9.

75. Duncan, C.P., Groffman, P.M., 1994. Comparing microbial parameters in natural and constructed wetlands. Journal of Environmental Quality 23, 298-304.

76. Easton, Z.M., Rogers, M., Davis, M., Wade, J., Eick, M., Bock, E., 2015. Mitigation of sulfate reduction and nitrous oxide emission in denitrifying environments with amorphous iron oxide biochar. Ecological Engineering 82, 605-613, https://doi.org/10.1016/j.ecoleng.2015.05.008.

77. Egger, M., Jilbert, T., Behrends, T., Rivard, C., Slomp, C.P., 2015. Vivianite is a major sink for phosphorus in methanogenic coastal surface sediments. Geochimica et Cosmochimica Acta 169, 217-235, https://doi.org/10.1016/j.gca.2015.09.012.

78. Erler, D.V., Eyre, B.D., Davison, L., 2008. The contribution of anammox and denitrification to sediment N_2 production in a surface flow constructed wetland. Environmental Science & Technology 42, 9144-9150, https://doi.org/10.1021/es801175t.

79. Erler, D.V., Eyre, B.D., Davison, L., 2010. Temporal and spatial variability in the cycling of nitrogen within a constructed wetland: a whole-system stable-isotope-addition experiment. Limnology and Oceanography 55 (3), 1172-1187, https://doi.org/10.4319/lo.2010.55.3.1172.

80. ESA, 2018. *Oro Loma Horizontal Levee Demonstration Project: Project Evaluation Report*. Prepared for the San Francisco Estuary Partnership.

81. Evans, L.J., Smillie, G.W., 1976. Extractable iron and aluminium and their relationship to phosphate retention in Irish soils. Journal of Irish Agricultural Research 15 (1), 65-73.

82. Evaristo, J., McDonnell, J.J., Clemens, J., 2017. Plant source water apportionment using stable isotopes: a comparison of simple linear, two-compartment mixing model approaches. Hydrological Processes 31 (21), 3750-3758, https://doi.org/10.1002/hyp.11233.

83. Fair, J.M., Heikoop, J.M., 2006. Stable isotope dynamics of nitrogen sewage effluent uptake in a semi-arid wetland. Environmental Pollution 140, 500-505, https://doi.org/10.1016/j.envpol.2005.08.005.

84. Freeman, L.A., Corbett, D.R., Fitzgerald, A.M., Lemley, D.A., Quigg, A., Steppe, C.N., 2019. Impacts of urbanization and development on estuarine ecosystems and water quality. Estuaries and Coasts 42, 1821-1838, https://doi.org/10.1007/ss12237-019-00597-z.

85. Foley, J., de Haas, D., Hartley, K., Lant, P., 2010. Comprehensive life cycle inventories of alternative wastewater treatment systems. Water Research 44, 1654-1666, https://doi.org/10.1016/j.watres.2009.11.031.

86. Flores-Verdugo, F.J., Day, Jr., J.W., Briseño-Dueñas, R., 1987. Structure, litter fall, decomposition, and detritus dynamics of mangroves in a Mexican coastal lagoon with an ephemeral inlet. Marine Ecology 35, 83-90.

87. Fry, B. *Stable Isotope Ecology*, Springer Science+Business Media, New York, NY, 2006.

88. Furukawa, Y., Barnes, H.L, 1995. Chapter 10: Reactions forming pyrite from precipitated amorphous ferrous sulfide. ACS Symposium Series 612, 194-205.

89. Gallagher, A., Scholes, R. 2017. *Unpublished data*.

90. Galletti, A., Verlicchi, P., Ranieri, E. Removal and accumulation of Cu, Ni, and Zn in horizontal subsurface flow constructed wetlands: contribution of vegetation and filling medium. Science of the Total Environment 408, 2010, 5097-5105, https://doi.org/10.1016/j.scitotenv.2010.007.045.

91. Galloway, J.N., Townsend, A.R., Erisman, J.W., Bekunda, M., Cai, Z., Freney, J.R., Martinelli, L.A., Seitzinger, S.P., Sutton, M.A., 2008. Transformation of the nitrogen cycle: recent trends, questions and potential solutions. Science 320, 889-892, https://doi.org/10.1126/science.1136674.

92. García, J., Rousseau, D., Morato, J., Lesage, E., Matamoros, V., Bayona, J., 2010. Contaminant removal processes in subsurface-flow constructed wetlands: a review. Critical Reviews in Environmental Science and Technology 40 (7), 561-661.

93. Gasparovic, L., Korenová, Z., Jelemensky, L., 2010. Kinetic study of wood chips decomposition by TGA. Chemical Papers 64(2), 174-181, https://doi.org/10.2478/s11696-009-0109-4.

94. Ge, Z., Wei, D., Zhang, J., Hu, J., Liu, Z., Li, R., 2019. Natural pyrite to enhance simultaneous long-term nitrogen and phosphorus removal in constructed wetlands: three years of pilot study. Water Research 148, 153-161, https://doi.org/10.1016/j.watres.2018.10.037.

95. Gedan, K.B., Kirwan, M.L., Wolanski, E., Barbier, E.B., Silliman, B.R., 2011. The present and future role of coastal wetland vegetation in protecting shorelines: answering recent challenges to the paradigm. Climatic Change 106, 7-29, https://doi.org/10.1007/s10584-010-0003-7.

96. Geng, Y., Ge, Y., Luo, B., Chen, Z., Min, Y., Schmid, B., Gu, B., Chang, J., 2019. Plant diversity increases N removal in constructed wetlands when multiple rather than single N processes are considered. Ecological Applications 29 (7), e01965, https://doi.org/10.5061/dryad.80nf679.

97. Ghermandi, A., van den Bergh, J.C.J.M., Brander, L.M., de Groot, H.L.F., Nunes, P.A.L.D., 2010. Values of natural and human-made wetlands: a meta-analysis. Water Resources Research 46 (12), https://doi.org/10.1029/2010WR009071.

98. Giblin, A.E., Tobias, C.R., Song, B., Weston, N., Banta, G.T., Rivera-Monroy, V.H., 2013. The importance of dissimilatory nitrate reduction to ammonium (DNRA) in the nitrogen cycle of coastal ecosystems. Oceanography 26 (3), 124-131, https://doi.org/10.5670/oceanog.2013.54.

99. Gill, R.A., Kelly, R.H., Parton, W.J., Day, K.A., Jackson, R.B., Morgan, J.A., Scurlock, J.M.O., Tieszen, L.L., Castle, J.V., Ojima, D.S., Zhang, X.S., 2002. Using simple environmental variables to estimate below-ground productivity in grasslands. Global Ecology & Biogeography 11, 79-86, https://doi.org/10.1046/j.1466-822X.2001.00267.x.

100. Gill, R.A., Jackson, R., 2000. Global patterns of root turnover for terrestrial ecosystem. New Phytologist 147, 13–31, https://doi.org/10.1046/j,1469-8137.2000.00681.x.

101. Grace, J.B., Anderson, T.M., Smith, M.D., Seabloom, E., Andelman, S.J., Meche, G., Weiher, E., Allain, L.K., Jutila, H., Sankaran, M., Knops, J., Ritchie, M., Willig, M.R., 2007. Does species diversity limit productivity in natural grassland communities? Ecology Letters 10, 680-689, https://doi.org/10.1111/j.1461-0248.2007.01058.x.

102. Granger, J., Sigman, D.M., Needoba, J.A., Harrison, P.J., 2004. Coupled nitrogen and oxygen isotope fractionation of nitrate during assimilation by cultures of marine phytoplankton. Limnology and Oceanography 49 (5), 1763-1773, https://doi.org/10.4319/lo.2004.49.5.1763.

103. Groffman, P.M., Altabet, M.A., Böhlke, J.K., Butterbach-Bahl, K., David, M.B., Firestone, M.K., Giblin, A.E., Kana, T.M., Nielsen, L.P., Voytek, M.A., 2006. Methods for measuring denitrification: diverse approaches to a difficult problem. Ecological Applications 16 (6), 2091-2122.

104. Grogan, P., Matthews, R., 2002. A modelling analysis of the potential for soil carbon sequestration under short rotation coppice willow bioenergy plantations. Soil Use and Management 18, 175-183, https://doi.org/10.1079/SUM2002119.

105. Gruber, N., Galloway, J.N., 2008. An earth-system perspective of the global nitrogen cycle. Nature 451, 293-296.

106. Guerra, E., Ventura F., Snyder, R.L., 2015. Crop coefficients: a literature review. Journal of Irrigation and Drainage Engineering 142 (3), 06015006, https://doi.org/10.1061/(ASCE)IR.1943-4774.0000983.

107. Guo, W., Cecchetti, A.R., Wen, Y., Zhou, Q., Sedlak, D.L., 2020. Sulfur cycle in a wetland microcosm: extended ^{34}S-stable isotope analysis and mass balance. Environmental Science & Technology 54 (9), 5498-5508.

108. Gustafsson, J.P. *Visual MINTEQ 3.1*; KTH (Royal Institute of Technology): Stockholm, Sweden, 2014.

109. Hang, Q., Wang, H., Chu, Z., Ye, B., Li, C., Hou, Z., 2016. Application of plant carbon source for denitrification by constructed wetland and bioreactor: review of recent development. Environmental Science and Pollution Research 23, 8260-8274, https://doi.org/10.1007/s11356-016-6324-y.

110. Hansen, L.S., Blackburn, T.H., 1991. Aerobic and anaerobic mineralization of organic material in marine sediment microcosms. Marine Ecology Progress Series 75, 283-291.

111. Harris-Lovett, S., Lienert, J., Sedlak, D.L., 2018. Towards a new paradigm of urban water infrastructure: identifying goals and strategies to support multi-benefit municipal wastewater treatment. Water 10 (9), 1127, https://doi.org/10.3390/w10091127.

112. Harris-Lovett, S., Lienert, J., Sedlak, D.L., 2019. A mixed-methods approach to strategic planning for multi-benefit regional water infrastructure. Journal of Environmental Management 233, 218-237, https://doi.org/10.1016/j.jenvman.2018.11.112.

113. Hastie, T., Tibshirani, R., Friedman, J., 2009. *The Elements of Statistical Learning.* Springer New York. https://doi.org/10.1007/978-0-387-84858-7

114. Headley, T.R., Kadlec, R.H., 2008. Conducting hydraulic tracer studies of constructed wetlands: a practical guide. Ecohydrology and Hydrobiology 7 (3-4), 269-282.

115. Healy, M., Cawley, A.M., 2002. Nutrient processing capacity of a constructed wetland in western Ireland. Journal of Environmental Quality 31, 1739-1747.

116. Heaton, T.H.E., 1986. Isotopic studies of nitrogen pollution in the hydrosphere and atmosphere: a review. Chemical Geology 59, 87-102, https://doi.org/10.1016/0168-9622(86)90059-X.

117. Heberger, M., Cooley, H., Herrera, P., Gleick, P.H., Moore, E., 2009. *Final paper: the impacts of sea-level rise on the California coast.* Prepared by: California Climate Change Center.

118. Heberger, M., Cooley, H., Herrera, P., Gleick, P.H., Moore, E., 2011. Potential impacts of increased coastal flooding in California due to sea-level rise. Climatic Change 109 (Supplement 1), 229-249, https://doi.org/10.1007/s10584-011-0308-1.

119. Heiskanen, A-S., Bonsdorff, E., Joas, M., 2019. Chapter 20 – Baltic Sea: A Recovering Future from Decades of Eutrophication. In: *Coasts and Estuaries: The Future*, 343-362, https://doi.org/10.1016/B978-0-12-814003-1.0020-4.

120. Heisler, J., Glibert, P.M., Burkholder, J.M., Anderson, D.M., Cochlan, W., Dennison, W.C., Dortch, Q., Gobler, C. J., Heil, C.A., Humphries, E., Lewitus, A., Magnien R., Marshall, H.G., Sellner, K., Stockwell, D.A., Stoecker, D.K., Suddleson, M., 2008. Eutrophication and harmful algal blooms: a scientific consensus. Harmful Algae 8 (1), 3-13, https://doi.org/10.1016/j.hal.2008.08.006.

121. Hill, A.R. Stream Chemistry and Riparian Zones. In: *Streams and Ground Waters* (Eds. Jones, J.B., Mulholland, P.J.), Academic Press, London, 2000.

122. Holtan, H., Kamp-Nielsen, L., Stuanes, A.O. Phosphorus in soil, water and sediment: an overview. In: Persson, G., Jansson, M. (Eds.), *Phosphorus in Freshwater Ecosystems. Developments in Hydrobiology,* vol. 48. Springer, Dordrecht, 1988.

123. Hopkins, J.B., Ferguson, J.M., 2012. Estimating the diets of animals using stable isotopes and a comprehensive Bayesian mixing model. PLoS ONE 7 (1), 1-13, https://doi.org/10.1371/journal.pone.0028478.

124. Howes, D.J., Fox, P., Hutton, P.H., 2015. Evapotranspiration from natural vegetation in the central valley of California: monthly grass reference-based vegetation coefficients and the dual crop coefficient approach. Journal of Hydrologic Engineering 20 (10), 04015004, https://doi.org/10.1061/(ASCE)HE.1943-5584.0001162.

125. Hsu, C., Hsieh, H., Yang, L., Wu, S., Chang, J., Hsiao, S., Su, H., Yeh, C., Ho, Y., Lin, H., 2011. Biodiversity of constructed wetlands for wastewater treatment. Ecological Engineering 37 (10), 1533-1545, https://doi.org/10.1016/j.ecoleng.2011.06.002.

126. Huang, G., Zhao, X., Su, Y., Zhao, H., Zhang, T., 2008. Vertical distribution, biomass, production and turnover of fine roots along a topographical gradient in a sandy shrubland. Plant and Soil 308, 201-212, https://doi.org/10.1007/s11104-008-9620-6.

127. Hug, L.A., Co, R. It takes a village: microbial communities thrive through interactions and metabolic handoffs. mSystems 3, 2018, e00152-17, https://doi.org/10.1128/mSystems.00152-17.

128. Hummel, M.A., Berry, M.S., Stacey, M.T., 2018. Sea level rise impacts on wastewater treatment systems along the U.S. coasts. Earth's Future 6, 622-633, https://doi.org/10.1002/2017EF000805.

129. Illmer, P., Schinner, F., 1995. Solubilization of inorganic calcium phosphates – solubilization mechanisms. Soil Biology Biochemistry 27 (3), 257-263.

130. Inamori, R., Wang, Y., Wamamoto, T., Zhang, J., Kong, H., Zu, K., Inamori, Y., 2008. Seasonal effect on N_2O formation in nitrification in constructed wetlands. Chemosphere 73, 1071-1077, https://doi.org/10.1016/j.chemosphere.2008.07.064.

131. Ingersoll, T.L., Baker, L.A., 1998. Nitrate removal in wetland microcosms. Water Research 32 (3), 677-684, https://doi.org/10.1016/S0043-1354(97)00254-6.

132. Jackson, M.B., Attwood, P.A., 1996. Roots of willow (*Salix viminalis* L.) show marked tolerance to oxygen shortage in flooded soils and in solution culture. Plant and Soil 187, 37-45.

133. Jarque, C. M., Bera, A. K., 1980. Efficient tests for normality, homoscedasticity and serial independence of regression residuals. Economics Letters 6 (3), 255–259. https://doi.org/10.1016/0165-1765(80)90024-5

134. Jasper, J.T., Jones, Z.L., Sharp, J.O., Sedlak, D.L., 2014a. Biotransformation of trace organic contaminants in open-water unit process treatment wetlands. 48 (9), 5136-5144, https://doi.org/10.1021/es500351e

135. Jasper, J.T., Jones, Z.L., Sharp, J.O., Sedlak, D.L., 2014b. Nitrate removal in shallow, open-water treatment wetlands. Environmental Science and Technology 48 (19), 11512-11520, https://doi.org/10.1021/es502785t.

136. Javanaud, C., Michotey, V., Guasco, S., Garcia, N., Anschutz, P., Canton, M., Bonin, P., 2011. Anaerobic ammonium oxidation mediated by Mn-oxides: from sediment to strain level. Research in Microbiology 162 (9), 848-857, https://doi.org/10.1016/j.resmic.2011.01.011.

137. Jäckel, U., Russo, S., Schnell, S., 2005. Enhanced iron reduction by iron supplement: a strategy to reduce methane emissions from paddies. Soil Biology and Biochemistry 37 (11), 2150-2154, https://doi.org/10.1016/j.soilbio.2005.03.003.

138. Jensen, J. R., 2007. Remote Sensing of the Environment: An Earth Resource Perspective, Prentice Hall: Upper Saddle River, NJ. 2nd ed. ISBN 0-13-188950-8.

139. Jones, Z.L., Jasper, J.T., Sedlak, D.L., Sharp, J.O., 2017. Sulfide-induced dissimilatory nitrate reduction to ammonium supports anaerobic ammonium oxidation (Anammox) in an open-water unit process wetland. Applied and Environmental Microbiology 83 (15), e00782-17.

140. Jørgensen, C.J., Jacobsen, O.S., Elberling, B., Aamand, J., 2009. Microbial oxidation of pyrite coupled to nitrate reduction in anoxic groundwater sediment. Environmental Science & Technology 43 (13), 4851-4857.

141. Kadlec, R.H., 2009. Comparison of free water and horizontal subsurface treatment wetlands. Ecological Engineering 35, 159-174, https://doi.org/10.1016/j.ecoleng.2008.04.008.

142. Kadlec, R.H., Wallace, S.D. *Treatment Wetlands*. 2nd Ed. CRC Press: Boca Raton, FL, 2009.

143. Kantawanichkul, S., Kladprasert, S., Brix, H., 2009. Treatment of high-strength wastewater in tropical vertical flow constructed wetlands planted with *Typha angustifolia* and *Cyperus involucratus*. Ecological Engineering 35, 238-247, https://doi.org/10.1016/j.ecoleng.2008.06.002.

144. Kao-Kniffin, J., Freyre, D.S., Balser, T.C., 2010. Methane dynamics across wetland plant species. Aquatic Botany 93, 107-113.

145. Kappler, A., Bryce, C., 2017. Cryptic biogeochemical cycles: unravelling hidden redox reactions. Environmental Microbiology 19 (3), 842-846.

146. Kaushal, S.S., Groffman, P.M., Band, L.E., Elliott, E.M., Shields, C.A., Kendall, C., 2011. Tracking nonpoint source nitrogen pollution in human-impacted watersheds. Environmental Science and Technology 45 (19), 8225-8232, https://doi.org/10.1021/es200889e.

147. Kendall, C., 1998. Chapter 16 – Tracing Nitrogen Sources and Cycling in Catchments. In: *Isotope Tracers in Catchment Hydrology*, 519-576, https://doi.org/10.1016/B978-0-444-81546-0.50023-9.

148. Kendall, C., Elliott, E.M., Wankel, S.D., 2007. Tracing anthropogenic inputs of nitrogen to ecosystems. In: *Stable Isotopes in Ecology and Environmental Science*, 2nd Ed., Eds: Michener, R., Lajtha, K., Blackwell Publishing, Malden, MA, USA, https://doi.org/10.1002/9780470691854.ch12.

149. Khorram, S., Wiele, C. F. van der, Koch, F. H., Nelson, S. A. C., & Potts, M. D. (2016). *Principles of applied remote sensing*. Springer. ISBN: 978-3-319-22559-3 978-3-319-22560-9.

150. Knight, R.L., 1997. Wildlife habitat and public use benefits of treatment wetlands. Water Science and Technology 35 (5), 35-43, https://doi.org/10.2166/wst.1997.0159.

151. Knight, R.L., Clarke, R.A., Jr., Bastian, R.K., 2001. Surface flow (SF) treatment wetlands as a habitat for wildlife and humans. Water Science and Technology 44 (11-12), 27-37, https://doi.org/10.2166/wst.2001.0806.

152. Knight, R.L., Walton, W.E., O'Meara, G.F., Reisen, W.K., Wass, R., 2003. Strategies for effective mosquito control in constructed treatment wetlands. Ecological Engineering 21, 211-232, https://doi.org/10.1016/j.ecoleng.2003.11.001.

153. Knowles, P.R., Griffin, P., Davies, P.A., 2010. Complementary methods to investigate the development of clogging within a horizontal sub-surface flow tertiary treatment wetland. Water Research 44, 320-330, https://doi.org/10.1016/j.watres.2009.09.028.

154. Ko, J.Y., Day, J.W., Lane, R.R., Day, J.N., 2004. A comparative evaluation of money-based and energy-based cost-benefit analyses of tertiary municipal wastewater treatment using forested wetlands vs. sand filtration in Louisiana. Ecological Economics 49, 331-347.

155. Koerselman, W., Meuleman, A.F.M., 1996. The vegetation N:P ratio: a new tool to detect the nature of nutrient limitation. Journal of Applied Ecology 33, 1441-1450, https://www.jstor.org/stable/2404783.

156. Kohzu, A., Miyajima, T., Tayasu, I., Yoshimizu, C., Hyodo, F., Matsui, K., Nakano, T., Wada, E., Fujita, N., Nagata, T., 2008. Use of stable nitrogen isotope signatures of riparian macrophytes as an indicator of anthropogenic N inputs to river ecosystems. Environmental Science & Technology 42, 7837-7841, https://doi.org//10.1021/es801113k.

157. Kucukali, S., Cokgor, S., 2009. Energy concept for predicting hydraulic jump aeration efficiency. Journal of Environmental Engineering 135(2), 105-107, https://doi.org/10.1061/(ASCE)0733-9372(2009)135:2(105).

158. Kumar, R., Pal, P., 2015. Assessing the feasibility of N and P recovery by struvite precipitation from nutrient-rich wastewater: a review. Environmental Science and Pollution Research 22, 17453-17464, https://doi.org/10.1007/s11356-015-5450-2.

159. Kuzovkina, Y.A., Volk, T.A., 2009. The characterization of willow (*Salix* L.) varieties for use in ecological engineering applications: co-ordination of structure, function and autecology. Ecological Engineering 35, 1178-1189, https://doi.org/10.1016/j.ecoleng.2009.03.010.

160. Kvet, J., 1982. *Production of organic matter in macrophyte stands (in Czech).* Proceedings of Macrophytes in Water Management, Water Hygiene, and Fishery; Dum Techniky CSVTS: Ceské Budejovice, Czech Republic, 73–81.

161. LaFond-Hudson, S., Johnson, N.W., Pastor, J., Dewey, B., 2018. Iron sulfide formation on root surfaces controlled by the life cycle of wild rice (*Zizania palustris*). Biogeochemistry 141, 95-106.

162. Lai, T.M., Shin, J.K., Hur, J., 2011. Estimating the biodegradability of treated sewage samples using synchronous fluorescence spectra. Sensors 11, 7382-7394, https://doi.org/10.3390/s110807382.

163. Lamers, L.P.M., Govers, L.L., Janssen I.C.J.M., Geurts, J.J.M., van der Welle, M.E.W., van Katwijk, M.M., van der Heide, T., Roelofs, J.G.M., Smolders, A.J.P., 2013. Sulfide as a soil phytotoxin–a review. Frontiers in Plant Science 4, 1-14, https://doi.org/10.3389/fpls.2013.00268.

164. Layman, C.A., Araujo, M.S., Boucek, R., Hammerschlag-Peyer, C.M., Harrison, E., Jud, Z.R., Matich, P., Rosenblatt, A.E., Vaudo, J.J., Yeager, L.A., Post, D.M., Bearhop, S., 2012. Applying stable isotopes to examine food-web structure: an overview of analytical tools. Biological Reviews 87, 545-562, https://doi.org/10.1111/j.1469-185X.2011.00208.x.

165. Le Corre, K.S., Valsami-Jones, E., Hobbs, P., Parsons, S.A., 2009. Phosphorus recovery from wastewater by struvite crystallization: a review. Critical Review in Environmental Science and Technology 39(6), 433-477, https://doi.org/10.1080/10643380701640573.

166. Le Maire, G., Marsden, C., Nouvellon, Y., Grinand, C., Hakamada, R., Stape, J. L., Laclau, J. P., 2011. MODIS NDVI time-series allow the monitoring of Eucalyptus plantation biomass. Remote Sensing of Environment 115 (10), 2613–2625. https://doi.org/10.1016/j.rse.2011.05.017.

167. Lee, C.Y., Lee, C.C., Lee, F.Y., Tseng, S.K., Liao, C.J., 2004. Performance of subsurface flow constructed wetland taking pretreated swine effluent under heavy loads. Bioresource Technology 92 (2), 173-179, https://doi.org/10.1016/j.biortech.2003.08.012.

168. Lee, S-H., Kim, S-Y., Kang, H., 2012. Effects of elevated CO_2 on communities of denitrifying bacteria and methanogens in a temperate marsh microcosm. Microbial Ecology 64, 485-498.

169. Lehman, P.W., Boyer, G., Satchwell, M., Waller, S., 2008 The influence of environmental conditions on the seasonal variation of *Microcystis* cell density and microcystins concentration in San Francisco Estuary. Hydrobiologia 600, 187-204.

170. Li, Y., Yu, S., Strong, J., Wang, H., 2012. Are the biogeochemical cycles of carbon, nitrogen, sulfur, and phosphorus driven by the "Fe^{III}-Fe^{II} redox wheel" in dynamic redox environments? Journal of Soils and Sediments 12, 683-693, https://doi.org/10.1007/s11368-012-0507-z.

171. Li, L., Davis, A.P., 2014. Urban stormwater runoff nitrogen composition and fate in bioretention systems. Environmental Science & Technology 48, 3403-3410.

172. Li, T., Wang, H., Dong, W., Liu, T., Ouyang, F., Zhang, Q., 2014. Phosphate removal during Fe(II) oxidation in the presence of Cu(II): characteristics and application for electro-plating wastewater treatment. Separation and Purification Technology 132, 388-395, https://doi.org/10.1016/j.seppur.2014.05.040.

173. Li, X., Hou, L., Lui, M., Zheng, Y., Yin, G., Lin, X., Cheng, L., Li, Y., Hu, X., 2015. Evidence of nitrogen loss from anaerobic ammonium oxidation coupled with ferric iron reduction in an intertidal wetland. Environmental Science & Technology 49, 11560-11568, https://doi.org/10.1021/acs.est.5b03419.

174. Li, X., Bellerby, R., Craft, C., Widney, S.E., 2018. Coastal wetland loss, consequences, and challenges for restoration. Anthropocene Coasts 1, 1-15, https://doi.org/10.1139/anc-2017-0001.

175. Liang, Y., Zhu, H., Bañuelos, G., Yan, B., Zhou, Q., Yu, X., Cheng, X. Constructed wetlands for saline wastewater treatment: a review. Ecological Engineering 98, 2017, 275-285, https://doi.org/10.1016/j.ecoleng.2016.11.005.

176. Lin, Y., Bhattacharyya, A., Campbell, A.N., Nico, P.S., Pett-Ridge, J., Silver, W.L., 2018. Phosphorus fractionation responds to dynamic redox conditions in a human tropical forest soil. Journal of Geophysical Research: Biogeosciences 123, 3016-3027, https://doi.org/10.1029/2018JG004420.

177. Lin, Y., Gross, A., O'Connell, C.S., Silver, W.L., 2020. Anoxic conditions maintained high phosphorus sorption in humid tropical forest soils. Biogeosciences 17, 89-101, https://doi.org/10.5194/bg-17-89-2020.

178. Lindley, M. 2014. *Ecotone Plan.* Oro Loma Wet Weather Equalization & Ecotone Demonstration Project, 100% Design. Prepared by ESA, San Francisco, CA for Oro Loma Sanitary District, San Lorenzo, CA.

179. Liptzin, D., Silver, W.L., 2009. Effects of carbon additions on iron reduction and phosphorus availability in a humid tropical forest soil. Soil Biology and Biochemistry 41, 1696-1702.

180. Lowe, J., Battalio, B., Brennan, M., Holmes, M., Niemi, E., Toms, C., 2013. *Final report: analysis of the costs and benefits of using tidal marsh restoration as a sea level rise adaptation strategy in San Francisco Bay.* Prepared by ESA PWA for The Bay Institute.

181. Lü, C., Yan, D., He, J., Zhou, B., Li, L., Zheng, Q., 2017. Environmental geochemistry significance of organic phosphorus: an insight from adsorption on iron oxides. Applied Geochemistry 84, 52-60, https://doi.org/10.1016/j.apgeochem.2017.05.026.

182. Maantay, J., Maroko, A., 2009. Mapping urban risk: flood hazards, race, & environmental justice in New York. Applied Geography 29 (1), 111-124, https://doi.org/10.1016/j.apgeog.2008.08.002.

183. Macdonald, B.C.T., White, I., Åström, M.E., Keene, A.F., Melville, M.D., Reynolds, J.K., 2007. Discharge of weathering products from acid sulfate soils after a rainfall event, Tweed

River, eastern Australia. Applied Geochemistry 22 (12), 2695-2705, https://doi.org/10.1016/j.apgeochem.2007.07.004.

184. Mach, V., Blaser, M.B., Claus, P., Chaudhary, P.P., Rulík, M., 2015. Methane production potentials, pathways, and communities of methanogens in vertical sediment profiles of river Sitka. Frontiers in Microbiology 6, 506, https://doi.org/10.3389/fmicb.2015.00506.

185. Mackey, A.P., Smail, G., 1996. The decomposition of mangrove litter in a subtropical mangrove forest. Hydrobiologia 332, 93-98.

186. Mambelli, S., Brooks, P.D., Sutka, R., Hughes, S., Finstad, K.M., Nelson, J.P., Dawson, T.E., 2016. High-throughput method for simultaneous quantification of N, C, and S stable isotopes and contents in organics and soils. Rapid Communications in Mass Spectrometry 30 (15), https://doi.org/10.1002/rcm.7605.

187. Mander, Ü., Dotro, G., Ebie, Y., Towprayoon, S., Chiemchairsri, C., Nogueira, S.F., Jamsranjav, B., Kasak, K., Truu, J., Tournebize, J., Mitsch, W.J. Greenhouse gas emissions in constructed wetlands for wastewater treatment: a review. Ecological Engineering 66, 2014, 19-35, https://doi.org/10.1016/j.ecoleng.2013.12.006.

188. Mariotti, A., Germon, J.C., Hubert, P., Kaiser, P., Letolle, R., Tardieux, A., Tardieux, P., 1981. Experimental determination of nitrogen kinetic isotope fractionation: some principles; illustration for the denitrification and nitrification processes. Plant and Soil 62, 413-430, https://doi.org/10.1007/BF02374138.

189. Matamoros, V., Bayona, J.M. Elimination of pharmaceuticals and personal care products in subsurface flow constructed wetlands. Environmental Science & Technology 40, 2006, 5811-5816, https://doi.org/10.1021/es0607741.

190. Mayo, A.W., Bigambo, T., 2005. Nitrogen transformation in horizontal levee subsurface flow constructed wetlands 1: model development. Physics and Chemistry of the Earth 30, 658-667, https://doi.org/10.1016/j.pce.2005.08.005.

191. McClelland, J.W., Valiela, I., 1998. Linking nitrogen in estuarine producers to land-derived sources. Limnology and Oceanography 43 (4), 577-585, https://doi.org/10.4319/lo.1998.43.4.0577.

192. McIntyre, R.E.S., Adams, M.A., Ford, D.J., Grierson, P.F., 2009. Rewetting and litter addition influence mineralisation and microbial communities in soils from a semi-arid intermittent stream. Soil Biology and Biochemistry 41, 92-101.

193. Meers, E., Rousseau, D.P.L., Blomme, N., Lesage, E., Du Laing, G., Tack, F.M.G., Verloo, M.G., 2005. Tertiary treatment of the liquid fraction of pig manure with *Phragmites australis*. Water, Air, and Soil Pollution 160, 15-26.

194. Meers, E., Tack, F.M.G., Tolpe, I., Michels, E., 2008. Application of a full-scale constructed wetland for treatment of piggery manure: monitoring results. Water Air Soil Pollution 193, 15-24, https://doi.org/10.1007/s11270-008-9664-5.

195. Megonigal, J.P., Neubauer, S.C., 2019. *Chapter 19: Biogeochemistry of Tidal Freshwater Wetlands*. In: Coastal Wetlands (2nd Edition), 641-683, https://doi.org/10.1016/B978-0-444-63893-9.00019-8.

196. Mengis, M., Schiff, S.L., Harris, M., English, M.C., Aravena, R., Elgood, R.J., MacLean, A., 1999. Multiple geochemical and isotopic approaches for assessing ground water NO_3^- elimination in a riparian zone. Ground Water 37 (3), 448-457, https://doi.org/10.1111/j.1745-6584.1999.tb01124.x.

197. Messer, T.L., Burchell, M.R., Böhkle, J.K., Tobias, C.R., 2017. Tracking the fate of nitrate through pulse-flow wetlands: a mesocosm scale ^{15}N enrichment tracer study. Ecological Engineering 106, 597-608, https://doi.org/10.1016/j.ecoleng.2017.06.016.

198. Minick, K.J., Mitra, B., Li, X., Noormets, A., King, J.S., 2019. Water table drawdown alters soil and microbial carbon pool size and isotope composition in coastal freshwater forested wetlands. Frontiers in Forests and Global Change 2 (7), 1-19.

199. Mitsch, W.J., Gosselink, J.G., 2000. The value of wetlands: importance of scale and landscape setting. Ecological Economics 35 (1), 25-33, https://doi.org/10.1016/S0921--8009(00)00165-8.

200. Mohamedali, T., Roberts, M., Sackmann, B., Kolosseus, A. 2011. *Puget Sound Dissolved Oxygen Model Nutrient Load Summary for 1999-2008.* Published by the Department of Ecology: University of Washington. https://fortress.wa.gov/ecy/publications/documents/1103057.pdf.

201. Molinos-Senante, M., Hernández-Sancho, F., Sala-Garrido, R., 2010. Economic feasibility study for wastewater treatment: a cost-benefit analysis. Science of the Total Environment 408, 4396-4402.

202. Moorman, M.C., Hoos, A.B., Bricker, S.B., Moore, R.B., García, A.M., and Ator, S.W., 2014, Nutrient load summaries for major lakes and estuaries of the Eastern United States, 2002: U.S. Geological Survey Data Series 820, 94 p., http://dx.doi.org/10.3133/ds820.

203. Moran, M.A., Hodson, R.E., 1989. Bacterial secondary production on vascular plant detritus: relationships to detritus composition and degradation rate. Applied and Environmental Microbiology 55 (9), 2178-2189.

204. Morris, J.T., Shaffer, G.P., Nyman, J.A., 2013. Brinson review: perspectives on the influence of nutrients on the sustainability of coastal wetlands. Wetlands 33, 975-988, https://doi.org/10.1007/s13157-013-0480-3.

205. Möbius, J., 2013. Isotope fractionation during nitrogen remineralization (ammonification): implications for nitrogen isotope biogeochemistry. Geochimica et Cosmochimica Acta 105, 422-432, https://doi.org/10.1016/j.gca.2012.11.048.

206. Möller, I., Kudella, M., Rupprecht, F., Spencer, T., Paul, M., van Wesenbeeck, B.K., Wolters, G., Jensen, K., Bouma, T.J., Miranda-Lange, M., Schimmels, S., 2014. Wave attenuation over coastal salt marshes under storm surge conditions. Nature Geoscience 7, 727-731.

207. Muerdter, C.P., Wong, C.K., LeFevre, G.H., 2018. Emerging investigator series: the role of vegetation in bioretention for stormwater treatment in the built environment: pollutant removal, hydrologic function, and ancillary benefits. Environmental Science: Water Research & Technology 4 (5), 592-612, https://doi.org/10.1039/C7EW00511C.

208. Murphy, A.E., Bulseco, A.N., Ackerman, R., Vineis, J.H., Bowen, J.L., 2020. Sulphide addition favours respiratory ammonification (DNRA) over complete denitrification and alters the active microbial community in salt marsh sediments. Environmental Microbiology https://doi.org/10.1111/1462-2920.14969.

209. Murray, T.E., 1995. The correlation between iron sulfide precipitation and hypolimnetic phosphorus accumulation during one summer in a softwater lake. Canadian Journal of Fisheries and Aquatic Sciences 52 (6), 1190-1194, https://doi.org/10.1139/f95-115.

210. National Atmospheric Deposition Program (NADP; NRSP-3). 2019. NADP Program Office, Wisconsin State Laboratory of Hygiene, 465 Henry Mall, Madison, WI 53706.

211. Neiff, J.J., Poi de Neiff, A., 1990. Litterfall, leaf decomposition and litter colonization of *Tessaria integrifolia* (compositae) in the Parana river floodplain. Hydrobiologia 203, 45-52.

212. Nivala, J., Knowles, P., Dotro, G., García, J., Wallace, S., 2012. Clogging in subsurface-flow treatment wetlands: measurement, modeling and management. Water Research 46, 1625-1640, https://doi.org/10.1016/j.watres.2011.12.051.

213. Novick, E., Senn, D.B., 2013. *External Nutrient Loads to San Francisco Bay.* Prepared by San Francisco Estuary Institute for the Regional Monitoring Program. https://sfbaynutrients.sfei.org/sites/default/files/NutrientLoadsFINAL_FINAL_Jan232014.pdf.

214. Oehmen, A., Lemos, P.C., Carvalho, G., Yuan, Z., Keller, J., Blackall, L.L., Reis, M.A.M., 2007. Advances in enhanced biological phosphorus removal: from micro to macro scale. Water Research 44, 2271-2300.

215. Ogle, K., Tucker, C., Cable, J.M., 2014. Beyond simple linear mixing models: process-based isotope partitioning of ecological processes. Ecological Applications 24 (1), 181-195, https://doi.org/10.1890/1051-0761-24.1.181.

216. Olila, O.G., Reddy, K.R., Stites, D.L., 1997. Influence of draining on soil phosphorus forms and distribution in a constructed wetland. Ecological Engineering 9, 157-169.

217. Ortiz-Llorente, M.J., Alvarez-Cobelas, M., 2012. Comparison of biogenic methane emissions from unmanaged estuaries, lakes, oceans, rivers and wetlands. Atmospheric Environment 59, 328-337.

218. Ozalp, M., Conner, W.H., Lockaby, B.G., 2007. Above-ground productivity and litter decomposition in a tidal freshwater forested wetland on Bull Island, SC, USA. Forest Ecology and Management 245, 31-43.

219. Öberg, G., Sandén, P., 2005. Retention of chloride in soil and cycling of organic matter-bound chlorine. Hydrological Processes 19 (11), 2123-2136, https://doi.org/10.1002/hyp.5680.

220. Pacaldo, R.S., Volk, T.A., Briggs, R.D. 2014. Carbon sequestration in fine roots and foliage biomass offsets soil CO_2 effluxes along a 19-year chronosequence of shrub willow (*Salix x dasyclados*) biomass crops. BioEnergy Research 7, 769-776, https://doi.org/10.1007/s12155-014-9416-x.

221. Paerl, H.W., Scott, J.T., 2010. Throwing fuel on the fire: synergistic effects of excessive nitrogen inputs and global warming on harmful algal blooms. Environment Science & Technology 44 (20), 7756-7758.

222. Paranychianakis, N.V., Tsiknia, M., Kalogerakis, N., 2016, Pathways regulating the removal of nitrogen in planted and unplanted subsurface flow constructed wetlands. Water Research 102, 321-329, https://doi.org/10.1016/j.watres.2016.06.048.

223. Parfitt, R.L., 1978. Anion adsorption by soils and soil materials. Advances in Agronomy 30, 1-50.

224. Parnell, A.C., Phillips, D.L., Bearhop, S., Semmens, B.X., Ward, E.J., Moore, J.W., Jackson, A.L., Grey, J., Kelly, D.,J., Inger, R., 2013. Bayesian stable isotope mixing models. Environmetrics 24 (6), https://doi.org/10.1002/env.2221.

225. Pataki, D.E., Ehleringer, J.R., Flanagan, L.B., Yakir, D., Bowling D.R., Still, C.J., Buchmann, N., Kaplan, J.O., Berry, J.A., 2003. The application and interpretation of Keeling plots in terrestrial carbon cycle research. Global Biogeochemical Cycles 17 (1), 1022, https://doi.org/10.1029/2001GB001850.

226. Pehlivanoglu, E., Sedlak, D.L., 2004. Bioavailability of wastewater-derived organic nitrogen to the alga *Selenastrum Capricornutum*. Water Research 38, 3189-3196, https://doi.org/10.1016/j.watres.2004.04.027.

227. Persson, G., Lindroth, A., 1994. Simulating evaporation from short-rotation forest: variations within and between seasons. Journal of Hydrology 156, 21-45, https://doi.org/10.1016/0022-1694(94)90069-8.

228. Phillips, D.L., 2001. Mixing models in analyses of diet using multiple stable isotopes: a critique. Oecologia 127, 166-170, https://doi.org/10.1007/s004420000571.

229. Phillips, D.L., 2012. Converting isotope values to diet composition: the use of mixing models. Journal of Mammalogy 93 (2), 342-352, https://doi.org/10.1644/11-MAMM-S-158.1.

230. Phillips, D.L., Gregg, J.W., 2001. Uncertainty in source partitioning using stable isotopes. Oecologia 127, 171-179, https://doi.org/10.1007/s004420000578.

231. Phillips, D.L., Inger, R., Bearhop, S., Jackson, A.L., Moore, J.W., Parnell, A.C., Semmens, B.X., Ward, E.J., 2014. Best practices for use of stable isotope mixing models in food-web studies. Canadian Journal of Zoology 92, 823-835, https://doi.org/10.1139/cjz-2014-0127.

232. Piñón-Villarreal, A.R., Bawazir, A.S., Shukla, M.K., Hanson, A.T., 2013. Retention and transport of nitrate and ammonium in loamy sand amended clinoptilolite zeolite. Journal of Irrigation and Drainage Engineering 139 (9), 755-765.

233. Planet Team, 2017. Planet Application Program Interface: In Space for Life on Earth. San Francisco, CA. https://api.planet.com.

234. Poi de Neiff, A., Neiff, J.J., Casco, S.L., 2006. Leaf litter decomposition in three wetland types of the Paraná River floodplain. Wetlands 26 (2), 558-566.

235. Postma, D., 1981. Formation of siderite and vivianite and the pore-water composition of a recent bog sediment in Denmark. Chemical Geology 31, 225-244.

236. Prasse, C., Wenk, J., Jasper, J.T., Ternes, T.A., Sedlak, D.L.,2015. Co-occurrence of photochemical and microbiological transformation processes in open-water unit process wetlands. Environmental Science and Technology 49 (24), 14136-14145, https://doi.org/10.1021/acs.est.5b03783.

237. Qiang, Y., 2019. Disparities of population exposed to flood hazards in the United States. Journal of Environmental Management 232, 295-304, https://doi.org/10.1016/j.jenvman.2018.11.039.

238. Qin, C., Liu, H., Liu, L., Smith, S., Sedlak, D., Gu, A.Z. 2016. Bioavailability and characterization of dissolved organic nitrogen and dissolved organic phosphorus in wastewater effluents. Science of the Total Environment 611, 47-53, https://doi.org/10.1016/j.scitotenv.2014.11.005.

239. Qualls, R.G., Richardson, C.J., 2000. Phosphorus enrichment affects litter decomposition, immobilization, and soil microbial phosphorus in wetland microcosms. Journal of the American Soil Science Society 64, 799-808.

240. Read, J., Wevill, T., Fletcher, T., Deletic, A., 2008. Variation among plant species in pollutant removal from stormwater in biofiltration systems. Water Research 42, 893-902, https://doi.org/10.1016/j.watres.2007.08.036.

241. Reinhardt, M., Müller, B., Gächter, R., Wehrli, B., 2006. Nitrogen removal in a small constructed wetland: an isotope mass balance approach. Environmental Science & Technology 40, 3313-3319, https://doi.org/10.1021/es052393d.

242. Rickard, D., Morse, J.W., 2005. Acid volatile sulfide (AVS). Marine Chemistry 97 (3-4), 141-197, https://doi.org/10.1016/j.marchem.2005.08.004.

243. Rittmann, B.E., McCarty, P.L. *Environmental Biotechnology: Principles and Applications*. 1st Ed. McGraw-Hill: New York, NY, 2001.

244. Rivett, M.O., Buss, S.R., Morgan, P., Smith, J.W.N., Bemment, C.D., 2008. Nitrate attenuation in groundwater: a review of biogeochemical controlling processes. Water Research 42 (16), 4215-4232, https://doi.org/10.1016/j.watres.2008.07.020.

245. Rodgers, T.F.M., Stiegler, A.N., Robitaille, R., Cecchetti, A.R., Jantunen, L., Sedlak, D.L., Diamond, M.L. Modeling organophosphate ester fate and transport in the Oro Loma living levee. *Manuscript in preparation.*

246. Rogers, K.H., Breen, P.F., Chick, A.J., 1991. Nitrogen removal in experimental wetland treatment systems: evidence for the role of aquatic plants. Research Journal of the Water Pollution Control Federation 63 (7), 934-941.

247. Rothe, M., Kleeberg, A., Hupfer, M., 2016. The occurrence, identification and environmental relevance of vivianite in waterlogged soils and aquatic sediments. Earth-Science Reviews 158, 51-64, https://doi.org/10.1016/j.earscirev.2016.04.008.

248. Ruttenberg, K.C., Sulak, D.J., 2011. Sorption and desorption of dissolved organic phosphorus onto iron (oxyhydr)oxides in seawater. Geochimica et Cosmochimica Acta 75, 4095-4112, https://doi.rog/10.1016/j.gca.2010.10.033.

249. Rütting, T., Boeckx, P., Müller, C., Klemedtsson, L., 2011. Assessment of the importance of dissimilatory nitrate reduction to ammonium for the terrestrial nitrogen cycle. Biogeoscience 8, 1779-1791, https://doi.org/10.5194/bg-8-1779-2011.

250. Rysgaard, S., Fossing, H., Jensen, M.M. Organic matter degradation through oxygen respiration, denitrification, and manganese, iron and sulfate reduction in marine sediments (the Kattegat and the Skagerrak). *Ophelia* **2001**, *55*(2), 77-91.

251. Rytter, R.M., Rytter, L., 1998. Growth, decay, and turnover rates of fine roots of basket willow. Canadian Journal of Forestry Research 28, 893–902, https://doi.org/10.1139/x98-063.

252. Rytter, R.M., 1999. Fine-root production and turnover in a willow plantation estimated by different calculation methods. Scandinavian Journal of Forest Research 14 (6), 526-537, https://doi.org/10.1080/02827589908540817.

253. Rytter, R.M., 2001. Biomass production and allocation, including fine-root turnover, and annual N uptake in lysimeter-grown basket willows. Forest Ecology and Management 140 (2-3), 177-192, https://doi.org/10.1016/S0378-1127(00)00319-4.

254. Rytter, R.M., 2013. The effect of limited availability of N or water on C allocation to fine roots and annual fine root turnover in *Alnus incana* and *Salix viminalis*. Tree Physiology 33, 924-939, https://doi.org/10.1093/treephys/tpt060.

255. Saeed, T., Sun, G., 2012. A review on nitrogen and organics removal mechanisms in subsurface flow constructed wetlands: dependency on environmental parameters, operating conditions and supporting media. Journal of Environmental Management 112, 429-448, https://doi.org/10.1016/jenvman.2012.08.011.

256. Salk, K.R., Erler, D.V., Eyre, B.D., Carlson-Perret, N., Ostrom, N.E. 2017. Unexpectedly high degree of anammox and DNRA in seagrass sediments: description and application of a revised isotope pairing technique. Geochimica et Cosmochimica Acta 211, 64-78, https://doi.org/10.1016/j.gca.2017.05.012.

257. Save the Bay, 2017. *Oro Loma Horizontal Levee Vegetation Report*. https://oroloma.org/wp-content/uploads/STB-Oro-Loma-Report_11.13.17.pdf.

258. Schipper, L.A., Vojvodic-Vukovic, M., 2001. Five years of nitrate removal, denitrification and carbon dynamics in a denitrification wall. Water Research 35 (14), 3473-3477, https://doi.org/10.1016/S0043-1354(01)00052-5.

259. Schipper, L.A., Barkle, G.F., Hadfield, J.C., Vojvodic-Vukovic, M., Burgess, C.P., 2004. Hydraulic constraints on the performance of a groundwater denitrification wall for nitrate removal from shallow groundwater. Journal of Contaminant Hydrology 69, 263-279, https://doi.org/10.1016/S0169-7722(03)00157-8.

260. Schipper, L.A., Cameron, S.C., Warneke, S., 2010. Nitrate removal from three effluents using large-scale denitrification beds. Ecological Engineering 36, 1552-1557.

261. Schmidt, C.A., Clark, M.W., 2012. Efficacy of a denitrification wall to treat continuously high nitrate loads. Ecological Engineering 42, 203-211, https://doi.org/10.1016/j.ecoleng.2012.02.006.

262. Schwede, D.B., Lear, G.G., 2014. A novel hybrid approach for estimating total deposition in the United States. Atmospheric Environment 92, 207-220, https://doi.org/10.1016/j.atmosenv.2014.04.008.

263. Schwarcz, H.P., 1991. Some theoretical aspects of isotope paleodiet studies. Journal of Archaeological Science 18, 261-273, https://doi.org/10.1016/0305-4403(91)90065-W.

264. Schwarzenbach, R.P., Escher, B.I., Fenner, K., Hofstetter, T.B., Johnson, C.A., von Gunten, U., Wehrli, B., 2006. The challenge of micropollutants in aquatic systems. Science 313, 1072-1077, https://doi.org/10.1126/science.1127291.

265. Seabold, Skipper, J. Perktold. "statsmodels: Econometric and statistical modeling with python." *Proceedings of the 9th Python in Science Conference.* 2010. http://conference.scipy.org/proceedings/scipy2010/pdfs/seabold.pdf.

266. Seifollahi-Aghmiuni, S., Nockrach, M., Kalantari, Z., 2019. The potential of wetlands in achieving the sustainable development goals of the 2030 agenda. Water 11, 609, https://doi.org/10.3390/w11030609.

267. Seitzinger, S., Harrison, J.A., Böhlke, J.K., Bouwman, A.F., Lowrance, R., Peterson B., Tobias C., van Drecht, G., 2006. Denitrification across landscapes and waterscapes: a synthesis. Ecological Applications 16 (6), 2064-2090, https://doi.org/10.1890/1051-0761(2006)016[2064:DALAWA]2.0.CO;2.

268. Sengupta, A., Sutala, M.A., McLaughlin, K. Howard, M., Teifenthaler, L., Von Bitner, T. *Terrestrial nutrient loads and fluxes to the Southern California Bight, USA.* Southern California Coastal Water Research Project. ftp://ftp.sccwrp.org/pub/download/DOCUMENTS/AnnualReports/2013AnnualReport/ar13_245_258.pdf.

269. Shackelford, C.D., Daniel, D.E., 1991. Diffusion in saturated soil. I: background. Journal of Geotechnical Engineering 117 (3), 467-484.

270. Shang, C., Stewart, J.W.B., Huang, P.M., 1992. pH effects on kinetics of adsorption of organic and inorganic phosphates by short-range ordered aluminum and iron precipitates. Geoderma 53, 1-14.

271. Shepard, C.C., Crain, C.M., Beck, M.W., 2011, The protective role of coastal marshes: a systematic review and meta-analysis. PLoS ONE, 6 (11), 1-11, https://doi.org/10.1371/journal.pone.0027374.

272. Shin, H-S., Kang, S-T., 2003. Characteristics and fates of soluble microbial products in ceramic membrane bioreactor at various sludge retention times. Water Research 37, 121-127.

273. Shuai, W., Jaffé, P.R., 2019. Anaerobic ammonium oxidation coupled to iron reduction in constructed wetland mesocosms. Science of the Total Environment 648, 984-992, https://doi.org/10.1016/j.scitotenv.2018.08.189.

274. Sigman, D.M., Casciotti, K.L., Andreani, M., Barford, C., Galanter, M., Böhlke, J.K., 2001. A bacterial method for the nitrogen isotopic analysis of nitrate in seawater and freshwater. Analytical Chemistry 73 (17), 4145-4153, https://doi.org/10.1021/ac010088e.

275. Sinton, L.W., Finlay, R.K., Reid, A.J., 1996, A simple membrane filtration-elution method for the enumeration of F-RNA, F-DNA and somatic coliphages in 100-ml water samples. Journal of Microbiological Methods, 25, 257-269, https://doi.org/10.1016/0167-7012(95)00100-X.

276. Slomp, C.P., Van der Gaast, S.J., Van Raaphorst, W., 1996. Phosphorus binding by poorly crystalline iron oxides in North Sea sediments. Marine Chemistry 52, 55-73.

277. Smil, V., 2000. Phosphorus in the environment: natural flows and human interferences. Annual Reviews of Energy and the Environment, 25, 53-88.

278. Smith, S., Takács, I., Murthy, S., Daigger, T., Szabó, A., 2008. Phosphate complexation model and its implications for chemical phosphorus removal. Water Environmental Research 80(5), 428-438, https://doi.org/10.1002/j.1554-7531.2008.tb00349.x.

279. Søvik, A.K., Mørkved, P.T., 2007 Nitrogen isotope fractionation as a tool for determining denitrification in constructed wetlands. Water Science & Technology 56 (3), 167-173, https://doi.org/10.2166/wst.2007.529.

280. Stadnyk, C.N. 2010. Root dynamics and carbon accumulation of six willow clones in Saskatchewan. M.Sc. thesis. University of Saskatchewan, Saskatoon.

281. Stelzer, R.S., Scott, J.T., Bartsch, L.A, Parr, T.B., 2014. Particulate organic matter quality influence nitrate retention and denitrification in stream sediments: evidence from a carbon burial experiment. Biogeochemistry 119, 387-402, https://doi.org/10.1007/s10533-014-9975-0.

282. Stiegler, A.N., Rodgers, T.F.M., Cecchetti, A.R., Sedlak, D.L., *Untitled manuscript in preparation*.

283. Stock, B.C., Semmens, B.X., 2013. MixSIAR GUI User Manual. Version 3.1. https://github.com/brianstock/MixSIAR. https://doi.org/10.5281/zenodo.56159.

284. Stock, B.C., Jackson, A.L., Ward, E.J., Parnell, A.C., Phillips, D.L., Semmens, B.X., 2018. Analyzing mixing systems using a new generation of Bayesian tracer mixing models. PeerJ 6:e5096, https://doi.org/10.7717/peerj.5096.

285. Strous, M., Kuenen, J.G., Jetten, M.S.M., 1999. Key physiology of anaerobic ammonium oxidation. Applied and Environmental Microbiology 65 (7), 3248-3250, https://doi.org/10.1128/AEM.65.7.3248-3250.1999.

286. Su, J.F., Zheng, S.C., Huang, T.L., Ma, F., Shao, S.C., Yang, S.F., Zhang, L.N., 2016. Simultaneous removal of Mn(II) and nitrate by the manganese-oxidizing bacterium *Acinetobacter* sp. SZ28 in anaerobic conditions. Geomicrobiology Journal 33 (7), 586-591.

287. Sumpter, J.P., Johnson, A.C., 2005. Lessons from endocrine disruption and their application to other issues concerning trace organics in the aquatic environment. Environmental Science and Technology 39 (12), 4321-4332, https://doi.org/10.1021/es048504a.

288. Sutton, M.A., Bleeker, A., 2013. The shape of nitrogen to come. Nature 494, 435-437.

289. Swanson, C.R., 2015. Annual and seasonal dissolved inorganic nutrient budgets for Humboldt Bay with implications for wastewater dischargers. Thesis (M.S.): Humboldt State University. http://humboldt-dspace.calstate.edu/bitstream/handle/10211.3/163081/Swanson_Charles_Fall2015.pdf?sequence=1.

290. Szilas, C.P., Borggaard, O.K., Hansen, H.C.B., Rauer, J., 1998. Potential iron and phosphate mobilization during flooding of soil material. Water, Air and Soil Pollution 106, 97-109, https://doi.org/10.1023/A:1004965631574.

291. Tai, Y-L., Dempsey, B.A., 2009 Nitrite reduction with hydrous ferric oxides and Fe(II): stoichiometry, rate, and mechanism. Water Research 43, 546-552, https://doi.org/10.1016/j.watres.2008.10.055.

292. Tcherkez, G., Tea, I., 2013. $^{32}S/^{34}S$ isotope fractionation in plant sulphur metabolism. New Phytologist 200, 44-53, https://doi.org/10.1111/nph.12314.

293. Tchobanoglous, G., Burton, F.L., Stensel, H.D. *Wastewater Engineering: Treatment and Reuse*. 5th Ed. McGraw-Hill: New York City, NY, 2013.

294. Tetra Tech, 2018. *Technical Support for Elkhorn Slough Nutrient Total Maximum Daily Load (TMDL) Development*. 1-60.

295. Thamdrup, B., 2012. New pathways and processes in the global nitrogen cycle. Annual Reviews of Ecology, Evolution and Systematics 43, 407-428, https://doi.org/10.1146/annurev-ecolsys-102710-145048.

296. Thomas, D.H., Rey, M., Jackson, P.E., 2002. Determination of inorganic cations and ammonium in environmental waters by ion chromatography with a high-capacity cation-exchange column. Journal of Chromatography A 956, 181-186, https://doi.org/10.1016/S0021-9673(02)00141-3.

297. Thornton, J.A., Harding, W.R., Dent, M., Hart, R.C., Lin, H., Rast, C.L., Rast, W., Ryding, S-O., Slawski, T.M., 2013. Eutrophication as a 'wicked' problem. Lake and Reservoirs: Research and Management 18, 298-316, https://doi.org/10.1111/lre.12044.

298. Tiedje, J.M.. *Ecology of denitrification and dissimilatory nitrate reduction to ammonium*. p. 179-244. *In* A.J.B. Zehnder (ed), Environmental Microbiology of Anaerobes. John Wiley and Sons: New York City, N.Y., 1988.

299. Tipping, E., Somerville, C.J., Luster, J., 2016. The C:N:P:S stoichiometry of soil organic matter. Biogeochemistry 130, 117-131, https://doi.org/10.1007/s10533-016-0247-z.

300. Torrentó, C., Cama, J., Urmeneta, J., Otero, N., Soler, A., 2010. Denitrification of groundwater with pyrite and *Thiobacillus denitrificans*. Chemical Geology 278, 80-91.

301. Tovilla, H.C., de la Lanza, E.G., 1999. Ecología, producción, y aprovechamiento del mangle *Conocarpus erectus* L. en Barra de Tecoanapa Guerroro, México. Biotropica 31, 121-134.

302. Truu, M., Juhanson, J., Truu, J., 2009. Microbial biomass, activity and community composition in constructed wetlands. Science of the Total Environment 407, 3958-3971.

303. Twilley, R.R., Lugo, A.E., Patterson-Zucca, C., 1986. Litter production and turnover in basin mangrove forest in southwest Florida. Ecology 676, 670-683.

304. Twilley, R.R., Pozo, M., García, V.H., Rivera-Monroy, V.H., Zambrano, R., Bodero, A., 1997. Litter dynamics in riverine mangrove forests in the Guaya River estuary, Ecuador. Oecologia 111, 109-122.

305. Ulrich, P.D., Sedlak, D.L., 2010. Impacts of iron amendment on net methylmercury export from tidal wetland microcosms. Environmental Science & Technology 44 (19), 7659-7665, https://doi.org/10.1021/es1018256.

306. Uselman, S.M., Qualls, R.G., Lilienfein, J., 2012. Quality of soluble organic C, N, and P produced by different types of litter: root litter versus leaf litter. Soil Biology & Biochemistry 54, 57-67, https://doi.org/10.1016/j.soilbio.2012.03.021.

307. USGS, 2014. *Amounts and Sources of Nutrients Delivered to Estuaries in the Gulf of Mexico*. https://archive.usgs.gov/archive/sites/water.usgs.gov/nawqa/sparrow/estuary/gom/index.html.

308. van de Broek, M., Temmerman, S., Merckx, R., Govers, G., 2016. Controls on soil organic carbon stocks in tidal marshes along an estuarine salinity gradient. Biogeosciences 13(24), 6611-6624, https://doi.org/10.5194/bg-13-6611-2016.

309. van den Berg, M., Wendel-Vos, W., van Poppel, M., Kemper, H., van Mechelen W., Maas, J., 2015. Health benefits of green spaces in the living environment: a systematic review of epidemiological studies. Urban Forestry & Urban Greening 14 (4), 806-816, https://doi.org/10.1016/j.ufug.2015.07.008.

310. van Groenigen, J.W., Huygens, D., Boeckx, P., Kuyper, Th.W., Lubbers, I.M., Rütting, T., Groffman, P.M., 2015. The soil N cycle: new insights and key challenges. SOIL 1, 235-256, https://doi.org/10.5194/soil-1-235-2015.

311. van Kessel, C., Clough, T., van Groenigen, J.W., 2009. Dissolved organic nitrogen: an overlooked pathway of nitrogen loss from agricultural systems? Journal of Environmental Quality 38, 393-401, https://doi.org/10.2134/jeq2008.0277.

312. Vidales, J.A., Gerba, C.P., Karpiscak, M.M., 2003. Virus removal from wastewater in a multispecies subsurface-flow constructed wetland. Water Environment Research 75 (3), 238-245, https://www.jstor.org/stable/25045689.

313. Vymazal, J., 2007. Removal of nutrients in various types of constructed wetlands. Science of the Total Environment 380 (1-3), 48-65.

314. Vymazal, J. (ed), *Water and Nutrient Management in Natural and Constructed Wetlands*. Springer: New York City, N.Y., 2010.

315. Vymazal, J., Švehla, J., Kröpfelová, L., Chrastný, V. Trace metals in *Phragmites australis* and *Phalaris arundinacea* growing in constructed and natural wetlands. Science of the Total Environment 380, 2007, 154-162, https://doi.org/10.1016/j.scitotenv.2007.01.057.

316. Wafar, S., Untawale, A.G., Wafar, M., 1997. Litterfall and energy flux in a mangrove ecosystem. Estuaries and Coastal Shelf Science 44, 111-124.

317. Wallis, J.P., Scholes, R., Cecchetti, A.R., Sedlak, D.L., 2017. Phosphorus and iron cycling in unit-process treatment wetlands. REU Abstract as Published through ReNUWIt, http://renuwiterc.org/wordpress/wp-content/uploads/pdf/Wallis_Abstract.pdf.

318. Walpersdorf, E., Bender Koch, C., Heiberg, L., O'Connell, D.W., Kjaergaard, C., Bruun Hansen, H.C., 2013. Does vivianite control phosphate solubility in anoxic meadow soils? Geoderma 193-194, 189

319. Wamsley, T.V., Cialone, M.A., Smith, J.M., Atkinson, J.H., Rosati, J.D., 2010. The potential of wetlands in reducing storm surge. Ocean Engineering 37, 59-68, https://doi.org/10.1016/j.oceaneng.2009.07.018.

320. Wang, F., Chapman, P.M., 1999. Biological implications of sulfide in sediment–a review focusing on sediment toxicity. Environmental Toxicology & Chemistry 18 (11), 2526-2532, https://doi.org/10.1002/etc.5620181120.

321. Wang, M., Chen, W., 2018 Generation and characterization of DOM in wastewater treatment processes. Chemosphere 201, 96-109, https://doi.org/10.1016/j.chemosphere.2018.02.124.

322. Webber, P.J., May, D.E., 1977. The magnitude and distribution of belowground plant structures in the alpine tundra of Niwot Ridge, Colorado. Arctic and Alpine Research 9(2), 157-174.

323. Wen, Y., Chen, Y., Zheng, N., Yang, D., Zhou, Q. 2010. Effects of plant biomass on nitrate removal and transformation of carbon sources in subsurface-flow constructed wetlands. Bioresource Technology 101 (19), https://doi.org/10.1016/j.biortech.2010.04.068.

324. Westerhoff, P., Mash, H., 2002. Dissolved organic nitrogen in drinking water supplies: a review, AQUA 51 (8), 415-448, https://doi.org/10.2166/aqua/2002/0038.

325. White, P.J., Broadley, M.R., 2001. Chloride in soils and its uptake and movement within the plant: a review. Annals of Botany 88 (6), 967-988, https://doi.org/10.1006/anbo.2001.1540.

326. Wiedmer, E., Senn-Irelt, B., 2006. Biomass and primary productivity of an *Alnus viridis* stand – a case study from the Schächental valley, Switzerland. Botanica Helvetica 116, 55-64, https://doi.org/10.1007/s00035-006-0758-7.

327. Wilby, F.V., 1969. Variation in recognition odor threshold of a panel. Journal of the Air Pollution Control Association 19 (2), 96-100.

328. Wild, A., 1950. The retention of phosphate by the soil. a review. Journal of Soil Science 1, 221.

329. Wilfert, P., Kumar, P.K., Korving, L., Witkamp, G-J., van Loosdrecht, M.C.M., 2015. The relevance of phosphorus and iron chemistry to the recovery of phosphorus from wastewater: a review. Environmental Science & Technology 49, 9400-9414, https://doi.org/10.1021/acs.est.5b00150.

330. Williams, P.B., Faber, P.B., 2009. Salt marsh restoration experience in San Francisco Bay. Journal of Coastal Research, Special Issue 27, 203-311.

331. Willems, H.P.L., Rotelli, M.D., Berry, D.F., Smith, E.P., Reneau, R.B., Mostaghimi, S., 1997. Nitrate removal in riparian wetland soils: effects of flow rate, temperature, nitrate concentration and soil depth. Water Research 31 (4), 841-849, https://doi.org/10.1016/S0043-1354(96)00315-6.

332. Witt, C., Gaunt, J.L., Galicia, C.C., Ottow, J.C.G., Neue, H-U., 2000. A rapid chloroform-fumigation extraction method for measuring soil microbial biomass carbon and nitrogen in flooded rice soils. Biology and Fertility of Soils 30, 510-519.

333. Wolch, J.R., Byrne, J., Newell, J.P., 2014. Urban green space, public health and environmental justice: the challenge of making cities 'just green enough'. Landscape and Urban Planning 125, 234-244, https://doi.org/10.1016/j.landurbplan.2014.01.017.

334. Wu, S., Vymazal, J., Brix, H., 2017. Critical review: biogeochemical networking of iron in constructed wetlands for wastewater treatment. Environmental Science & Technology 53, 7930-7944, https://doi.org/10.1021/acs.est.9b00958.

335. Xiao, X., Agustí, S., Pan, Y., Yu, Y., Li, K., Wu, J., Duarte, C.M., 2019. Warming amplifies the frequency of harmful algal blooms with eutrophication in Chinese coastal waters. Environmental Science & Technology 53 (22), 13031-13041, https://doi.org/10.1021/acs.est.9b03726.

336. Xu, X., Thornton, P.E., Post, W.M., 2013 A global analysis of soil microbial biomass carbon, nitrogen and phosphorus in terrestrial ecosystems. Global Ecology and Biogeography 22, 737-749.

337. Yang, W.H., Weber, K.A., Silver, W.L., 2012a. Nitrogen loss from soil through anaerobic ammonium oxidation coupled to iron reduction. Nature Geosciences Letters 5, 538-541, https://doi.org/10.1038/NGEO1530.

338. Yang, X., Huang, S., Wu, Q., Zhang, R., 2012b. Nitrate reduction coupled with microbial oxidation of sulfide in river sediment. Journal of Soils and Sediments 12, 1435-1444.

339. Yao, W., Millero, F.J., 1996. Adsorption of phosphate on manganese dioxide in seawater. Environmental Science and Technology 30, 536-541, https://doi.org/10.1021/es950290x.

340. Yavitt, J.B., Fahey, T.J. 1986. Litter decay and leaching from the forest floor in *Pinus contorta* (Lodgepole Pine) ecosystems. Journal of Ecology 74(*2*), 525-545, http://www.jstor.com/stable/2260272.

341. Yin, T., Chen, H., Reinhard, M., Yi, X., He, Y., Gin, K.Y-H. Perfluoroalkyl and polyfluoroalkyl substances removal in a full-scale tropical constructed wetland system treating landfill leachate.

342. Young, P., 1996. The "new science" of wetland restoration. Environmental Science & Technology 30 (7), 292A-296A.

343. Yu, S-I., R, H-M., 2009. Natural ^{15}N abundance of plant and soil inorganic-N as evidence for over-fertilization with compost. Soil Biology and Biochemistry 41(7), 1541-1547, https://doi.org/10.1016/j.soilbio.2009.04.014.

344. Zaiontz, C., 2018. Real statistics using Excel. www.real-statistics.com.

345. Zhang, Y-C., Slomp, C.P., Broers, H.P., Bostick, B., Passier, H.F., Böttcher, M.E., Omoregie, E.O., Lloyd, J.R., Polya, D.A., van Cappellen, P., 2012. Isotopic and microbiological signatures of pyrite-driven denitrification in a sandy aquifer. Chemical Geology 300-301, 123-132, https://doi.org/10.1016/j.chemgeo.2012.01.024.

346. Zhang, M., Zhang, T., Shao, M.F., Fang, H.H.P., 2009. Autotrophic denitrification in nitrate-induced marine sediment remediation and *Sulfurimonas denitrificans*-like bacteria. Chemosphere 76, 677-682, https://doi.org/10.1016/j.chemosphere.2009.03.066.

347. Zhang, W., Lei, Q., Li, Z., Han, H., 2016. Temporal variation of nitrogen balance within constructed wetlands treating slightly polluted water using a stable nitrogen isotope experiment. Environmental Science and Pollution Research 23, 2677-2683, https://doi.org/10.1007/s11356-015-5485-4.

348. Zhai, X., Piwpuan, N., Arias, C.A., Headley, T., Brix, H., 2013. Can root exudates from emergent wetland plants fuel denitrification in subsurface flow constructed wetlands? Ecological Engineering 61P, 555-563, https://doi.org/10.1016/j.ecoleng.2013.02.014.

349. Zheng, X., Sun, P., Han, J., Song, Y., Hu, Z., Fan, H., Lv, S., 2014. Inhibitory factors affecting the process of enhanced biological phosphorus removal (EBPR) – a mini-review. Process Biochemistry 49, 2207-2213, https://doi.org/10.1016/j.procbio.2014.10.008.

350. Zhou, Y., Xing, X-H., Liu, Z., Cui, L., Yu, A., Feng, Q., Yang, H., 2008. Enhanced coagulation of ferric chloride aided by tannic acid for phosphorus removal from wastewater. Chemosphere 72, 290-298, https://doi.org/10.1016/j.chemosphere.2008.02.028.

351. Ziajahromi, S., Neale, P.A., Rintoul, L., Leusch, F.D.L. Wastewater treatment plants as a pathway for microplastics: Development of a new approach to sample wastewater-based microplastics. Water Research 112, 2017, 93-99, https://doi.org/10.1016/j.watres.2017.01.042.

352. Zhuiykov, S., 2012. Solid-state sensors monitoring parameters of water quality for the next generation of wireless sensor networks. Sensor and Actuators B: Chemical 161, 1-20, https://doi.org/10.1016/j.snb.2011.10.078.

Appendix A: Supporting Information for Chapter 2

A.1 Horizontal levee test facility cell design details related to treatment types

Treatments were varied among the test facility wetland cells based on topography, soil type, and planting regime (Table A-1). Detailed descriptions of each of these treatments are provided in sections A.1.1, A.1.2 and A.1.3.

Table A-1: Wetland treatments employed at the test facility.

Treatment ID	Cells	Topography	Topsoil Type	Planting Regime
Swale-Depression	A, B, C	Swale-depression	Fine topsoil	Wet meadow*
Wet Meadow, Fine	D, E, F	Uniform grade	Fine topsoil	Wet meadow
Wet Meadow, Coarse	G, I, K	Uniform grade	Coarse topsoil	Wet meadow
Willow	H, J, L	Uniform grade	Coarse topsoil	Riparian

*See section A.1.3 for more information about the differences between the swale-depression wet meadow planting regimes and other cells.

A.1.1 Topography

Two types of topography were used in the construction of wetland cells. In the first topography type (Figure A-1), the wetland surface was sloped evenly at a 1:30 grade over the length of the cell. This topography is called a uniform grade. In the second topography type, wetland cells were additionally graded from the sides of the wetland cells toward the center to create a swale-type channel through which a small surface flow could pass over the wetland surface (Figure A-2). This topography is referred to as a swale-depression topography (Lindley, 2014).

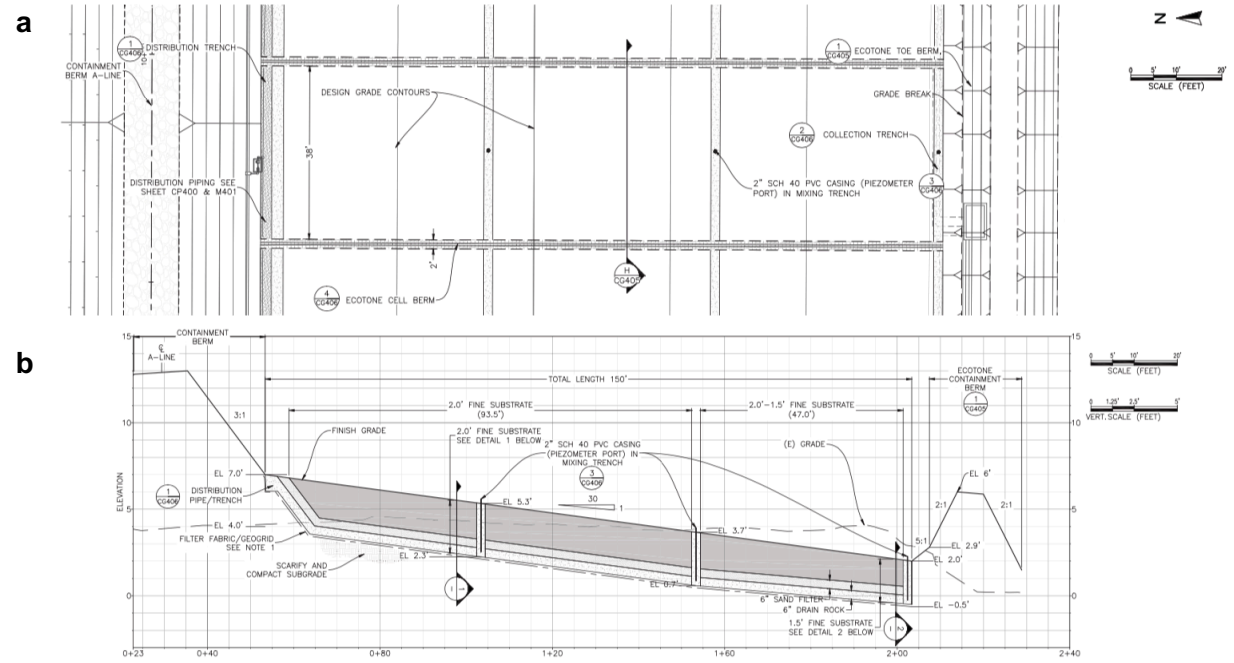

Figure A-1: Design schematics for wetland cells with uniformly sloped topography: (a) a plan view and (b) a section view (Lindley, 2014).

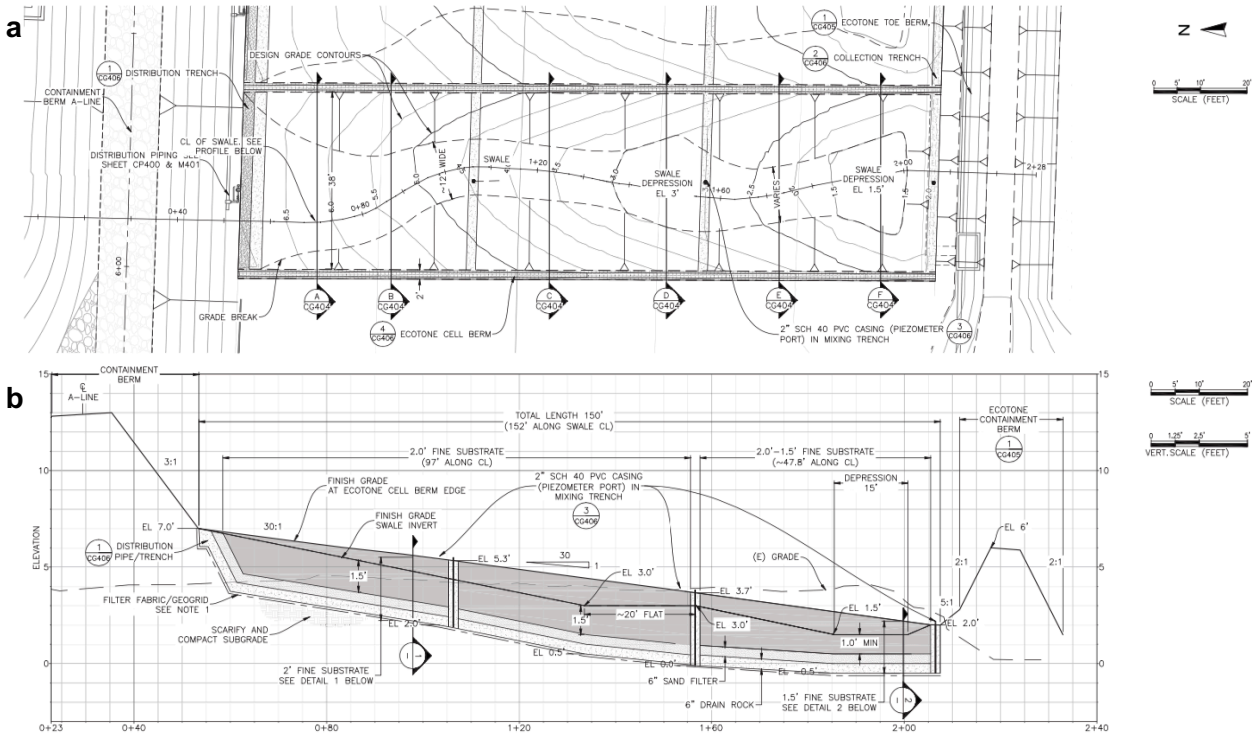

Figure A-2: Design schematics for wetland cells with swale-depression topography: a) a plan view and (b) a section view (Lindley, 2014).

A.1.2 Soil type

Two soil mixtures were used for the topsoil in the wetland cells: a coarse mixture and a fine mixture. Topsoil layers were underlain with drainage layers of sand and gravel (each 15 cm in depth), amended with wood chips (Redwood or Douglas Fir) of <2 cm in size mixed in at 30% by volume. Topsoil types consisted of combinations four different types of media from various sources: gravel, sand, bay mud and aged wood fines. Bay mud consisted of a fine clay mud loam excavated on site during construction from a depth of 0.5-2.0 m. Wood fines consisted of the same wood chip materials described previously < 0.5 cm in size and aged for a minimum of 1 year by composting prior to use. The media sources met the following specs (Lindley, 2014):

Table A-2: Gravel grain size specifications.

Sieve Size	Acceptable Range	ASTM Test
1”	100%	D 422
3/8”	40-100%	D 422
Passing #4	10-40%	D 422
Passing #8	10-33%	D 422
Passing #30	5-15%	D 422
Passing #50	0-7%	D 422
Passing #200	<1%	D 422

Table A-3: Sand grain size specifications.

Sieve Size	Acceptable Range	ASTM Test
3/8”	100%	D 422
Passing #4	90-100%	D 422
Passing #8	75-97%	D 422
Passing #30	35-55%	D 422
Passing #50	10-30%	D 422
Passing #200	<1%	D 422

The fine topsoil mixture consisted of 60% (v/v) bay mud, 30% (v/v) sand and 10% (v/v) wood fines. The coarse topsoil mixture consisted of 50% (v/v) bay mud, 50% (v/v) sand and 10% (v/v) wood fines (Lindley, 2014).

A.1.3 Planting regimes and plant community establishment

Two primary planting regimes were applied to treatment cells. The first planting regime was employed to mimic a wet meadow habitat consisting mainly of grasses, rushes, sedges, herbs, forms and subshrubs. The second planting regime was used to mimic a riparian willow wetland containing willows, shrubs, and some grasses as well, though willows had crowded out most other plant species within 2 years of planting in those cells. The first planting regime was applied with minor modifications to the amount of each species planted to wetland cells with a swale-depression topography. All plants used in the sloped wetland cells are native plant species collected from around San Francisco Bay and propagated on site in raised beds by Save the Bay (https://savesfbay.org/) staff. Additional information regarding the collection, propagation and transplanting of native plant species at the test facility are available in a report (Save the Bay, 2017). The plant species used in each of the planting regimes are listed in order based on the number of plants transplanted onto the wetland slopes (which roughly corresponds to species density) in Table A-4 and Table A-5 below:

Table A-4: Plants used in the wet meadow planting regime. Numbers in parentheses correspond to the amount of each species planted in swale-depression cells. Shaded cells represent plants that were only planted in swale-depression cells (Save the Bay, 2017).

Common Name	Species Name	# Planted per Cell
Creeping wild rye	*Elymus triticoides*	2800 (2100)
Baltic rush	*Juncus balticus*	1050 (1050)
Iris-leaved rush	*Juncus xiphiodes*	700 (525)
Marsh baccharis	*Baccharis glutinosa*	350 (263)
Clustered field sedge	*Carex praegracilis*	350 (263)
Santa Barbara sedge	*Carex barbarae*	350 (88)
Western golden rod	*Euthamia occidentalis*	350 (263)
California aster	*Symphyotrichum chilense*	350 (263)
Mugwort	*Artemisia douglasiana*	350 (263)
California loosestrife	*Lythrum californicum*	350 (263)
Pale spikerush	*Eleocharis macrostachya*	(1225)
Common rush	*Juncus effuses*	(350)
Alkali bulrush	*Bolboschoenus maritimus*	(88)

Table A-5: Plants used in the riparian wetland planting regime (Save the Bay, 2017).

Common Name	Species Name	# Planted per Cell
Arroyo willow	*Salix lasiolepsis*	700
California blackberry	*Rubus ursinus*	525
Clustered field sedge	*Carex praegracilis*	385
Santa Barbara sedge	*Carex barbarae*	385
Marsh baccharis	*Baccharis glutinosa*	175
California rose	*Rosa californica*	175
Red osier dogwood	*Cornus sericea*	88
Black elderberry	*Sambus nigra*	88

Vegetation monitoring, including line-transect and quadrat sampling methods, conducted in 2018 indicated that slope vegetation methods produced a dense, diverse native plant community with limited encroachment by invasive and non-native species (<2% of plants identified). The species listed above continued to dominate the plant communities in their respective cells throughout the monitoring period. Full vegetation monitoring results are not provided in the Final Evaluation Report (ESA, 2018).

Plant biomass data detailing the increase in plant biomass over time in the horizontal levee system will be discussed in subsequent publications. Photos showing the progression of plant community growth at the test facility are shown here.


b


c


d


e

Figure A-3: Photos showing the progression of plant growth throughout the monitoring period. Photo (a) shows the horizontal levee during construction and (b) shows plants being transplanted onto the slope in November of 2015. Photo (c) shows vegetation establishment in April 2016 and (d) shows plant growth by the end of the first full growing season in October of 2016. Photos (e) and (f) show dense vegetation growth that established by (e) July 2017 and (f) June 2018.

A.2 Operational conditions related to flow rates and flow measurements

Over the course of this monitoring period, the influent flow to the subsurface wetland was applied at three levels: approximately 184, 130 and 66 L min^{-1}. This is displayed in the timeline presented in Figure 2-3. Table A-6 below presents the flow rates going into each individual cell.

Table A-6: Influent flow rates for individual wetland cells in L min^{-1}. Readings correspond to average flow readings for the 3-6 days preceding the sampling date (depending on the availability of data). Highlighted cells represent values that estimated from either (1) visual readings of the flow meters taken in the field at the time of sampling or (2) through taking the difference of the total flow and the sum of the measured flow rates from other cells.

	Wetland Cell												
Date	A	B	C	D	E	F	G	H	I	J	K	L	Total
6/1/17	28.6	8.3	17.8	10.2	5.3	12.4	7.2	23.8	24.8	0.0*	24.1	20.6	184
6/15/17	32.5	6.6	17.4	9.6	4.6	8.3	8.1	23.2	31.9	0.0*	25.2	15.3	184
6/27/17	37.1	5.1	17.0	7.7	5.0	12.3	9.3	24.4	33.9	0.0*	26.5	6.0	184
7/14/17	39.0	7.2	20.3	10.2	3.0	11.7	9.7	19.3	41.8	0.0*	23.0	0.1	184
8/3/17	32.4	21.1	12.5	19.7	11.9	19.0	8.1	19.5	28.4	0.0*	17.7	0.6	184
9/1/17	29.5	19.8	10.9	18.6	14.3	16.6	25.2	17.5	16.2	0.0*	15.7	0.0*	184
11/6/17	2.7	17.2	7.4	16.3	8.1	15.5	40.2	15.7	2.7	0.0*	14.9	0.3	131
12/15/17	13.6	14.6	10.6	11.3	14.3	14.6	15.1	6.0	13.6	0.0*	15.4	1.1	131
2/8/18	15.7	19.0	12.8	14.2	37.4	20.5	14.9	8.2	18.9	0.0*	19.5	2.0	192
3/8/18	12.6	16.2	12.0	13.5	21.7	8.4	11.5	5.7	16.2	10.9	15.7	9.3	164
4/5/18	12.5	13.6	8.4	9.5	12.8	8.3	11.5	6.0	16.0	37.9	10.8	13.9	162
5/2/18	10.5	10.6	7.3	7.4	1.7	7.0	10.6	5.0	13.5	37.8	8.6	17.9	137
5/17/18	14.0	10.5	10.1	10.0	13.5	9.3	8.2	6.1	17.9	45.7	10.1	25.6	181
6/5/18	12.3	12.2	8.6	8.7	6.9	8.2	10.5	5.1	15.7	41.2	9.1	20.1	159
6/20/18	14.0	13.0	9.2	9.9	10.9	9.3	9.0	5.0	9.8	45.4	10.8	25.8	173
7/3/18	17.2	4.9	25.7	4.2	5.7	3.8	5.8	7.3	5.0	7.2	3.0	5.8	92
8/1/18	14.1	12.7	10.3	2.4	2.4	2.0	3.1	4.0	2.8	4.2	3.1	4.6	66
8/15/18	16.4	11.6	9.6	1.9	2.1	1.6	2.7	3.7	2.5	3.4	2.6	4.0	62
9/5/18	12.6	14.0	12.7	2.6	3.4	2.4	3.7	4.8	2.6	3.8	3.3	5.0	71
9/17/18	13.5	10.8	7.6	1.7	0.6	1.2	2.7	3.1	2.4	3.2	2.5	3.2	53
10/11/18	13.7	15.6	13.1	2.9	3.4	2.6	3.5	5.2	3.4	4.6	3.3	6.9	79
11/7/18	13.7	15.6	13.1	2.9	3.4	2.6	4.0	5.3	3.4	4.6	3.3	6.9	79
11/26/18	13.7	15.6	13.1	2.9	3.4	2.6	4.0	5.3	3.4	4.6	3.3	6.9	79
1/10/19	13.7	15.6	13.1	2.9	3.4	2.6	4.0	5.3	3.4	4.6	3.3	6.9	79
2/7/19	9.8	11.0	9.1	2.5	3.4	2.6	3.2	4.5	3.4	4.6	3.3	6.9	64
3/19/19	9.8	11.0	9.1	2.5	3.4	2.6	3.2	4.5	3.4	4.6	3.3	6.9	64
4/15/19	12.2	13.6	11.2	3.0	4.2	3.2	4.0	5.6	4.2	5.7	4.1	8.5	79

*During early portions of the sampling period, cells J and L had their influent distribution pipes clogged by willow roots. For this reason, influent flow rates of 0 were recorded for cell J between June 2017 and February 2018, and between September of 2017 for cell L.

During the monitoring period, two operational regimes were employed. During the first operational regime, nitrified wastewater effluent flowed through the free water surface wetland first and then through the horizontal levee in series. During the second operational regime, the two wetlands were fed independently, in parallel. How water was conveyed to the horizontal levee slope in these two operational regimes is illustrated in Figure 2-1 with the blue and orange flow paths, respectively. The

dates during which these flow regimes were employed are delineated in the timeline in Figure 2-3, next to the label “Flow Regime”.

Additionally, hydraulic optimization of the individual wetland cells occurred in three phases throughout the monitoring period. This was achieved by using valves at the influent to each cell to modulate flow rates going into individual cells. In the first phase, influent valves were left open (April 2017 through June 2017). However, this led to wide variations in the flow rate received by each cell. In the second phase of hydraulic optimization, which lasted from June 2017 through July of 2018, flows were throttled to equalize the fraction of overland flow observed in each cell. Finally, in the last phase of hydraulic optimization (July 2017-present), cells D through L were throttled to eliminate overland flow in those cells. The dates for these hydraulic optimization phases are also presented in Figure 2-3. The fraction of water flowing over the surface of each cell was calculated as described in Chapter 2 by performing a mass balance on nitrate. The level of throttling into each cell was determined based on these overland flow calculations. Data presented in the text of this study related to “hydraulically optimized” cells in phase 3 comes from cells D-L on dates after July 2018.

A.3 Tracer tests

Hydraulic tracer tests were conducted using reagent grade lithium bromide (>99%; Sigma-Aldrich, Saint Louis, MO, USA) dissolved in deionized water and then injected into the wetland at various locations. Tests were performed in a variety of cells (cells D-H) over multiple dates to characterize overland and subsurface flow hydrology.

An initial test was conducted in April 2018, which captured the hydraulic conditions in the overland flow water, using 1.0 L of a 50 g L^{-1} LiBr solution injected into the influent pump station, with hourly grab samples collected for 51 hours from the effluent of cell G. Grab samples were collected every 1-3 hours from the effluent of cell G using automated Teledyne ISCO Compact Portable Samplers (Clipper Controls, CA, USA). Concentrations of Li^+, Br^- and Cl^- are plotted over time in Figure A-4.

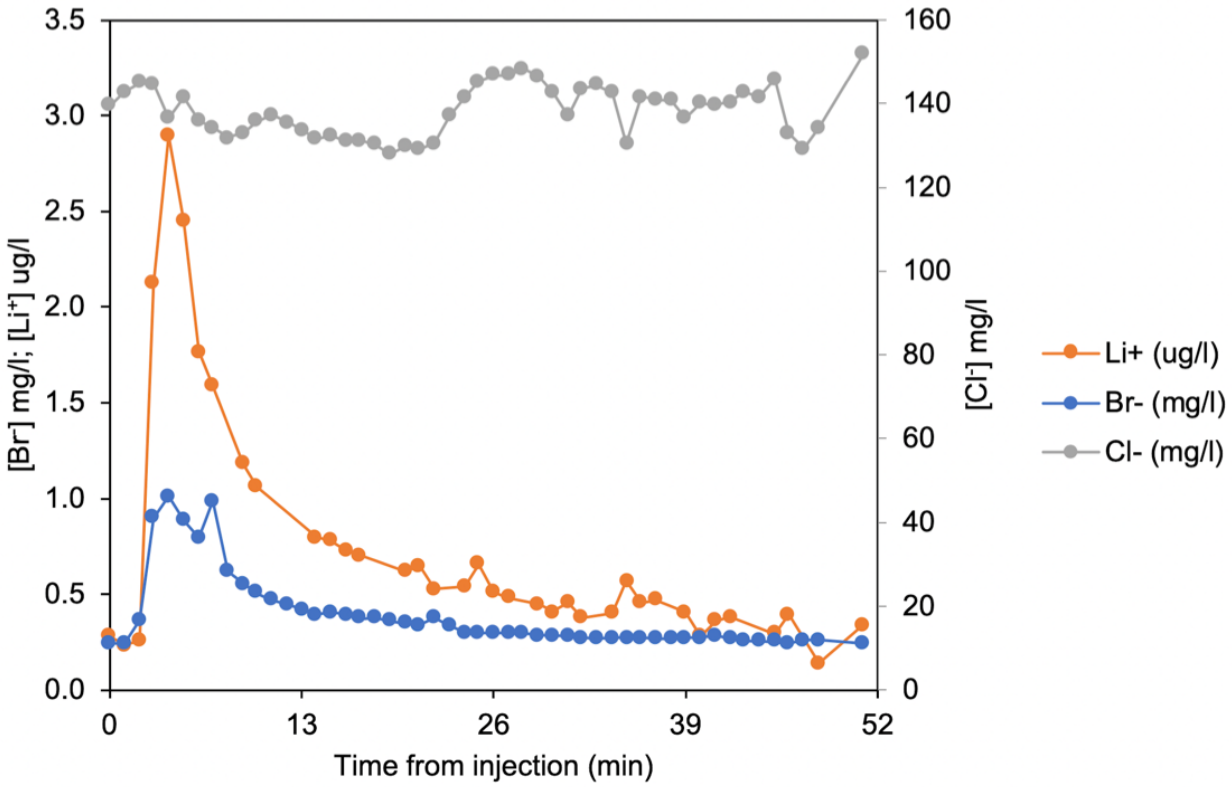

Figure A-4: Concentrations of Li^+, Br^- and Cl^- in the effluent from cell G during the April 2018 tracer test.

Mean hydraulic residence times for the overland flow water were calculated in cell G on this date using both Li^+ and Br^- data according to previously described methods (Headley and Kadlec, 2007; Benjamin and Lawler, 2013). Mean residence times were calculated as 10.8 hr and 12.0 hr respectively, averaging 11.4 hr. Three additional tests were performed in July 2017, with 1.0 L of a 30 g L^{-1} LiBr solution injected directly into the influent pump station. Over the next 24-99 hours, grab samples were collected every 2-3 hours from the effluent of cells E, F and/or G. Samples were collected only for cell E on July 4, 2018 (Figure A-5) with samples collected from cells E, F and G on July 11, 2018 (Figure A-6).

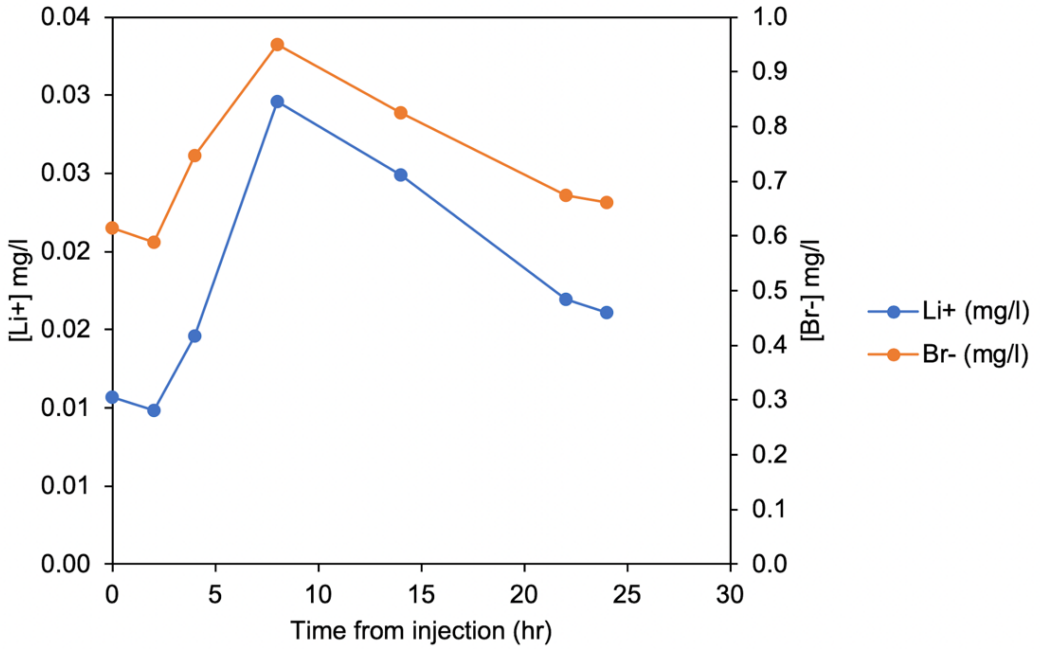

Figure A-5: Concentrations of Li^+, Br^- and Cl^- in the effluent from cell E during the July 4, 2018 tracer test.

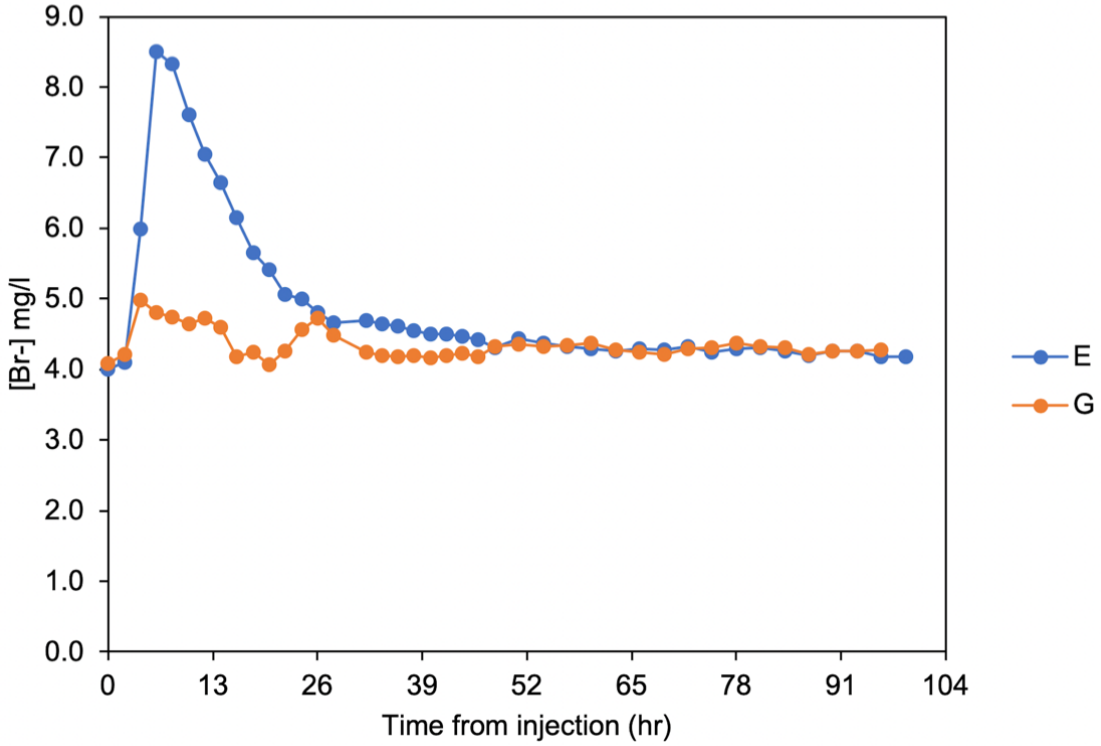

Figure A-6: Concentrations of Br^- in the effluent from cells E and G on July 11, 2018 tracer test. Data for lithium was unavailable on this date and samples from cell F are not shown because there were large data gaps due to instrument malfunction.

Mean hydraulic residence times were again calculated in the overland flow on these dates. For July 4, 2018, mean residence times were calculated as 11.1 hr and 12.9 hr (using Br^- and Li^+ respectively), averaging 12.0 hr for cell E. On July 11, 2018, mean residence times were calculated as 17.7 hr and 22.4 hr for cells E and G respectively. It is important to note that overland flow rates in G were significantly lower than in cell E during this period of time, which likely explains the significantly higher overland flow residence time in that cell.

Additional tracer tests were conducted in cells D, G and H in January 2019, with 1.0 L of a 30 g L^{-1} LiBr solution injected directly into the influent pump station. At this time, applied flow rates were decreased in these cells to eliminate overland flow so that tracer tests could be conducted to measure subsurface residence times. Over the next 800 hours, grab samples were collected every 2-7 hours from the effluent of those cells. Unfortunately, these tracer tests were inconclusive because reliable tracer peaks could not be identified (an example is shown for cell D in Figure A-7) likely due to a combination of precipitation events, high background noise and concentrations of analytes that were too close to quantification limits.

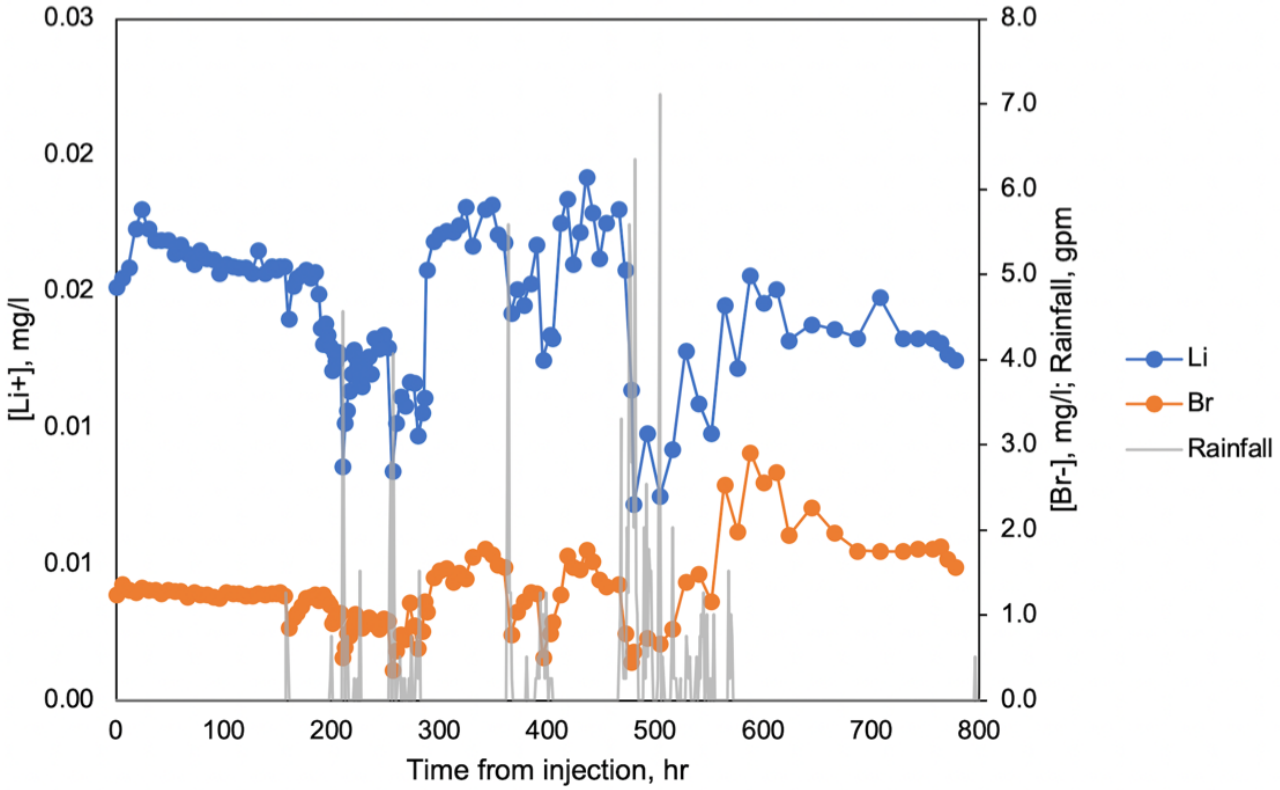

Figure A-7: Tracer test data collected from cell D in January 2019.

Because residence times could not be calculated from the January 2019 tracer tests, additional tests were conducted. In March and June 2019, tracer was injected directly into the subsurface at a depth of 0.8 m below the ground surface (i.e., into the coarse gravel sublayer) by pumping 0.03-1.0 L of 30 g L^{-1} LiBr into a set of two porewater samplers. Tracer was injected into the coarse sublayers of the subsurface because we expect insignificant flows of water to pass through the surface soil layers based on the respective hydraulic conductivities of those layers. Samples were then collected manually at varying time intervals (30 minutes to 24 hours) using porewater samplers at distances between 30 cm and 15 m downgradient along the flow-path. Tracer test samples were collected at depths of 0.8 m

below the ground surface. During the March 2019 test (Figure A-8), samples were injected at 0.8 m below the ground surface ~4 m from the influent of cell F in the center of the cell. Samples were then collected 15 cm downstream on 5-15 min intervals over the next 2 hr.

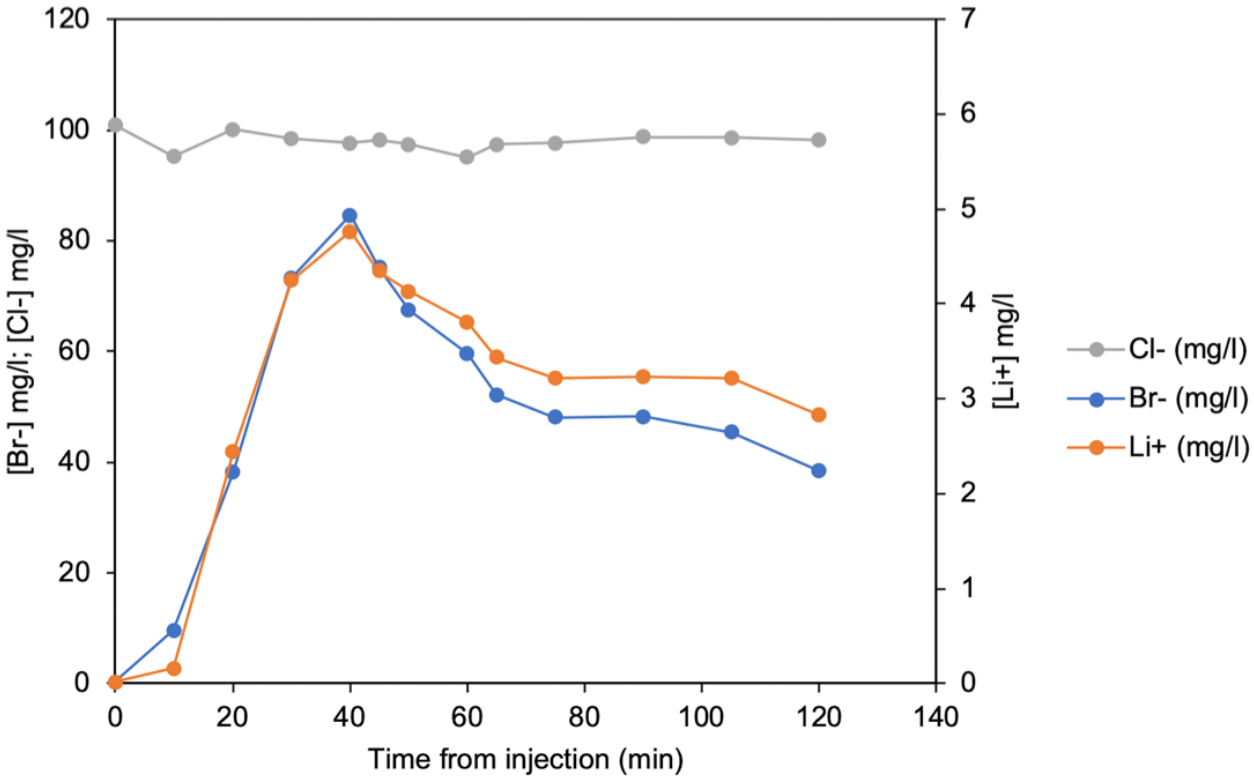

Figure A-8: Tracer test data collected from cell F in March 2019.

Both Li^+ and Br^- peaks experienced significant tailing and concentrations of neither analyte reached background concentrations within the test period. However, estimates of subsurface mean hydraulic residence times could still be derived from these data. Mean residence times were approximately 59 min and 61 min (for Br^- and Li^+ respectively) in the 15 cm section of the subsurface, which corresponds to 12.2 d and 12.7 d with an average of 12.5 d if extrapolated to the entire slope. Because the tail of the tracer test was not fully characterized, it is likely that this value is an underestimate with actual mean residence times in the subsurface possibly up to 20 d or greater.

The final set of subsurface tracer tests were conducted in cell F starting on June 25, 2019. 1.0 L of 30 g L^{-1} LiBr tracer was pumped into a set of two porewater samplers in the center of the wetland cell 15 m from the influent. Samples were collected at 23 m and 31 m from the influent (7 m and 16 m from the injection point) at 20, 22, 23, 46, and 94 hr after tracer injection. Measurements of lithium and bromide in those samples are presented in Figure A-9. Over the 94 hours of monitoring, a significant increase in concentrations of both lithium and bromide over background levels was observed in samples collected at 7 m downstream of the injection point, with concentrations beginning to increase somewhere between 23 and 46 hours after injection. Over the monitoring period, a significant increase in concentrations of lithium or bromide was not observed at the sampling location 16 m downstream. These data were consistent with the estimates from the preliminary subsurface tracer test in March 2019, which suggested that we would have expected mean residence times of ~50 hr and ~110 hr for

subsurface distances of 7 m and 16 m respectively. Because the tracer peak was not fully characterized within 100 hr, it is possible (and likely) that mean residence times in the subsurface may exceed 20-25 d. However, it is important to note that subsurface flow rates may have been particularly low in cell F during this second sampling event because porewater samples were difficult to collect at depth in certain locations suggesting that the water table in this cell was lower than normal.

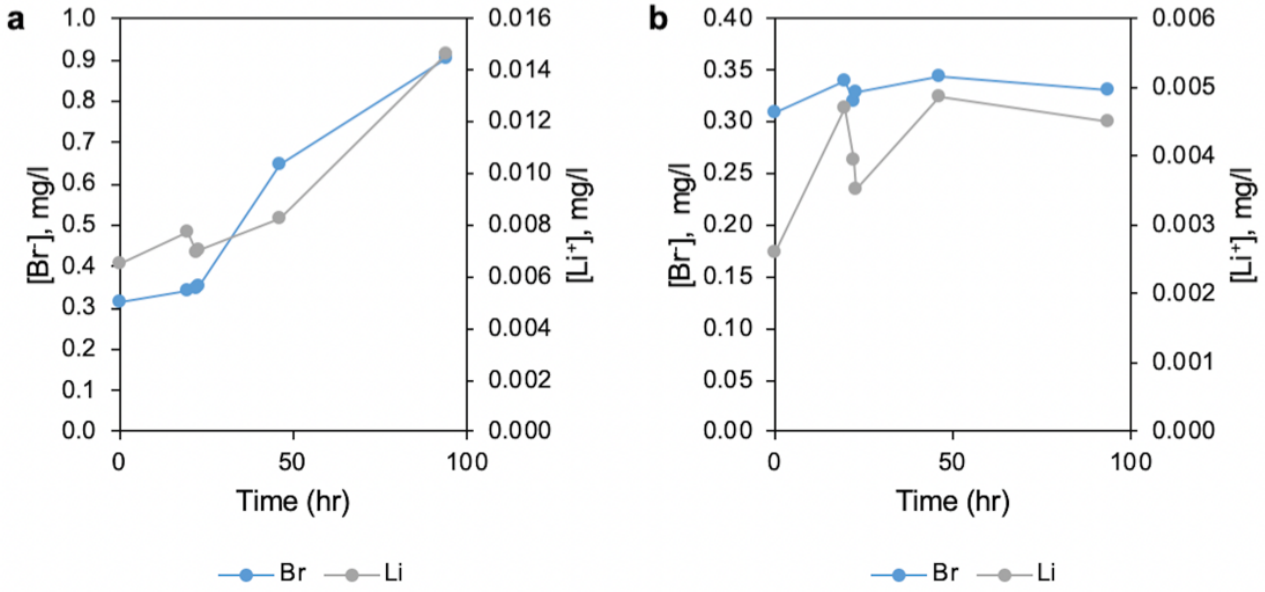

Figure A-9: Lithium and bromide measurements taken at distances (a) 7 m and (b) 16 m from the injection point for the June 2019 tracer test.

A.4 Bird survey results

On 12/2/2017, Amy Chong and Diony Gamoso, both Biological Sciences Technicians with the Presidio Trust, did a bird census at the Oro Loma Sanitary District. Specifically, our surveys were in the Ecotone Slope and the Wet Weather Equalization Basin. The project team included the Oro Loma Sanitary District, ESA, U.C. Berkeley, consultant Peter Baye, Save The Bay, and Bay Institute. The restoration project was implemented in 2015 and 2016. We were curious what species of birds were now using these newly created habitats.

Method: We used an Area Search method for our census. This consisted of us slowly walking the perimeter of the two sites, identifying bird species present by both sight and calls. We also included any species observed using the berms that border each site. We tried not to double-count birds and were conservative in our estimates of numbers. Hence, the total number for each species observed is likely on the low side. Specific habitat usage (ex. "in willows"), was often noted.

I. Ecotone Slope
Time: 08:45-10:10am, Weather: Hazy, calm, approx. 50 degrees F

Note: W = winter range R = within year-round range for this species

Species	#	W or R	Notes
1. White-tailed Kite	2	R	One was hovering (hunting) over site
2. Golden-crowned Sparrow	1	W	
3. White-crowned Sparrow	1	R	
4. Song Sparrow	6	R	
5. Black Phoebe	2	R	One of them on berm
6. Common Yellowthroat	1	R	In Cattails
7. Marsh Wren	1	R	In Cattails
8. Western Meadowlark	3	R	On berm
9. Anna's Hummingbird	2	R	In willows
10. American Crow	2	R	On berm
11. Fox Sparrow	2	W	In willows
12. Yellow-rumped Warbler	6	W	In willows

Note: we also heard 1 Pacific chorus frog at this location

II. Wet Weather Equalization Basin
Time: 10:45-11:47am, Weather: Hazy, calm, approx 56 degrees F

Species	#	W or R	Notes
1. Mallard	31	R	15 females,16 males; in water
2. Northern Shoveler	4	W	3 females, 1 male; in water
3. Snowy Egret	2	R	
4. Black Phoebe	2	R	
5. Great Egret	1	R	
6. White-crowned Sparrow	9	R	Small flocks feeding amid weedy edges of ponds, or weedy berms
7. American Crow	4	R	
8. Golden-Crowned Sparrow	2	W	
9. Western Meadowlark	2	R	On weedy berm
10. Song Sparrow	2	R	On weedy berm, or pond edges
11. Savannah Sparrow	5	R	On weedy berm
12. Lesser Goldfinch	5	R	On weedy berm

Comments:

We both had a fun morning doing the survey! We were happy to see that the project site has developed so nicely.

There were some species that tended to use microhabitats within the sites. For example, the Yellow-rumped Warblers, Fox Sparrows, and Anna's Hummingbirds, were all associated with the willows. The Cattails seemed to provide preferred foraging sites for the Common Yellowthroat and Marsh Wren. Even the weedy berms, covered with senesced annual plants provided good foraging habitat to the different sparrows – likely finding dropped seeds.

We are already excited about coming back in the Spring to do a breeding bird survey!

Appendix B: Supporting Information from Chapter 3

B.1 Elemental cycling in the horizontal levee

In wetland sediments, biogeochemical cycles of different elements are coupled by microorganisms, which utilize diverse substrates to fuel their metabolisms (Burgin et al., 2011). Mineral precipitation and dissolution can also couple elemental cycles. For example, iron cycling is linked to the carbon cycle not only through microbial Fe-reduction, but also through the precipitation of iron carbonate minerals, like siderite (Postma, 1981). We assessed the internal cycling of nitrogen, manganese, iron and sulfur in the following sections to understand the links between elemental cycles in these systems.

B.1.1 Internal nitrogen cycling mechanisms

In horizontal levees, plants are not harvested and therefore plant uptake is only a storage mechanism for nitrogen rather than an ultimate removal mechanism. There are only a few mechanisms that can explain gaseous release of nitrogen to the atmosphere. For example, anammox and denitrification convert nitrate (and ammonium in the case of anammox) to $N_{2(g)}$. However, processes like dissimilatory nitrate reduction to ammonium (DNRA) merely convert nitrogen between aqueous species without removing it from the system. In the case of DNRA, because nitrogen remains in a reactive form, it can continue to be cycled and is concerning because the product of this reaction (ammonium) can be exported in the effluent and can still cause eutrophication. Details regarding nitrogen cycling within the horizontal levee is presented in the following sections.

Ammonium can be transformed by a variety of mechanisms. Ammonium can be converted to nitrite and nitrate via nitrification or Feammox, directly to $N_{2(g)}$ via anammox, into organic forms through assimilation into microbial or plant biomass and can also exchange with potassium to be stored in the layers of phyllosilicate clays (van Groenigen et al., 2015). Because the horizontal levee was operated with a continuously saturated subsurface, decreasing ammonium concentrations were likely caused primarily by assimilation into microbial and plant biomass and to a lesser extent by anaerobic processes, such as anammox and Feammox (Yang et al., 2012a). Ammonium fixation into clay minerals may also have played a role in removal. Nitrification could be transforming a fraction of the applied ammonium in aerobic hotspots supplied with oxygen by plant roots, though we would only expect this to be significant in cells planted with willows. Additionally, Feammox occurs when microorganisms oxidize ammonium to nitrite using Fe(III)-oxides (Thamdrup, 2012; Li et al., 2015; Shuai et al., 2019) and it is possible that cryptic nitrogen cycling could have occurred in which ammonium were converted to nitrite by Feammox only to be rapidly denitrified or removed by anammox. Though we did not observe evidence of it, the role Feammox played could have been significant based on the large amount of iron stored in the soil layers (~2200 kmol of Fe).

Nitrite was likely removed through the same processes as nitrate (e.g., denitrification), though a fraction of nitrite could also be transformed by abiotic processes (Tai and Dempsey, 2009; Li et al., 2012).

DON decreased by approximately 35% in the subsurface. The fact that removal rates for dissolved organic nitrogen were slow is not surprising: anaerobic degradation of organic compounds is often slower than under aerobic conditions (Hansen and Blackburn, 1991). A variety of additional processes,

such as decomposition and solubilization of particulate organic nitrogen, may also have occurred in the horizontal levee subsurface and could explain the relatively low DON removal observed (Li and Davis, 2014; van Kessel et al., 2009).

B.1.2 Trends in concentrations of $Mn_{(aq)}$, $Fe_{(aq)}$ and sulfate

Changes in porewater concentrations of manganese and iron give us important information about the reduction of Mn(III/IV)- and Fe(III)-oxides. Fe(III) and Mn(IV), the forms of the metals that were likely present prior to the introduction of wastewater, are sparingly soluble under the pH conditions in the wetland. In contrast, Mn(II) and Fe(II) tend to be much more soluble under many conditions.

Porewater Mn and Fe concentrations increased in the first few meters of the wetland as nitrate concentrations decreased, with strong negative correlations between those metals and nitrate (Spearman's rho values were -0.66 and -0.45, for Mn and Fe respectively). Conversely, Mn and Fe concentrations were positively correlated with each other (Spearman's rho = +0.75). Therefore, we concluded that the dissolved Mn and Fe detected in the porewater were in the +2 oxidation state and that reduction of Mn- and Fe-oxides was occurring coincident with nitrate reduction. Dissolved concentrations of Mn and Fe increased steadily in the first 15 m of the slope (Figure 3-17) minus a few outliers. Porewater concentrations of these species did not tend to increase substantially after this point. Concentrations of porewater sulfate decreased by over 90% over the wetland slope though the distance at which this reduction occurred varied significantly seasonally (Figure 3-16) and based on wetland cell type (Figure 3-17).

When porewater data were segregated by cell type, significant differences in concentrations of $Mn_{(aq)}$ ($p < 0.001$), $Fe_{(aq)}$ ($p < 0.01$) and sulfate ($p < 0.05$) were observed between cells planted with willows versus those planted with a wet meadow plant community. In particular, sulfate concentrations were significantly higher in willow cells (Figure 3-17). In those cells, sulfate concentrations did not decrease significantly until around the 15 m of the slope where they decreased by >93% ($p < 0.001$). This was likely caused by the unique adaptations of willows to waterlogged conditions. Willows are particularly tolerant to oxygen stress in inundated soils (Jackson and Attwood, 1996), due to their ability to supply oxygen to the subsurface (Armstrong, 1968) through extensive rooting zones (Kuzovkina and Volk, 2009). This supply of oxygen can re-oxidize $Mn(II)_{(aq)}$, $Fe(II)_{(aq)}$ and reduced sulfur, leading to lower aqueous concentrations of Mn(II) and Fe(II), and ostensibly reduced rates of sulfate reduction. In contrast, wet meadows likely had shallower rooting zones, supplying less oxygen to deeper layers where microbial processes dominate.

Appendix C: Supporting Information from Chapter 4

C.1 Biomass measurements and regression development

Different types of imagery have been used previously for forest biomass prediction, including Radar, LiDAR and optical imagery (le Maire et al., 2011). Although Radar and LiDAR data provide high accuracy estimates of biomass, these data are not as readily available or often lack spatial and temporal frequency of optical sensor imagery. In this study, we estimated above-ground biomass using temporally resolved multispectral satellite data of the field site to calculate vegetation index values for the areas of individual wetland cells across four sampling dates. Methods consisted of four main steps: (1) biomass sampling; (2) computing vegetation indices from remote sensing data; (3) fitting regressions to the biomass and vegetation indices; (4) assessing the error and performance of the regressions; and, (5) applying the regression to generate estimates of biomass.

Seasonal changes in standing biomass followed consistent trends that were modeled using polynomial regressions to estimate peak standing biomass on an annual basis. To determine the total amount of biomass produced by plants throughout the year (i.e., net primary production), values of peak standing biomass were multiplied by biomass turnover rates (i.e., biomass turnover (yr^{-1}) = net primary production (kg m^{-2} yr^{-1})/peak standing biomass (kg m^{-2})). Biomass turnover rates were estimated based on literature values and measurements conducted at the field site (Table C-4).

C.1.1 Biomass sampling

Biomass samples were collected in 0.25 m^2 square quadrats on four dates, in 8 of the 12 wetland cells (Figure C-1). Sampling points were collected via GPS (for 2019 dates) or by measurement offsets from a known location (for 2017 dates). The biomass sampling locations were selected via stratified random sampling (24 samples in 2017), or strategically sampled to target high biomass areas, to provide an upper bound for regression (19 samples in 2019) (Figure C-1). Biomass samples were collected by harvesting all living plant biomass to the ground surface in the 0.25 m^2 quadrats. In January 2019, dead biomass (litter) was also collected to allow for calculations of biomass turnover rates.

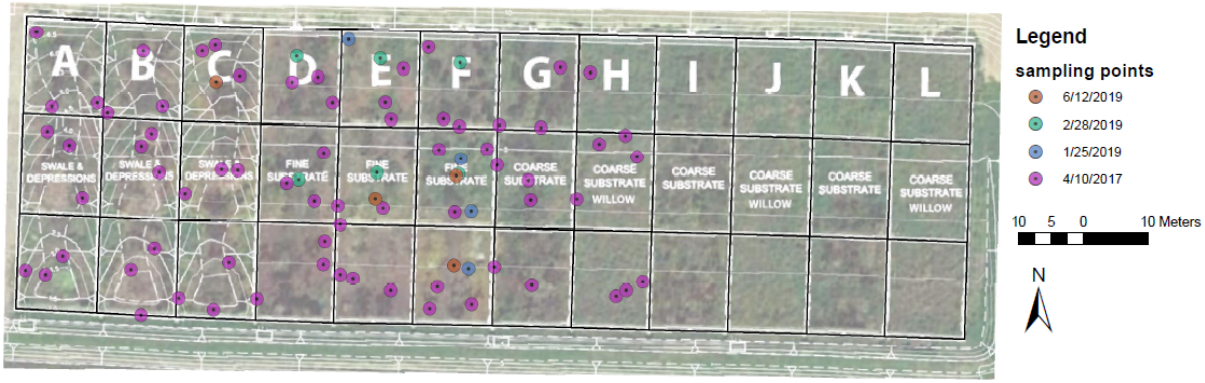

Figure C-1: Location and dates of biomass samples.

Biomass samples were not collected from cells I-L on dates when samples were geolocated due to logistical and time constraints. For cells J and L, there were logistical difficulties associated with collecting full *S. lasiolepis* samples and samples from cell H were collected to be considered representative of the willow cells. However, samples were collected from cells I-L in January 2017, at which time biomass measurements in those cells (median of 0.53 kg m^{-2}) were not statistically different ($p = 0.15$) from samples collected from other cells (0.48 kg m^{-2}).

Boxplots showing the mean biomass measurements by wetland cell for 2017 and 2019 are shown in Figure C-2. On average, biomass values were higher for 2019 (1.13 kg/m^2) compared to 2017 (0.41 kg/m^2). Two biomass outliers (one per year) were identified that fell outside of the maximum interquartile range; these were omitted from further analysis.

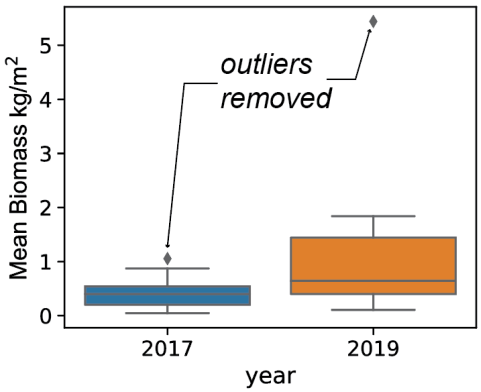

Figure C-2: Boxplots of mean cell biomass for 2017 and 2019 sampling dates. The line in the center of the box represents the median. Biomass outliers are shown as points for 2017 and 2019, which were subsequently dropped from the analysis.

C.1.2 Vegetation indices

For each sampling date, we downloaded a corresponding satellite image from Planet Labs with 0% cloud cover (PlanetScope Scene imagery, 4-band, 3.7 m spectral resolution) (Planet Team, 2017). These images were imported into ArcGIS, resampled to 0.25 m resolution and clipped to the boundary of the wetland. Biomass sampling dates and corresponding satellite image dates are summarized in Table C-1.

Table C-1: Biomass sampling dates, image date, number of points and sampling method.

Biomass Sampling Date	Planet Date	$n_{samples}$	$n_{cell\ thirds}$	$n_{samples\ per\ cell\ third}$	Method
4/10/2017	4/3/2017	70	24	3	Stratified random
1/25/2019	1/24/2019	3	3	1	Upper bound
2/28/2019	2/22/2019	6	6	1	Upper bound
6/12/2019	6/12/2019	10	4	2.5	Upper bound

Normalized vegetation indices take advantage of the differential absorption and reflectance of energy in the red and near-infrared regions between vegetation and impervious area to identify vegetated areas (Jensen, 2007). Different greenness indices can discriminate among different parts of the landscape.

Therefore, we tested the correlation between above-ground biomass measurements and three different vegetation indices: (1) Simple Ratio; (2) Normalized Difference Vegetation Index; and, (3) Green Normalized Vegetation Index.

The aptly named Simple Ratio (SR) is the simplest vegetation index, calculated as the ratio of red and near-infrared bands (Equation C-1), and is responsive to changes in biomass or leaf area index (Jensen, 2007). Because the SR is not normalized, values are not bounded by -1 or 1. If the red and NIR reflectance are very similar, the SR value is approximately 1 and indicates areas of bare soil or impervious material. If NIR is much higher than red reflectance (as is the case with green vegetation), the SR value is very high (e.g., > 30).

Unlike SR, Normalized Difference Vegetation Index (NDVI) and Green Normalized Vegetation Index (GNDVI) are normalized indices that range from -1 to 1. The NDVI index quantifies the differential absorption and reflectance of energy of photosynthetic objects (vegetation) and non-photosynthetic objects (Khorram et al., 2016). The NDVI is calculated by normalizing the difference between red and near-infrared bands (Equation C-2). GNDVI is a modified form of NVDI that uses green instead of red visible light (Equation C-3). In this way, GNDVI is more sensitive to the chlorophyll content of the vegetation (it uses the difference between the reflectance at the "green peak" and the reflectance of NIR light).

$$SR = \frac{Red}{NIR}$$ **Equation C-1**

$$NDVI = \frac{NIR-Red}{NIR+Red}$$ **Equation C-2**

$$GNDVI = \frac{NIR-Green}{NIR+Green}$$ **Equation C-3**

We computed NDVI, GNDVI, and SR across the wetland for each sampling date. For each biomass sampling date, NDVI, GNDVI, and SR values from the corresponding image were spatially averaged within each cell-third zone using 'zonal statistics' tool in ArcGIS. This approach reduced potential bias and error associated with sample point locations and provided adequate spatial resolution for subsequent calculations. These data, along with average biomass values within each cell third for each sampling date, were imported into Python for further analysis.

Scatter plots showing biomass vs. vegetation indices with outliers removed are shown in Figure C-3.

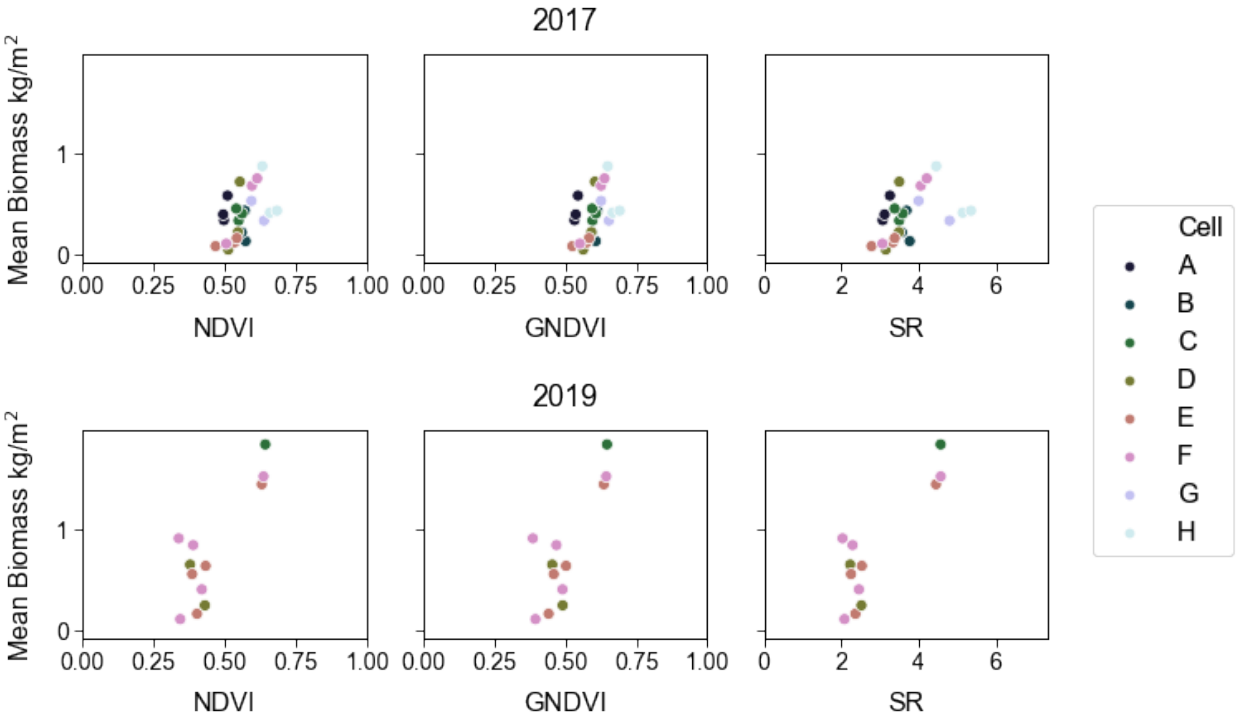

Figure C-3: Above-ground mean biomass (kg/m^2) vs. vegetation indices. Upper plot shows NDVI, GNDVI, and SR for 2017, lower plot shows NDVI, GNDVI, and SR for 2019. Outliers were removed.

C.1.3 Regression development

Prior to developing predictive models, we evaluated the merit of using linear regression by determining whether the data satisfies three principle assumptions for linear regression. These three principle assumptions are: (1) the data are well-described by linear regression; (2) the errors are random and homoscedastic (un-biased); and, (3) the residuals (and thus the data as a whole) are normally distributed. The first of these assumptions using the Harvey-Collier test for linearity, which tests the null hypothesis that the mean of the residual errors is zero. We evaluated the second assumption using the Breusch-Pagan Lagrange Multiplier test for homoskedasticity, which tests the null hypothesis that the residual variance does not depend on the x variable (Breusch and Pagan, 1979). We tested the third assumption using the Jarque-Bera test, which tests the null hypothesis that the data is normally distributed against an alternative that the data follow some other distribution (Jarque and Bera, 1980). Each of these diagnostic tests were computed using the Python "statsmodel" package (Seabold et al., 2010).

Table C-2 summarizes p-values for the linearity and homoskedasticity tests and r^2 values for residual normality test. Most of the p-values resulting from these tests are insignificant ($p > 0.05$), with the exception of the linearity test using 2019 biomass vs. NDVI and GNDVI; these tests resulted in p-values of 0.03 and 0.02, respectively. This suggests that the regressions resulting from 2019 biomass data and NDVI and from the 2019 biomass data and GNDVI are non-linear. All other assumptions (homoskedasticity and random residuals) were satisfied ($p > 0.05$) for all regressions.

Table C-2: p-values of diagnostic tests for linearity assumptions.

Test	Assumption	p-value					
		NDVI		*GNDVI*		*SR*	
		2017	*2019*	*2017*	*2019*	*2017*	*2019*
Harvey Collier	H_o: data are linear	0.71	0.03*	0.90	0.02*	0.50	0.06
Breusch-Pagan Lagrange	H_o: homoskedasticity	0.34	0.16	0.63	0.19	0.29	0.14
Jarque-Bera	H_o: normally distributed	0.36	0.82	0.35	0.66	0.36	0.76

* Indicates statistical significance ($p \leq 0.05$); reject H_o.

For our final model, we fit an ordinary least squares (OLS) regression based on SR statistic for both 2017 and 2019. This choice avoids potential non-linearity exhibited in the NDVI and GNDVI regressions for 2019 data. The OLS model consists of a single independent variable (in this case, SR) to predict the dependent variable (biomass). Separate regressions were developed for 2017 and 2019, taking the form of Equation C-4 and Equation C-5:

$$Y_{2017} = X \times (\beta_{2017} \pm \varepsilon_{2017}) \quad \textbf{Equation C-4}$$

$$Y_{2019} = X \times (\beta_{2019} \pm \varepsilon_{2019}) \quad \textbf{Equation C-5}$$

Where *Y* is the dependent response variable (biomass), β is the slope coefficient, X the independent variable (NDVI, GNDVI, or SR), and ε the random error. Per the assumptions of linearity (described above), the random error term, ε, is assumed to follow a normal distribution with a mean of 0 and variance σ^2. The OLS method estimates β given X and Y, such that the sum of the squared prediction errors is minimized.

C.1.4 Error and performance

We conducted two tests of performance. First, we evaluated error through a single leave-one-out analysis, in which each regression was trained on 70% of samples (training set) and evaluated on the remaining 30% of samples (test set). However, small changes in training data can result in very different series of splits (Hastie et al. 2001), which can significantly impact results. For this reason, we repeated the above analysis across different subsets of training data by varying the random seed (i.e., how the data are split into training and testing sets). These tests give an estimate of the OLS model out-of-sample error – i.e., how well the regression predicts data it was not trained on. Regression performance was evaluated using the coefficient of determination (R^2) and normalized root-mean-square error (NRMSE) of prediction on our testing dataset. The NRMSE represents the root-mean-square-error normalized by the range of observed biomass values. Error metrics for the OLS regressions are shown in Table C-3.

Table C-3: Error metrics for OLS regression of above ground biomass (kg/m^2) for 2017 and 2019.

Metric	Single train-test split		Mean of 10 train-test splits	
	2017	*2019*	*2017*	*2019*
R^2 (unitless)	0.18	0.54	0.07	0.51
NRMSE (%)	29%	25%	32%	26%

The single train-test split gave more favorable results, but these results were more likely to be biased by a favorable training set than the average of 10 train-test splits. A better estimate of error was from the mean of 10 train-test splits. This suggests that for data on which the regression was not trained, we

can expect a mean R^2 of 0.07 and 0.51 and NRMSE of 32% and 26% for 2017 and 2019, respectively.

The final 2017 and 2019 SR regressions (trained on all the data) and 95% CIs (around the slope) take the form of Equation C-6 and Equation C-7:

$$\text{2017 biomass (kg/m}^2\text{)} = \text{SR} \times 0.1034 \text{ (95\% CI = -0.0792, + 0.1275)} \quad \textbf{Equation C-6}$$

$$\text{2019 biomass (kg/m}^2\text{)} = \text{SR} \times 0.2924 \text{ (95\% CI = -0.2189, + 0.3658)} \quad \textbf{Equation C-7}$$

The final 2017 and 2019 regressions are plotted along with the SR and biomass data in Figure C-4 and have R^2 values of 0.17 and 0.26, respectively. These R^2 values are slightly higher than the R^2 values presented in Table C-3 because the final regression is trained and tested on all of the data, rather than trained on a subset of the data and tested on unseen data.

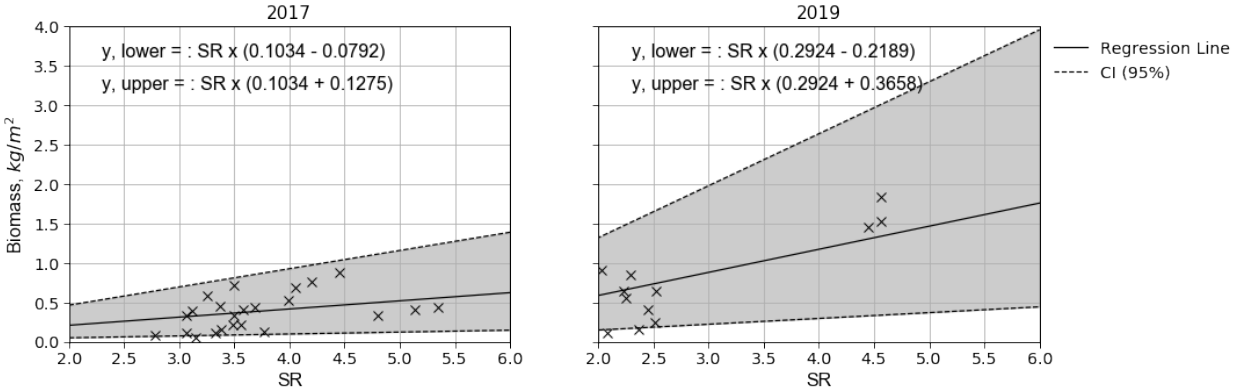

Figure C-4: Final OLS regressions for 2017 and 2019 with 95% confidence intervals on the slope.

C.1.5 Estimation of biomass and limitations

The OLS SR-biomass regressions were applied to cell-third SR values from the isotope sampling dates. The resulting biomass values (in kg m^{-2}) for each cell-third and each date were then used to estimate peak annual biomass, net primary production (section 4.2.6) and uptake of nitrogen (both overall and from wastewater). There are a few sources of potential error with this approach. First, because regressions were developed for 2017 and 2019, but not for 2018 (no biomass sampling was conducted in 2018), we used the average of the 2017 and 2019 regression estimates for the 2018 biomass values. Second, biomass samples were only collected from cells A through H, but not from I though J due to time constraints during sampling days and logistical difficulties with sampling willows. It is possible that these shortcomings in the sampling methods induced bias in the regression results. However, given that we observed similar ranges of SR values over time (i.e., in 2016, 2017, 2018, and 2019) and space (i.e., in cells A through H and I through J), we believe that these regressions are representative of the wetlands as a whole.

Table C-4: Literature and calculated values for turnover rates.

Rate (yr^{-1})	Above or below ground	Reference
0.96	Above ground, willow	Amichev et al, 2012
0.07	Above ground, trees	Wiedmer and Senn-Ilert, 2006
0.50	Roots	Grogan and Matthew, 2002
2.1	Roots	Berhongaray et al., 2013
2.4	Roots	Berhongaray et al., 2013
4.9	Roots	Rytter, 1999
5.8	Roots	Rytter, 1999
0.20	Above ground, willow	Webber and May, 1977
0.90	Roots	Stadnyk, 2010
1.1	Roots	Stadnyk, 2010
0.45	Roots	Rytter and Rytter, 1998
2.1	Roots	Rytter and Rytter, 1998
0.20	Roots	Rytter and Rytter, 1998
5.0	Roots	Rytter and Rytter, 1998
2.2	Roots	Rytter and Rytter, 1998
0.8	Roots	Rytter and Rytter, 1998
1.2	Roots	Rytter and Rytter, 1998
1.3	Roots	Rytter and Rytter, 1998
2.0	Roots	Rytter and Rytter, 1998
0.56	Roots	Gill and Jackson, 2000
0.10	Roots	Gill and Jackson, 2000
0.56	Roots	Gill and Jackson, 2000
5.0	Roots	Rytter, 2013
2.4	Roots	Rytter, 2013
3	Roots	Pacaldo et al., 2014
1.4	Roots	Huang et al., 2008
1.0	Roots	Huang et al., 2008
1.9	Roots	Huang et al., 2008
1.3	Roots	Huang et al., 2008
6.4	Roots	Rytter, 2001
6.8	Roots	Rytter, 2001
1	Above ground, willow	van de Broek et al., 2015
0.21	Above ground, willow	Gill and Jackson, 2000
1.3	Tall emergent macrophytes	Kvet, 1982
4.4	*Typha* spp.	Davis, 1989
3.5	Wetlands, low	Davis, 1994
10	Wetlands, high	Davis, 1994
1.3	Not specified, wetlands	Kadlec and Wallace, 2009
1.0	Macrophyte, low	Mitsch and Gosselink, 2000
2.0	Macrophyte, high	Mitsch and Gosselink, 2000
4.2	Wet meadow, median composite, 2016	This study
5.0	Wet meadow plants, high, 2016	This study
3.3	Wet meadow plants, low, 2016	This study
4.2	Wet meadow, median composite, 2019	This study
15	Wet meadow plants, high, 2019	This study
1.7	Wet meadow plants, low, 2019	This study

C.2 Additional details regarding foliar and soil isotope samples

C.2.1 Differences between baseline foliar and soil isotope measurements

Between October 2016 and April 2017, average $\delta^{15}N$ and $\delta^{34}S$ values in foliar samples were 5.7 ± 0.5‰ and 0.0 ± 1.1‰, respectively, while soil samples collected in April 2016 had average $\delta^{15}N$ and $\delta^{34}S$ values of 5.7 ± 0.5‰ and 0.5 ± 2.1‰, respectively. Only prior to May 2016 were significant differences ($p < 0.05$) between foliar and soil samples observed, when $\delta^{15}N$ for *S. lasiolepis* and *J. balticus* were 8.8 ± 3.8‰ and 2.6 ± 3.2‰, respectively and $\delta^{34}S$ values were 0.5 ± 2.0‰ and -2.7 ± 2.1‰ (these data are not included in Figure 4-7). It is important to note that these samples were collected within 6 months after the plants had been transplanted to the horizontal levee and differences in values may have been due to isotope signature differences between soils in the horizontal levee and those in the beds where the plants were germinated and propagated.

C.2.2 Unexpectedly high foliar nitrogen isotope signatures

Among foliar samples collected in the first 10 m of the wetland slope, 65% exhibited higher $\delta^{15}N$ values than those measured in the influent nitrate from the most recent water sampling dates. This suggests that plant nitrogen is not simply a mixture of soil and influent nitrate sources, but rather that: (1) there was an undetected source of nitrogen; or, (2) wastewater nitrate became more enriched in ^{15}N prior to plant uptake. The former is unlikely because there are no reported natural sources of nitrogen that have such high $\delta^{15}N$ values (Kendall, 1988; Craine et al., 2015), whereas progressive enrichment of nitrate in ^{15}N in subsurface systems is a widely observed phenomenon (Böttcher et al., 1990; Aravena and Robertson, 1998; Mengis et al., 1999) and is often driven by denitrification (Kendall, 1998).

Therefore, we concluded that denitrification was rapidly and progressively enriching nitrate in ^{15}N in the subsurface, leading to higher $\delta^{15}N$ measurements in plants than would be expected based on the influent measurements. It is also possible, though unlikely, that plants in the wetland were discriminating against ^{15}N during uptake due to luxury consumption of nutrients, but we find this unlikely as the authors are not aware of this having been shown in any previous studies of plant uptake of nitrogen. Rather, past studies have shown that isotopic signatures of plants still continue to match their source of nitrogen under luxury consumption conditions (Yun and Ro, 2009).

C.2.3 Shifts in soil nitrogen isotope signatures

Measurements of soil $\delta^{15}N$ from samples collected in April 2017 exhibited a significant shift from previous values ($p < 0.001$; two-tailed t test), but in the opposite direction ($\delta^{15}N_{soil,\ April\ 2017} = 4.6 \pm 0.5‰$) of the shifts that were observed in foliar $\delta^{15}N$ measurements. Significant shifts were not observed ($p = 0.49$; two-tailed t test) in $\delta^{34}S$ values in soil.